Molecular Genetics of Chorea-Acanthocytosis

Carol N. M. Dobson-Stone

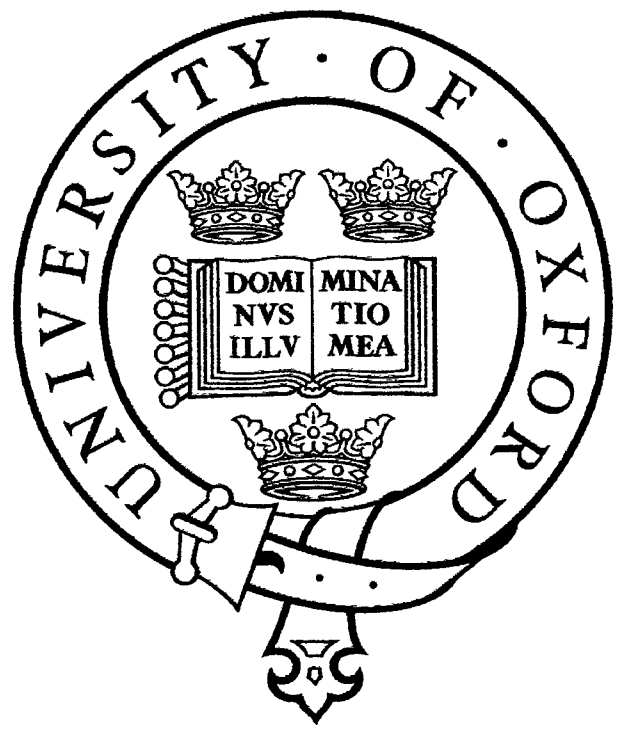

Wolfson College
University of Oxford

A thesis submitted for the degree of Doctor of Philosophy
Hilary 2004

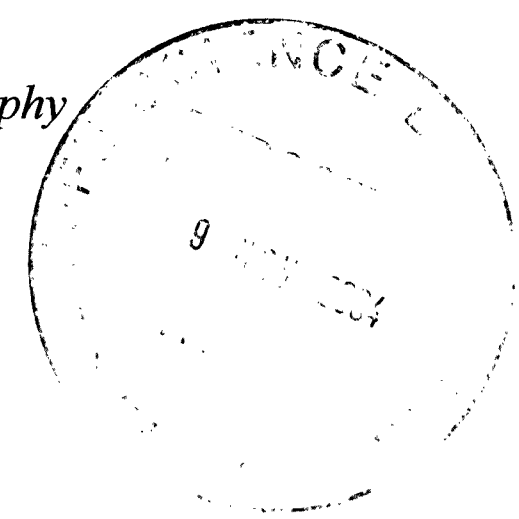

Carol N. M. Dobson-Stone
Wolfson College, University of Oxford

Molecular Genetics of Chorea-Acanthocytosis

Abstract

Chorea-acanthocytosis (ChAc) is an autosomal recessive neurological disorder whose characteristic features include hyperkinetic movements and abnormal red blood cell morphology. The disorder shares features with Huntington's disease and McLeod syndrome (MLS), and can sometimes be difficult to distinguish clinically from the latter. In 1997, ChAc was linked to a 6-cM region on chromosome 9q21-22. A novel gene, *CHAC*, was identified in the critical region. *CHAC* (now renamed *VPS13A*) encodes a large protein called chorein, with a yeast homologue implicated in protein sorting.

In this study, all 73 exons plus flanking intronic sequence in *VPS13A* were screened for mutations in 83 unrelated ChAc patients. We identified 88 different *VPS13A* mutations in 72 probands, comprising six deletions of entire exons, 22 nonsense, 36 frameshift, 19 splice-site and five missense mutations. This disorder therefore shows substantial allelic heterogeneity: however, evidence for common inheritance of the EX70_73del mutation in four French Canadian pedigrees indicates a possible founder effect in this population.

Expression of *VPS13A* appears to be ubiquitous, as determined by tissue-specific analysis of mRNA and chorein distribution. However, chorein expression was markedly reduced or undetectable in lymphoblasts, fibroblasts and erythrocyte membranes from 14 ChAc patients. In contrast, MLS cells showed chorein expression similar to control levels, suggesting that loss of chorein expression is a diagnostic feature of ChAc.

Yeast two-hybrid analysis of six different ~600 amino-acid chorein fragments was used to screen a human brain cDNA library for proteins that may interact with chorein. One fragment interacted weakly with constructs derived from transcription factor NF-κB, putative protein phosphatase PP2Cη and TAB2, a protein implicated in the mitogen-activated kinase cascade. Although exogenously expressed chorein and TAB2 did not appear to colocalise, co-immunoprecipitation experiments supported an interaction between the two proteins, suggesting an avenue for future research into chorein function.

Submitted for the degree of Doctor of Philosophy, Hilary 2004

Declaration

All the work in this thesis was performed by the author in the Wellcome Trust Centre for Human Genetics, Faculty of Clinical Medicine, University of Oxford, except as detailed below:

Mutational analysis of *VPS13A* in patients with chorea-acanthocytosis (Chapter 3), Wave I: Luca Rampoldi was responsible for cloning the *CHAC* gene (*VPS13A*). I assisted him with mutation detection of the original 11 ChAc probands. I also reconfirmed the mutations in these probands by restriction digest or sequencing, and checked that mutations co-segregated with the disease haplotypes in the respective families.

Wave II: Lorne Lonie performed the DHPLC analysis of the Wave II cohort. I performed PCR amplification and hybridisation of the proband samples, and all post-DHPLC procedures.

Wave III: Lorne Lonie performed the DHPLC analysis of the Wave III cohort. Under my supervision, Lea Filippone and Sarah Westbury performed PCR amplification and hybridisation of the proband samples, and sequencing analysis of DHPLC variants. I reconfirmed the mutations in these probands by sequencing, and checked that mutations co-segregated with the disease haplotypes in the respective families.

The work reported in this thesis has not been submitted for any other degree in this or any other university or institute of learning.

Acknowledgements

During the course of this study, I was the recipient of a Wellcome Trust Prize Studentship. I would like to thank the patients and their families, who have made this study possible, and the numerous clinicians who were involved in patient sample collection. In particular, Prof Adrian Danek was the driving force behind collection of patient samples and clinical data, and was always ready to give help and advice on the clinical aspects of this study.

I would also like to thank Prof Tony Monaco for his brilliant supervision and encouragement throughout my time at the Wellcome Trust Centre. Despite the many demands on his time, he was always quick to reply with sensible answers to my stupid questions, and has provided the gold standard by which I shall measure all future bosses! Drs Luca Rampoldi and Antonio Velayos-Baeza, the former and current post-doc on the ChAc project, have also been extremely generous with their time and wisdom and have been instrumental in the success of this study.

Additional thanks go to the rest of the Monaco group for all their help in scientific and non-scientific matters, and for making the past six years at the Wellcome Trust Centre seem more like fun than work. Our lab neighbours, the Genomics group and the former Hovnanian group, were always willing to give technical advice and much-needed reagents. Outside the lab, I am indebted to Jan Trinder for all her help and the 'lucky touch' that ensured acceptance of my manuscripts! My non-scientific friends have always been supportive, and listened politely without yawning to my moans about experiments not going to plan, for which I am very grateful.

Above all, I would like to thank my parents and the rest of my rapidly expanding family for all their love, and the support they have shown in my every endeavour since I was old enough to hold a pen. Special thanks to my husband, without whom I wouldn't have eaten or otherwise functioned properly over the past three months, and for always being there to rescue me from irretrievable geekiness.

Glossary of abbreviations used in this thesis

5FOA	5-fluoroorotic acid
aa	amino acid
ABL	abetalipoproteinemia
AD	activation domain
AT	annealing temperature
BCA	bicinchonic acid
BLAST	basic local alignment sequence tool
bp	base pair
BSA	bovine serum albumin
C-	carboxy
cDNA	complementary DNA
CGD	chronic granulomatous disease
ChAc	chorea-acanthocytosis
CK	creatine kinase
cM	centimorgan
CMV	cytomegalovirus
CT	computed tomography
DB	DNA-binding domain
DHPLC	denaturing high-performance liquid chromatography
dH_2O	deionised water
DMD	Duchenne muscular dystrophy
DNA	deoxyribonucleic acid
dNTP	deoxynucleoside-5'-triphosphate
DTT	dithiothreitol
EBV	Epstein-Barr virus
EDTA	ethylenediaminetetraacetic acid
EGFP	enhanced green fluorescent protein
EST	expressed sequence tag
gDNA	genomic DNA
GST	glutathione-S-transferase
h	hour
HARP	hypoprebetalipoproteinemia, acanthocytosis and retinitis pigmentosa
HBL	familial hypobetalipoproteinemia
HD	Huntington's disease
HDL2	Huntington's disease-like 2
-His	histidine-deficient
HSS	Hallervorden-Spatz syndrome
IKK	IκB kinase
IκB	inhibitor of NF-κB
IL-1	interleukin-1
IPTG	isopropylthio-β-D-galactoside
kb	kilobase pair
kDa	kilodalton
LB	Luria broth
-Leu	leucine-deficient
LiAc	lithium acetate

M	molar
mA	milliamps
MAP	mitogen-activated protein
MAPKKK	MAP kinase kinase kinase
mg	milligram
min	minute
ml	millilitre
MLS	McLeod syndrome
mM	millimolar
MRI	magnetic resonance imaging
mRNA	messenger RNA
MTP	microsomal triglyceride transfer protein
Mw	molecular weight
μg	microgram
μl	microlitre
μm	micrometer (micron)
μM	micromolar
N-	amino
NF-κB	nuclear transcription factor kappa B
ng	nanogram
nm	nanometre
nt	nucleotide
OD	optical density
OPMD	oculopharyngeal muscular dystrophy
ORF	open reading frame
PBS	phosphate-buffered saline
PCR	polymerase chain reaction
PDI	protein disulfide isomerase
PEG	polyethylene glycol
PET	positron emission tomography
PKAN	pantothenate kinase-associated neurodegeneration
pmol	picomole
PMSF	phenylmethylsulphonyl fluoride
PP2Cη	protein phosphatase 2C eta
PTC	premature termination codon
PVC	prevacuolar compartment
RFLP	restriction fragment length polymorphism
RNA	ribonucleic acid
RNAse	ribonuclease
RT-PCR	reverse transcriptase polymerase chain reaction
s	second
sarkosyl	N-lauryl sarcosine, sodium salt
SDS-PAGE	sodium dodecyl sulphate polyacrylamide gel electrophoresis
STE	saline Tris-EDTA
SV40	simian virus 40
TAB2	TAK1-binding protein 2
TAE	Tris-acetate EDTA
TAK1	transforming growth factor β-activated kinase 1
TBE	Tris-borate EDTA
TBS	Tris-buffered saline

TEMED	tetramethylethylenediamine
TF	transcription factor
TGN	*trans*-Golgi network
TPR	tetratricopeptide repeat
-Trp	tryptophan-deficient
U	unit
UBA	ubiquitin-associated
-Ura	uracil-deficient
UTR	untranslated region
UV	ultraviolet
vps	vacuolar protein sorting
X-Gal	5-bromo-4-chloro-3-indolyl-β-D-galactopyranoside
Y2H	yeast two-hybrid

Contents

List of tables and figures

Index of Tables

List of Figures

Chapter 1: Introduction

'Acanthocyte', meaning 'thorny cell', is a descriptive term for a particular type of abnormal erythrocyte characterised by irregular cytoplasmic projections. Secondary acanthocytosis can occur post-splenectomy (Ward 1979), and as a result of malnutrition (due to, e.g., anorexia) (Takeshita *et al.* 2002), liver disease (Chitale *et al.* 1998), or myelodysplasia (Doll *et al.* 1989). Hereditary acanthocytosis is found together with neurological abnormalities in a rare constellation of disorders, collectively termed neuroacanthocytosis. Chorea-acanthocytosis, the subject of this thesis, is one of these disorders. Other neuroacanthocytoses include McLeod syndrome, abetalipoproteinemia and homozygous hypobetalipoproteinemia. Additional diseases, such as Hallervorden-Spatz syndrome and Huntington's disease-like 2, can occasionally include acanthocytosis as a phenotype.

1.1 Clinical features of chorea-acanthocytosis

In 1968, a North American family was described with circulating acanthocytes and a distinctive neurological disorder (Estes *et al.* 1967). Such an association had previously been observed in the recessive disorder abetalipoproteinemia (Bassen and Kornzweig 1950; Schwartz *et al.* 1961). However, no abnormality in serum lipids was detected in this family, and in another pedigree with similar symptoms: reports on these two families in 1968 concluded that they were suffering from a clinically distinct syndrome (Critchley *et al.* 1968; Levine *et al.* 1968). This disorder has been termed variously

Levine-Critchley syndrome (Sakai *et al.* 1985), amyotrophic chorea with acanthocytosis (Kito *et al.* 1980), neuroacanthocytosis (Yamamoto *et al.* 1982) and choreoacanthocytosis (Sakai *et al.* 1981), but it is now most commonly known as chorea-acanthocytosis.

1.1.1 General features of chorea-acanthocytosis

Chorea-acanthocytosis (ChAc, OMIM 200150) is a multisystem degenerative neurological disorder, characterised by progressive dyskinesia and aberrant erythrocyte morphology. No estimates of its prevalence have been made, but the disorder appears to be more common in Japan (Kuroiwa *et al.* 1984; Oshima *et al.* 1985): approximately 50 of the 200 or so cases reported to date are Japanese. ChAc does not appear to be geographically restricted: cases have been reported in Northern and Southern Europe (Sotaniemi 1983; Serra *et al.* 1986), North and South America (Critchley *et al.* 1968; Gross *et al.* 1985), India (Bharucha and Bharucha 1989), Africa (Feinberg *et al.* 1991), China (Ong *et al.* 1989) and the Middle East (Bohlega *et al.* 2003). The onset of neurological symptoms is usually delayed until 25-45 years of age, but can occur as early as the first decade or as late as the seventh (Hardie *et al.* 1991; Rampoldi *et al.* 2002). The course of the disease is progressive and death usually occurs after 7-14 years, often due to respiratory complications directly or indirectly linked to the movement disorder. It is not rare for patients to commit suicide (Alonso *et al.* 1989; Johnson *et al.* 1998). There is as yet no long-term treatment for this disorder.

1.1.2 Movement disorders in ChAc

As the name implies, chorea is often the dominant neurological symptom in ChAc. Chorea is commonly described as random, abrupt, irregular, involuntary movements that flow from body part to body part in a chaotic manner. Chorea often resembles fragments of normal movement, and many individuals with chorea incorporate the involuntary movements into motor patterns that appear voluntary. Choreatic limb movements in ChAc patients broadly resemble those seen in Huntington's disease (HD) (Shibasaki *et al.* 1982). In addition, the orofacial region is usually affected; in contrast with HD, self-mutilation of tongue and lips (Sakai *et al.* 1981; Kuroiwa *et al.* 1984) is often seen. Orofacial dyskinesia can also lead to dysarthria and dysphagia, commonly in the form of feeding dystonia. Vocalisations and motor tics reminiscent of those seen in Tourette syndrome are often observed (Hardie *et al.* 1991); however, coprolalia is reported in only a few cases (Bird *et al.* 1978; Spitz *et al.* 1985).

Dystonia, characterised by involuntary muscle spasms that produce twisting postures of different body parts, is also common: it has been reported as the presenting symptom in a few cases (de Yebenes *et al.* 1988; Peppard *et al.* 1990; Hardie *et al.* 1991). The hyperkinetic state can gradually progress to parkinsonism (Sakai *et al.* 1985; Hardie *et al.* 1991; Ishikawa *et al.* 2000) - this has been explained as an initial supersensitivity of brain dopamine receptors followed by progressive pre- and postsynaptic degeneration (Spitz *et al.* 1985). However, rare patients presenting with parkinsonism have also been reported (Spitz *et al.* 1985; Bostantjopoulou *et al.* 2000). In short, the gamut of involuntary movements associated with basal ganglia dysfunction is exhibited in ChAc.

1.1.3 Neuropsychiatric features

Epileptic seizures are common in ChAc - a study of 40 Japanese cases reported seizures as the second most common presenting symptom after chorea (Kuroiwa *et al.* 1984), and they have been the presenting symptom in European cases (Malandrini *et al.* 1993; Aasly *et al.* 1999). A neuropsychiatric review of nine ChAc patients revealed that personality change, with impulsive and distractible behaviour or apathy was most common, and obsessive-compulsive features might also occur (Kartsounis and Hardie 1996). Other psychiatric and behavioural features seen in ChAc include aggression (Alonso *et al.* 1989; Malandrini *et al.* 1993), anxiety (Feinberg *et al.* 1991), depression (Rinne *et al.* 1994b), disinhibition (Sorrentino *et al.* 1999) and lying (Yamamoto *et al.* 1982). Cognitive impairment is common, with deficits in memory, attention and executive skills observed (Kartsounis and Hardie 1996), but intellectual deterioration appears to be mild compared with HD (Medalia *et al.* 1989).

1.1.4 Brain pathology

As expected from the dyskinesia associated with the disorder, ChAc appears to be primarily a disease of the basal ganglia. Typical post-mortem analyses reveal marked atrophy and astrogliosis of the caudate and putamen, with associated enlargement of the lateral ventricles, similar findings to that in HD. The globus pallidus is also often atrophied, but to a lesser extent (Bird *et al.* 1978; Sobue *et al.* 1986; Alonso *et al.* 1989; Feinberg *et al.* 1991). Rinne *et al.* (1994) observed that the thalamus, substantia nigra and anterior horns of the spinal cord were abnormal in 30-50% of previous brain autopsies; and that the subthalamic nucleus, midbrain, pons, medulla, cerebellum and cerebral cortex were apparently unaffected. However, ocular motor abnormalities suggest that the brainstem is involved in the pathology of some ChAc cases

(Gradstein *et al.* 2003). More extensive nigral degeneration was observed in post-mortem studies of two cases with overt parkinsonian features (Rinne *et al.* 1994a).

Computed tomography (CT) and magnetic resonance imaging (MRI) studies are consistent with the post-mortem analyses (see Figure 1.1a). MRI shows increased signal in caudate and putamen on T2- weighted images (Hardie *et al.* 1991; Malandrini *et al.* 1993; Tanaka *et al.* 1998). Serra *et al.* (1987) used CT to measure caudate size in five patients with suspected ChAc and found that the extent of shrinkage was very similar to that in HD patients. Mild diffuse cerebral atrophy has been observed using CT (Sotaniemi 1983; Spitz *et al.* 1985; Malandrini *et al.* 1993; Hirayama *et al.* 1997), but the degree of cerebral cortex degeneration observed in HD (Vonsattel *et al.* 1985) does not appear to be typical for ChAc.

Positron emission tomography (PET) findings show marked glucose hypometabolism of caudate and putamen in ChAc patients (Hosokawa *et al.* 1987; Dubinsky *et al.* 1989). Tanaka *et al.* (1998) found global reduction in cerebral blood flow and oxygen metabolism, with marked reduction in caudate and putamen, and less in frontal lobes. Another study showed significant blood flow decrease in the frontal lobe only (Delecluse *et al.* 1991). An [^{18}F]-fluorodopa-uptake PET study showed evidence of selective degeneration of dopaminergic projections from the nigra compacta to the posterior putamen in neuroacanthocytosis patients; altered [^{11}]C-raclopride uptake implied loss of striatal dopamine D2 receptors (Brooks *et al.* 1991). The authors suggested that this could explain why choreic and parkinsonian signs are both seen in ChAc.

1.1.5 Peripheral nerve and muscle pathology

Reduction or absence of deep tendon reflexes, indicative of a motor neuropathy and not observed in HD, is highly characteristic of ChAc (Sakai *et al.* 1981; Sotaniemi 1983). There is negligible reduction of motor and sensory nerve conduction velocity (Sobue *et al.* 1986; Vita *et al.* 1989; Tanaka *et al.* 1998). Nerve biopsies show a moderate decrease in density of myelinated fibres (Ohnishi *et al.* 1981; Vita *et al.* 1989). Muscle atrophy is a common feature of ChAc and can sometimes occur before dyskinesia (Kito *et al.* 1980; Serra *et al.* 1986). Muscle CT scans of two ChAc patients showed selective symmetrical lower leg atrophy (Ishikawa *et al.* 2000). Electromyograms of suspected ChAc patients generally show high amplitude and long duration potentials, indicating neurogenic abnormalities (e.g., (Ohnishi *et al.* 1981; Gross *et al.* 1985; Vita *et al.* 1989; Tanaka *et al.* 1998)). Muscle biopsies are also compatible with a chronic neurogenic muscular atrophy (Ohnishi *et al.* 1981; Serra *et al.* 1986; Vita *et al.* 1989). When myopathic changes are observed in ChAc, they are considered secondary to the chronic denervation (Limos *et al.* 1982).

1.1.6 Laboratory findings

Apart from acanthocytosis, the most common laboratory findings in ChAc are elevated serum muscle-specific creatine kinase (CK) levels (Danek *et al.* 2004). Levels of other enzymes, such as muscle and liver transaminases and lactate dehydrogenase are sometimes also elevated (Serra *et al.* 1986; Tanaka *et al.* 1998). These findings may be due to an often subclinical muscular atrophy (Danek *et al.* 2004). Two ChAc patients showed increased levels of tissue transglutaminase, a cross-linking enzyme involved in assembly of macromolecular structures (Melone *et*

al. 2002). One female with confirmed ChAc showed absence of serum aprebetalipoprotein (Bohlega *et al.* 1998; Bohlega *et al.* 2003).

1.1.7 Treatment

Medication for ChAc is aimed primarily at relieving dyskinesia and psychiatric symptoms, or controlling epileptic seizures. Although the latter is often successful, standard neuroleptics are often of little effect (Wihl *et al.* 2001; Burbaud *et al.* 2002). High-frequency stimulation of the motor thalamus has been shown to improve trunk spasms but not dysarthria or hypotonia (Burbaud *et al.* 2002); a similar technique used in the globus pallidus did not have any long-term effect (Wihl *et al.* 2001). Similarly, excisions in the same areas have had only partial success (Ohnishi *et al.* 1981; de Yebenes *et al.* 1988; Fujimoto *et al.* 1997).

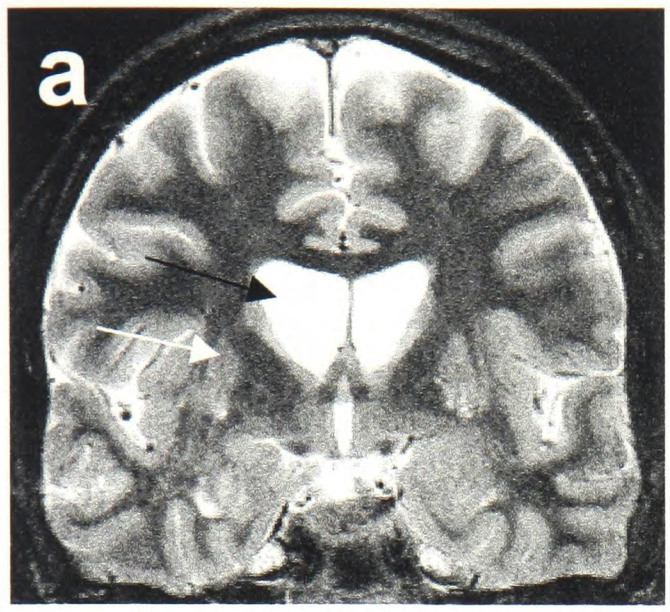

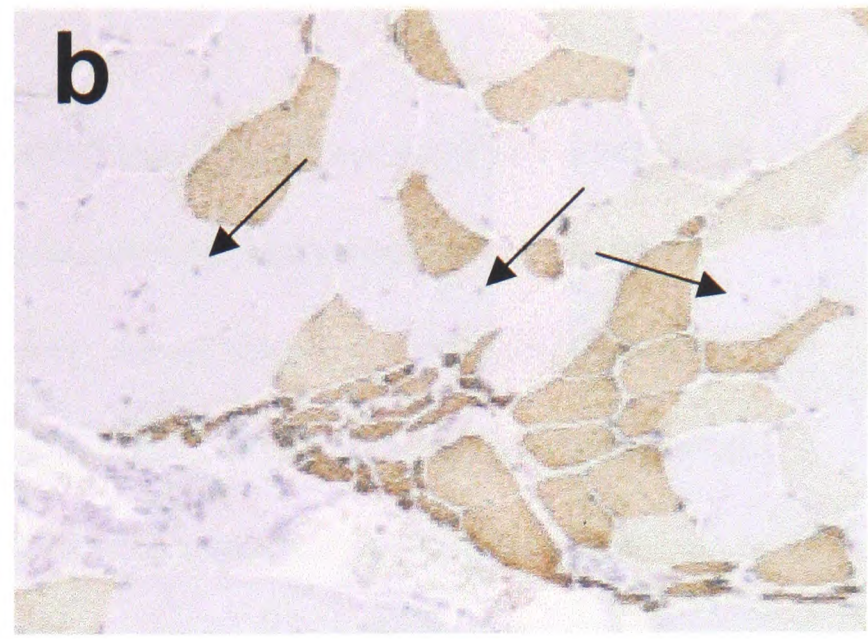

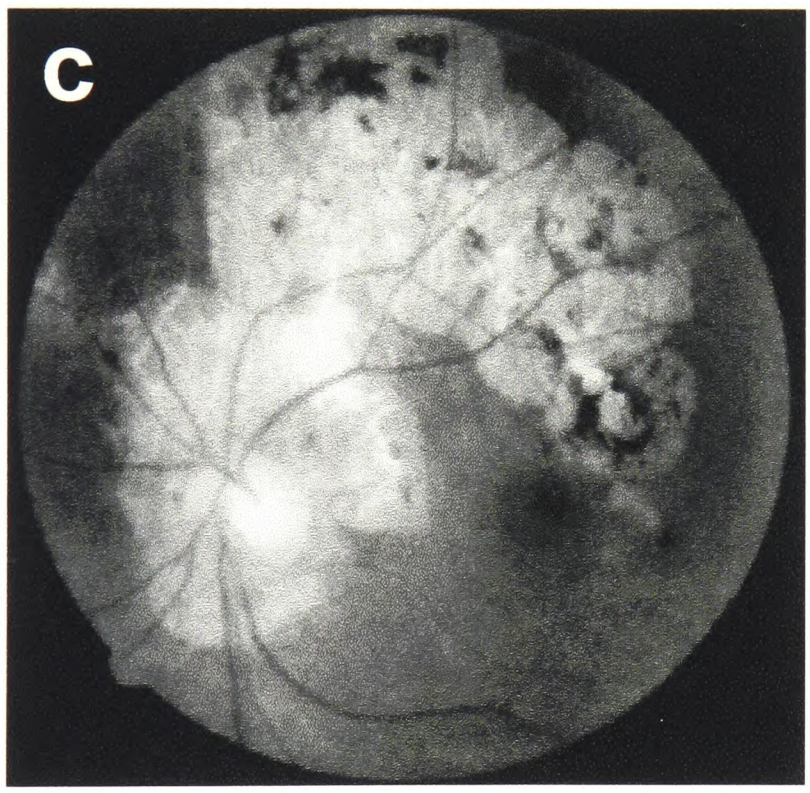

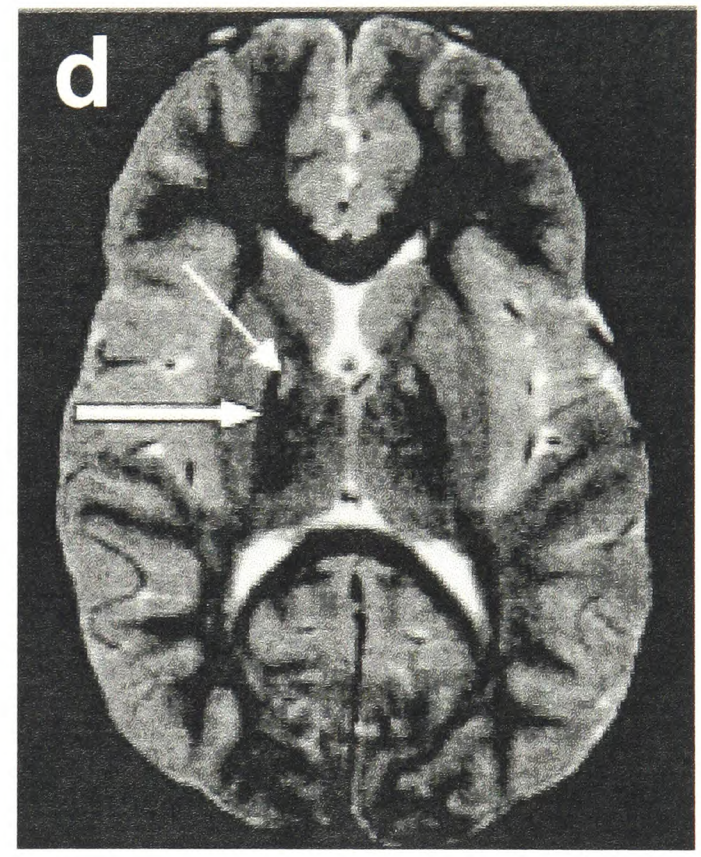

Figure 1.1 - Clinical features of neuroacanthocytoses. a, Basal ganglia degeneration in ChAc. MRI scan taken in the frontal plane, showing pronounced atrophy of the heads of the caudate nuclei with subsequent widening of the lateral ventricles (black arrow), and incipient atrophy of the putamen (white arrow) *(taken from Danek* et al., *2004)*. **b, Myopathy in MLS.** Immunohistochemistry of quadriceps muscle stained for fast myosin, showing fibre-type grouping, fibre atrophy, centralised nuclei (arrows) and variability of fibre diameter *(taken from Jung* et al., *2001*). **c, Retinitis pigmentosa in ABL.** Right retinal fundoscope of an ABL patient showing degeneration of the retinal pigment (*taken from Al-Shali* et al., *2003*). **d, 'Eye of the tiger' sign in HSS.** T2-weighted MRI scan taken in the lateral plane, showing hypointensity (thick arrow) with a central region of hyperintensity (thin arrow) in the medial globus pallidus (*taken from Hayflick* et al., *2003*).

1.2 Other neuroacanthocytoses: McLeod syndrome

Kell is a complex blood group system with more than 20 serologically recognised erythrocyte antigens. Certain Kell antigens are very immunogenic, so the Kell serotype is the next most important determinant of transfusion compatibility after ABO and Rhesus. The McLeod phenotype, characterised by weak expression of the Kell antigens and absence of the otherwise ubiquitous Kx antigen, was first recognised and named after the propositus by Allen *et al.* (1961). This phenotype is rare: again, no estimates of prevalence have been recorded, but Swash *et al.* (1983) noted that of 300,000 donors screened over three years in a British blood transfusion centre, only two with the McLeod phenotype were detected. Sixteen years after the phenotype was described, Wimer *et al.* (1977) discovered that the red cells in the propositus showed acanthocytosis, reduced *in vivo* survival and a compensated haemolytic state. Hepatomegaly and splenomegaly were subsequently observed in a New Zealand pedigree (Symmans *et al.* 1979). McLeod syndrome (MLS) was originally introduced to neurologists as a benign myopathy (Swash *et al.* 1983), but it is now appreciated that the clinical spectrum of the disorder includes severe neurological impairment, and some cases can be difficult to distinguish clinically from ChAc (Takashima *et al.* 1994; Stevenson and Hardie 2001; Danek 2002). In fact, some cases where neurological symptoms were initially ascribed to ChAc are now known to have MLS (e.g., Family L in (Hardie *et al.* 1991); case in (Faillace *et al.* 1982)), and it is likely that misdiagnosed cases of MLS remain in the literature.

1.2.1 Clinical features

The description of 22 men with the McLeod phenotype by Danek *et al.* (2001) illustrates the range of clinical features typically associated with this disorder. Liver and/or spleen enlargement was observed in 40% of the patients examined. Two-thirds of patients showed signs of cardiac disease, with a cardiac cause of death suspected in 4/5 patients. All tested patients showed areflexia or hyporeflexia, with lower limb tendons being more affected. Muscle weakness, primarily of the lower limbs, was detected in two-thirds of patients. Muscle involvement in MLS was initially recognised by Marsh *et al.* (1981), and since then has been well documented. Muscle biopsies even in subclinical cases show features of active muscle fibre necrosis and regeneration (Swash *et al.* 1983; Dotti *et al.* 2000). In addition to this myopathy, there appear to be neuropathic changes, including fibre-type grouping, in other muscle biopsies (Witt *et al.* 1992; Malandrini *et al.* 1994; Jung *et al.* 2001a) (see Figure 1.1b). Electromyographic studies usually detect the neurogenic component of the atrophy (Dotti *et al.* 2000; Danek *et al.* 2001). A muscle CT scan of three MLS patients revealed selective and symmetrical atrophy of lower limb muscles (Ishikawa *et al.* 2000). In one patient, muscle necrosis led to severe rhabdomyolysis (Jung and Brandner 2002). The muscle atrophy is reflected in laboratory findings. Elevated creatine kinase in the serum of MLS patients was first noted by Marsh *et al.* (1981) and has since been observed in nearly every patient investigated. Serum lactate dehydrogenase activity is also slightly elevated in most MLS patients (Marsh *et al.* 1981; Danek *et al.* 2001).

The age of onset of neurological features in the McLeod cohort reported by Danek *et al.* (2001) ranged from 26 - 61. Seizures were reported in 23% of patients.

Psychopathologic features, including emotional lability, anxiety and depression, inappropriate behaviour, hallucinations and paranoia, were present in at least 45% of the group. Moderate cognitive deficits were discovered in over half of those examined. The majority of MLS patients show some form of movement disorder: as in ChAc, chorea appears to be the most common manifestation, but its onset is generally later - the mean age of onset is early fifties, compared with mid-twenties for ChAc (Rampoldi *et al.* 2002). Facial tics, involuntary vocalisations and tongue movements and dysarthria have all been reported: in contrast to ChAc, though, tongue and lip biting seems to be rare. The similarities in dyskinesia between ChAc and MLS is partly explained by the similar brain pathology - MLS patients also show atrophy of the caudate nucleus by CT (Danek *et al.* 1994; Malandrini *et al.* 1994) and MRI scans show an altered signal in the caudate and putamen (Dotti *et al.* 2000). PET studies indicate that glucose metabolism is absent in the basal ganglia and low in the frontal and parietal cortex (Dotti *et al.* 2000).

1.2.2 Genetics

Analysis of a large New Zealand family segregating the McLeod phenotype (Symmans *et al.* 1979) proved the assumption of X-linked recessive inheritance (Wimer *et al.* 1977). Female carriers show mosaicism for expression of Kell antigens, implying that the McLeod locus is subject to X-inactivation (Marsh *et al.* 1975b; Wimer *et al.* 1977). Several boys with chronic granulomatous disease (CGD) and the McLeod phenotype had been reported (Marsh *et al.* 1975a), so the deletion of Xp21 in a patient with Duchenne muscular dystrophy (DMD), CGD, retinitis pigmentosa and MLS (Francke *et al.* 1985) implied that the gene responsible for MLS lay in this chromosomal region. Using deletion analysis of patients with different combinations

of MLS, CGD and DMD, Bertelson *et al.* (1988) placed the MLS locus between the CGD and the DMD loci. Ho *et al.* (1992) narrowed the critical region to 150-380 kilobases within Xp21. They subsequently identified point mutations in two unrelated McLeod patients in a novel gene, *XK*, thereby identifying it as the gene responsible for the disorder (Ho *et al.* 1994).

XK is arranged in three exons. Its cDNA has an open reading frame (ORF) of 1335 nucleotides, encoding a predicted protein of 444 amino acids. At time of writing, 24 different *XK* mutations had been reported (21 reviewed in (Rampoldi *et al.* 2002); (Russo *et al.* 2002; Jung *et al.* 2003; Singleton *et al.* 2003)). Most of these are mutations likely to lead to absence of XK protein; the mutations appear to be evenly distributed throughout the *XK* gene sequence (Rampoldi *et al.* 2002).

1.2.3 Possible functions of XK

The *XK* gene is expressed highest in foetal liver and adult skeletal muscle, slightly lower in heart, brain and pancreas, and in low levels in other tissues (Ho *et al.* 1994). XK protein is predicted to contain 10 transmembrane regions and 14 potential phosphorylation sites, with a large extracellular loop between the third and fourth transmembrane domains. Khamlichi *et al.* (1995) purified Kx as an immunocomplex with Kell, and demonstrated by amino-acid sequencing that this was identical to XK. They also showed that XK is covalently attached to Kell via a disulphide bond. Interestingly, although XK is present as a complex with Kell in erythrocytes, immunohistochemistry studies have shown that in skeletal muscle, Kell localises to the cell membrane but XK is predominantly in the sarcoplasmic reticulum (Jung *et al.* 2001b).

Kell is a single membrane-spanning protein with a large extracellular region (Lee *et al.* 1991) and shows homology to mammalian endopeptidases, which process a variety of peptide hormones. Kell is primarily expressed in erythroid tissues and testis, but weak expression is seen in many other tissues (Russo *et al.* 2000). *In vitro* studies showed that Kell preferentially cleaves big endothelin-3, a peptide involved in multiple biological processes, including the regulation of vascular tone (Lee *et al.* 1999). Endothelins are neurotrophic factors at low concentrations and cytotoxic at high concentrations, suggesting that endothelin-related mechanisms might be implicated in neurodegeneration (Kataoka *et al.* 1995; Ehrenreich *et al.* 2000). It is therefore tempting to speculate that endothelins could play an important role in the pathogenesis of MLS. However, the simple absence of Kell and its activities on the plasma membrane cannot be the cause of McLeod syndrome, since individuals with the Kell null phenotype, lacking all Kell antigens, show no clinical or haematological abnormalities (Lee *et al.* 2000).

XK shows the same topographical arrangement in the membrane as Na^+ Cl^--dependent neurotransmitter receptors. However, it has very little amino-acid homology with these receptors, and initial studies showed no difference between McLeod and normal red cells in uptake of various substrates (Ho *et al.* 1994). XK shares 19% identity and 37% similarity with CED-8 in *Caenorhabditis elegans* (Stanfield and Horvitz 2000). CED-8, like XK, is predicted to have 10 transmembrane regions and is located on the plasma membrane. Studies on *Ced-8* loss-of-function mutations imply that the gene is involved in the execution step of programmed cell death, downstream of the caspase CED-3. The human homologue of CED-3, caspase-

8, is thought to play a crucial role in the striatal neurodegeneration in Huntington's disease (Hackam *et al.* 2000; Gervais *et al.* 2002). Stanfield *et al.* (2000) propose that XK may also function in apoptosis in humans and the late onset neurodegeneration associated with McLeod syndrome is a consequence of a disruption in apoptosis. However, as homology between the two proteins is not extensive, any conclusions drawn on XK's function based on comparison with CED-8 should be treated with caution.

As McLeod myopathy bears a striking resemblance to that in female carriers of a DMD mutation (Dubowitz 1985; Witt *et al.* 1992), it is conceivable that dystrophin is important in the muscular manifestations of MLS. However, muscle biopsies of two MLS patients showed normal expression and distribution of dystrophin, implying that XK and dystrophin do not interact in any substantial way (Carter *et al.* 1990).

Clues to XK function can be provided from analysis of the amino-acid substitutions established as causal mutations in MLS. Three such missense mutations have been reported so far (Danek *et al.* 2001; Russo *et al.* 2002; Jung *et al.* 2003). The cysteine involved in the C294R mutation is predicted to alter the structural stability of the XK protein (Danek *et al.* 2001). COS-1 cells were transfected with XK cDNA encoding an R222G substitution that had been observed in a MLS patient (Russo *et al.* 2002). The mutant protein was expressed but did not travel to the cell surface. However, no neurological examination was reported for this patient, and so the clinical consequences of this altered XK localisation are not known. Substitution E327K has also been associated with the McLeod serological phenotype (Jung *et al.* 2003). Again, the mutant XK was not presented on the erythrocyte surface - but remarkably,

despite extensive investigations, no clinical or subclinical cerebral or neuromuscular signs and symptoms of MLS were found. This implies that XK physiologic function is not necessarily related to XK/Kell complex formation.

1.3 Other neuroacanthocytoses: abetalipoproteinemia

Abetalipoproteinemia (ABL, OMIM 200100) was initially described by Bassen and Kornzweig (Bassen and Kornzweig 1950), who noted an association of the signs of lipid malabsorption, acanthocytosis, pigmentary degeneration of the retina and ataxia with hypocholesterolemia. ABL is characterised by the absence of plasma lipoproteins that contain apolipoprotein B and low plasma concentrations of triglyceride and cholesterol. It may present in infancy with failure to thrive but can present in young adults as a spinocerebellar degenerative disorder with peripheral neuropathy and a pigmented retinopathy (see Figure 1.1c). About 100 cases have been reported worldwide. About a third of these cases are from consanguineous marriages: family studies suggested autosomal recessive transmission. The majority of obligate heterozygotes are reported to have normal lipid levels (Berriot-Varoqueaux *et al.* 2000).

1.3.1 Clinical features

The initial presentation of ABL in infancy is of lipid intolerance with steatorrhoea, vomiting and abdominal swelling. Intestine endoscopy reveals a white mucosa in the duodenum and jejunum due to storage of lipids by the enterocytes (Delpre *et al.* 1978). Liver biopsies consistently show hepatic steatosis (Collins *et al.* 1989).

Chronic malabsorption of lipids leads to lipid-soluble vitamin deficiency. If untreated, the classical neurological course of ABL includes diminution and then loss of deep tendon reflexes, then progressive alteration of proprioreception, cerebellar syndrome and muscular atrophy of both neurogenic and myogenic origin (Wichman *et al.* 1985; Higuchi *et al.* 1993; Berriot-Varoqueaux *et al.* 2000). This atrophy leads to progressive impaired mobility. The first ophthalmological signs in ABL are alterations in night and colour vision, then a decrease in visual acuity, which can deteriorate to blindness (Berriot-Varoqueaux *et al.* 2000). Some patients exhibit moderate to severe anaemia due to haemolysis and shortening of erythrocyte half-life (Simon and Ways 1964). Abnormalities in coagulation have also been observed (Caballero and Buchanan 1980). At least five cases of rapidly evolving cardiac insufficiency leading to premature death have been reported (e.g., (Dische and Porro 1970)).

1.3.2 Treatment

The neurological symptoms of ABL are very similar to those in monkeys (Fitch and Dinning 1963) and rats (Machlin *et al.* 1977; Towfighi 1981) with vitamin E deficiency. Deficiency of vitamins A and K is believed to contribute to the visual disturbances and occasional blood coagulation problems (Caballero and Buchanan 1980; Bieri *et al.* 1984). Therefore, patients are typically managed by restricting dietary uptake of long-chain fatty acids, and administering supplements of essential fatty acids and vitamins A, E and K. Early diagnosis and treatment of ABL is needed to stall progression of retinal and neurological symptoms (Berriot-Varoqueaux *et al.* 2000).

1.3.3 Genetics

Wetterau *et al.* (1992) reported that a defect in the microsomal triglyceride transfer protein (MTP) might be a proximal cause of ABL. MTP is a dimeric lipid transfer protein consisting of the multifunctional protein disulfide isomerase (PDI) and a unique 97-kDa subunit. Intestinal biopsies of ABL patients revealed absence of the large subunit, although PDI was detected. Triglyceride transfer activity was undetectable. The primary involvement of MTP in ABL was confirmed later on by the cloning of the gene encoding the large subunit, *MTP*, and the identification of *MTP* mutations in patients with ABL (Sharp *et al.* 1993). Twenty-three *MTP* mutations associated with ABL have now been reported. These were reviewed by Rampoldi *et al.* (2002), who observed that the mutations seem to cluster in the middle and C-terminal domains of the protein. Four missense mutations have been identified - one of these, S590I, seems to be associated with a milder disease course (Wang and Hegele 2000; Al-Shali *et al.* 2003).

1.3.4 Function of MTP

MTP is expressed primarily in liver and intestine, although it is also observed in heart, kidney and testis. MTP has extensive amino-acid homology with vitellogenin, a transport and storage lipoprotein found in egg-laying invertebrates (Wahli 1988). A model of MTP by Mann *et al.*, based on this similarity, predicts an N-terminal β-barrel domain, followed by a 300-aa α-helical domain, responsible for MTP interaction with PDI (Mann *et al.* 1999). *In vitro* assays have established that MTP binds and shuttles individual lipid molecules between membranes (Atzel and Wetterau 1994). The following model of apolipoprotein synthesis has been proposed (Olofsson *et al.* 1999). Addition of lipid to ApoB begins cotranslationally in the

endoplasmic reticulum. A small ApoB-containing lipoprotein particle is formed in the first step of lipoprotein assembly. Additional triglyceride is added in the second step assembly, probably by fusion of ApoB particle with a preformed triglyceride droplet. Cell-free binding assays, co-immunoprecipation and yeast two-hybrid studies (reviewed in (Gordon and Jamil 2000)) suggest that initiation of lipidation of nascent apoB may occur through a direct association with MTP. This early lipidation may be required to allow the nascent polypeptide to fold properly and therefore avoid targeting by Hsp70 for proteasome degradation. Experiments with transgenic animals support a primary role for MTP in ApoB lipid loading. Homozygous MTP knockout mice die in midgestation, suggesting a rather different role of MTP in rodent embryological development (Raabe *et al.* 1998), but conditional knockout of hepatic MTP leads to complete loss of plasma ApoB100 (Chang *et al.* 1999; Raabe *et al.* 1999).

1.4 Other neuroacanthocytoses: hypobetalipoproteinemia

Familial hypobetalipoproteinemia (HBL, OMIM 107730) is a codominant disorder. Heterozygotes have plasma levels of cholesterol and ApoB below the fifth percentile and are typically asymptomatic with no acanthocytes (Schonfeld 2003), although recent reports reveal hepatic steatosis in a large proportion of heterozygotes (Tarugi and Lonardo 1997; Schonfeld *et al.* 2003). The frequency of HBL heterozygotes is estimated to be 1/500 - 1/1000 in Western populations (Linton *et al.* 1993). Homozygotes have extremely low levels of apoB; clinically they are very variable and severe cases are indistinguishable from ABL, with neuro-ophthalmological complications and acanthocytes (Herbert *et al.* 1983). Vitamin E treatment is also standard for these cases, but, as in ABL, doesn't reverse the acanthocytosis (Hegele and Miskie 2002).

1.4.1 Genetics

Young *et al.* (1987; 1988) demonstrated that mutations in the *APOB* gene on chromosome 2 cause some cases of HBL. Over 40 mutations have now been described (reviewed in (Schonfeld 2003)). Most of the reported mutations are nonsense or frameshift mutations that prevent translation of full-length apoB-100. Seven families with no linkage to the *APOB* locus show evidence of linkage to chromosome 3p21 (Yuan *et al.* 2000; Neuman *et al.* 2002), but other families show linkage to neither locus (Schonfeld 2003) and their genetic lesion is yet to be determined.

1.5 Other syndromes associated with acanthocytosis

1.5.1 Hallervorden-Spatz syndrome

The term 'Hallervorden-Spatz syndrome' (HSS) applies to a spectrum of disorders that share the common features of neurodegeneration and iron accumulation in the brain. A characteristic MRI finding in T2-weighted images is decreased signal intensity from the globus pallidus with a central area of increased signal (the 'eye of the tiger' sign, see Figure 1.1d). Classic HSS is an autosomal recessive disorder that presents in childhood with dystonia, dysarthria and rigidity and leads to mental deterioration and an early death. Some patients show retinal degeneration (Hayflick 2003). Atypical HSS has a later onset and a more slowly progressive course. Mutations in the *PANK2* gene, encoding pantothenate kinase 2, are responsible for all classic HSS and a third of atypical HSS (Zhou *et al.* 2001; Hayflick *et al.* 2003): consequently, this disorder is now known as pantothenate kinase-associated neurodegeneration (PKAN, OMIM 234200). Acanthocytosis was first associated with PKAN by Roth *et al.* (1971), and was reported in eight percent of a large cohort of PKAN patients with classic symptoms (Hayflick *et al.* 2003). Since acanthocytosis is not routinely sought in PKAN, its true prevalence in this disorder may be higher. PKAN mutations have also been found in patients with the eye of the tiger sign and acanthocytosis, retinitis pigmentosa and hypoprebetalipoproteinemia (HARP syndrome) (Ching *et al.* 2002; Houlden *et al.* 2003). Pantothenate kinase is a key regulatory enzyme in the biosynthesis of coenzyme A, which plays a central role in intermediary and fatty acid metabolism (Abiko 1967). Interestingly, the *Drosophila* pantothenate kinase hypomorphic mutant shows impaired neurologic co-ordination (Afshar *et al.* 2001).

1.5.2 Huntington's disease-like 2

Walker *et al.* (2002) described a pedigree with autosomal dominant inheritance of a progressive neurodegenerative disorder comprising chorea, dementia, parkinsonism and acanthocytosis. Based on its similarities to the ChAc phenotype, they called the disorder 'autosomal dominant chorea-acanthocytosis'. The affected individuals in this family were subsequently found to harbour the trinucleotide repeat expansion within the gene *JPH3* that has been associated with Huntington's disease-like 2 (HDL2) (Holmes *et al.* 2001; Walker *et al.* 2003). In light of these findings, the blood of six additional HDL2 patients was screened: and one showed acanthocytes (Walker *et al.* 2003). *JPH3* codes for junctophilin-3, a component of the junctional complex that anchors plasma membrane to endoplasmic reticulum, and that may be involved in the functional coupling between cell-surface voltage sensors and intracellular calcium channels (Nishi *et al.* 2000; Takeshima *et al.* 2000). Junctophilin-3 knockout mice show impaired motor co-ordination (Nishi *et al.* 2002).

1.6 The basis of acanthocytosis

1.6.1 Erythrocyte structure

The red blood cell membrane is composed of a lipid bilayer to which is anchored a filamentous network of proteins that underlie the cytoplasmic side of the membrane (reviewed in (Marchesi *et al.* 1976; Mohandas and Gascard 1999; Gascard and Mohandas 2000); see Figure 1.2a). About 52% of the membrane mass is protein, 40% is lipid and 8% is carbohydrate. The phospholipid bilayer provides physical continuity to the membrane and serves as the matrix in which transmembrane proteins reside. The membrane skeleton consists of several protein components, the most abundant of which is spectrin. Spectrin is a flexible, rod-like molecule. It is a heterodimer, with the subunits intertwined side-to-side. The heterodimers associate head-to-head to form tetramers; the tail ends associate with short oligomers of actin, in a ternary complex with protein 4.1R that is further stabilised by interaction with adducin. This membrane skeleton is principally linked to the lipid bilayer by ankyrin, which associates with the transmembrane band 3 protein and spectrin; and by the binding of glycophorin C in the bilayer to 4.1R. This composite protein structure plays a critical role in regulating cell shape, mechanical properties and structural stability. The ability of the red cell to undergo extensive deformation is essential, not only for its function (its diameter, 8 μm, far exceeds that of the capillaries, 2-3 μm), but also for its survival (Mohandas and Chasis 1993).

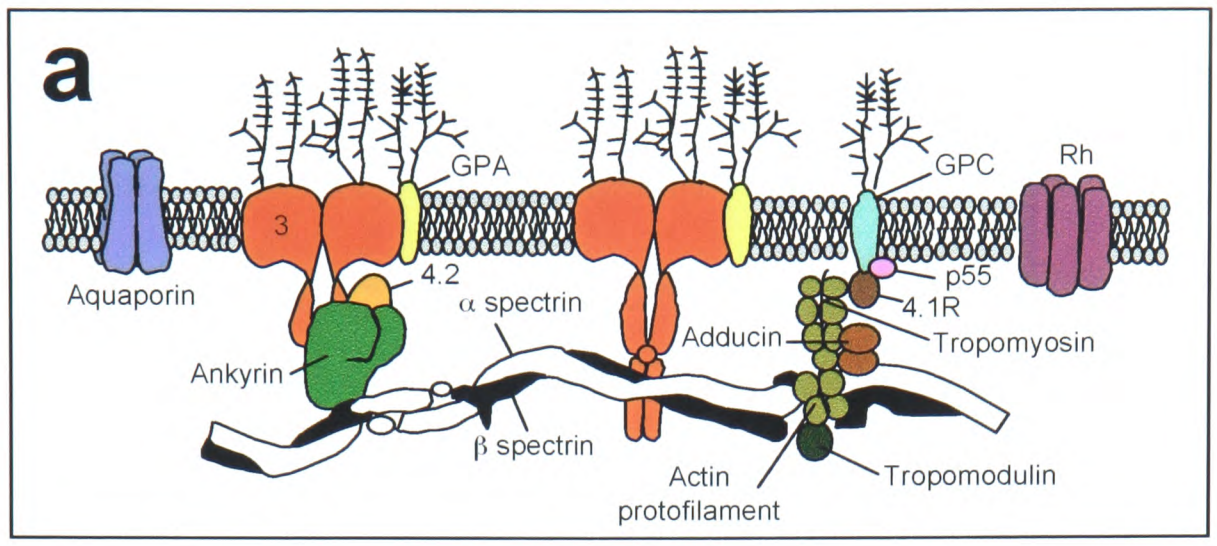

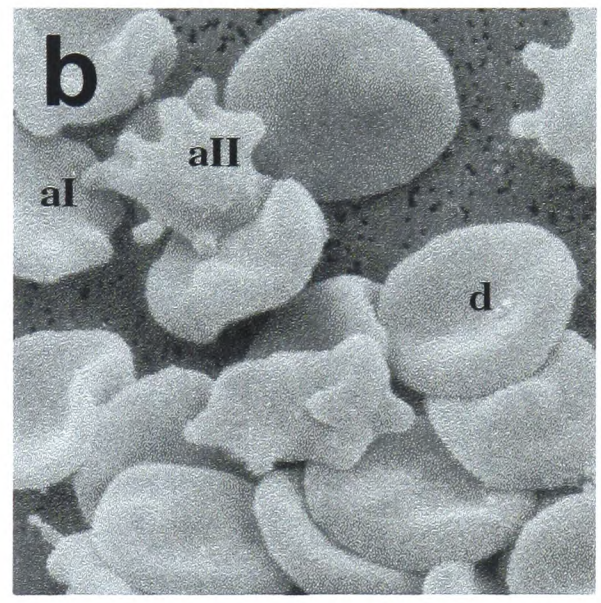

Figure 1.2 - Normal and abnormal erythrocyte structure. a, Organisation of the erythrocyte plasma membrane. Ankyrin and protein 4.1R bind glycophorin C (GPC) and band 3, respectively, to the spectrin/actin cytoskeleton. Additional proteins, including protein 4.2, protein p55, adducin, tropomyosin and tropomodulin, participate in regulation of these interactions *(adapted from Gascard and Mohandas, 2000).* **b, Acanthocytosis.** Scanning electron microscopy of peripheral blood from a ChAc patient reveals many stage I (aI) and stage II (aII) acanthocytes, together with a few morphologically normal discocytes (d) *(taken from Danek* et al., *2004).*

1.6.2 Normal and aberrant erythrocyte morphology

Normal erythrocyte shape is that of a biconcave disk, the discocyte. The bilayer couple hypothesis of red cell shape, proposed by Sheetz and Singer (1974), states that the asymmetric expansion of the outer leaflet leads to spiculated forms such as acanthocytes and echinocytes, while expansion of the inner leaflet leads to formation of stomatocytes (rounded cells with internal invaginations). Acanthocytes are defined as dense, slightly contracted red cells with a number of irregularly spaced, thorny surface protrusions, some with terminal bulbs (Brecher and Bessis 1972); see Figure 1.2b). Echinocytes have more abundant and evenly distributed surface projections that have a much broader base in relation to length. The distinction between acanthocytes and echinocytes is important, as healthy individuals may have up to 3% echinocytosis in a peripheral blood smear (Dacie 1985). In contrast, acanthocytes are not normally found in the blood. Unlike echinocytes, the formation of acanthocytes cannot be readily induced. Studies on ABL patients show that the *in vivo* deformation of the membrane is irreversible and produced after erythrocytes pass into the peripheral circulation (Bassen and Kornzweig 1950).

1.6.3 Detection of acanthocytes

Reported percentages of acanthocytes in affected individuals' blood vary widely. Patients with ABL usually have over 50% acanthocytosis (Berriot-Varoqueaux *et al.* 2000). In contrast, patients with ChAc or McLeod syndrome are usually in the 5-50% range (Hardie *et al.* 1991). There appears to be no correlation between degree of acanthocytosis and severity of symptoms or length of disease course. In addition, some patients with molecularly confirmed ChAc have exhibited no acanthocytes during the disease course (Malandrini *et al.* 1993; Johnson *et al.* 1998), or only many

years after the onset of neurological symptoms (Sorrentino *et al.* 1999). It is not clear how much variability in acanthocytosis can be accounted for by differing laboratory procedures. For highest sensitivity of acanthocyte detection, wet film preparations of blood diluted 1:1 with heparinised saline have been recommended (Feinberg *et al.* 1991). However, routine haematological investigations typically utilise dried blood smears of whole blood, which were not sensitive enough to determine abnormalities in 2/3 patients with confirmed ChAc (Storch *et al.* 2004).

1.6.4 Factors in acanthocyte formation

ChAc blood cells that are initially morphologically normal show a dramatic increase in sensitivity to stresses that induce echinocytic change (Feinberg *et al.* 1991; Terada *et al.* 1999). ChAc red blood cells exhibit an increased density (Clark *et al.* 1989; Terada *et al.* 1999); and reduced deformability (Villegas *et al.* 1987; Clark *et al.* 1989), possibly due to decreased membrane fluidity (Oshima *et al.* 1985; Villegas *et al.* 1987). Since the major components of cell membrane are lipid, protein and carbohydrate, abnormalities in any one of these must be considered. The carbohydrate moiety is not known to be involved in morphology of red cells (Galey *et al.* 1978). Instead, studies on the formation of acanthocytes have focussed on the lipid and protein contributions.

1.6.5 Role of lipids

The outer and inner leaflets of the normal erythrocyte membrane differ in lipid composition (Rothman and Lenard 1977), and the lipid fluidity of the outer leaflet exceeds that of the inner (Cogan and Schachter 1981). In ABL, it is generally believed that an altered lipid composition is responsible for the acanthocytosis. Global amounts

are little changed, but the ratio of sphingomyelin to lecithin is always increased. The phospholipid fatty acid composition is deficient in linolenic and arachidonic acids, and increased in saturated fatty acids (Berriot-Varoqueaux *et al.* 2000). This alteration produces a decrease in fluidity (Cooper 1977), which Flamm and Schachter (1982) demonstrated was restricted to the outer leaflet of the erythrocyte membrane. The imbalance in lipid composition is probably related to the absence of betalipoprotein in the plasma. Normal erythrocytes acquire an acanthocytic form when transfused into ABL patients (Frezal *et al.* 1961). However, *in vitro* incubation of normal red cells with ABL plasma doesn't induce this change (Schwartz *et al.* 1961; Cooper and Gulbrandsen 1971), which suggests the deformation is not due to a simple passive exchange of lipids between erythrocyte and plasma.

In contrast, studies on the lipid contribution to acanthocytosis in ChAc have been more equivocal. Sakai *et al.* (1991) noted a decrease in linolenic acid in ChAc erythrocytes, and abnormal composition of the fatty acids covalently bound to membrane proteins. Clark *et al.* (1989) enriched the acanthocyte population in ChAc blood by density-gradient centrifugation and found an increase in the ratio of sphingomyelin to phospholipids. However, other studies have reported no significant differences in red blood cell membrane lipid or fatty acid composition (Villegas *et al.* 1987; Hardie *et al.* 1991; Olivieri *et al.* 1997). Oshima *et al.* (1985) also found no definite abnormalities in the phosphatide content, or cholesterol/phospholipid ratio, so suggested that distortion of the membrane in ChAc acanthocytes is caused by factors other than the lipid components.

1.6.6 Role of proteins

Proteins are known to play a role in membrane fluidity (Cooper *et al.* 1980). It is therefore possible that a dysfunction of lipid-protein or protein-protein interaction could lead to acanthocytosis. A freeze-fracture study of ChAc erythrocyte membranes showed a marked increase of intramembranous particle-free areas (Ueno *et al.* 1982). This was not replicated by Clarke *et al.* (1989), but recent studies have demonstrated focal changes in the compactness of membrane protein networks in ChAc erythrocytes (Terada *et al.* 1999). Sodium dodecyl sulphate polyacrylamide gel electrophoresis (SDS-PAGE) of freshly prepared erythrocyte membranes shows no gross abnormalities in ChAc protein composition or mobilities (Feinberg *et al.* 1991; Bosman *et al.* 1994). However, SDS-PAGE of older preparations indicate that ankyrin and bands 3 and 4.2 are self-digested faster in ChAc patients than in healthy controls, possibly due to a conformational defect in the junction between spectrin and band 3 (Asano *et al.* 1985). Western blotting also shows increased fragmentation of band 3 in some patients (Bosman *et al.* 1994).

There is additional evidence for the involvement of band 3 in acanthocytic change. Band 3 is a ubiquitous protein. In red blood cells, it mediates the exchange of anions across the membrane (Cabantchik and Rothstein 1974; Lepke *et al.* 1976), maintains acid-base balance and is the binding site for several glycolytic enzymes and haemoglobin (Strapazon and Steck 1977; Salhany and Shaklai 1979; Kliman and Steck 1980). Band 3 undergoes an as-yet uncharacterised initial change during cellular ageing. Following this, band 3 degrades and becomes 'senescent cell antigen'. A physiologic IgG autoantibody binds to this and initiates cellular removal (Kay 1981). Bruce *et al.* (1993) discovered that two siblings showing acanthocytosis but no

other clinical features were homozygous for a P896L mutation in band 3 protein, which increased its apparent electrophoretic mobility and anion transport and decreased the number of ankyrin-binding sites (Kay *et al.* 1994). ChAc erythrocytes show immunologic characteristics of aged band 3, and antibodies to brain anion transporter have been isolated from the sera of ChAc patients (Kay *et al.* 1990a; Kay *et al.* 1990b). Kay *et al.* propose that an alteration in conformation in band 3 in ChAc patients leads both to acanthocytosis in erythrocytes, and premature destruction of neurons in the basal ganglia. How directly or indirectly the band 3 alteration is linked to the primary genetic defect in ChAc is not yet clear.

The structural defect of McLeod syndrome red cells may also lie in the protein composition as there appears to be no abnormality or deficiency in McLeod erythrocyte phospholipids (Galey *et al.* 1978; Kuypers *et al.* 1985), and they show normal transport of phospholipids (Redman *et al.* 1988). Ballas *et al.* (1990) demonstrated that MLS red cells showed decreased deformability, partly due to a reduction in surface area and partly to intrinsic membrane stiffness. The obvious primary protein candidates for structural changes in McLeod erythrocytes are XK and Kell, since they are both transmembrane proteins whose presence is abolished or greatly reduced in this disorder. As previously discussed (section 1.2.3), the absence of Kell cannot be a primary cause for acanthocytosis, since Ko individuals have morphologically normal erythrocytes. Suspicion has therefore rested on the XK protein. However, apart from Kell, XK was not shown to associate with any transmembrane or membrane-associated proteins (Russo *et al.* 1998), and certain individuals in whom membrane XK was undetectable did not show acanthocytosis

(Jung *et al.* 2003). The exact basis for acanthocytic change in MLS, as in ChAc, is therefore still to be elucidated.

1.7 Genetics of ChAc

1.7.1 Mode of inheritance

The mode of transmission of ChAc was originally unclear. A few kindreds with apparent autosomal dominant inheritance have been reported (Levine *et al.* 1968; Kito *et al.* 1980; Marson *et al.* 2003; Saiki *et al.* 2003), but no studies have shown unequivocal evidence of dominant transmission. Ironically, it is possible that the original family reported by Levine *et al.* (1968) was a manifestation of McLeod syndrome with skewed female X-inactivation (R Hardie, personal communication). In any case, the vast majority of familial cases that have been reported show ChAc in only one generation, and there are a relatively high number of cases from consanguineous parents (e.g., (Bird *et al.* 1978; Sakai *et al.* 1981; Yamamoto *et al.* 1982; Sotaniemi 1983; Spitz *et al.* 1985; Serra *et al.* 1986; Alonso *et al.* 1989; Tanaka *et al.* 1998)), implying that the 'classic' ChAc neurological phenotype is an autosomal recessive trait. In contrast, semidominant inheritance of acanthocytosis has been observed in some pedigrees (Sotaniemi 1983; Dubinsky *et al.* 1989; Ueno *et al.* 2001).

1.7.2 CHAC positional cloning

Rubio *et al.* (1997) performed a genome-wide linkage screen using 11 families of diverse geographical origin segregating for ChAc. The disorder was linked in all

families to a 6-centimorgan interval on chromosome 9q21-q22, flanked by the recombinant markers *GATA89A11* and *D9S1843* (see Figure 1.3a). This result was confirmed by homozygosity-by-descent analysis in offspring from consanguineous marriages, and indicated that ChAc is indeed an autosomal recessive disorder. A partial yeast artificial chromosome contig was constructed and 17 transcripts were mapped in the ChAc critical region. Two of these, *GNAQ* and *GNA14*, encode members of the guanine nucleotide-binding protein α-subunit family (Simon *et al.* 1991). *GNAQ* and *GNA14* were screened for mutations in ChAc patients but no significant changes were found (Rubio *et al.* 1999).

We subsequently identified a novel gene, denoted *CHAC*, in this critical region. Direct sequencing of probands from the 11 families used for linkage analysis revealed 16 different *CHAC* mutations likely to disrupt or abolish gene function (Rampoldi *et al.* 2001). Another group who independently identified the gene reported one additional mutation, a deletion of exons 60 and 61, in three families from the same region in Japan (Ueno *et al.* 2001). *CHAC* has recently been renamed *VPS13A*, to acknowledge its similarity with *VPS13/SOI1* in *Saccharomyces cerevisiae* (Velayos-Baeza *et al.* 2004).

1.7.3 Genomic structure of VPS13A

VPS13A is organised in 73 exons, spanning about 240 kilobases of the genome, as shown in Figure 1.3. It has multiple splice forms (Velayos-Baeza *et al.* 2004), but there are two predominant transcripts as determined by expressed sequence tag (EST) analysis and reverse-transcription polymerase-chain reaction (RT-PCR). Transcript 1A contains exons 1 to 68 and 70 to 73, therefore skipping exon 69, which has an in-

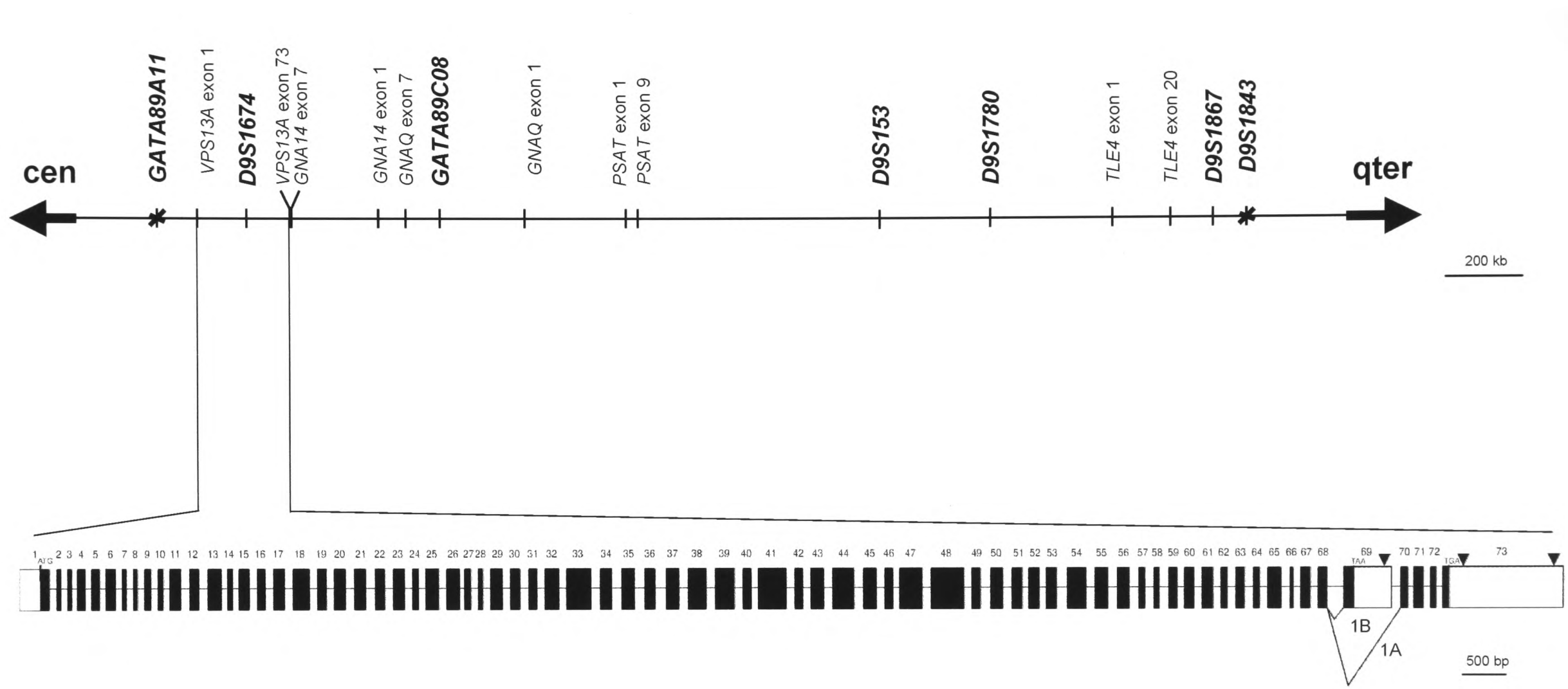

Figure 1.3 - Physical map of the *CHAC* region on chromosome 9q21-q22 and genomic structure of *VPS13A*. a, Schematic of the *CHAC* critical region defined by the recombinant markers (✖) *GATA89A11* and *D9S1843*. The localisation of polymorphic markers (**bold**) and known genes is shown. Positions of markers and genes are derived from the UCSC Genome Browser July 2003 assembly (http://genome.ucsc.edu/cgi-bin/hgGateway). **b, Intron/exon organisation of *VPS13A*.** Exons are indicated as thick bars (white blocks represent 5' and 3' UTRs). Introns are depicted as thin lines and are not scaled. The start ATG is located at position 260 in the transcript sequence. The two major splicing variants 1A (exons 1-68 + 70-73) and 1B (exons 1-69) are shown. The locations of polyadenylation signals in exon 69 and exon 73 are indicated by triangles.

Fig 1.3

frame stop codon. It has a full-length sequence of 11262 bp containing an ORF of 9525 nt and a 3' untranslated region (UTR) sequence of 1477 bp. Analysis of ESTs and cDNA clones suggests the preferential use of one consensus and one alternative polyadenylation signal at positions 10863 and 9715 (from the initiating ATG), respectively. Transcript 1B comprises exons 1-69. It is 10050 bp long, containing an ORF of 9288 nt. This encodes a protein of 3095 aa which lacks the 111 aa encoded by exons 70 to 73 and has 32 new amino acids at the C-terminus. The 500 bp 3' UTR contains one consensus polyadenylation signal at position 9776. The protein encoded by these transcripts is called chorein.

1.8 Chorein

Little is known of chorein's structure or function. Chorein is annotated in the SWISSPROT database as having 10 tetratricopeptide repeats (TPRs). The TPR is a loosely conserved 34-aa motif widespread in evolution, with eight residues conserved in terms of size, hydrophobicity and spacing (Lamb *et al.* 1995; Blatch and Lassle 1999). TPR-containing proteins are involved in a number of processes, including cell-cycle control, stress response, mitochondrial and peroxisomal protein transport and neurogenesis (Goebl and Yanagida 1991): there appears to be no common biochemical function linking these proteins. TPRs are predicted to form two amphipathic helices that can mediate TPR-TPR interactions (Hirano *et al.* 1990; Sikorski *et al.* 1990), although many interactions between TPR and non-TPR-containing proteins have been reported (Blatch and Lassle 1999). Computer searches of chorein's sequence do not identify any other known structural motifs or domains,

and the number of putative transmembrane domains in chorein diverges widely between different prediction programs. Initial clues to chorein's function must therefore come from analysis of its protein homologues.

1.8.1 Chorein orthologues

Chorein seems to belong to a novel gene family, as shown in Figure 1.4. It is very highly conserved (83% identities, 90% positives) in mouse. It has a lower degree of sequence similarity (20-29% identities, 39-48% positives) with five proteins of comparable size: the putative protein products T08G11.1 and CG2093, of *Caenorhabditis elegans* and *Drosophila melanogaster* respectively, the protein Vps13p of *Saccharomyces cerevisiae* and two orthologues in *Schizosaccharomyces pombe*. The sequence similarity significantly increases (up to 49% identities for the *Drosophila* and *C. elegans* proteins) in the amino (N-) and carboxy (C-) termini, where matches can also be found with a VPS13-like protein of *Arabidopsis* and the protein TipC of *Dictyostelium*. As these proteins are of an unusually large size and show strong conservation of the terminal domains, it is likely that they have all descended from a common ancestor.

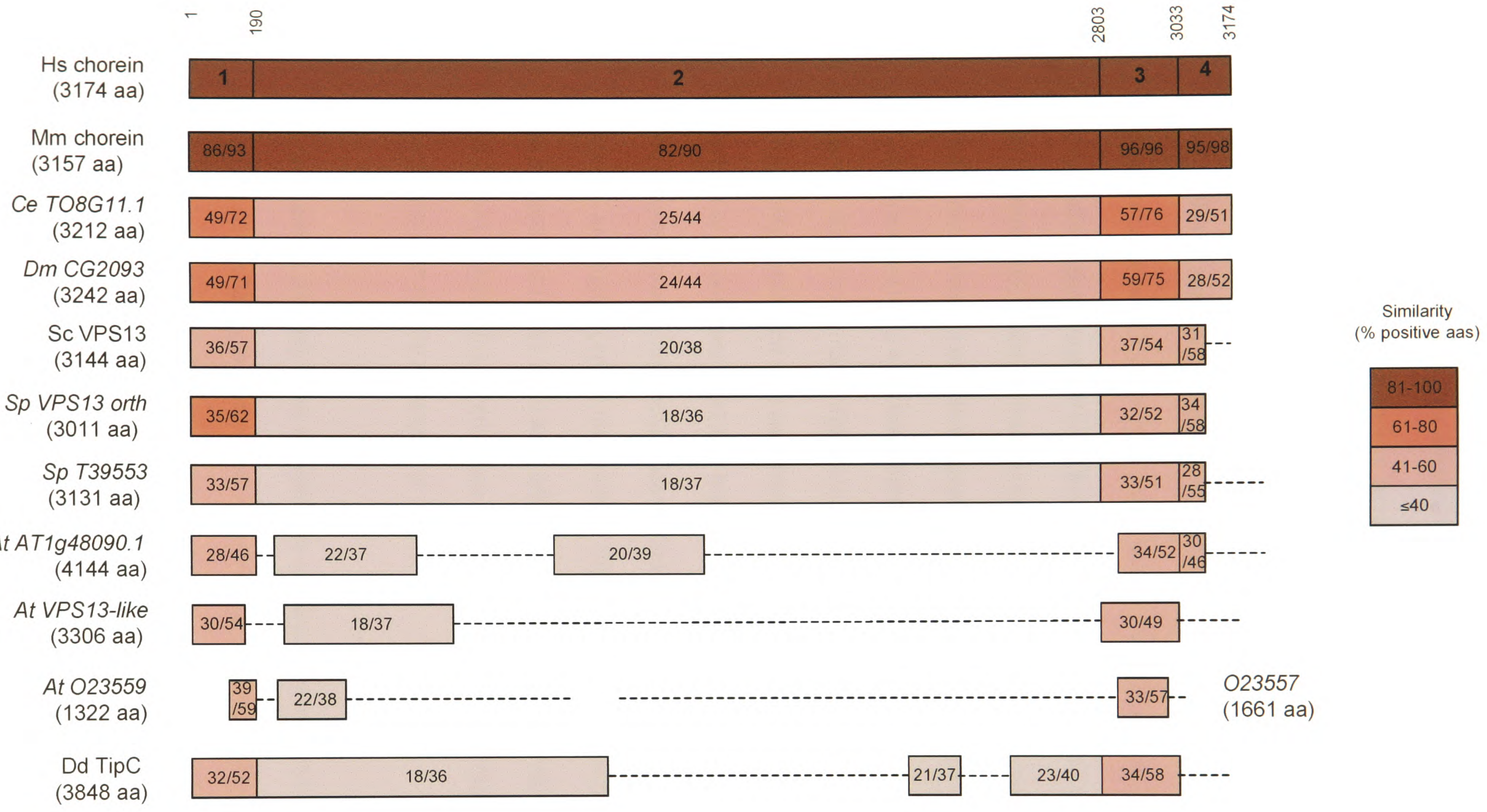

Figure 1.4 - Putative chorein orthologues. Schematic representation of the homology of hypothetical (*italics*) and known proteins with chorein. Chorein regions 1-4 (indicated at top) were separately analysed using the NCBI pairwise blastp program (http://www.ncbi.nlm.nih.gov/blast/bl2seq/bl2.html). Numbers within each region correspond to degree of sequence similarity with chorein. Only those regions with significant similarity are shown. Dashed lines connect regions originating from the same protein; different products believed to comprise part of the same protein, as based on physical map positions, are shown on the same line. 25/44, 25% identical/44% positive amino acids; Hs, *Homo sapiens;* Mm, *Mus musculus*; Ce, *Caenorhabditis elegans;* Dm, *Drosophila melanogaster;* Sc, *Saccharomyces cerevisiae;* Dd, *Dictyostelium discoideum;* Sp, *Schizosaccharomyces pombe;* At, *Arabidopsis thaliana;* orth, orthologue.

Fig 1.4

Of the proteins for which experimental evidence is available, the closest orthologue of chorein is Vps13p in *S. cerevisiae*. In yeast, *vps* genes encode proteins required for proper trafficking from the Golgi to the vacuole (Banta *et al.* 1988; Raymond *et al.* 1992). Vps13p (also reported as Soi1p) is a highly charged, 3144-aa protein (Redding *et al.* 1996). It appears to promote the cycling of the *trans*-Golgi network (TGN) transmembrane proteins Kex2p, Vps10p and Ste13p, between the TGN and the prevacuolar compartment (PVC) (Redding *et al.* 1996; Brickner and Fuller 1997). The PVC corresponds to the multivesicular body/late endosome in mammalian cells. Vps13p antagonises a retention signal at the TGN and, at the PVC, promotes the entry of proteins containing a retrieval signal in retrograde transport vesicles. It appears to exist in a high molecular weight heterooligomeric or homooligomeric complex peripherally associated with membranes, and is present at very low levels in cells. Brickner *et al.* note that Vps13p's highly conserved domains at the N- and C-termini, with a monotonous amino acid composition rich in aliphatic and charged residues in between, are reminiscent of intermediate filament proteins (Fuchs and Weber 1994), and suggest that it may form a cytoskeletal element that physically links the TGN and PVC. Vps13p has subsequently been implicated in the trafficking of insulin via its interaction with Kex2p (Zhang *et al.* 2001).

In nonhumans, the only other significantly similar known protein is TipC. The *tipC* gene encodes a 3848-aa protein that is implicated in *Dictyostelium* development (Stege *et al.* 1999). When exogenous nutrients are depleted, *Dictyostelium* amoebae stop growing and aggregate to produce a multicellular mound. A critical process in the morphogenesis of *Dictyostelium discoideum* is the formation of the tip at the apex of the mound that extends after an extracellular matrix surrounds each aggregate

(Loomis 1982). *tipC* mutants aggregate normally to the mound stage, but instead of forming a single tip from each mound as in wild type, the mutants extend multiple tips (Stege *et al.* 1999). The authors suggest that the *tipC* mutants have some defect in the cell sorting that enables morphogenesis beyond the aggregate stage.

1.8.2 The human VPS13 family

We have recently characterised the structure of three new human genes encoding proteins similar to chorein, located on chromosomes 1p36, 8q22 and 15q21 (Velayos-Baeza *et al.* 2004) (see Figure 1.5). Like chorein, their closest yeast homologue is also Vps13p: we have therefore named the genes *VPS13B* (on chromosome 8q22), *VPS13C* (15q21) and *VPS13D* (1p36). All are large genes with a high number of exons spanning 208 - 864 kilobases of genomic sequence. *VPS13C* is most similar to *VPS13A* and may have arisen by recent gene duplication: intragenic duplication of multiple exons also seems to be a common feature of these genes. Each gene is expressed ubiquitously and has at least two major alternatively spliced forms: interestingly, RT-PCR analysis revealed a brain-specific splice-form expression pattern for all genes except *VPS13A*. Computer analysis predicts that VPS13D contains an ubiquitin-associated (UBA) domain, present in some proteins involved in the ubiquitination pathway; and that a VPS13C splicing isoform contains a lysine-rich motif. Neither domain is predicted in chorein.

VPS13B has recently been reported as *COH1*: eight different mutations leading to a premature termination codon (PTC) and one missense mutation in *COH1* were found in 31 patients with Cohen syndrome (Kolehmainen *et al.* 2003). This disorder presents in childhood: its clinical characteristics include a nonprogressive psychomotor retardation, microcephaly, hypotonia and joint laxity, retinochoroidal dystrophy, myopia, and neutropenia (Kivitie-Kallio and Norio 2001). The limited similarity between the phenotype of Cohen syndrome and ChAc patients is perhaps reflected in the fact that of the four human VPS13 proteins, chorein and VPS13B share the least homology, mainly restricted to the N- and C-termini.

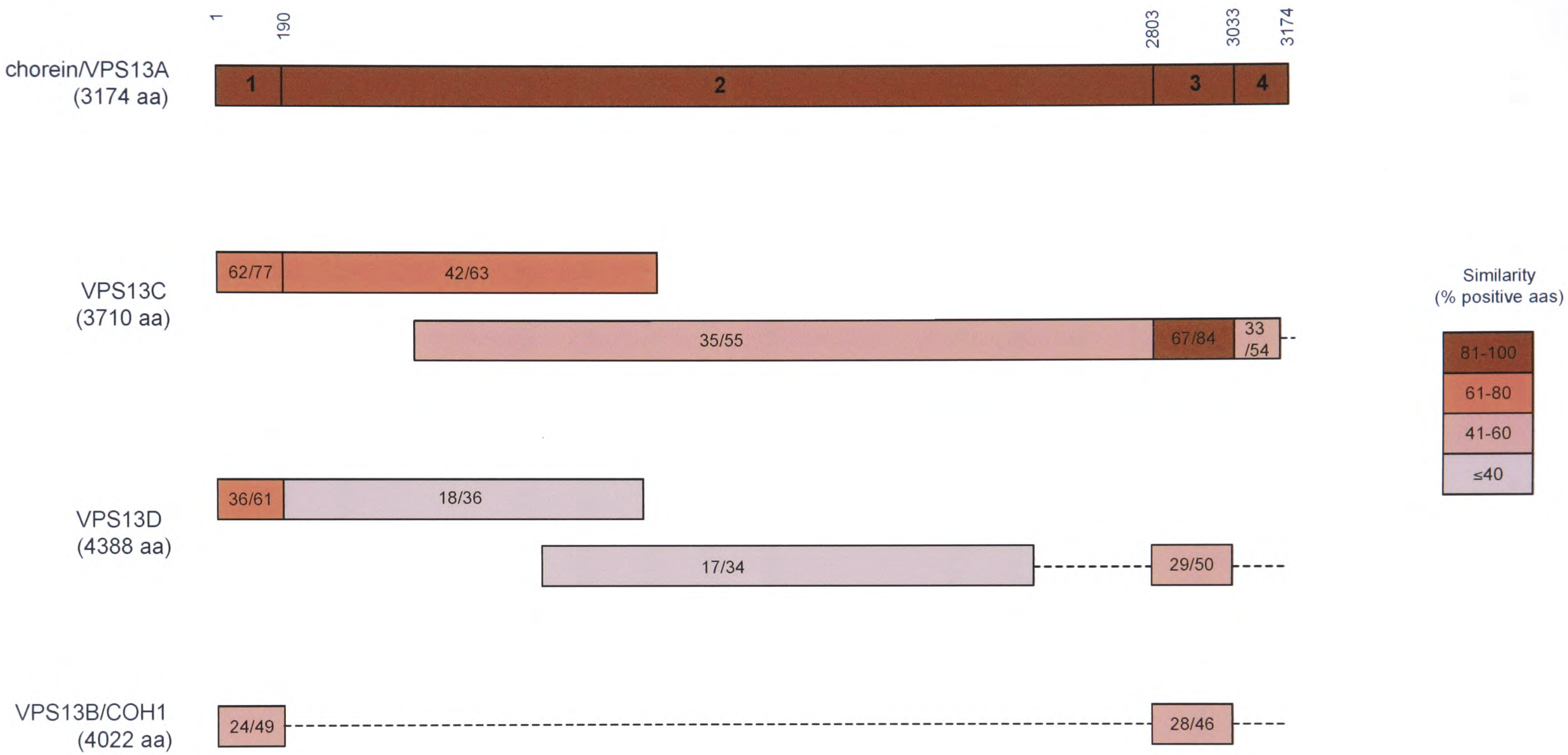

Figure 1.5 - The human VPS13 family. Schematic representation of the homology of human VPS13 proteins with chorein. Chorein regions 1-4 (indicated at top) were separately analysed using the NCBI pairwise blastp program (http://www.ncbi.nlm.nih.gov/blast/bl2seq/bl2.html). Splice variant 1A was used for each protein. Numbers within each region correspond to degree of sequence similarity with chorein. Dashed lines connect regions originating from the same protein. VPS13C and VPS13D show overlapping alignments against region 2 of chorein: this probably reflects intramolecular duplications that have occurred in the evolution of these two proteins. Key: 62/77, 62% identical/77% positive amino acids.

Fig 1.5

1.9 Research strategy

This thesis describes the mutations identified in 11 ChAc families with linkage to chromosome 9q21-22, thus demonstrating that mutations in *VPS13A* are responsible for chorea-acanthocytosis. *VPS13A* encodes a large, evolutionarily conserved protein called chorein. Other than the assumption that chorein plays a similar role to its structural homologue in *Saccharomyces cerevisiae*, little can be said of its potential function or how its absence leads to the ChAc phenotype. As the first step towards addressing these issues and to obtain an idea of the mutational spectrum of this disorder, an additional 72 unrelated probands with ChAc were screened for *VPS13A* mutations (**Chapter 3**).

VPS13A expression was investigated at the mRNA level by Northern blot and RT-PCR analysis. Polyclonal antisera raised against an N-terminal region of the protein were subsequently generated. The antisera were used for immunoblot detection in a range of tissues, in order to investigate the normal distribution of chorein expression, and to determine the effect of various *VPS13A* mutations on chorein expression in ChAc patients (**Chapter 4**).

As the molecular pathways involved in chorein function and pathogenesis of ChAc are completely unknown, a yeast-two hybrid screen was used to search for potential chorein-interacting proteins. In order to verify the interaction and determine its biological significance, co-immunoprecipitation and immunolocalisation studies were performed on a putative chorein-binding partner (**Chapter 5**).

Chapter 2: Materials and Methods

This chapter describes the techniques used in this study. Reagents were purchased from Sigma, unless otherwise stated. All enzymatic reactions were set up on ice, and all other procedures were performed at room temperature, unless otherwise stated. Reagent compositions not detailed in the text are listed in Tables 2.1 - 2.3.

2.1-2.10 NUCLEIC ACID TECHNIQUES

2.1 Preparation of nucleic acids

2.1.1 Extraction of genomic DNA from blood

Genomic DNA (gDNA) was extracted from 5-10 ml peripheral blood using the Nucleon® Genomic DNA Extraction Kit BACC2 (Tepnel Life Sciences, plc), according to manufacturer's instructions. Briefly, erythrocytes were lysed by incubation in a high-sucrose solution. The lymphocytes were pelleted and then lysed in buffer containing 1% sodium dodecyl sulphate (SDS). Samples were deproteinised by addition of sodium perchlorate, before extraction of proteins by treatment with chloroform and Nucleon resin. DNA was precipitated by addition of 2 volumes of cold absolute ethanol. The DNA 'jellyfish' precipitate was removed with an inoculating loop, briefly washed in 70% ethanol and allowed to air dry, before resuspension in 300-600 µl 0.1 x TE, pH 8.0. If no jellyfish was visible, the mixture was kept at -20°C for ≥ 2 h, then subjected to centrifugation at 2200*g* for 30 min. The pellet was washed by addition of 70% ethanol and centrifugation at 2200*g* for 5 min.

The washed pellet was allowed to air dry and was then resuspended in 300 µl 0.1 x TE, pH 8.0.

2.1.2 Extraction of gDNA from lymphoblastoid/fibroblast cell lines

Lymphoblastoid cells were grown to maximal density in a 75-cm^2 tissue culture flask. The cells were then pelleted and washed, as described in section 2.11.4. Fully confluent fibroblasts were trypsinised as described in section 2.11.3 before pelleting. Washed cell pellets were resuspended by vortexing in 5 ml transport buffer containing 0.2 mg/ml proteinase K, and incubated with shaking at 55°C overnight. Deproteinisation and all subsequent steps were performed (with scaled-up volumes) according to the Nucleon BACC2 kit instructions. Due to their high protein content, cell digests were often extracted twice with chloroform before precipitation of DNA.

2.1.3 Preparation of recombinant DNA from bacteria - minipreps

Escherichia coli transformed with high-copy plasmids were cultured overnight in 4 ml Luria Broth (LB). 1 ml was removed for preparation of glycerol stocks (section 2.10.5). The remaining 3 ml were processed using the QIAprep Spin Miniprep kit (QIAGEN), according to manufacturer's instructions. Plasmid DNA was eluted in 50 µl 10 mM Tris.Cl buffer, pH 8.5.

2.1.4 Preparation of recombinant DNA from bacteria - maxipreps

E. coli transformed with yeast two-hybrid cDNA library constructs (section 2.21.4) were cultured overnight in 50 ml Terrific Broth. The overnight culture was processed using the QIAGEN Plasmid Maxi Kit and a QIAGEN-tip 500 column, according to manufacturer's instructions. Plasmid DNA was resuspended in 200 µl TE, pH 8.0.

2.1.5 Extraction of RNA

Total RNA was extracted from cultured cells using TRIzol® Reagent (Invitrogen), following the manufacturer's instructions. RNA from 1-4 x 10^6 cells was resuspended in 60 µl RNase-free water.

2.2 Polymerase chain reaction (PCR)

All PCRs were carried out on a PTC-225 thermal cycler (MJ Research). Primer sequences, and the corresponding $MgCl_2$ concentrations and annealing temperatures (ATs) used, are listed in Appendix 1.

2.2.1 Standard PCR

Standard reactions contained 1x PCR buffer, 1-4 mM $MgCl_2$ (both from Applied Biosystems), 0.2 pmol/µl each forward and reverse primer, 0.2 mM dNTPs and 0.02 U/µl AmpliTaq Gold polymerase (Applied Biosystems). The PCR template was 32-40 ng gDNA, unless otherwise stated. Reactions were typically conducted in a total volume of 50 or 100 µl. Amplification conditions were typically as follows: initial denaturation and polymerase activation step of 95°C for 18 min; 30 cycles of denaturation at 95°C for 30 s, AT for 30 s, elongation at 72°C for 30 s; final elongation at 72°C for 10 min. For amplification of 500-bp to 1-kb fragments, the elongation cycle step was increased to 1 min.

2.2.2 PCRs for denaturing high-performance liquid chromatography analysis

When amplifying gDNA for mutation screening by denaturing high-performance liquid chromatography (DHPLC) (section 2.8.2), care had to taken to reduce PCR error. Reactions were set up as above, except that a proofreading polymerase mix was used (9:1 volume mix of AmpliTaq Gold polymerase: *PfuTurbo* DNA Polymerase (Stratagene)), at 0.2 µl per 50 µl reaction. To reduce unspecific primer annealing, a 'touchdown' program was used. Thermocycling was carried out as follows: 95°C for 15 min; a touchdown of 14 cycles (95°C for 30 s; AT + 7.5°C with –0.5°C per cycle for 30 s; 72°C for 30 s); 25 standard PCR cycles; 72°C for 7 min. Amplification of GC-rich *VPS13A* exon 1 was carried out as above, except that deaza dGTP-dNTP mix was substituted for standard dNTPs, and thermocycling was performed on a GeneAmp® PCR System 9700 (Applied Biosystems).

2.2.3 Long template PCR

Amplification of 1.2-2 kb fragments from 3 µl lymphoblastoid first-strand cDNA (section 2.2.5) was performed using r*Tth* DNA polymerase XL (Applied Biosystems), according to manufacturer's instructions. Thermocycling was carried out as follows: 94°C for 2 min; 34 cycles of 94°C for 15 s, 60°C for 30 s, 72°C for 2 min; 72°C for 10 min. Amplification of 3-6 -kb fragments from 40 ng gDNA was performed using BIO-X-ACT™ Long DNA Polymerase (Bioline Ltd), according to manufacturer's instructions. Thermocycling was carried out as follows: 95°C for 5 min; AT for 1 min; 30 cycles of 68°C for 4-7 min, 95°C for 30 s, AT for 30 s; 68°C for 10 min.

2.2.4 Colony PCR

This technique was used to screen large numbers of bacterial colonies for the construct of interest. Colonies were suspended in 50 µl dH_2O. 5 µl of this suspension was used as template in a standard PCR reaction, scaled down to 25 µl total volume. The remaining colony suspension from a PCR-positive clone was used to inoculate an overnight culture for subsequent miniprep (section 2.1.3).

2.2.5 Reverse-transcription PCR (RT-PCR)

Total RNA (5 µg), diluted in water to 29.5 µl total volume, was denatured at 70°C for 10 min then cooled on ice. First strand cDNA was synthesised by reverse transcription in a 50 µl reaction containing 100 ng random hexanucleotides (Amersham Biosciences), 40 U RNAsine Ribonuclease Inhibitor (Promega), 1 mM dNTPs, 1 x first strand buffer, 10 mM dithiothreitol (DTT) and 200 U Superscript RNAse H Reverse Transcriptase (all from Invitrogen). Reactions were incubated at 37°C for 45 min, and were then stored at -20°C until needed. Standard 25-µl PCRs (section 2.2.1) or long-template PCRs (section 2.2.3) were performed using 2.5 µl RT reaction as template. To analyse tissue distribution of *VPS13A* mRNA, Human Multiple Tissue cDNA (MTC™) Panel 1 (CLONTECH Laboratories, Inc) was used as template - 2 µl were used in a 25-µl PCR.

2.3 Agarose gel electrophoresis

DNA molecules were resolved according to size using standard agarose gel electrophoresis. 2% agarose gels were typically used, but for separation of molecules

greater than 1 kb, 1% gels were used. For restriction analysis of <500-bp fragments, 3-4% gels were used. Agarose was melted in 1 x Tris-acetate EDTA (TAE) buffer (Bio-Rad Laboratories). After cooling to below 50°C, ethidium bromide was added to 0.4 mg/ml. Samples were mixed with agarose loading buffer before being loaded on the gel and subjected to electrophoresis at 110-160 mA. 1Kb PLUS DNA ladder (Invitrogen) was used as size standard. Analytical gels were visualised and photographed using an AlphaImager™ 1220 (Flowgen). Preparative gels were visualised using a UV transilluminator; the DNA fragment of interest was excised and purified as in section 2.5.

2.4 Quantification of DNA and RNA

2.4.1 Spectrophotometric quantification

DNA and RNA were quantified by measuring the optical density at 260 nm (OD_{260}) of appropriate dilutions on a DU 640 Spectrophotometer (Beckman Coulter Bioresearch), or of undiluted samples on the NanoDrop® ND-1000 Spectrophotometer (NanoDrop Technologies, Inc). Concentrations were calculated according to Sambrook *et al.* (1989):

DNA concentration (ng/µl) = OD_{260} x dilution x 50

RNA concentration (ng/µl) = OD_{260} x dilution x 40

2.4.2 Quantification on agarose gel

Estimates of DNA yield from PCRs and post-digest purifications were made after electrophoresis alongside known quantities of *Hin*dIII-digested λ DNA (Invitrogen) and comparison of band intensities.

2.5 PCR product/restriction digest purification

Column purification of all DNA >100 bp from a reaction was achieved using the QIAquick PCR Purification Kit (QIAGEN), according to manufacturer's instructions. If multiple samples were to be purified, the 96-well MultiScreen™ MANU 030 PCR purification plate (Millipore) was used. Samples were added to the plate, which was attached to a vacuum manifold until wells became dry. Samples were eluted by addition of dH_2O to wells, and incubation with shaking for 10 min. DNA from a 50-µl PCR would typically be eluted in 30 µl dH_2O. Purification of specific DNA fragments from agarose gel was performed with the GENECLEAN® SPIN kit (Qbiogene), according to manufacturer's instructions.

2.6 Nucleic acid hybridisation protocols

2.6.1 Southern blot detection

Transfer. Genomic DNA (8 μg) digested with restriction endonuclease was subjected to electrophoresis on a 1% agarose gel. The gel was photographed alongside a ruler to enable accurate sizing of DNA fragments, then incubated in Southern denaturing solution for 40 min. A sheet of 3MM chromatography paper (Whatman International Ltd), saturated in and in contact with denaturing solution, was placed on a glass plate. The gel was then placed upside down on the paper, and Saran wrap was placed around the gel edges to prevent evaporation. Hybond-N+ nylon transfer membrane (Amersham Biosciences) was placed on the gel, followed by three sheets of water-soaked 3MM paper. A stack of paper towels, followed by a glass plate and a 1-kg weight were placed on top, to allow transfer of DNA to the membrane by capillary action. Transfer proceeded overnight; the membrane was then soaked in Southern neutralising solution for 30 min, and in 2x SSC buffer (Invitrogen) for 10 min, before being air dried and baked at 80°C for 2 h.

Probe labelling. cDNA probes were labelled with ^{32}P-dCTP by random priming, using the Megaprime labelling kit (Amersham Biosciences) according to manufacturer's instructions. Labelled probes were purified through a ProbeQuant™ G-50 Micro Column (Amersham Biosciences), by centrifugation at 700*g* for 2 min. The purified probe was denatured at 95°C for 5 min and then cooled on ice.

Hybridisation. Blotted membranes were incubated in 20 ml hybridisation buffer by rotation at 42°C for at least four hours. The labelled probe was then added, and hybridisation proceeded at 42°C overnight.

Washing and detection. Hybridised membranes were washed with 3x SSC, 0.1% SDS for 15 min at 65°C with shaking. The wash was repeated with 2x SSC, 0.1% SDS. Damp membranes were wrapped in Saran wrap and exposed to X-OMAT imaging film (Kodak) at -70°C. After 2-7 days exposure, films were developed using an X150 X-ograph developer (X-ograph Imaging Systems).

Stripping. Residual probe was stripped from hybridised membranes by addition of boiling 0.5% SDS and incubation at room temperature for 3 h with shaking. Membranes were exposed to film to detect efficiency of stripping.

2.6.2 Northern blot detection

A Human Multiple Tissue Northern (MTN®) Blot (CLONTECH Laboratories, Inc) was used for analysis of *VPS13A* mRNA distribution. Radioactive cDNA probes were prepared and the blot was hybridised as above. The hybridised membrane was washed twice in 0.5x SSC, 0.5% SDS for 30 min (once at room temperature, once at 65°C) with shaking. The washed membrane was exposed, developed and stripped as above, except that exposure time was shorter (2 h for *β-actin* probe, 2 days for *VPS13A* probe).

2.7 DNA sequencing analysis

During assembly of plasmid constructs, inserts were fully sequenced by fluorescent dye terminator sequencing prior to further manipulation. At every subsequent cloning step, ligation junctions were sequenced to check integrity. PCR products were also sequenced for mutation detection (section 2.8). Earlier experiments used slab gel electrophoresis on the ABI PRISM 377 DNA sequencer (section 2.7.1); this was later superseded by capillary electrophoresis on the ABI PRISM 3700 DNA Analyser (section 2.7.2) (both instruments from Applied Biosystems). Fluorescent samples were protected from the light as far as possible.

2.7.1 Sequencing on ABI 377

Sequence reactions were performed using the BigDye™ Terminator Cycle Sequencing Ready Reaction Kit (Applied Biosystems). The 20-µl reaction contained 30-90 ng purified PCR product or 200-500 ng plasmid DNA, 4 µl terminator premix, 10 pmol primer and 4 µl sequencing buffer. Thermocycling was as follows: 96°C for 5 min; 30 cycles of 96°C for 10 s, 50°C for 5 s, and 60°C for 4 min. Unincorporated nucleotides were removed by sodium acetate-ethanol precipitation as follows. 0.1 volumes of 3 M sodium acetate, pH 4.6 and 2.5 volumes of cold absolute ethanol were added to each sequencing reaction, which were then incubated on ice for 25 min. The samples were pelleted by centrifugation at 2200*g* for 30 min at 4°C, and pellets were washed by centrifugation for 5 min in room temperature 70% ethanol. Pellets were air dried before being resuspended in 2 µl ABI 377 loading buffer. Samples were denatured at 95°C for 3 min and cooled on ice, before being subjected to electrophoresis on a 4.2% polyacrylamide sequencing gel in 1x Tris-borate EDTA

(TBE) buffer. Sequences were analysed by means of the Sequencing Analysis and Sequence Navigator programs (both from Applied Biosystems).

2.7.2 Sequencing on ABI 3700

The 20-µl sequencing reaction contained 10-40 ng purified PCR product or 150-300 ng plasmid DNA, 4 µl BigDye version 3.1 terminator premix, 10 pmol primer and 2 µl BigDye buffer (Applied Biosystems). Thermocycling was as above (section 2.7.1). To aid purification, 0.1 volumes of 125 mM EDTA were added to samples prior to addition of sodium acetate/ethanol as before (section 2.7.1). Incubation at room temperature for 15 min was followed by centrifugation as before. Sample plates were inverted and briefly spun at 185*g* to remove the supernatant. The pellet wash was performed at 1650*g* for 15 min at 4°C. Air dried pellets were resuspended in 20 µl 50% (v/v) Hi-Di™ formamide (Applied Biosystems) and denatured as above. Denatured samples were stored at 4°C before electrophoresis. Sequences were analysed as above.

2.8 Mutation detection protocols

2.8.1 Strategy

PCR products were generated from gDNA as in section 2.2 and subjected to electrophoresis to check for large insertions/deletions. *XK* exons and flanking intronic sequences were screened for mutations by direct sequencing of PCR products, as in section 2.7. *XK* primers used solely in sequencing reactions are listed in Appendix 1. Most exons of *VPS13A* were analysed by DHPLC, as in section 2.8.2. However, for 11 exons (exons 2, 16, 29, 33, 35, 48, 49, 50, 66, 67 and 72), analysis by DHPLC was not appropriate, either because PCR product yield was low or because the amplicon contained a high frequency polymorphism. These exons were therefore sequenced directly. The presence of each mutation was verified in the proband and any available family members by restriction enzyme analysis (section 2.10.1) or sequencing. The DNA of 50 control individuals was analysed to check for the presence of any missense mutations identified in Wave I (section 3.1). Wave II missense or exonic splice-site mutations (section 3.2) were checked in 192 control individuals (European Collection of Cell Cultures) by restriction enzyme analysis. Where the mutations did not provide a restriction fragment polymorphism, a diagnostic restriction site was introduced by PCR mutagenesis (primer sequences in Appendix 1).

2.8.2 DHPLC analysis

PCR amplification was performed as in section 2.2.2. Amplification products from probands were combined in a 3:1 ratio with the appropriate wild-type homozygous amplicon. To optimise the formation of heteroduplexes, samples were heated to 95°C for 4 min, followed by 42 cycles of 95°C with –1.6°C per cycle for 1 min. The

reannealed samples were stored at -20°C before DHPLC analysis on the WAVE™ DNA Fragment Analysis System (Transgenomic). Samples that showed a variant DHPLC pattern were further analysed by direct sequencing (section 2.7).

2.9 Haplotype analysis

Polymorphic microsatellite markers *GATA89A11*, *D9S1674*, *GATA89CO8*, *D9S153*, *D9S1780* and *D9S1867* flanking *VPS13A* were used in order to define haplotypes in the *CHAC* critical region. Fluorescently labelled primers specific for the markers were used in standard PCR amplification (section 2.2.1), except that 0.8 pmol/μl each primer, 1.28 mM dNTPs and 0.04 U/μl AmpliTaq Gold DNA polymerase were used, in a total reaction volume of 25 μl. PCR product yield was estimated for each marker following agarose gel electrophoresis (section 2.3), and products were diluted in dH_2O and pooled as required. 1.5 μl of dilutions were combined with 0.1 μl GeneScan® 400HD ROX size standard (Applied Biosystems) and 10 μl Hi-Di Formamide, then subjected to capillary electrophoresis on the ABI PRISM 3770. Samples were analysed using the Genotyper program (Applied Biosystems).

2.10 Molecular cloning

Most techniques in this section are based on standard protocols (Sambrook *et al.* 1989).

2.10.1 Restriction digestion

Digests were performed using restriction endonucleases (New England BioLabs, Inc), according to manufacturer's instructions. Enzymes were subsequently heat inactivated at the recommended temperature for 25 min. To verify construct identity in plasmid DNA minipreps (section 2.1.3), 1 µl of miniprep was typically digested in a 30 µl reaction with 2.5-10 U enzyme for 2 h. For mutation confirmation in patient and control PCR amplicons (section 2.8.1), 5 µl of purified PCR product was typically digested with 5-20 U enzyme in a 30 µl reaction overnight. Preparative digests, used in plasmid construct assembly, typically digested 1-5 µg DNA overnight in 50-100 µl reaction volume. Digests were subjected to electrophoresis (section 2.3) and the desired DNA fragment was subsequently excised and purified. If gel purification was not desired, a second digest cleaving only the unwanted fragment was performed for 2 h, prior to column purification (section 2.5).

2.10.2 Modification of restriction fragment ends

DNA fragment ends were occasionally modified after restriction digestion (section 2.10.1) in order to permit correct DNA ligation (section 2.10.3). Samples were subsequently column- or gel purified (section 2.5) before further processing.

Filling-in of 5' overhangs - 44 µl digestion reaction was combined with 5 µl of dNTPs (330 µM) and 1 µl of DNA polymerase I Klenow fragment (Amersham Biosciences, 1 U/µl) and incubated at room temperature for 30 min.

Polishing of 3' overhangs - T4 DNA polymerase was used for this process, since its 3'-5' exonuclease activity is ~1000 times more efficient than that of Klenow fragment. 45 µl digestion reaction was combined with 2.5 µl of dNTPs (2 mM), 1.5 µl dH_2O and 1 µl of T4 DNA polymerase (Invitrogen, 1-8 U/µl) and incubated at 37°C for 15 min. The reaction was stopped by addition of 2.5 µl 0.5 M EDTA.

2.10.3 Ligation

Ligation were typically calculated to combine a 3:1 molar ratio of insert to vector, using the following calculation:

$$\frac{Av \times Si}{Sv} \times R = Ai$$

where: Av = amount of vector (ng); Si = size of insert (kb); Sv = size of vector (kb); R = molar ratio of insert to vector; Ai = amount of insert (ng).

Standard ligations - Restriction-digested (section 2.10.1) vector and insert were purified (section 2.5) and combined in a 10 µl reaction volume containing 1 x ligase buffer and 2.5 U of T4 DNA ligase (both in Rapid DNA Ligation kit, Roche). The

reaction was incubated at room temperature for ≥1 h, and then transformed into competent *E. coli* (section 2.10.4).

Cloning of PCR fragments - To provide a ready source of product for downstream cloning procedures, PCR products were cloned using the pGEM®-T Vector System (Promega), according to manufacturer's instructions. Briefly, 2 µl of PCR product/pGEM-T Vector ligation reaction were heat-shock transformed into competent *E. coli* (section 2.10.4) and recovered in 1 ml SOC medium (Invitrogen). 100 µl of the transformation culture were plated on to LB-ampicillin agar supplemented with 0.5 mM isopropylthio-β-D-galactoside (IPTG) and 80 µg/ml 5-bromo-4-chloro-3-indolyl-β-D-galactopyranoside (X-Gal) and incubated overnight at 37°C. Interruption of the β-galactosidase gene by the PCR product insert allows discrimination between positive (white, β-galactosidase inactive) and negative (blue, β-galactosidase active) colonies.

2.10.4 Transformation of E. coli

Due to the high transformation efficiency of the technique, electroporation was used to introduce 1 µl of yeast plasmid miniprep (section 2.21.7) into electrocompetent DH10B cells (Invitrogen), according to manufacturer's instructions. All other plasmids were introduced into bacteria via heat-shock transformation, as detailed below.

Heat-shock transformation (standard) - 50 µl of chemically competent XL-1 Blue Supercompetent cells (Stratagene) or DH5α cells were combined with 5 µl ligation reaction (section 2.10.3) and incubated on ice for 20 min. Cells were heat-shocked at 42°C for 30 s (DH5α) or 45 s (XL-1 Blue) and then placed on ice for 2 min. The cells were supplemented with 250-450 µl SOC medium, before incubation with shaking at 37°C for 1 h. Aliquots of the culture (1/20 and 1/2 total volume) were subsequently plated on to LB-agar plates containing the appropriate antibiotic and incubated overnight at 37°C.

Quick transformation protocol - For propagation of intact plasmids conferring ampicillin resistance, 5 µl of DH5α cells were combined with 50 ng of miniprep DNA and placed on ice for 5 min. Cells were heat-shocked, cooled on ice and supplemented with SOC medium as above. The ampicillin-resistance gene is rapidly expressed in transformant cells and so no 37°C recovery period is required when transforming intact plasmids. The entire transformant mixture was therefore directly plated on to an LB-ampicillin agar plate and incubated as above.

Transformation of bacterial expression vectors - One Shot® BL21 Star™ (DE3) chemically competent cells (Invitrogen) were used for efficient, high-level expression of recombinant fusion protein, required for production of chorein antigen (section 2.12). They were transformed with 50 ng of intact plasmid DNA according to manufacturer's recommendations. BL21 cells are not recommended for long-term propagation of constructs, so expression vectors were maintained in XL1-Blue cells.

2.10.5 Preparation and revival of glycerol stocks

For long-term storage of plasmid constructs, glycerol stocks of transformant bacteria were prepared. An aliquot of overnight culture (810 µl) was combined with 190 µl sterile 80% glycerol, snap frozen on dry ice and stored at -80°C. Cells were revived by scraping off ~20µl of the frozen mixture and streaking on to an LB-antibiotic agar plate, which was then incubated at 37°C overnight.

Table 2.1 - Composition of reagents used for nucleic acid techniques

Reagent	Composition	Notes[a]
TE buffer, pH x	10 mM Tris.Cl, pH x 1 mm EDTA, pH 8.0	Autoclave
Transport buffer	100 mM NaCl 10 mM Tris.Cl, pH 8.0 25 mM EDTA, pH 8.0 0.5% SDS	Add SDS after autoclaving
Terrific Broth (100 ml)	90 ml Terrific Broth premix 10 ml 10x K salts	Combine under sterile conditions
Terrific Broth premix (500 ml)	6 g bactotryptone 12 g yeast extract 2 ml glycerol	Autoclave
10x K salts (100 ml)	2.31 g KH_2PO_4 12.54 g K_2HPO_4	Autoclave
Deaza-dGTP-dNTP mix	2.5 mM 7-deaza dGTP 2.5 mM dGTP 5 mM dATP 5 mM TTP 5 mM dCTP	Use 2 µl in 50 µl PCR
10x agarose loading buffer	1 mg/ml bromophenol blue 1 mg/ml xylene cyanole FF 30% (v/v) glycerol 1 x TBE	Store at 4°C
Southern denaturing solution	1.5 M NaCl 0.5 M NaOH	
Southern neutralising solution	1.5 M NaCl 0.5 M Tris.Cl, pH 7.5	
Hybridisation buffer	50% formamide 4 x SSC 50 mM Na_2PO_4, pH 7.2 1 mM EDTA 8% dextran sulphate 1% SDS 10x Denhart's solution (Sigma) 100 µg/ml herring sperm DNA 25 µg/ml yeast tRNA	Mix first four reagents at 50°C until dissolved. Add dextran & SDS and stir until dissolved. Cool to 37°C , then add Denhart's, DNA and tRNA. Store at 37°C.
ABI377 loading buffer (5 ml)	1 ml 50 mg/ml blue dextran in 25 mM EDTA 4 ml formamide	Store at 4°C
Sequencing gel (for 30 gels)	324 g urea 93.6 ml 40% acrylamide 19:1 9 g amberlite resin (Applied Biosciences)	Mix to dissolve urea and deionise mixture Filter and add 180 ml 5x TBE Degas for 15 min Store at 4°C
LB-agar (1 l)	20 g LB base (Sigma) 15 g agar (Becton Dickinson)	Autoclave, then cool to <50°C before supplementing with 100 µg/ml ampicillin, 50µg/ml kanamycin, 10µg/ml gentamicin, or 12.5 µg/ml chloramphenicol

[a]: Reagents are stored at room temperature unless otherwise stated

2.11 CELL CULTURE TECHNIQUES

2.11.1 Cell lines

The following human cell lines were used in this study: HeLa (cervical carcinoma, (Scherer and Hoogasian 1954)); MRC-5 SV2 (SV40- transformed foetal lung fibroblast, (Huschtscha and Holliday 1983)); 293T (embryonic kidney fibroblast, transformed with Ad5 DNA, (Graham *et al.* 1977)); H4 (neuroglioma, (Arnstein *et al.* 1974; Day and Ziolkowski 1979)), RD (rhabdomyosarcoma, (McAllister *et al.* 1969)); Hep3B (hepatocarcinoma, (Aden *et al.* 1979; Knowles *et al.* 1980)); and K562 (multipotential myelogenous leukaemia, (Lozzio *et al.* 1981)). Patient and control peripheral blood leucocytes were used to prepare EBV-transformed lymphoblastoid cell lines (European Collection of Cell Cultures). COS-7 (SV40-transformed African green monkey kidney fibroblasts, (Gluzman 1981)) and CHO-KI (Chinese hamster ovary cells, (Puck *et al.* 1958; Kao and Puck 1968)) cell lines were also used. Collaborators (Maria Teresa Dotti, University of Siena, Italy and Saidi Mohiddin, National Heart Lung and Blood Institute, US) kindly provided primary skin fibroblasts from ChAc patients; Natalie Wilson kindly provided some from a healthy control. All cell culture reagents were purchased from Sigma, unless otherwise stated.

2.11.2 Maintenance of cells

Non-adherent cells (lymphoblastoid and K562 cell lines) were grown in RPMI-1640 media supplemented with 10% foetal bovine serum, 100 U/ml penicillin/streptomycin and 2 mM L-glutamine. All other cells were grown in Dulbecco's modified Eagle medium, supplemented as above. Cells were grown within 25-, 75- or 175-cm^2 tissue culture flasks (BD Biosciences) and incubated at 37°C with 5% CO_2.

2.11.3 Harvesting and subculture of adherent cells

When cells were confluent, the medium was removed and phosphate-buffered saline (PBS) was used to wash the cells. Washed cells were lifted from the flask by incubation with Trypsin-versene EDTA for 3 min, followed by brisk agitation. Trypsinised cells were transferred to centrifuge tubes, supplemented with growth medium (which contains a trypsin inhibitor) and subjected to centrifugation at 150*g* for 5 min. The cell pellet was resuspended in an appropriate volume of medium, and cells were counted using a haemocytometer if required for downstream applications (e.g., immunofluorescence (section 2.20) or transfection (section 2.11.6)). A 5 to 10-fold dilution was used to subculture cells.

2.11.4 Harvesting and subculture of non-adherent cells

Cells grown to maximal density in 50 ml growth medium in a 75-cm^2 flask were transferred to a centrifuge tube and pelleted as above. When required, cells were washed by resuspension in PBS and recentrifugation. A 10-fold dilution was used to subculture cells.

2.11.5 Preparation and revival of frozen stocks

Pelleted cells from a 75-cm^2 flask were gently resuspended in 4 ml cold cell freeze mix (RPMI-1640 supplemented with penicillin/streptomycin, 30% foetal bovine serum and 10% dimethyl sulphoxide) and 1-ml aliquots quickly transferred to cryovials. These were wrapped in bubble wrap to prevent rapid freezing, and the package was placed at -80°C overnight. Cryovials were subsequently transferred to liquid nitrogen storage tanks. Cells were revived from frozen stocks by a 1-min

incubation in a 37°C waterbath, followed by resuspension in growth medium. Non-adherent cells were pelleted by centrifugation and resuspended in 10 ml fresh growth medium before transferral to a 25-cm^2 flask. Adherent cells were transferred to a 75- or 175-cm^2 flask and incubated overnight. The medium was replaced the following day.

2.11.6 Transfection of 293T and MRC5-SV2 cells

DNA constructs were transfected into cells by means of GeneJuice™ Transfection Reagent (Novagen, Inc), according to manufacturer's instructions. GeneJuice is a proprietary formulation of polyamines optimised for efficient transport of DNA. For co-immunoprecipitation experiments, 10-cm diameter tissue culture plates were each seeded with 1.5 x 10^6 cells and allowed to settle for 4-16 h. Equimolar amounts of plasmid (corresponding to 5 μg of plasmid pCMVT-TAB2, 5 μg of pcD4-chac2 and 10 μg of pcDFchac8) were transfected in various combinations: each transfection mixture contained 30 μl GeneJuice. For immunofluorescence experiments (section 2.20), a poly-L-lysine-coated 13-mm diameter coverslip was placed in each well of a 24-well tissue culture plate and seeded with 5 x 10^4 cells. Per well, 4.5 μl GeneJuice was combined with 1 μg of pcDFchac8 and/or 0.5 μg of pCMV-TAB2 and transfected as above. Cells were processed 36-48 h post-transfection.

2.12-2.20 PROTEIN TECHNIQUES

2.12 Preparation of recombinant antigen

2.12.1 Expression of recombinant protein in bacterial cultures

A colony of BL21-Star (DE3) transformant bacteria (section 2.10.4) was inoculated into 5-10 ml LB-ampicillin and incubated with shaking at 37°C overnight. This starter culture was then diluted 1/10 in LB-ampicillin and incubated as before until bacterial growth reached log phase (measured as OD_{600} of 0.6 - 0.8), usually after ~90 min. Aliquots of the culture were either supplemented with 0.1 mM IPTG to induce protein expression, or left without supplementation. Induction was allowed to proceed at a variety of temperatures and lengths of time to determine optimal protein expression conditions, as described in sections 4.2.1-4.2.3. Aliquots were removed at various time points - 100 µl of whole culture were stored at 4°C until required for standard PAGE (section 2.15.1), while 400 µl were fractionated as below. For large-scale preparation of recombinant protein, starter cultures were scaled up to 100 ml.

2.12.2 Fractionation of bacterial cell lysates

Aliquots of a log phase culture (section 2.12.1) were spun at 2200*g* for 10 min and cell pellets were resuspended in 50 µl pellet solubilisation buffer. Cell suspensions were sonicated in an FB11002 sonicating waterbath (Fisher Scientific) for 5 min, and then subjected to centrifugation as before. The supernatant (soluble fraction) was transferred to a new tube; the pellet (insoluble fraction) was resuspended in 50 µl pellet solubilisation buffer. Both fractions were stored at 4°C until analysis by standard PAGE (section 2.15.1) and Coomassie staining (section 2.16).

2.12.3 Solubilisation of glutathione-S-transferase (GST)-chor1

Solubilisation of recombinant fusion protein by addition of the sodium salt of the alkyl anionic detergent N-laurylsarcosine (sarkosyl) was performed after the method of Frangioni and Neel (1993). A 500-ml log phase bacterial culture was pelleted by centrifugation at 3000*g* for 10 min at 4°C. The pellet was washed by resuspension in 25 ml ice-cold PBS and centrifugation as before. The washed pellet was resuspended in 12 ml ice-cold sodium-Tris-EDTA (STE) and digested with 100 μg/ml of lysozyme for 15 min on ice. To enhance subsequent GST binding to glutathione (section 2.12.4), DTT was added to 10 mM; 10% sarkosyl solution in STE was then added to 1.5% final concentration. After a 1-min sonication in an ice bath, the mixture containing solubilised fusion protein was subjected to centrifugation in a 40-ml round-bottomed tube at 27000*g*, 4°C for 40 min. The supernatant was passed through a 0.45-μm syringe filter and transferred to a 50-ml centrifuge tube, where 10% Triton X-100 and STE were added to give a final concentration of 2% Triton X-100 in 25 ml total volume. This mixture was rocked for 30 min at room temperature to allow sequestration of sarkosyl by Triton X-100, which facilitates efficient GST-glutathione binding. For large-scale solubilisation of GST-chor1, sixteen 500-ml cultures were processed as above, pooling samples prior to addition of Triton X-100 to give eight 50-ml mixtures.

2.12.4 Purification of GST-chor1

Recombinant GST-chor1 fusion protein was purified on glutathione Sepharose beads (Amersham Biosciences) according to a protocol adapted from the manufacturer and Frangioni and Neel (1993).

Small-scale purification - As it proved impossible to purify soluble GST-chor1 in the absence of detergent, multiple small-scale purifications were performed containing various combinations of different detergents and other additives, as detailed in section 4.2.3. A typical small-scale optimisation trial used 1-ml aliquots of Triton-treated GST-chor1 mixture (section 2.12.3) in microcentrifuge columns with 50-µl bed volume of glutathione-agarose (MicroSpin™ GST Purification Module, Amersham Biosciences), after column equilibration according to the manufacturer's recommendations.

Large-scale purification - Once the purification conditions had been optimised, the following scaled-up protocol was used. Four 1.33-ml aliquots of 75% glutathione bead suspension were each transferred to 15-ml centrifuge tubes, and washed by centrifugation in 10 ml STE at 650*g*, 4°C for 2 min. This was followed by a wash with STE supplemented with sarkosyl and DTT (STE-SD). The equilibrated beads were resuspended in 1 ml STE-SD to give a 50% slurry. The eight 50-ml Triton-treated GST-chor1 mixtures (section 2.12.3) were each rocked with 1 ml bead slurry for 1 h at room temperature to allow association of GST-chor1 with the glutathione beads. Pairs of tubes containing bead-protein mixture were pooled and passed through an empty PD-10 column (Amersham Biosciences), thus generating four fusion protein-bound columns, each with a 1-ml bed volume. Each column was washed with 400 ml STE-SD, and the washed beads from each column were resuspended in 1 ml STE-SD and pooled to a 15-ml tube. A thrombin recognition site located between GST and chor1 allowed release of the chorein moiety from the glutathione beads - 160 U thrombin protease (Amersham Biosciences) were added and the suspension was

rocked overnight at room temperature. The following day, the suspension was transferred to a new PD-10 column and the 4-ml eluate was collected (eluate 1). Three more eluates were collected (eluate 2, 4 ml; eluate 3, 2 ml; eluate 4, 2 ml) by allowing the appropriate volume of STE-SD to pass though the column. The beads were finally resuspended in 4 ml STE-SD and aliquots of the eluates and beads were subjected to electrophoresis to assess purity and estimate yield of chor1 antigen by comparison with bovine serum albumin standards, as shown in Figure 4.3c.

2.12.5 Antigen concentration and immunisation

Eluates 1 and 2 were pooled and concentrated in a Vivaspin 6 centrifugal concentrator column with a 10-kDa exclusion filter (Vivascience AG), according to manufacturer's recommendations. The 0.5-ml sample was transferred to a microfuge tube; the column was then washed out with 0.5 ml STE-SD, which was added to the sample. The total protein concentration of the purified chor1 antigen was measured using the bicinchonic acid method (BCA protein assay kit, Pierce), according to manufacturer's instructions. Several 40-µl aliquots (~160 µg protein) were made and stored at -80°C until required. Immunisation of rabbits SK274 and SK275 with chor1 was performed by Eurogentec Bel SA (Herstal, Belgium); the serum collected 87 days post-immunisation was designated anti-chor1.

2.13 Protein sample preparation

2.13.1 Yeast cell lysate preparation

Yeast cultures were grown to log phase ($OD_{600} \approx 0.4$-0.5) and 5 ml were pelleted by centrifugation at 970*g* for 5 min. Cell pellets were washed by resuspension in 1.5 ml dH_20 and centrifugation at 6000*g* for 30 s. Washed pellets were resuspended in 2 volumes of ice-cold yeast cell lysis buffer. To shear the cells, 2 pellet volumes of sterile acid-washed 710-1180 -μm diameter glass beads were added and the mixture was vortexed for three bursts of 30 s, and then sonicated in an ice bath for 5 min. Samples were denatured for 5 min at 100°C and spun at 16000*g* for 1 min. The supernatant was transferred to a new tube and subjected to standard PAGE (section 2.15.1) and Western blotting (section 2.17).

2.13.2 Mammalian cell lysate preparation

Cells were harvested and pelleted as in sections 2.11.3 - 2.11.4. Cell pellets were washed with ice-cold PBS then lysed in 10 pellet volumes of ice-cold mammalian cell lysis buffer. After 20 min incubation on ice, lysates were clarified by centrifugation at 16000*g* at 4°C for 20 min. The supernatant (soluble fraction) was transferred to a new tube. If required, the pellet (insoluble fraction) was resuspended in 100 μl lysis buffer. Protein concentrations were measured using the BCA assay as in section 2.12.5. The OD_{562} of the samples was measured on a SpectraMAX 190 plate reader (Molecular Devices). Fractions were stored at -20°C until required.

2.13.3 Erythrocyte membrane preparation

Erythrocyte membranes were prepared after the method of Dodge *et al.* (1963). However, to enable batch processing of patient blood, the protocol was modified to utilise blood samples frozen at -20°C. Whole blood was thawed at room temperature and 2.5 ml were added to 10 ml of ice-cold erythrocyte wash solution in a 15 ml centrifuge tube. The mixture was spun at 3400*g*, 4°C for 10 min and all but the bottom 2 ml was removed by pipetting. The remaining mixture was split into two 1.5 ml microcentrifuge tubes and spun at 16000*g*, 4°C for 5 min. All but 250 µl of the supernatant was removed, taking care not to disturb the loose pellet. Most erythrocytes were already lysed by the freeze-thawing, but any intact cells were now lysed by trituration in 1 ml of a hypotonic erythrocyte lysis solution. This was followed by centrifugation at 16000*g*, 4°C for 5 minutes. The loose pellet of membranes was washed multiple times in 1 ml erythrocyte lysis solution followed by centrifugation as above, until it could be clearly distinguished from a solid pellet of clotted material. The two loose pellets from each original sample were pooled and transferred to a fresh tube. Washing in erythrocyte lysis solution proceeded as above, until the supernatant remained colourless. Membranes were stored at -20°C until required. Membrane yield was presumably dependent on initial erythrocyte count and varied from 100-200 µl: 2.5 µl of this were combined with 4 µl dH_2O and prepared for electrophoresis (section 2.15) and Western blotting (section 2.17).

2.14 Dot blotting

Three dilutions of purified chor1 antigen (section 2.12.5; 25, 50, 100 ng/μl) were prepared and 2 μl of each were spotted on to Hybond ECL Nitrocellulose Membrane (Amersham Biosciences). The membrane was dried at 60°C for 5 min and then cooled, prior to immunodetection as in section 2.17.2.

2.15 SDS-polyacrylamide gel electrophoresis (SDS-PAGE)

Standard PAGE was initially used for all applications. However, we discovered that even on 5% polyacrylamide gels full-length chorein could not be detected, and so gradient PAGE was employed whenever this was necessary. Rainbow™ coloured protein molecular weight markers (Amersham Biosciences) were used as size standard. After SDS-PAGE, proteins were either stained with Coomassie blue (section 2.16) or detected by Western blot analysis (section 2.17).

2.15.1 Standard PAGE

Protein samples were mixed with PAGE sample buffer and denatured at 100°C for 10 min. The denatured samples were subjected to electrophoresis in 1x PAGE running buffer on 10% or 12.5% polyacrylamide gels in the XCell Surelock™ Mini-Cell system (Invitrogen). To improve separation of proteins, gels were cast with a ~5 mm top layer of stacking gel. Electrophoresis proceeded at 80 V for 50 min, then at 120 V until the dye front had passed through the gel.

2.15.2 Gradient PAGE

All products were purchased from Invitrogen. Protein samples were mixed with NuPAGE™ LDS Sample Buffer and Sample Reducing Agent and incubated at 70°C for 10 min. Samples were then subjected to electrophoresis on precast NuPAGE Novex Tris-acetate gels (3-8% polyacrylamide gradient), under denaturing and reducing conditions. Electrophoresis proceeded at 150 V for 80-90 min.

2.16 Coomassie staining

Polyacrylamide gels were gently agitated in Coomassie blue stain for 1 h, then agitated in multiple changes of Coomassie destain until protein bands were clearly visible. Gels were placed on 3MM Whatman paper and dried in a 583 Gel Dryer (Bio-Rad Laboratories) for 40 min at 80°C.

2.17 Western blot analysis

2.17.1 Transfer of proteins

The XCell II™ Blot Module (Invitrogen) was used for electrophoretic transfer of proteins. Proteins on standard polyacrylamide gels were transferred for 1 h at 26 V to nitrocellulose membranes, in 1x Western transfer buffer. Proteins on gradient gels were transferred according to manufacturer's instructions, on to Invitrolon™ polyvinylidene difluoride membranes (Invitrogen). To check equal loading of erythrocyte membrane preparations (section 2.13.3), blots were agitated for 15 min in 0.1% Ponceau S solution (Sigma), followed by brief destaining in dH_2O until protein

bands were clearly visible. Blots were subsequently destained completely in 1x Tris-buffered saline with Tween-20 (TBS-T) before downstream processing.

2.17.2 Immunodetection

All incubation steps were performed with agitation to enable even distribution of reagent. To reduce background signal, blots were blocked overnight at 4°C in 5% powdered non-fat milk dissolved in 1x TBS-T. The following day, blots were incubated in primary antibody diluted in 1% milk in TBS-T for 1 h at room temperature. Primary antibodies used were: rabbit anti-chor1 (section 2.12.5, 1:5000 dilution); rabbit anti-myc (Invitrogen, 1:500); rabbit anti-FLAG (Sigma, 1:2000); mouse anti-early endosome antigen 1 (Transduction Laboratories, 1:5000); mouse anti-myc (ICRF, 1:2000); mouse anti-T7 (Novagen, Inc, 1:10000); and mouse anti-GAL4 DB (Santa Cruz Biotechnology, Inc, 1:200). Blots were subsequently washed by three 20-min incubations in TBS-T, and then incubated with horseradish peroxidase-conjugated goat anti-mouse or anti-rabbit secondary antibodies (1/5000 dilution, Bio-Rad Laboratories), as for the primary incubation. Blots were washed as before, then proteins were visualised using the Enhanced Chemiluminescent (ECL) plus Western Blotting Detection System (Amersham), according to manufacturer's instructions. If required for reprobing, blots were stripped according to the ECL instructions and stored at 4°C in TBS-T until required.

2.18 Antibody purification and processing

Anti-chor1 antibodies were purified from antiserum according to the following protocol. To avoid degradation of antibodies, all reagents and procedures were at 4°C unless otherwise stated.

2.18.1 Column preparation

NHS-activated Sepharose 4 Fast Flow bead suspension (Amersham Biosciences, 1 ml) was briefly spun at 620*g*. The supernatant was removed by decanting and beads were washed twice by brief centrifugation in 10 ml 5 mM HCl. The acidified beads were tumbled overnight in a 2-ml microcentrifuge tube with ~1.5 mg purified chor1 antigen (section 2.12.5). The following day, beads were spun for 5 min at 700*g*, transferred to a 15-ml tube, washed twice by brief centrifugation in 10 ml STE-S and incubated on ice for 2 h in 100 mM Tris.Cl, pH 8.0. The resin was then washed sequentially: in 10 ml of 100 mM Tris.Cl, 500 mM NaCl; then 10 ml of 100 mM sodium acetate, pH 4.0, 500 mM NaCl. This sequential wash was repeated three times and followed by two washes in PBS: the beads were then transferred to a PD-10 column and kept in PBS until required. For long-term storage of the resin, 0.1% Na azide and 20% ethanol in PBS were used.

2.18.2 Serum treatment

10 ml anti-chor1 serum (section 2.12.5) was dialysed against five changes of 1 l PBS over a period of 24 h. The dialysed serum was passed through a 0.2 μm syringe filter and tumbled with the drained antigen-conjugated beads overnight. The column was drained the following day, and 3-ml washes of PBS were passed through until no

excess protein was found in the wash, as determined by OD_{280} measurement (~5-6 washes). Column-bound antibodies were eluted with 2-ml fractions of 100 mM glycine, pH 3.0 and immediately neutralised with 50 µl 1 M Tris, pH 9.0. This was repeated until little protein was found in the eluate, measured as above (6 elutions). Eluates were pooled as appropriate after Coomassie analysis (section 2.16), supplemented with 0.1% Na azide and adjusted to pH 7.4, before aliquoting and storage at -20°C.

2.18.3 Antibody depletion assay

For antibody depletion experiments, the chor1 antigen-conjugated Sepharose column used in antibody purification (section 2.18.1) was employed. Anti-chor1 antiserum was diluted 1/2500 in TBS. Half was passed three times through the column, while half was left untreated. Both serum preparations were subsequently adjusted to the appropriate dilution for use in Western blotting (section 2.17).

2.19 Co-immunoprecipitation

Per immunoprecipitation (IP), 6 µg *(6 µl MαT7)* of primary antibody were combined with 10 µl Protein G Sepharose™ 4 Fast Flow beads (Amersham Biosciences) and a total of 250 µl IP buffer in a microcentrifuge tube and tumbled for 2 h at room temperature, to allow formation of the antibody-bead complex. The antibody-bead complex was washed five times by a 5-s centrifugation at 16000*g* in 500 µl IP buffer and kept on ice until required. Cell lysates were prepared as in section 2.13.2 (but using IP buffer for cell lysis) and tumbled with 20 µl protein G at 4°C for 1 h. This mixture was then subjected to centrifugation at 16000*g* for 5 min to pellet unspecific protein G-binding proteins. The supernatant was combined with washed antibody-bead complex and tumbled at 4°C overnight to allow precipitation of antibody-bound protein. The beads were then washed five times in 500 µl IP buffer and resuspended in PAGE sample buffer. Samples were denatured and loaded on to duplicate acrylamide gels for subsequent electrophoresis (section 2.15) and Western blotting (section 2.17).

2.20 Immunofluorescence (IF)

MRC5-SV2 and 293T cells grown on 13-mm coverslips in a 24-well plate (section 2.11.6) were processed for indirect immunofluorescence as follows. Cells were washed with 1 ml PBS (prewarmed to 37°C to avoid dislodging of loosely-adhered 293T cells) and then inverted to remove the wash. Cells were fixed with 0.5 ml of room-temperature 4% paraformaldehyde in PBS, or 0.5 ml of ice-cold methanol. Paraformaldehyde fixation retains the native structure of the proteins, while methanol denatures them, thus enabling presentation of different epitopes for antibody recognition. Fixation proceeded at room temperature for 10 min, followed by four washes in 0.6 ml IF wash solution. To reduce background signal, fixed cells were incubated in IF block solution for 30 min at room temperature, prior to incubation for 1 h in primary antibody. Primary antibodies used were rabbit anti-chor1 (section 2.12.5; 1:1000 dilution in 200 µl IF block), rabbit anti-FLAG (1:500) and mouse anti-T7 (1:500). Cells were washed five times with IF wash and then incubated with fluorescent dye-conjugated secondary antibody as before, but kept in the dark. Secondary antibodies used were Alexa Fluor® 594-conjugated goat anti-rabbit (red) and Alexa Fluor 488-conjugated goat anti-mouse (green) (both from Molecular Probes, 1:500 dilution). Cells were washed as before, then coverslips were removed from the wash and mounted on to a microscope slide with ~10 µl Fluoromount-G (Southern Biotechnology Associates, Inc). Slides were stored at 4°C, before examination within 24 h under the MRC 1024 confocal microscope system using Lasersharp 2000 software (both from Bio-Rad Laboratories).

Table 2.2 - Composition of reagents used for protein techniques

Reagent	Composition	Notes[a]
Pellet solubilisation buffer	1x PBS 1% Triton X-100	Store at 4°C Add 1x protease inhibitor cocktail (Sigma) and 1 mM Phenyl methyl sulphonyl fluoride (PMSF) immediately before use
STE	10 mM Tris.Cl, pH 8.0 1 mM EDTA 150 mM NaCl	
STE-SD	1x STE 0.1% sarkosyl 1 mM DTT	Sterile filter Make fresh each time
Yeast cell lysis buffer	2.5x PAGE sample buffer	Add 1 mM PMSF immediately before use
Mammalian cell lysis buffer	50 mM Tris.Cl, pH 8.0 150 mM NaCl 1% Triton X-100	Store at 4°C Add 1x protease inhibitor cocktail immediately before use
Erythrocyte wash solution	5 mM Na_2HPO_4, pH 8.0 0.9 % NaCl	Store at 4°C Add 1x protease inhibitor cocktail immediately before use
Erythrocyte lysis solution	5 mM Na_2HPO_4, pH 8.0	Store at 4°C Add 1x protease inhibitor cocktail immediately before use
5x PAGE sample buffer	10% (w/v) SDS 50% (v/v) glycerol 25% (v/v) β-mercaptoethanol 250 mM Tris.Cl, pH 6.8 0.1 mg/ml bromophenol blue	Freeze in aliquots at -20°C for long term storage
10x PAGE running buffer	250 mM Tris 2 M glycine 1% (w/v) SDS	Don't adjust pH
x% polyacrylamide gel	X% 37.5:1 acrylamide 1 x separating buffer	Make fresh each time Add 150 µl 10% (w/v) ammonium persulphate and 15 µl TEMED to polymerise 16 ml gel
4x separating buffer	1.5 M Tris 0.4% (w/v) SDS	Adjust pH to 8.8
Stacking gel	4% 37.5:1 acrylamide 1x stacking buffer	Make fresh each time Add 100 µl 10% (w/v) ammonium persulphate and 15 µl TEMED to polymerise 10 ml gel
2x stacking buffer	0.5 M Tris 0.2% (w/v) SDS	Adjust pH to 6.8
Coomassie blue stain	2.5 mg/ml Coomassie Brilliant Blue 45% (v/v) ethanol 10% (v/v) acetic acid	Filter before use Protect from light
Coomassie destain	10% (v/v) ethanol 10% (v/v) acetic acid	
10x Western transfer buffer	240 mM Tris 200 mM glycine	Don't adjust pH Add 20% methanol when preparing 1x stock

Table 2.2 - Composition of reagents used for protein techniques

Reagent	Composition	Notes[a]
TBS-T	1x TBS 0.1% Tween-20 (BDH)	
10x TBS	9% (w/v) NaCl 100 mM Tris.Cl, pH 7.5	
10x IP buffer	0.5 M Tris.Cl, pH 7.8 1.5 M NaCl 10 mM EDTA, pH 8.0 1% Triton X-100	Autoclave, store at 4°C Add 0.2% (w/v) iodoacetamide, 1 mM PMSF and 1x protease inhibitor cocktail to 1x stock immediately before use
IF wash solution	1x TBS 0.1% (v/v) Triton X-100 0.02% sodium azide	
IF block solution	1 x TBS 0.1% (v/v) Triton X-100 10 mg/ml fish gelatine	Store at 4°C

[a]: Reagents are stored at room temperature unless otherwise stated

2.21 YEAST TWO-HYBRID PROTOCOLS

The yeast two-hybrid (Y2H) system used in this study was the ProQuest™ Two-Hybrid System with Gateway™ Technology (Invitrogen). This system employs yeast strain MaV203. This strain contains auxotrophic mutations in the *LEU2* and *TRP1* genes to allow selection of bait and prey constructs, respectively. Three reporter genes, *HIS3*, *lacZ* and *URA3* are also engineered with GAL4-activated promoter sequences in this strain. Induction of *HIS3* and *URA3* allow two-hybrid-dependent transcription activation to be monitored by cell growth on plates lacking histidine (-His) or uracil (-Ura), respectively. Induction of *lacZ* results in a blue colour when assayed with X-Gal. Induction of *URA3* also results in conversion of 5-fluoroorotic acid (5FOA) to the toxic compound 5-fluorouracil: growth of cells containing interacting proteins is thus inhibited on 5FOA-supplemented medium. This phenotype is capable of detecting weaker bait-prey interactions than assaying for growth on -Ura medium can detect.

2.21.1 Y2H library screen strategy

VPS13A cDNA fragments were transferred through site-specific recombination (section 2.21.3) into the bait vector pDEST32. Small-scale transformation (section 2.21.5) was used to introduce bait constructs into MaV203. DNA from a human brain cDNA library (section 2.21.4) was introduced into bait-transformed yeast by large-scale transformation (section 2.21.6). Double transformants were assayed for reporter gene activity as recommended in the ProQuest instruction manual (Invitrogen). To account for false positives arising from mutation of the host yeast, clones were further analysed by retransformation (section 2.21.2).

2.21.2 Retransformation strategy

As recombinant DNA extracted from yeast is refractory to molecular analysis, plasmids were extracted from putative positive colonies by miniprep (section 2.21.7), and electroporated into bacteria (section 2.10.4). Prey constructs were obtained after miniprep of transformant bacteria (section 2.1.3), were cotransformed with the relevant bait into fresh yeast by small-scale transformation (section 2.21.5) and were then assayed for reporter gene induction as before.

2.21.3 Assembly of Y2H bait and prey constructs

The strategy for bait and prey construction is illustrated in Figures 5.1 & 5.2. The Gateway™ Technology uses the lambda site-specific recombination system to facilitate transfer of heterologous DNA sequences flanked by *att* sites. BP Clonase™ enzyme mix was used to catalyse recombination of *attB*-flanked PCR product with *attP*-containing donor vector pDONR221 to generate entry vector containing *attL*-flanked insert. Following verification of the entry vector by sequencing (section 2.7), LR Clonase™ enzyme mix was used to catalyse its recombination with *attR*-containing yeast two-hybrid destination vectors pDEST32 and pDEST22. Recombination reactions were transformed into Library Efficiency DH5α competent *E. coli* (Invitrogen) by heat shock (section 2.10.4). Donor and destination vectors contain the *ccdB* gene, which is lost upon recombination. CcdB protein inhibits DNA gyrase and thus growth of sensitive *E. coli* strains, which allows negative selection of unrecombined vectors.

2.21.4 Preparation of Y2H cDNA library

The library used in this study was Human Brain ProQuest Pre-made cDNA Library (Invitrogen), which uses cDNA isolated from a 27-year old male. This library is cloned into pEXP-AD502 prey vector and has an average cDNA insert size of 1.9 kb. Glycerol stocks of DH10B bacteria transformed with the library (~1.3 colony-forming units) were inoculated into 50 ml Terrific Broth and incubated with shaking at 30°C overnight. DNA was subsequently extracted by maxiprep (section 2.1.4).

2.21.5 Small-scale polyethylene glycol/lithium acetate (PEG/LiAc) transformation of yeast

The following technique provides enough competent yeast for seven transformations. Five colonies were suspended in 50 µl dH_2O, plated out on to YPAD-agar and incubated at 30°C overnight. The following day, the lawn of cells was resuspended in 5 ml YPAD and the OD_{600} of this suspension was measured. Enough suspension was used to inoculate 100 ml YPAD to an initial OD_{600} of 0.2. This starter culture was incubated with shaking at 30°C until yeast reached log phase ($OD_{600} \approx$ 0.4-0.5, usually after ~3 h incubation). Yeast cells were harvested by centrifugation at 970*g* for 5 min and the cell pellet was washed by resuspension in 40 ml sterile dH_20 and centrifugation at 240*g* for 10 min. Cells were then washed as before in 20 ml TE/LiAc solution and the cell pellet was adjusted to a final volume of 350 µl with TE/LiAc. The competent cells were stored at room temperature and used within 30 min of preparation. Carrier DNA was prepared by denaturing 10 mg/ml sonicated salmon sperm DNA (Invitrogen) at 100°C for 5 min and cooling on ice. Transformations were performed by combining 50 µl competent cell suspension with 5 µl carrier DNA and 100 ng each plasmid in a screw-cap microfuge tube. PEG/LiAc solution (300 µl) was

added and the sample was inverted to mix. Samples were incubated in a 30°C waterbath for 30 min with occasional mixing, then heat-shock transformed by a 5-min incubation in a 42°C waterbath. Samples were cooled on ice for 2 min and then spun at 6000*g* for 30 s. The pellet of transformed cells was resuspended in 500 µl sterile dH_2O. The suspension was then plated on to SC agar with the appropriate drop-out supplements. For cotransformation of yeast with two constructs, 100 µl of suspension were plated; for transformation with single constructs, 100 µl of a 1/10 dilution were plated. Plates were incubated for 48 h at 30°C before analysis of colonies.

2.21.6 Large-scale PEG/LiAc transformation of yeast

Large-scale transformation of yeast proceeded largely as for small-scale transformation (section 2.21.5), with the following modifications. Three lawn plates of yeast transformed with the relevant bait construct were prepared. Lawns were resuspended in 15 ml SC-Leu and used to inoculate a 350-ml SC-Leu starter culture in a 2-l capacity conical flask. The culture was grown to log phase and cells were pelleted, and then washed in 140 ml sterile dH20, followed by 70 ml TE/LiAc. Competent cells were resuspended to a final volume of 1.6 ml; as a negative control, a 75-µl aliquot was taken into a screw-cap microfuge tube and combined with 5 µl carrier DNA and 775 ng empty prey vector pEXP-AD502, then 450 µl PEG/LiAc. The remainder was combined in a 50-ml tube with 100 µl carrier DNA and 15 µg human brain cDNA library, then 9 ml PEG/LiAc. After incubation at 30°C, cells were heat-shocked at 42°C for 15 min with occasional mixing. After cooling, library-transformed cells were pelleted by centrifugation at 240*g* for 10 min, then resuspended to a final volume of 24 ml; the control transformed-cells were spun at 6000*g* for 30 s and resuspended to a final volume of 1.2 ml. To estimate the total

number of transformants, 100-µl aliquots of 1:10, 1:100 and 1:1000 dilutions of the cell suspension were spread on to 10-cm SC-Leu-Trp agar plates. The undiluted suspension was spread on to 15-cm SC-Leu-Trp-His plates (400 µl per plate). SC-Leu-Trp-His agar had been supplemented with 50 mM 3-amino-1, 2, 4-triazole to suppress leaky expression of the *HIS3* gene. Plates were incubated for 60 h at 30°C before removal of visible cell growth by replica cleaning with sterile velvets and reincubation for 60-72 h.

2.21.7 Extraction of recombinant DNA from yeast

Five yeast transformant colonies were inoculated into 5 ml SC-Leu-Trp medium and incubated with shaking at 30°C for ~24 h. 1 ml was then pelleted by centrifugation at 14000*g* for 30 s. Cells were lysed by suspension in 100 µl yeast alkaline lysis solution. Lysis was stopped after 15 min by sequential addition of 500 µl 1x TE, pH 7.5 and 60 µl 3 M sodium acetate. To remove proteins, 600 µl TE-saturated phenol: chloroform: isoamyl alcohol (25:24:1) was added and the mixture was vortexed for 2 min, and subjected to centrifugation at 14000*g* for 2 min. The upper aqueous phase was transferred to a new microfuge tube and treated again with phenol: chloroform: isoamyl alcohol as before. Ice-cold isopropanol (650 µl) was then added, and the mixture was incubated at -20°C for ≥ 30 min. After centrifugation at 14000*g* for 5 min, every trace of supernatant was removed and the DNA pellet was washed by centrifugation as before in 100 µl 70% ethanol. The air-dried pellet was resuspended in 10 µl TE, pH 7.5 and stored at -20°C.

Table 2.3 - Composition of reagents used for yeast two-hybrid techniques

Reagent	Composition	Notes[a]
SC medium (1 l)	6.7 g yeast nitrogen base without aa 1.35 g aa-purine mix	Autoclave, add 50 ml autoclaved 40% glucose Supplement with sterile-filtered solutions: 8 ml 20 mM uracil 8 ml 100 mM His 8 ml 100 mM Leu 8 ml 40 mM Trp (protect from light)
SC-Leu-Trp	As above	As above, but supplement with glucose, uracil and His only
Aa-purine mix	2 g each of all standard aa except His, Leu, Trp 2 g adenine hemisulphate	
TE/LiAc solution	1x TE, pH 7.5 100 mM lithium acetate	Prepare from filter-sterilised stocks of 1 M lithium acetate and 10x TE Prepare TE/LiAc solution immediately before use
PEG/LiAc solution	1x TE, pH 7.5 100 mM lithium acetate 40% PEG-3350	Prepare from filter-sterilised stocks of 1 M lithium acetate, 10x TE and 50% PEG-3350 Prepare PEG/LiAc solution immediately before use
Yeast alkaline lysis solution	3% SDS 0.2 N NaOH	Prepare fresh each time

[a]: Reagents are all stored at room temperature.

Chapter 3: Mutational analysis of *VPS13A* in patients with chorea-acanthocytosis

The entire coding and flanking intronic sequence in *VPS13A* was screened for mutations in 83 unrelated patients with chorea-acanthocytosis. These patients were organised into three cohorts, Waves I, II and III.

3.1 Wave I

Our initial cohort comprised the 11 previously reported ChAc families linked to chromosome 9q21-q22 (Rubio *et al.* 1997). We screened the proband from each family by direct sequencing of all 73 exons of *VPS13A*. We identified four homozygous and 12 heterozygous mutations, finding at least one mutation in all probands analysed (Table 3.1 & Figure 3.1). Co-segregation of the mutations with the disease haplotypes was confirmed in all available family members using the verification method outlined in Table 3.1.

3.1.1 Description of mutations

Patients in families CHAC3, 5 & 7 are heterozygous for nonsense mutations 622C>T, 6700C>T and 9109C>T, respectively (Table 3.1 & Figure 3.1). All three mutations are substitutions in the arginine codon CGA, generating a TGA premature termination codon (PTC).

Nine different insertions or deletions leading to a shift in the reading frame were identified (Table 3.1 & Figure 3.1). Patients in families CHAC1 and 3 are heterozygous for the single base-pair insertions 6404_6405insT and 4419_4420insA, respectively. CHAC4 patients are homozygous for insertion of a dinucleotide (3557_3558insAC) and a heterozygous 4 base-pair insertion 9289_9290insTTTG was found in CHAC7 patients. CHAC2 and CHAC8 patients are homozygous and CHAC11 patients are heterozygous for deletions of a single base pair at positions 1592, 1115 and 237, respectively. Heterozygous deletions of a dinucleotide (2833_2834del) and a tetranucleotide (9429_9432del) were found in affected members of families CHAC10 and 11, respectively. All nine frameshift mutations are predicted to lead to introduction of a PTC in the *VPS13A* transcript.

Affected members of CHAC5 harbour a heterozygous substitution of A to C at the splice-acceptor dinucleotide AG of intron 48 (Table 3.1 & Figure 3.1). As RNA was not available from this family, it was not possible to determine the precise effect of this mutation on splicing. However, input of this base change into the SpliceView program (http://l25.itba.mi.cnr.it/~webgene/wwwspliceview.html) revealed that the new junction sequence is too divergent from the consensus to score as a splice-site. We therefore predict that this mutation is likely to cause aberrant splicing of the *VPS13A* mRNA transcript.

Three different missense mutations were identified in this screen (Table 3.1 & Figure 3.1). CHAC1 patients are heterozygous for the base change 269T>A, which results in substitution of isoleucine to lysine at position 90. CHAC6 affected individuals harbour the homozygous change 4354T>C, which leads to substitution of proline for serine at position 1452. Individuals with ChAc in family CHAC9 are heterozygous for the base change 8162A>G, which leads to replacement of tyrosine by cysteine at position 2721. None of the three amino-acid substitutions was found in 100 control chromosomes.

Table 3.1 - *VPS13A* disease mutations identified in Wave I

Family[a]	Location	DNA change[b]	Protein change[b]	Mutation type	Verification method
CHAC1	Exon 4	269T>A (ht)	I90K[c]	Missense	Sequencing
	Exon 48	6404_6405insT (ht)	S2136KfsX1	Frameshift	*Dde*I
CHAC2*	Exon 17	1592del (hm)	I531KfsX6	Frameshift	Sequencing
CHAC3	Exon 9	622C>T (ht)	R208X	Nonsense	Sequencing
	Exon 38	4419_4420insA (ht)	G1474RfsX6	Frameshift	Sequencing
CHAC4*	Exon 33	3557_3558insAC (hm)	V1187LfsX11	Frameshift	Sequencing
CHAC5	Exon 48	6700C>T (ht)	R2234X	Nonsense	*Taq*I
	Intron 48	6775-2A>C (ht)	(SA: no score (wt = 82))[d]	Splice site	*Sty*I
CHAC6*	Exon 37	4354T>C (hm)	S1452P[c]	Missense	Sequencing
CHAC7	Exon 68	9109C>T (ht)	R3037X	Nonsense	Sequencing
	Exon 71	9289_9290insTTTG (ht)	T3098CfsX11	Frameshift	Sequencing
CHAC8*	Exon 13	1115del (hm)	K372SfsX1	Frameshift	Sequencing
CHAC9	Exon 59	8162A>G (ht)	Y2721C[c]	Missense	Sequencing
	?	?	?	?	
CHAC10	Exon 27	2833_2834del (ht)	K945EfsX10	Frameshift	Sequencing
	?	?	?	?	
CHAC11	Exon 4	237del (ht)	E80KfsX10	Frameshift	Sequencing
	Exon 72	9429_9432del (ht)	R3143SfsX4	Frameshift	Sequencing

[a]: Families are asterisked where we had prior evidence of homozygosity by descent (Rubio *et al.*, 1997). [b]: Nucleotides and amino acids are numbered according to the cDNA sequence of *VPS13A* isoform 1A reported by Rampoldi *et al.* (2001) as *CHAC* isoform A (GenBank accession no. NM_033305), with the adenosine of the initiation codon assigned position 1. Mutation nomenclature is as recommended by the Human Genome Variation Society (http://www.genomic.unimelb.edu.au/mdi/mutnomen/index.html). [c]: Not found in 100 control chromosomes. [d]: Wild type and mutant DNA sequence flanking the splice site was entered into the SpliceView program (http://l25.itba.mi.cnr.it/~webgene/wwwspliceview.html) - the scores produced are shown.
Key: ?, second heterozygous mutation not found; ex, exon; int, intron; SA, splice acceptor

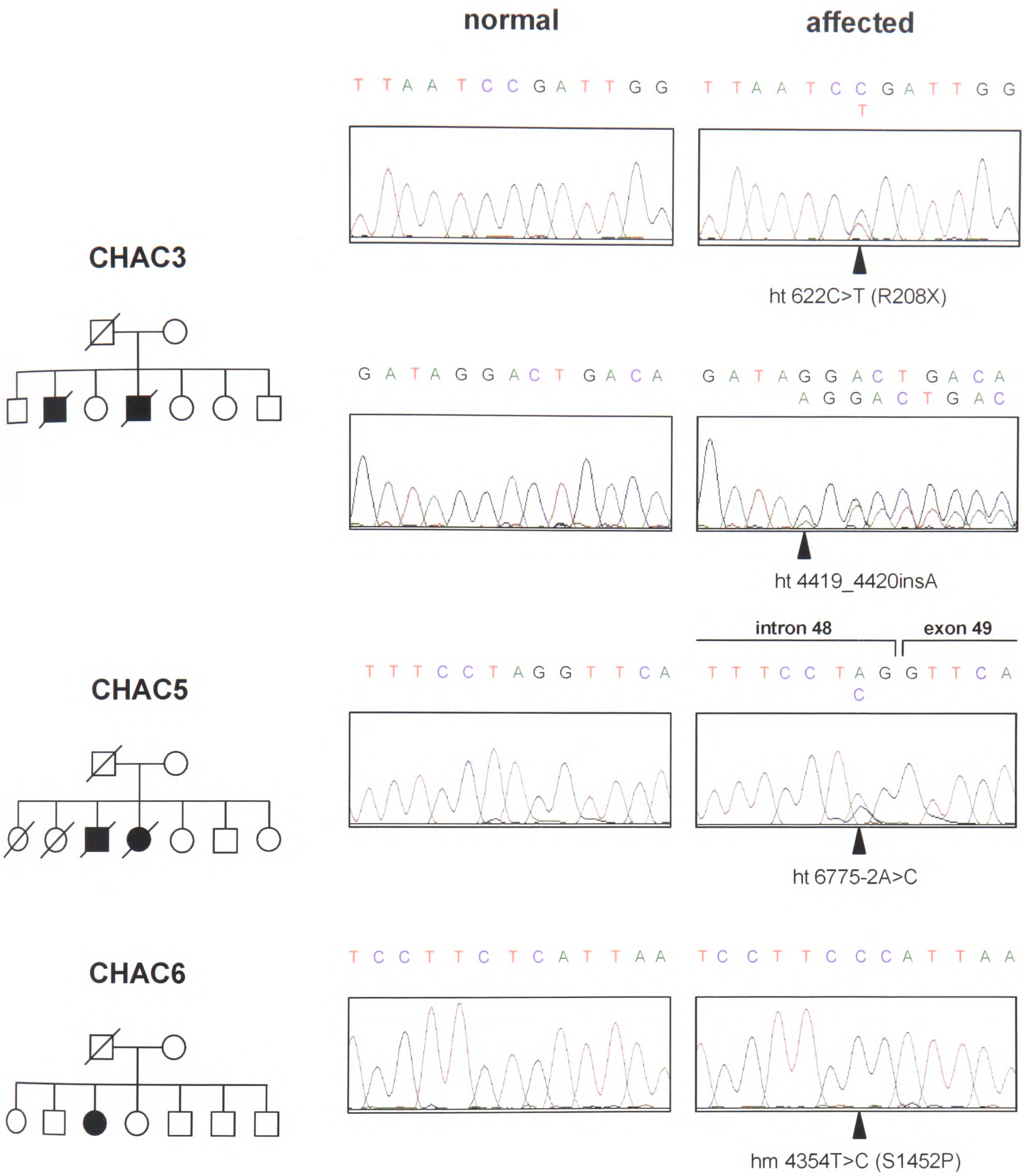

Figure 3.1 - Identification of *VPS13A* mutations in patients with ChAc. The pedigrees of families CHAC3, CHAC5 and CHAC6 are shown alongside sequences generated by direct sequencing of genomic DNA amplicons from (left) a control individual and (right) the relevant proband. The sequences illustrate respectively nonsense, frameshift, splice-site and missense mutations found in these families. Affected individuals are indicated in the pedigree by filled symbols, unaffected by open symbols. Arrowheads indicate the position of the mutation in the proband sequence. For heterozygous mutations, the mutant allele sequence is displayed below the wild-type sequence.
Key: ht = heterozygous, hm = homozygous

Fig 3.1

3.2 Wave II

3.2.1 XK *screening*

Forty-five probands with symptoms compatible with ChAc were initially included in the follow-up to Wave I. As most families in this cohort were not big enough to permit linkage analysis, and the symptoms of MLS can be similar to ChAc (Danek *et al.* 2004), we wished to exclude involvement of the *XK* gene before proceeding with the *VPS13A* screen. For 11 probands, Kell serotyping had been performed: these patients did not show the weak Kell antigen response characteristic of MLS. For the remaining 34 probands, no Kell serotyping data was available. Of these, 17 were either female or had an affected female in their pedigree, which was very unlikely to be consistent with X-linked recessive inheritance of the McLeod phenotype. This left 17 probands, who were screened for mutations in the *XK* gene by direct sequencing of all three exons and flanking intronic sequence. This revealed that one proband was hemizygous for a nonsense mutation in *XK* exon 3, 707G>A (W236X). A second patient was hemizygous for deletion of nucleotides 856-860 in the same exon. This 5-bp deletion causes a shift of reading frame at aa position 285, leading to a PTC 15 codons downstream.[1] As both these mutations were likely to disrupt XK function, these patients were excluded, leaving 43 probands with suspected ChAc.

[1] We subsequently reported these patients as MLS cases 11 and 22, respectively (Danek *et al.* 2001).

3.2.2 VPS13A *screening*

The entire coding and flanking intronic sequence in *VPS13A* was screened for mutations by denaturing high-performance liquid chromatography (DHPLC) in 43 unrelated patients with chorea-acanthocytosis. This revealed 57 different mutations likely to cause disease in 39 probands (Table 3.2). Only three of these mutations had been previously identified, in different families, in our Wave I cohort. All available family members were screened for the relevant mutation(s) using the verification method outlined in Table 3.2; in each case, the mutation(s) co-segregated consistently with the affection status. In seven patients only one heterozygous mutation was found; in four patients with typical symptoms of ChAc, no disease mutations were found.

3.2.3 Nonsense mutations

Seventeen different base substitutions that result in PTCs were identified (Table 3.2). Three of these mutations (1549G>T, 3109A>T, 5920G>T) result in substitution to a TAA stop codon; three other mutations (3157C>T, 6419C>G, 9219C>G) result in substitution to a TAG stop codon. The remaining 11 mutations in this group result in substitution to a TGA stop codon: the majority of these (7/11, 64%) arise in CGA arginine codons. The 5920G>T mutation was found to be homozygous not only in proband II-5, but also his affected mother (see Figure 3.2a).

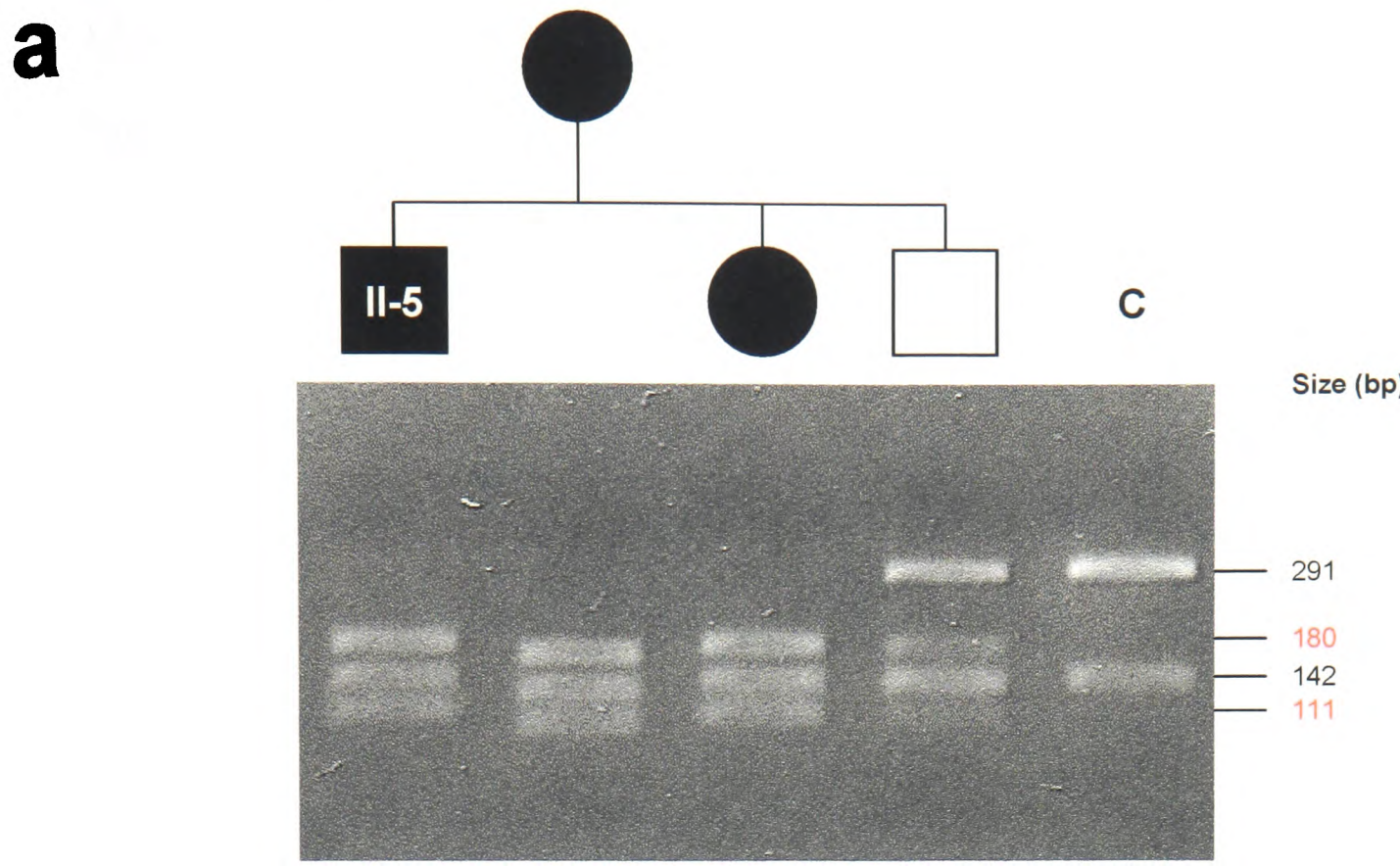

Figure 3.2 - Analysis of *VPS13A* mutations in pseudodominant ChAc families. a, Restriction fragment length polymorphism (RFLP) analysis of exon 45 in Wave II family 5. The mutation 5920G>T (E1974X) creates a *Dra*I site: bands corresponding to the mutant allele are indicated in red. **b,** Segregation of mutations in Wave II family 8. The father in this pedigree showed some mild dyskinesia, hence the grey shading. The left-hand panel shows RFLP analysis of exon 72. The splicing mutation 9474G>A destroys a *Scr*FI site: the band corresponding to the mutant allele is indicated in red. The right-hand panel shows sequencing analysis of exon 29. An arrowhead indicates the position of the mutation (3109A>T (K1037X)).

3.2.4 Splice-site mutations

Fifteen different mutations are predicted to result in altered *VPS13A* mRNA splicing (Table 3.2). Twelve of these are located in introns: they directly alter the highly conserved AG or GT dinucleotides of the intronic splice-acceptor or splice-donor sites, respectively. Mutation 883-1_892del spans intron 11 and exon 12. Although it deletes 10 nucleotides of exon 12 and could therefore shift the reading frame of the *VPS13A* mRNA, we consider its primary effect to be on splicing, since the new intron/exon junction formed (attctttagTATTTCAGTATTAT → attctttaTTAT) is widely divergent to the consensus splice-acceptor sequence. The remaining two splice-site mutations (7806G>A & 9474G>A) alter the 3' nucleotide in exons 55 and 72, respectively. The first substitution occurs within the sequence CCGgtaata → CCAgtaata: although both trinucleotides CCG and CCA code for proline, this exon/intron junction no longer conforms to the splice-donor consensus. The same is true of mutation 9474G>A in proband II-8: the substitution AGGgtaaat → AGAgtaaat does not affect the coding for arginine 3158, but does abolish the splice-donor site. Interestingly, the father of proband II-8 is homozygous for this mutation (see Figure 3.2b) and shows mild features of the disease. Both exonic splice-site mutations were found to be absent in 192 control individuals using the verification methods indicated in Table 3.2. In each case, input of these base changes into the SpliceView program revealed that the new junction sequence was too divergent from the consensus to score as a splice-site (Table 3.2).

3.2.5 Missense mutations

Only two different base changes resulting in potentially pathogenic, non-conservative amino-acid substitutions were identified (3283G>C & 7378T>C, Table 3.2). Mutation 3283C>G results in the substitution of alanine to proline at position 1095. Mutation 7378T>C results in the substitution of tryptophan to arginine at position 2460. Neither of these missense mutations was found when screening 192 normal individuals using the verification methods outlined in Table 3.2.

3.2.6 Insertion/deletion mutations

Twenty different insertions or deletions were identified that lead to a shift in the reading frame, introducing a PTC (Table 3.2). These comprise 11 1-bp deletions, two 1-bp insertions, two 2-bp deletions, three 4-bp deletions and one deletion each of five and 14 base pairs. Mutation 2029_2031delins27 involves the deletion of the trinucleotide CAT and the insertion of the 27-nucleotide sequence ATATACTAATATCTGCTTCTTTTGGAC. This mutation results in a net increase of 24 nucleotides, so does not shift the reading frame: however, the third trinucleotide that is introduced is a PTC. In probands II-6 and II-42, it was not possible to amplify exon 23 and exons 70-73, respectively. Southern analysis of the appropriate regions revealed that proband 6 was homozygous for an approximately 7-kb deletion covering exon 23, and that proband 42 was homozygous for a deletion of at least 13 kb removing the four terminal exons of *VPS13A* (Figure 3.3a & b).

Table 3.2 - *VPS13A* disease mutations identified in Wave II

Location	DNA change[a]	Protein change[a]	Proband no.[c]	Verification method
Nonsense				
Exon 9	622C>T[b]	R208X[b]	II-12 (ht), II-27* (hm), II-39 (ht)	Sequencing
Exon 17	1549G>T	E517X	II-3 (ht)	*Apo*I
Exon 18	1616C>G	S539X	II-18 (ht)	*Tfi*I
Exon 25	2593C>T	R865X	II-9 (hm)	*Taq*I
Exon 29	3109A>T	K1037X	II-8 (ht)	Sequencing
Exon 30	3157C>T	Q1053X	II-15* (hm)	Sequencing
Exon 34	3889C>T	R1297X	II-38 (ht)	Sequencing
Exon 37	4355C>G	S1452X	II-35 (ht)	Sequencing
Exon 37	4411C>T	R1471X	II-26 (ht)	*Sty*I
Exon 45	5920G>T	E1974X	II-5* (hm)	*Dra*I
Exon 46	6094C>T	R2032X	II-4 (ht)	*Bsr*I
Exon 48	6419C>G	S2140X	II-24 (ht)	*Ban*II
Exon 48	6494G>A	W2165X	II-10 (hm)	Sequencing
Exon 50	7005G>A	W2335X	II-36 (ht)	*Ple*I
Exon 56	7867C>T	R2623X	II-23 (ht)	Sequencing
Exon 68	9109C>T[b]	R3037X[b]	II-1 (ht)	*Tsp*45I
Exon 70	9219C>G	Y3073X	II-13 (ht)	Sequencing
Splice site				
Intron 11	883-1_892del	(SA: no score (wt = 82))[d]	II-22 (ht)	Sequencing
Intron 17	1595+1G>A	(SD: no score (wt = 86))	II-36 (ht)	Sequencing
Intron 17	1596-2A>C	(SA: no score (wt = 89))	II-16 (ht)	Sequencing
Intron 17	1596-1G>C	(SA: no score (wt = 89))	II-35 (ht)	Sequencing
Intron 21	2170+1G>A	(SD: no score (wt = 85))	II-26 (ht)	*Hph*I
Intron 22	2288+2T>C	(SD: no score (wt = 83))	II-2 (ht)	Sequencing
Intron 36	4242+1G>T	(SD: no score (wt = 93))	II-40 (hm)	Sequencing
Intron 40	4956+1G>T	(SD: no score (wt = 83))	II-12 (ht)	Sequencing
Exon 55	7806G>A[e]	(SD: no score (wt = 76))	II-3 (ht)	*Hpa*II
Intron 61	8472-1G>C	(SA: no score (wt = 88))	II-2 (ht)	Sequencing
Intron 65	8907+2T>A	(SD: no score (wt = 75))	II-16 (ht)	Sequencing
Intron 70	9275+1G>A	(SD: no score (wt = 80))	II-1 (ht)	*Mae*III
Intron 70	9276-2A>T	(SA: no score (wt = 92))	II-41 (ht)	Sequencing
Intron 71	9399+2_+8del	(SD: no score (wt = 92))	II-14 (ht)	Sequencing
Exon 72	9474G>A[e]	(SD: no score (wt = 81))	II-8 (ht)	*Scr*FI
Missense				
Exon 31	3283G>C[e]	A1095P	II-21 (ht)	*Bst*XI
Exon 53	7378T>C[e]	W2460R	II-28 (hm)	*Aci*I
Frameshift				
Exon 13	994del	A332LfsX9	II-7 (ht)	Sequencing
Exon 13	1125_1128del	S375RfsX22	II-11 (ht)	Sequencing
Exon 14	1187_1188del	F396fsX0	II-17* (hm)	Sequencing
Exon 14	1208_1211del	Q403RfsX5	II-23 (ht)	Sequencing
Exon 20	2029_2031delins27	H677delinsIYX	II-29 (ht)	*Psh*AI
Exon 34	3847del	L1283WfsX6	II-33 (hm)	*Bsr*I
Exon 36	4216del	V1406CfsX19	II-38 (ht)	*Sty*I
Exon 37	4346del	S1449FfsX4	II-19 (ht)	*Mbo*II
Exon 39	4835del	P1612QfsX29	II-21 (ht)	*Bsr*I
Exon 41	5253_5266del	F1751LfsX13	II-13 (ht)	*Dra*I

Table 3.2 - *VPS13A* disease mutations identified in Wave II

Location	DNA change[a]	Protein change[a]	Proband no.[c]	Verification method
Exon 46	6059del	P2020LfsX8	II-37 (hm)	*Hph*I
Exon 47	6283del	S2095QfsX9	II-7 (ht)	Sequencing
Exon 49	6804_6805insG	S2269VfsX6	II-39 (ht)	*Ava*II
Exon 49	6828del	V2277LfsX11	II-41 (ht)	Sequencing
Exon 53	7339_7340insT	Y2447LfsX4	II-20 (ht)	Sequencing
Exon 57	7985_7989del	P2662RfsX5	II-32 (ht)	Sequencing
Exon 57	8007del	K2669NfsX21	II-22 (ht)	*Hpa*I
Exon 61	8390del	G2797DfsX1	II-14 (ht)	*Mnl*I
Exon 70	9190del	V3064SfsX16	II-24 (ht)	Sequencing
Exon 72	9429_9432del[b]	R3143SfsX4[b]	II-34 (ht)	*Bsr*I
Exon 72	9431_9432del	E3144VfsX5	II-29 (ht)	*Pfl*MI
Gross deletion				
Exon 23	EX23del	(unknown)[f]	II-6* (hm)	Southern blot
Exons 70-73	EX70_EX73del	(unknown)	II-42 (hm)	Southern blot

[a]: Nucleotides and amino acids are numbered according to the cDNA sequence of *VPS13A* isoform 1A reported by Rampoldi *et al.* (2001) as *CHAC* isoform A (GenBank accession no. NM_033305), with the adenosine of the initiation codon assigned position 1. Mutation nomenclature is as recommended by the Human Genome Variation Society (http://www.genomic.unimelb.edu.au/mdi/mutnomen/index.html). [b]: Mutations that were identified in a Wave I family previously. [c]: Probands are asterisked where we had prior knowledge that they were offspring of a consanguineous pairing. [d]: Wild-type and mutant DNA sequence flanking each splice site was entered into the SpliceView program (http://l25.itba.mi.cnr.it/~webgene/wwwspliceview.html) - the scores produced are shown. [e]: Not found in 384 control chromosomes. [f]: skipping of this exon in *VPS13A* mRNA would lead to a frameshift.
Key: hm, homozygous; ht, heterozygous; SA, splice acceptor; SD, splice donor; wt, wild type.

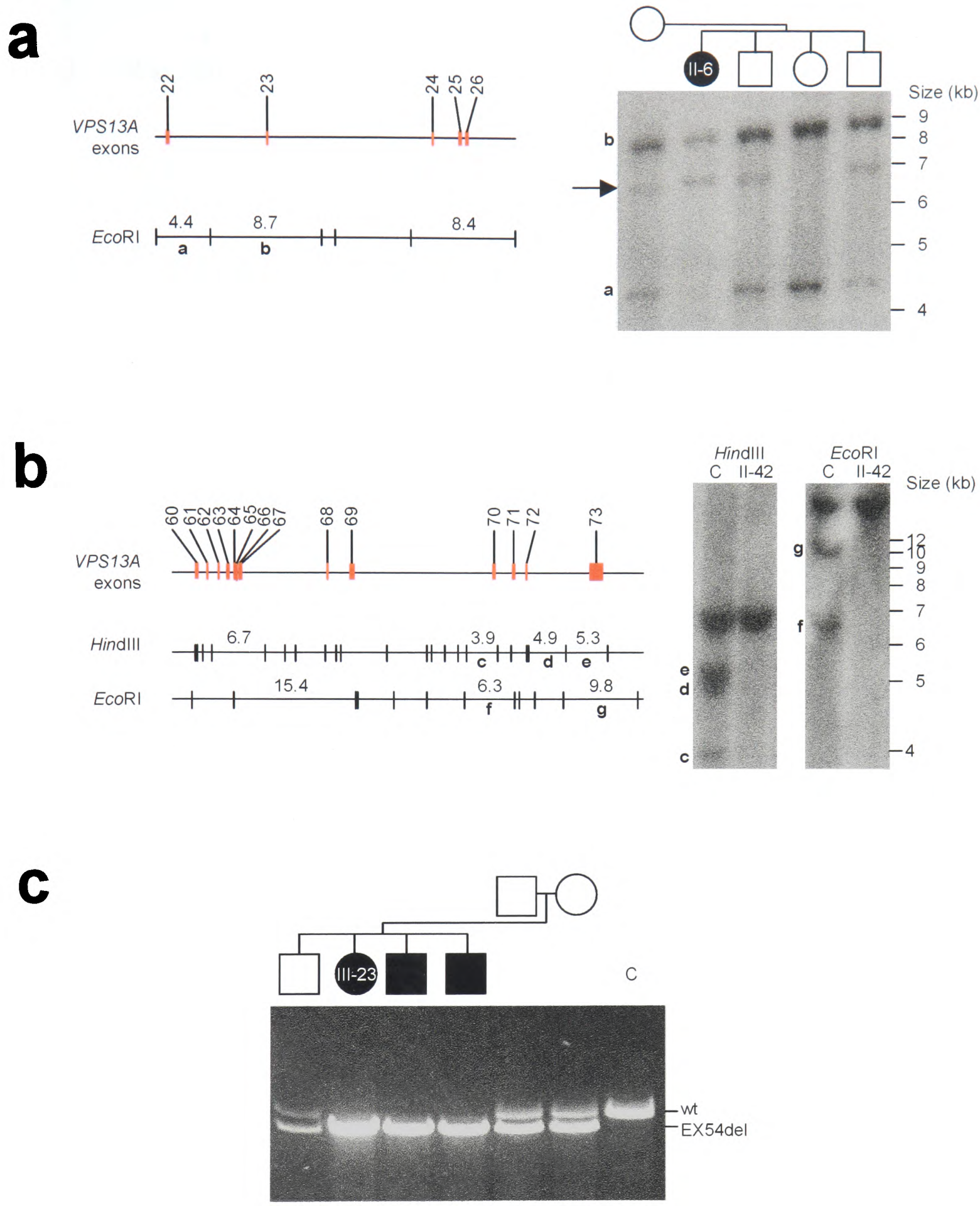

Figure 3.3 - Analysis of gross deletions in *VPS13A*. a, Southern blot analysis of proband II-6 EX23del mutation. PCR primers KIAArt13 & KIAArt11 (see Appendix 1) were used to generate a 563-bp cDNA probe containing exons 22-26. A scaled restriction map of the normal locus is shown on the left; hybridisation of the probe to an *Eco*RI digest of the proband family is shown on the right. The abnormal restriction fragment is arrowed; restriction fragments that are absent in the proband are labelled a & b. **b**, Southern blot analysis of proband II-42 EX70_73del mutation. PCR primers 222006fp6 & BCD3239fp1 (see Appendix 1) were used to generate a 710-bp cDNA probe containing exons 65-68 & 70-73. Scaled restriction maps of the normal locus are shown on the left; hybridisation of the probe to *Hin*dIII and *Eco*RI digests of a control and proband II-42 is shown on the right. Restriction fragments that are absent in the proband are labelled c-g. **c**, Long-range PCR analysis of proband III-23 EX54del mutation. The forward primer for exon 53 and reverse primer for exon 55 (see Appendix 1) were used to amplify a region spanning exons 53-55. The wild-type allele (wt) is 5797 bp; the deletion allele (del) is approximately 4 kb. Key: C, healthy control.

3.3 Wave III

3.3.1 XK *screening*

The Wave III cohort comprised 29 probands with suspected ChAc. As for Wave II, patients with no affected females in the pedigree and with no Kell serotyping data were screened for mutations in the *XK* gene. No mutations likely to cause McLeod syndrome were identified, and so all 29 probands were included in the *VPS13A* screen.

3.3.2 VPS13A *screening*

DHPLC was again employed to screen *VPS13A* in the 29 probands of Wave III. This revealed 27 different mutations likely to cause disease in 22 probands (Table 3.3). Nine of these mutations have been identified before in Wave I or II. Co-segregation of the relevant mutation with affection status was verified by sequencing of all available family members. In three patients only one heterozygous mutation was found; in seven patients with typical symptoms of ChAc, no disease mutations were found.

3.3.3 Nonsense mutations

Six different nonsense mutations were identified (Table 3.3). Three of these substitutions result in generation of a TAA stop codon; the remaining three lead to TGA stop codons.

3.3.4 Splice-site mutations

Five different mutations are predicted to lead to altered *VPS13A* mRNA splicing (Table 3.3). Mutation 188-5T>G occurs within the intron 3/exon 4 junction. The unusual sequence of the wild-type junction, caaaaaatgtagGTA, does not in fact score as a splice site when using the SpliceView program. In contrast, the new sequence scores 77 as a splice acceptor, but the predicted intron-exon junction is 4 bases upstream, i.e., caaaaaaag][gtagGTA. As it does not score with this program, it is not possible to predict how splicing at the wild-type junction is affected by the T>G substitution. However, the activation of a cryptic splice site near this sequence is likely to have an adverse effect. In proband III-15, the splice-donor sequence at the exon 6/intron 6 junction is altered from GATgtaagt (SpliceView score 83) to GATgtaaat (no score). The three remaining mutations directly alter the highly conserved intronic splice-acceptor (AG) or splice-donor (GT) dinucleotides.

3.3.5 Insertion/deletion mutations

Eleven different insertions or deletions leading to a shift in the reading frame were identified (Table 3.3). These include three 1-bp deletions, three 2-bp deletions, one 2-bp insertion and two 4-bp deletions. An insertion of the octanucleotide AACAAAAA, and a compound deletion of two nucleotides with insertion of an A, was also identified. All eleven mutations generate a PTC in the *VPS13A* mRNA transcript. Homozygous deletions of one or more exons were found in six probands (Figure 3.3): two of these (III-6 & III-24) shared the same deletion of exons 70-73 as Wave II proband 42. The 7-exon gene encoding G alpha subunit 14 (*GNA14*) lies in a tail-to-tail arrangement with *VPS13A* (Figures 1.3 & 3.4). PCR analysis of families II-

42, III- 6 & III-24 revealed that *GNA14* exons 6 & 7 could not be amplified in affected family members, implying that the deletion actually extends across the intergenic region between *VPS13A* and *GNA14* and encompasses the last two exons of *GNA14* (Figure 3.4).

Table 3.3 - *VPS13A* disease mutations identified in Wave III

Location	DNA change[a]	Protein change[a]	Proband no.[c]
Nonsense			
Exon 13	1078C>T	Q360X	III-22 (ht)
Exon 22	2191C>T	R731X	III-30 (ht)
Exon 23	2347C>T	Q783X	III-19* (hm)
Exon 37	4355C>G[b]	S1452X[b]	III-29 (ht)
Exon 37	4411C>T[b]	R1471X[b]	III-3 (hm)
Exon 41	5084T>A	L1695X	III-36 (ht)
Splice site			
Intron 3	188-5T>G	(SA: 77 (wt = no score))[d]	III-26 (ht)
Intron 6	495+1G>A	(SD: no score (wt = 83))	III-8 (ht)
Intron 6	495+5G>A	(SD: no score (wt = 83))	III-15 (ht)
Intron 17	1596-1G>C[b]	(SA: no score (wt = 89))	III-29 (ht)
Intron 36	4242+1G>T[b]	(SD: no score (wt = 93))	III-11* (hm)
Frameshift			
Exon 5	372_373ins8	V125NfsX3	III-22 (ht)
Exon 33	3557_3558insAC[b]	V1187LfsX11[b]	III-31 (hm)
Exon 35	3995_3996delinsA	F1332fsX0	III-30 (ht)
Exon 38	4428_4431del	G1478LfsX5	III-36 (ht)
Exon 39	4724del	P1575LfsX2	III-14 (hm)
Exon 40	4903_4906del	K1635VfsX5	III-15 (ht)
Exon 45	5909_5910del	E1970VfsX3	III-7 (ht)
Exon 46	6059del[b]	P2020LfsX8[b]	III-2 (hm)
Exon 49	6828del[b]	V2277LfsX11[b]	III-9 (ht)
Exon 67	9065_9066del	Q3022RfsX9	III-9 (ht)
Exon 72	9431_9432del[b]	E3144VfsX5[b]	III-18 (hm)
Gross deletion			
Exons 2-3	EX2_EX3del	(unknown)	III-20* (hm)
Exons 8-9	EX8_EX9del	(unknown)	III-13* (hm)
Exons 46-50	EX46_EX50del	(unknown)	III-33 (hm)
Exon 54	EX54del	(unknown)[f]	III-23 (hm)
Exons 70-73	EX70_EX73del[b]	(unknown)	III-6 (hm), III-24* (hm)

[a]: Nucleotides and amino acids are numbered according to the cDNA sequence of *VPS13A* isoform 1A reported by Rampoldi *et al.* (2001) as *CHAC* isoform A (GenBank accession no. NM_033305), with the adenosine of the initiation codon assigned position 1. Mutation nomenclature is as recommended by the Human Genome Variation Society (http://www.genomic.unimelb.edu.au/mdi/mutnomen/index.html). [b]: Mutations that were identified in a Wave I or II family previously. [c]: Probands are asterisked where we had prior knowledge that they were offspring of a consanguineous pairing. [d]: Wild-type and mutant DNA sequence flanking each splice site was entered into the SpliceView program (http://l25.itba.mi.cnr.it/~webgene/wwwspliceview.html) - the scores produced are shown. [e]: Not found in 384 control chromosomes. [f]: skipping of this exon in *VPS13A* mRNA would lead to a frameshift.
Key: hm, homozygous; ht, heterozygous; SA, splice acceptor; SD, splice donor; wt, wild type.

a

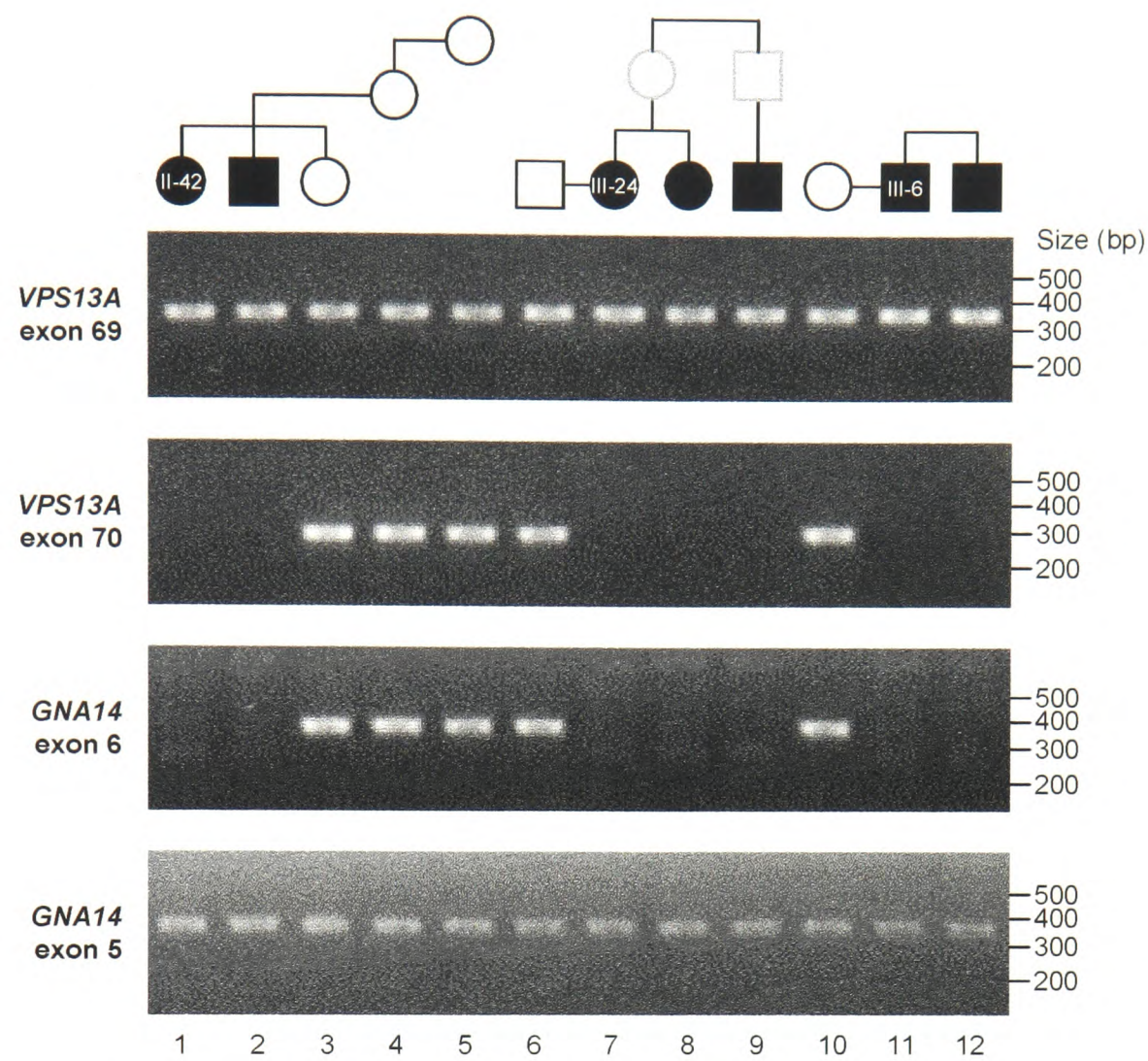

b

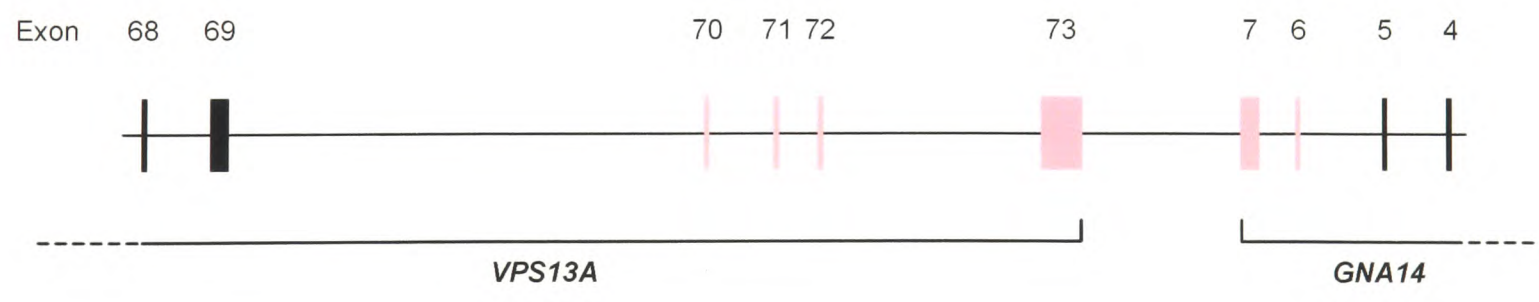

Figure 3.4 - Further characterisation of *VPS13A* EX70_73del mutation. a, PCR amplification of *VPS13A* exons 69 & 70, and *GNA14* exons 6 & 5, in families II-42, III-24 & III-6 (see Appendix 1 for primer sequences). Pedigrees are indicated at the top of the figure - family members who were not analysed are outlined in grey. **b**, Scaled map of chromosome 9 region covering the 3' ends of *VPS13A* and *GNA14* genes. Exons that cannot be amplified in probands II-42, III-6 & III-24 are shown in pink.

3.4 Exonic polymorphisms

During the course of screening Waves I-III, 24 additional exonic variants were identified (Table 3.4). Seventeen of these are silent mutations, as the nucleotide substitutions do not alter the amino acid coding. The remaining seven changes were concluded to be neutral variants, despite leading to amino-acid substitutions. This was because they were either present only in unaffected relatives, or on the same chromosome as disease-causing mutations. Interestingly, one of the so-called 'silent' mutations (1020A>G) in exon 13 occurs in the nucleotide sequence GAAGTAAAT. The new sequence scores 84 on the SpliceView program as a splice-donor site, GAG][GTAAAT (the splice-donor site in intron 13 that is usually used scores 79). Proband II-18 is heterozygous for this change and an S539X mutation in exon 18 (Table 3.2). The exon 13 change was also found on 1 of 384 control chromosomes, so it is doubtful that this represents a pathogenic variant. However, we cannot exclude the possibility that it could lead to the ChAc phenotype in combination with a heterozygous nonsense mutation. The base change 4509A>G in exon 38, identified in proband WIII-21, may also activate a cryptic splice-site: while the wild-type sequence GTCTTTCAAGAAA does not score, the altered sequence scores 80 as a potential splice-acceptor site, GTCTTTCA**G**][GAAA. The splice-acceptor site in intron 37 that is usually used scores 85. Analysis of mRNA splicing in this proband would be required to discover whether this base change is a neutral or pathogenic variant.

Table 3.4 - Exonic polymorphisms identified in *VPS13A*

Exon	DNA change[a]	Protein change[a]	Frequency in ChAc proband chromosomes
13	1020A>G	None[b]	1/166
14	1197T>C	None	1/166
18	1695C>G	F565L	2/166
26	2693T>C	V898A	4/166
26	2718A>G	None	2/166
26	2814A>G	None	1/166
29	3045G>A	None	21/166
29	3108T>C	None	2/166
33	3645C>A	None	2/166
38	4469G>A	R1490K	1/166
38	4509A>G	None[b]	1/166
39	4760A>G	Y1587C	0/166[c]
44	5583A>G	None	22/166
45	5917G>A	V1973I	9/166
45	5979C>T	None	2/166
46	6027C>T	None	19/164
46	6039C>A	None	1/164
47	6252A>G	None	1/164
48	6492T>C	None	40/164
48	6531C>T	None	2/164
54	7457T>C	I2486T	1/164
63	8571T>C	None	21/166
67	9069A>G	None	84/166
73	9515C>T	P3172L	2/160

[a]: Nucleotides and amino acids are numbered according to the cDNA sequence of *VPS13A* isoform 1A reported by Rampoldi *et al.* (2001) as *CHAC* isoform A (GenBank accession no. NM_033305), with the adenosine of the initiation codon assigned position 1. [b]: Possibly affects RNA splicing: see section 3.4. [c]: Mutation found in a healthy member of Wave I family CHAC6.

3.6 Summary

This chapter describes the mutational analysis of *VPS13A* in 83 unrelated patients with suspected chorea-acanthocytosis. Eighty-eight different changes likely to disrupt chorein function were found in 72 patients, comprising six deletions of entire exons, 22 nonsense, 36 frameshift, 19 splice-site and five missense mutations. In 12 patients, only one heterozygous mutation was found; for 11 patients with typical symptoms of ChAc, no mutations were found. Twelve mutations were shared by one or more apparently unrelated patients, leaving 76 mutations that were only identified in a single family. In addition, 24 exonic *VPS13A* variants were identified: 17 of these were synonymous, while seven were non-synonymous changes.

Chapter 4: Analysis of *VPS13A* expression

4.1 Distribution of *VPS13A* mRNA expression

In order to determine the tissue distribution of *VPS13A* mRNA, we analysed its expression by using a human adult multiple-tissue Northern blot. As shown in Figure 4.1a, hybridisation with a cDNA probe corresponding to *VPS13A* exons 7-17 shows a broad high-molecular-weight band. There are two polyadenylation signals present in exon 73, which generate a 10- or 11-kb variant of transcript 1A (exons 1-68, 70-73). Transcript 1B (exons 1-69) is predicted to be 10 kb long. The broad band seen on the Northern blot is therefore likely to correspond to these three variants. A signal could be detected in all the tissues analysed (although weak in some), suggesting ubiquitous expression of *VPS13A*. This result was confirmed by RT-PCR experiments on a multiple-tissue cDNA panel and in RNA isolated from fibroblasts and a lymphoblastoid cell line (Fig. 4.1b).

a

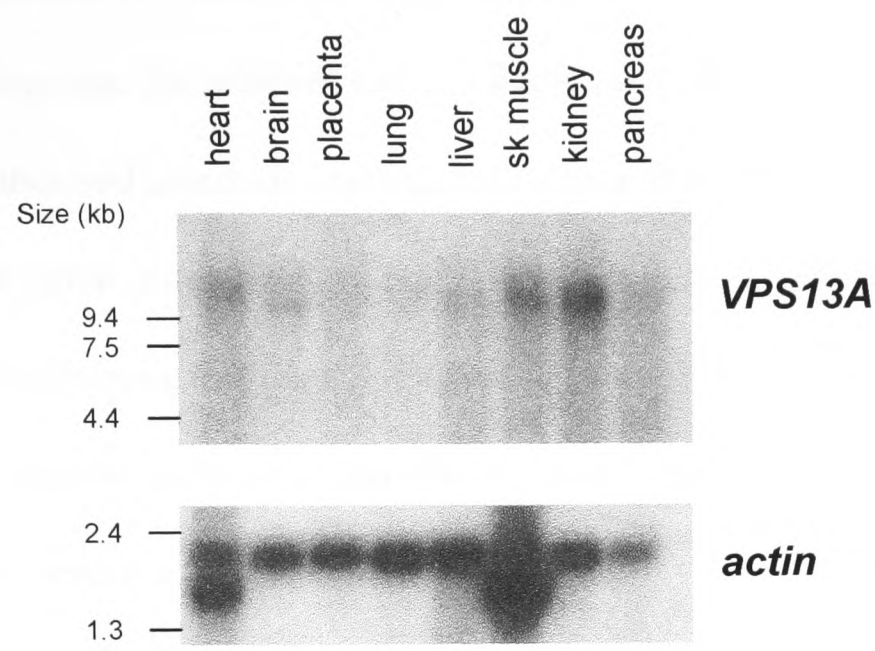

b

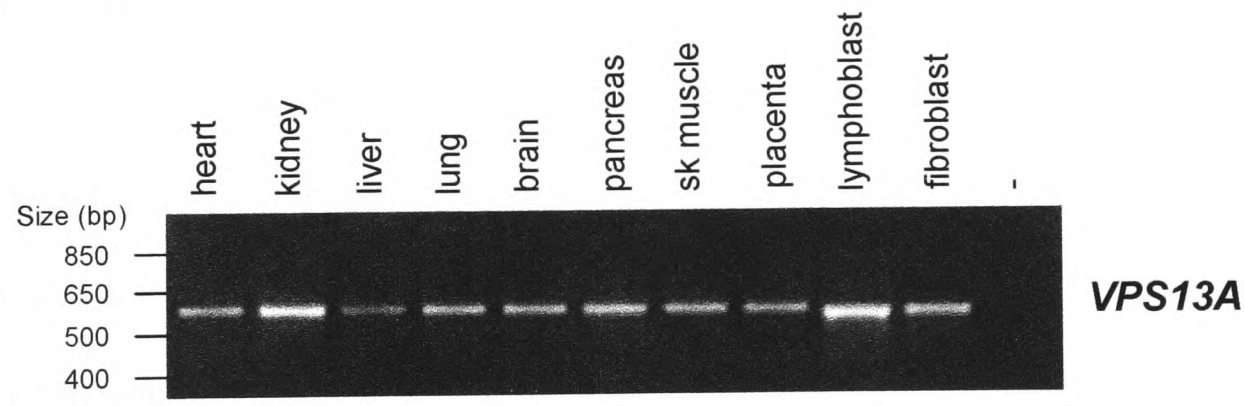

Figure 4.1 - Expression analysis of *VPS13A* mRNA. a, Adult human multiple-tissue Northern blot analysis. PCR primers KIAArt22 and KIAArt15 (see Appendix 1) were used to generate a 1028-bp cDNA probe containing *VPS13A* exons 7-17. The 2-kb β-actin probe supplied with the Northern blot (section 2.6.2) was used as control. **b**, RT-PCR analysis on an adult human multiple-tissue cDNA panel and lymphoblast and fibroblast cDNA. PCR primers KIAArt13 and KIAArt11 (see Appendix 1), amplifying a region containing *VPS13A* exons 22-26, were used. The expected PCR product (563 bp) is present in all the tissues analysed.
Key: Sk, skeletal; -, PCR negative control.

4.2 Chorein-specific rabbit polyclonal antibody production

A desirable reagent for the functional characterisation of any gene product is an antibody that recognises the relevant protein. Early on in the characterisation of *VPS13A*, we synthesised a peptide corresponding to amino acids 2572-2593 of chorein to raise a rabbit polyclonal antibody. However, the specificity of detection was poor (data not shown). We therefore decided to generate an antibody against a larger region of chorein, in the hope that the increased number of potential epitopes in the antigen would result in a more effective antibody.

4.2.1 Expression of GST-chorein fusion proteins

I assembled three bacterial expression vectors containing cDNA fragments encoding chorein amino acids 27-326, 1189-1502 & 2756-3055, fused to glutathione-S-transferase (GST), according to the scheme illustrated in Figure 4.2a. Each construct (pGEX-chac1, pGEX-chac2 and pGEX-chac3) was transformed into a bacterial strain engineered for efficient, inducible recombinant protein expression. Duplicate cultures of transformants were grown to log phase at 37°C, and protein expression was then induced at 18, 30 or 37°C. Expression levels of the fusion protein were investigated by SDS-PAGE at two, four and six hours post induction. As shown in Figure 4.2b, maximal expression of GST-chor1 was detected after six hours induction at 37°C; maximal expression of GST-chor2 was detected after six hours induction at either 30 or 37°C. I was not able to detect GST-chor3 expression (Figure 4.2b, bottom panel), so continued with GST-chor1 and GST-chor2 only.

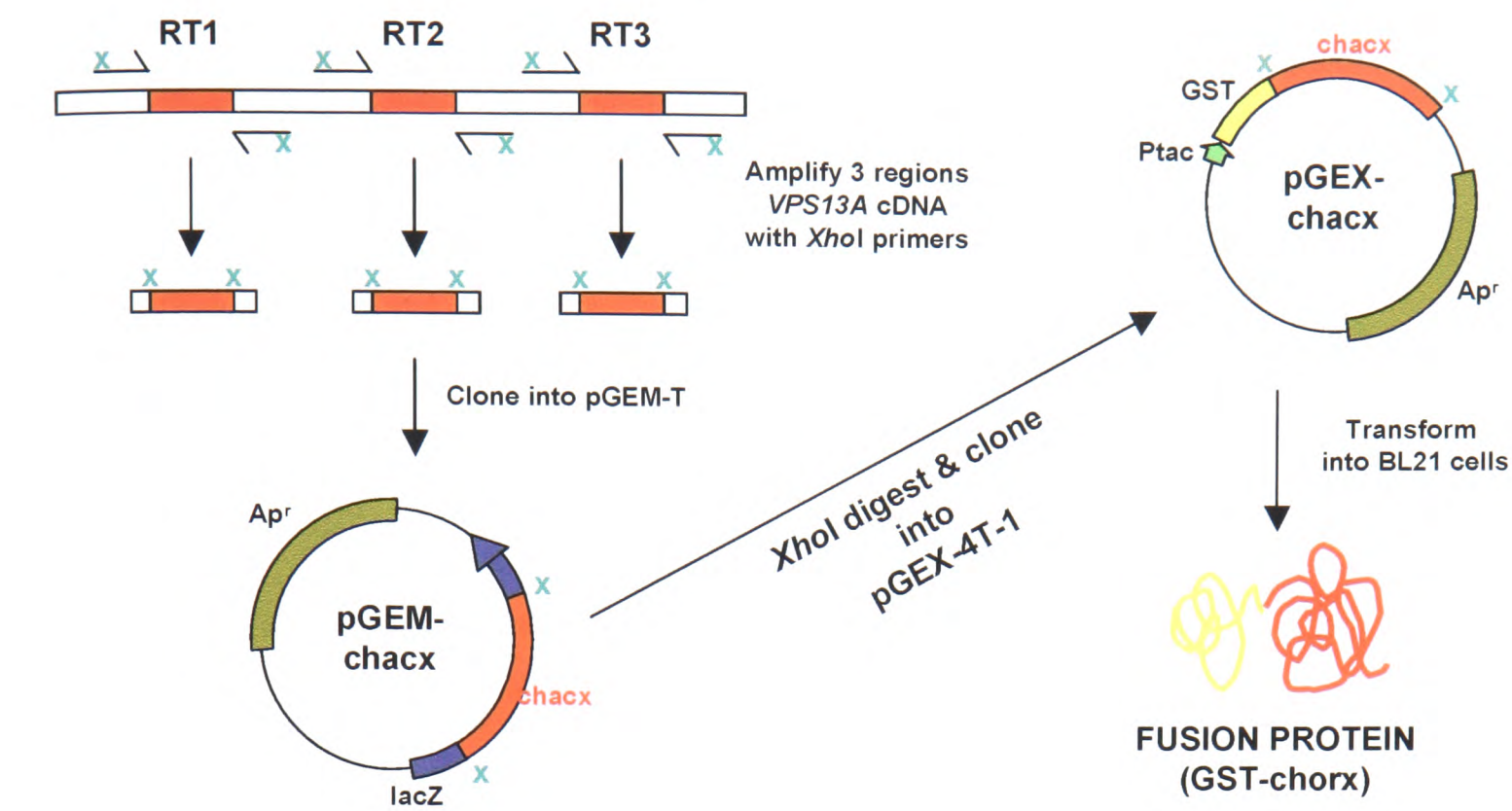

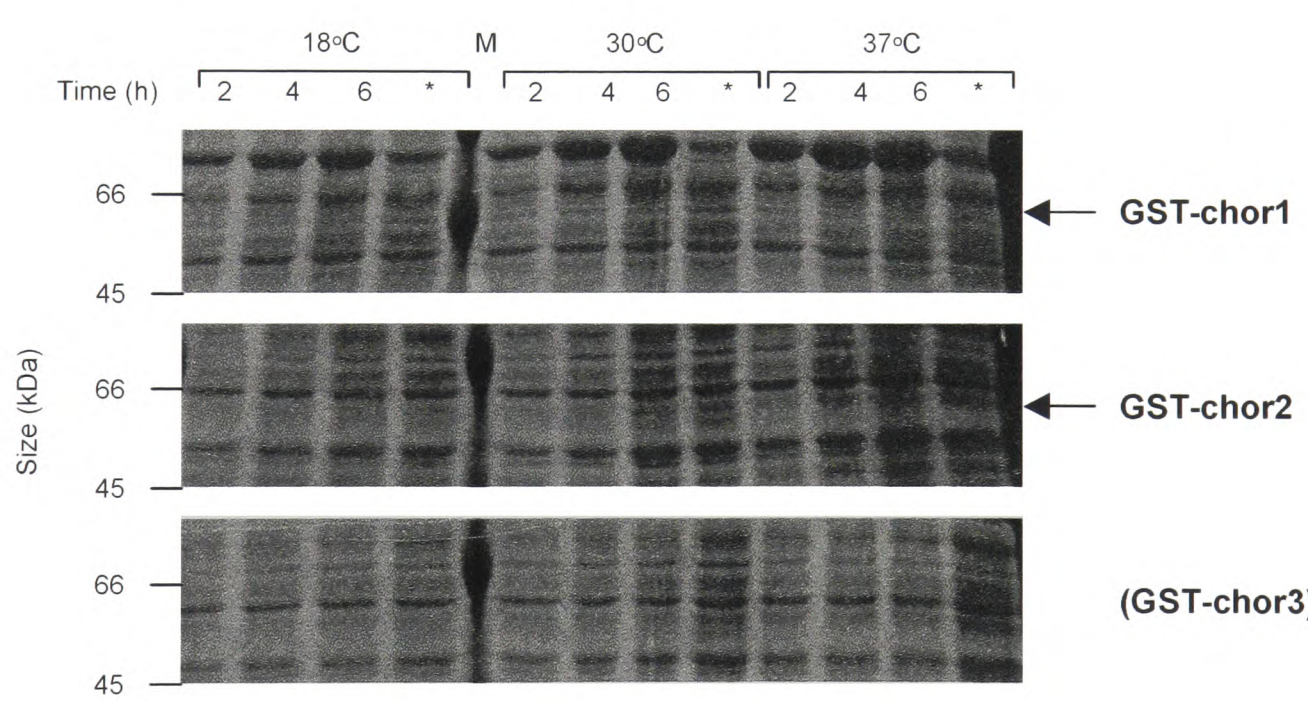

Figure 4.2 - Expression of GST-fusion proteins in bacteria. a, Strategy for construction of pGEX-chac1, pGEX-chac2 and pGEX-chac3 (pGEX-chacx) and expression of GST-chorx. Three regions of *VPS13A* cDNA (RT1, nucleotides 79-978; RT2, nucleotides 3568-4507; RT3, nucleotides 8269-9166) were amplified using primers containing 5' *Xho*I sites (primers: XhoRT1F & -R, XhoRT2F & -R, XhoRT3F & -R; see Appendix 1). Purified PCR products were ligated into the TA cloning vector, pGEM-T. Inserts of the resultant constructs were fully sequenced before being liberated by *Xho*I digestion and ligated into the bacterial expression vector, pGEX-4T1. Ligation junction sequences were sequenced and correct constructs were transformed into BL21 bacteria for IPTG-inducible expression of fusion protein. **b**, Induction trials for GST-chorx expression. Crude bacterial lysates prepared 2, 4 & 6 h after induction at different temperatures were subjected to electrophoresis on a 10% polyacrylamide gel, followed by staining with Coomassie blue. Arrows indicate bands corresponding to GST-fusion protein (predicted molecular weight ~61 kDa).
Key: X, *Xho*I site; Ptac, IPTG-inducible promoter; Amp^r, ampicillin resistance gene; *, 6h uninduced control; M, size marker.

4.2.2 Fractionation of GST-chor1 & -chor2 crude lysates

Overexpression of recombinant protein in bacteria can lead to incorrect folding and aggregation into insoluble inclusion bodies (Frangioni and Neel 1993). Indeed, when I induced expression of chorein fusion protein at 37°C, it was all found in the insoluble fraction (see Figure 4.3a). I therefore investigated the effects of different induction temperatures on the solubility of GST-chor1 and GST-chor2 fusion proteins. I also attempted to influence protein solubility by addition of 6% ethanol upon induction. This is thought to encourage overproduction of chaperones, which can facilitate correct folding of the recombinant protein (Thomas and Baneyx 1997). However, as shown in Figure 4.3b, lowering of induction temperature did not have a measurable effect on GST-chor1 solubility; and when ethanol was added little or no fusion protein was detected. Similar results were obtained with GST-chor2; and even when induced overnight at 16°C, no soluble GST-chor1 or GST-chor2 was detected (data not shown). My next strategy was therefore to solubilise the fusion protein post extraction. As overall levels of GST-chor1 expression were higher than GST-chor2 (Figure 4.2b), I decided to proceed with the former.

4.2.3 Solubilisation and purification of chor1 antigen

To maximise expression of GST-chor1, I induced the pGEX-chac1 transformant culture overnight at 37°C. Solubilisation of the fusion protein by addition of sarkosyl and purification on glutathione-agarose beads was achieved largely as described by Frangioni and Neel (1993). However, it was necessary to include detergent in all bead washing and fusion protein cleavage steps to prevent precipitation of chor1. Duplicate small-scale purifications using 0.01-0.9% sarkosyl, 2% Triton X-100, 2% Tween-20, 2% n-octyl, β-D-glucopyranoside and 1-5 mM DTT in various combinations

established that the optimal post-binding buffer was 0.1% sarkosyl, 1 mM DTT (data not shown). As shown in Figure 4.3c, the eluates (E1-E4) were not entirely pure – as well as chor1, they contained uncleaved GST-chor1 and GST. The estimated purity of the pooled chor1 eluate was 73%: attempts to increase this purity by, e.g., decreasing the thrombin cleavage time, or reincubating the post-cleavage eluate with glutathione-agarose beads, were unsuccessful (data not shown). Sarkosyl, a strong ionic detergent, partially denatures proteins, so its presence may have destabilised the GST-glutathione binding. Eluates E1-E3 (Figure 4.3c) were pooled and used to raise anti-chor1 polyclonal antisera in rabbits SK274 and SK275.

4.3 Testing of anti-chor1 antisera

I initially tested the specificity of the anti-chor1 antisera 59 days post-immunisation by dot blot of chor1 antigen. Comparison with preimmune sera showed that antisera from both rabbits were specific, and able to detect 50 ng of chor1 even when diluted to 1:10000, as shown in Figure 4.4.

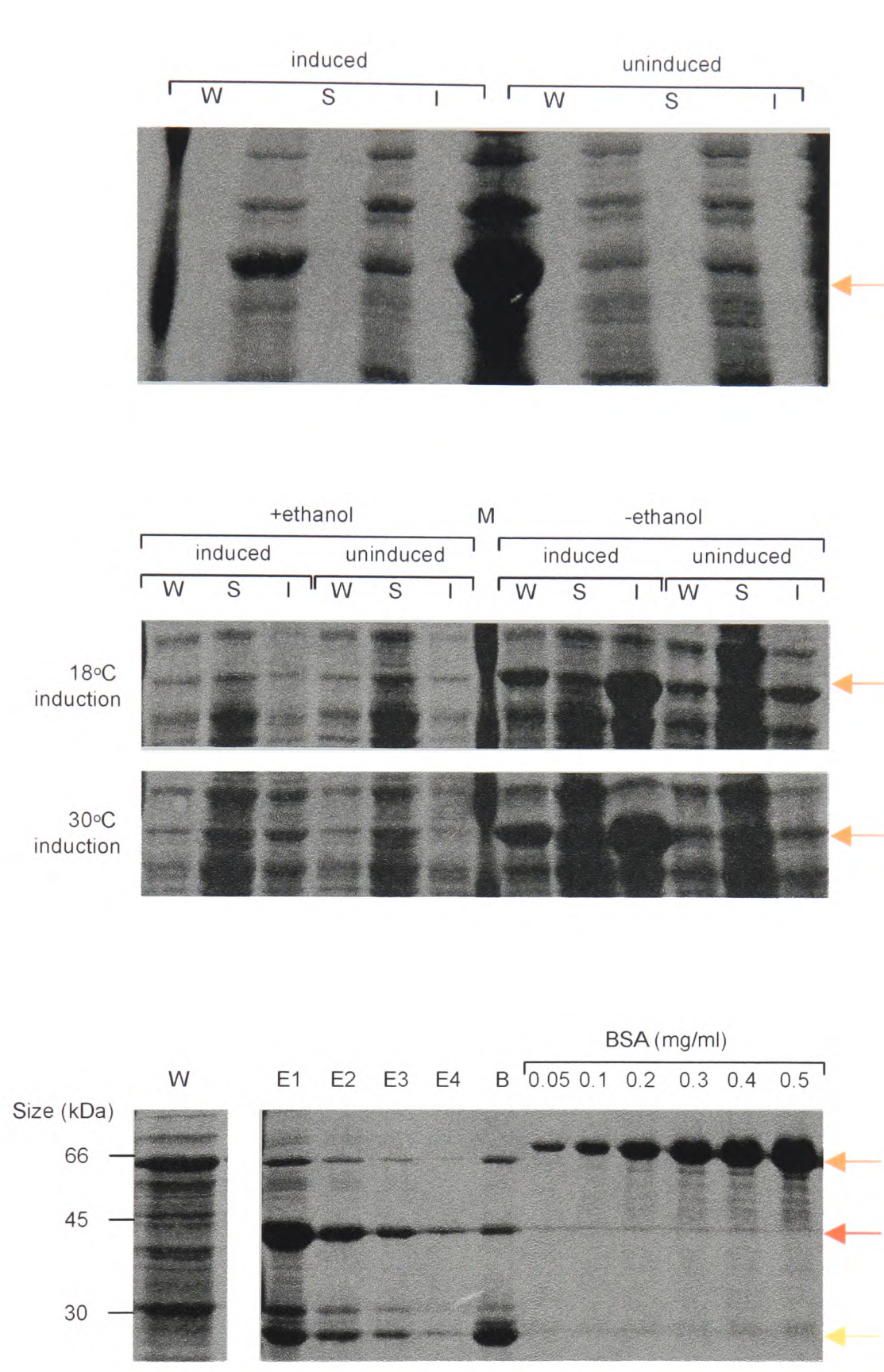

Figure 4.3 - Expression and purification of GST-chor1. Samples were separated on a 10% polyacrylamide gel, followed by staining with Coomassie blue. **a**, Fractionation of recombinant GST-chor1. Bacteria transformed with pGEX-chac1 were grown to log phase and induced at 37 °C for 6 h before being centrifuged: the pellet was separated into soluble and insoluble fractions. **b**, Effect of ethanol and temperature on GST-chor1 solubility. Bacterial cultures were induced for 6 h at 18 or 30°C in the presence (+) or absence (-) of 6% ethanol, and were then fractionated. **c**, Samples from various stages of the purification of chor1 from bacteria expressing GST-chor1 (for details see section 2.12.4). Bands corresponding to GST-chor1, chor1 and GST are arrowed in orange, red and yellow, respectively. Key: W, whole crude bacterial lysate; S, soluble fraction; I, insoluble fraction; E1-E4, eluates 1-4; B, glutathione-sepharose beads post-thrombin cleavage; BSA, bovine serum albumin standards.

Fig 4.3

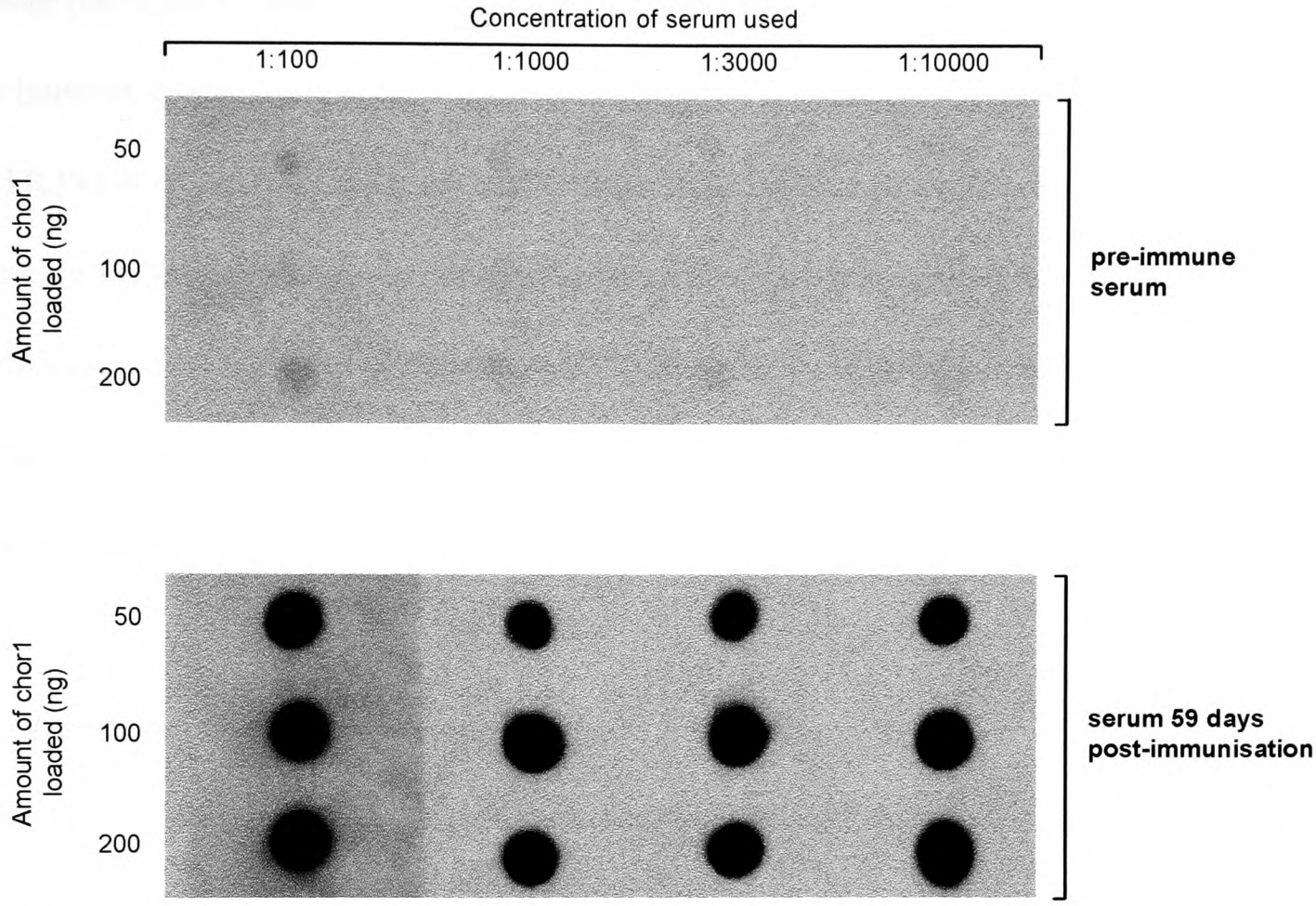

Figure 4.4 - Dot blot analysis of anti-chor1 antiserum. Dot blotting was performed as detailed in Materials and Methods, using pre-immune serum and serum 59 days post-chor1 immunisation, both from rabbit SK274. Similar results were obtained with rabbit SK275 (data not shown).

4.3.1 Detection of exogenous chorein

Figure 4.5a & b shows Western blot analysis of lysates from mammalian cells transfected with different chorein-fusion expression constructs. pcD4e encodes a 47-kDa N-terminal region of chorein. When probed with anti-chor1 antiserum, the insoluble fraction of cells transfected with this construct (Figure 4.5a, lane 3) shows a single band of approximately 50 kDa that is absent in untransfected cells (lanes 1 & 2). FITR293-CAG-1.1 is a cell line stably transfected with a construct encoding full-length chorein fused at its C-terminus to enhanced green fluorescent protein (EGFP). This fusion protein has a predicted Mw of 390 kDa. In these cells, a broad band > 220 kDa was detected by anti-chor1 (Figure 4.5b, lane 1). Interestingly, a slightly smaller band was seen in cells that were not expressing recombinant protein (lanes 2-5).

4.3.2 Detection of endogenous chorein

In order to explore whether the high-molecular-weight band detected in untransfected cells was indeed chorein, I prepared lysates from ChAc patient (P) and control (C) lymphoblastoid cell lines. These were analysed by Western blot using anti-chor1 antiserum, as shown in Figure 4.5c. A band running above the 220-kDa marker was detected in control cells (lane 5) - this is consistent with the predicted molecular weight of chorein, which is 360 kDa. P is the proband from Wave I family CHAC2. As discussed in section 3.1.1, CHAC2 patients are homozygous for the frameshift mutation 1592del that leads to a premature stop codon in exon 17 of the *VPS13A* gene. They are therefore predicted to be unable to express full-length chorein. As Figure 4.5c shows, the high molecular-weight band seen in control cells was absent in P cells (lane 6). This signal was not detected using pre-immune serum (lanes 1 & 2),

or when using serum depleted in chor1-binding antibodies (lanes 3 & 4), thereby confirming the specificity of the detection.

4.4 Purification of anti-chor1 antibody

In an attempt to further increase detection specificity, I purified chor1-binding antibodies from the anti-chor1 antiserum by antigen affinity purification, as shown in Figure 4.6a. Although the purification was successful and the optimum dilution of antibody for endogenous chorein was determined, there appeared to be little difference in specificity between the antibody and the antiserum from which it was purified (Figure 4.6b). Subsequent analyses confirmed this view (data not shown), so we decided to continue using the antisera for Western blot detection.

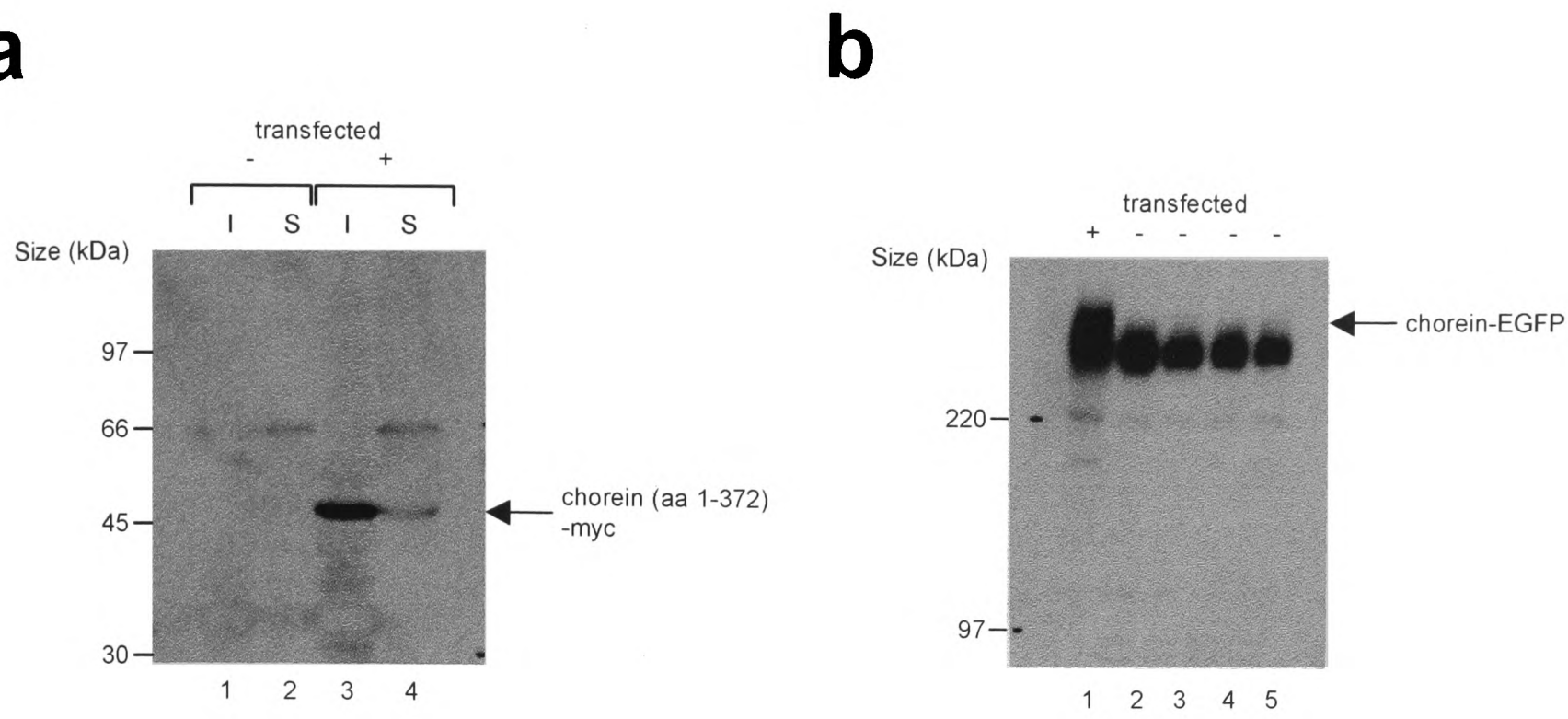

Figure 4.5 - Detection of exogenous and endogenous chorein. **a**, Western blot analysis of transiently-transfected cells. COS-1 cells were either transfected with N-terminal chorein construct pcD4e (+), or were mock-transfected (-). Cell lysates were prepared 48 h post-transfection and subjected to electrophoresis on a 10% polyacrylamide gel. Immunodetection was performed with a 1:30000 dilution of rabbit SK275 serum 59 days post-chor1 immunisation. **b**, Western blot detection of exogenous and endogenous chorein. Lysates were prepared from Flp-In T-Rex 293 cells (Invitrogen) stably transfected with full-length chorein construct (cell line FITR293-CAG-1.1, +), or from untransfected 293T cells (-). Lysates were separated on a 3-8% polyacrylamide gradient gel; immunodetection was performed with a 1:5000 dilution of rabbit SK275 serum 87 days post-chor1 immunisation. Bands corresponding to chorein fusion proteins are arrowed. **c**, Specificity of chorein detection by western blot analysis. 20-μg protein samples from lymphoblastoid cell lines were separated by SDS-PAGE and analysed by western blot. Blots were analysed with preimmune serum (lanes 1 & 2) or anti-chor1 antiserum (lanes 3-6). Anti-chor1 antiserum was either run through a column bound with chor1 antigen to remove chor1-binding antibodies (+, lanes 3 & 4) or left untreated (-, lanes 5 & 6). Immunodetection of early endosome antigen 1 (EEA1) shows equal loading of samples.
Key: I, insoluble fraction; S, soluble fraction; C, healthy control; P, proband of family CHAC2 .

Construct pcD4e and stable cell line FITR293-CAG-1.1 were kindly provided by Antonio Velayos.

a

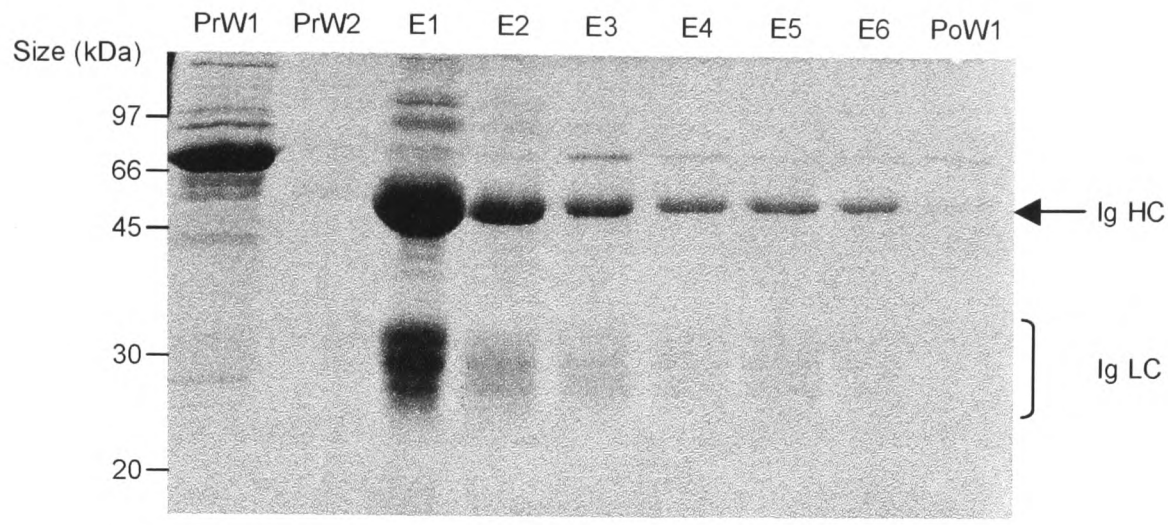

b

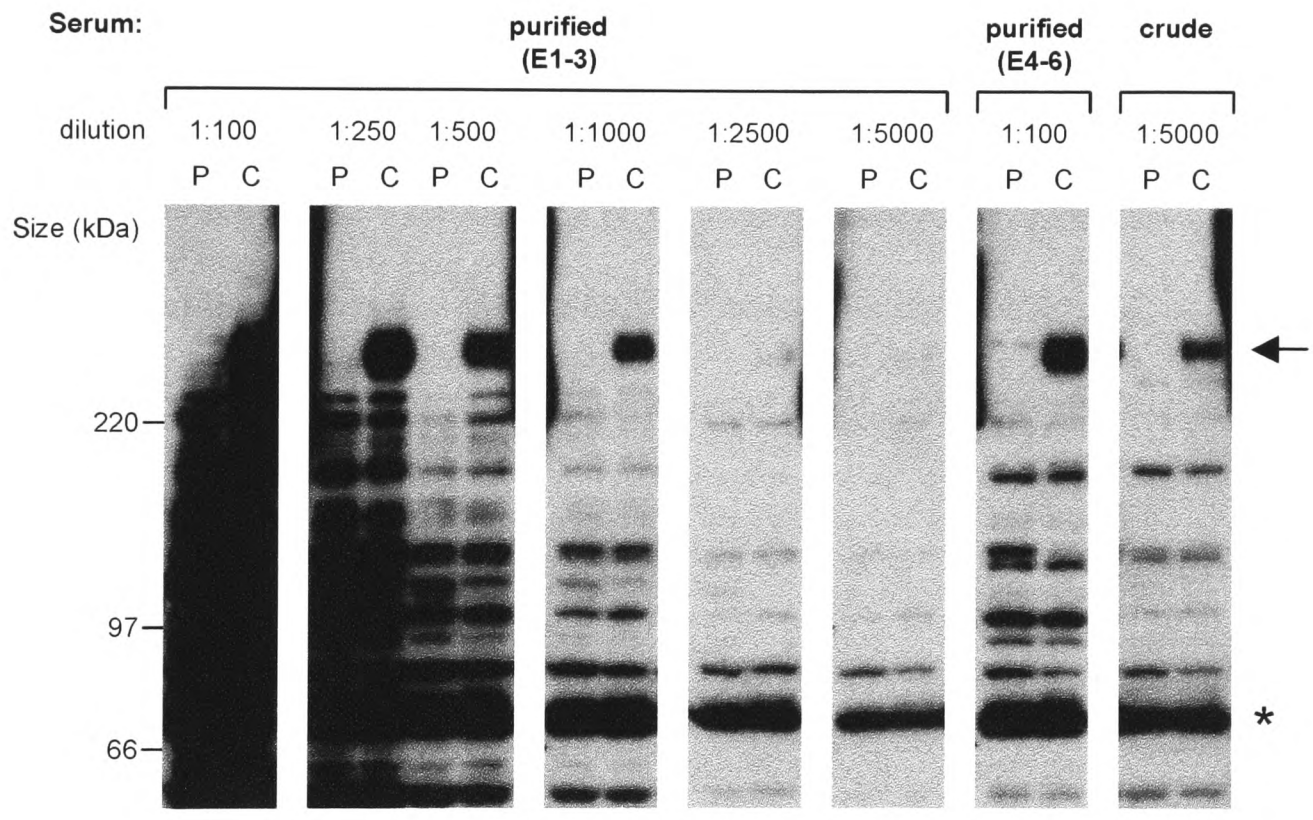

Figure 4.6 - Purification of anti-chor1 antiserum. **a**, Samples from various stages of the purification of anti-chor1 antibodies from rabbit SK274 serum 87 days post-chor1 immunisation. Serum was purified by affinity chromatography using a column containing bound chor1 antigen (details of procedure in section 2.18.3). 16 µl of a 1:10 dilution of pre-elution column wash 1 (PrW1) and neat aliquots of pre-elution wash 2 (PrW2), eluates 1-6 (E1-6) and post-elution column wash 1 (PoW1) were subjected to electrophoresis on a 12.5% polyacrylamide gel, which was then stained with Coomassie blue. Eluates containing purified anti-chor1 antibodies were subsequently pooled into two fractions, E1-3 and E4-6. **b**, Titration of purified E1-3 dilutions for Western blot analysis. Lysates prepared from control (C) and ChAc patient (P) lymphoblastoid cell lines were subjected to electrophoresis on a 3-8% polyacrylamide gel. Immunodetection was performed with different dilutions of E1-3, E4-6 and crude anti-chor1 antiserum. The band corresponding to chorein is arrowed; a ~70-kDa band that cross-reacts strongly with anti-chor1 is asterisked. Optimal dilution of E1-3 appears to be 1:1000. Similar results were obtained for purification of anti-chor1 antibodies from rabbit SK275 antiserum, except that the optimal dilution for E1-3 was 1:2500.

4.5 Analysis of chorein distribution

Lysates were prepared from a variety of cell lines routinely used in tissue culture techniques. Human cell lines were derived from cervical carcinoma (HeLa), foetal lung (MRC-5 SV2), embryonic kidney (293T), lymphoblasts (lymph), neuroglioma (H4), rhabdomyosarcoma (RD), hepatocarcinoma (Hep3B) and myelogenous leukaemia (K562). Lysates were also prepared from two non-human cell lines (COS-7, from African green monkey kidney; and CHO-KI, from Chinese hamster ovary). All 10 cell-line lysates were analysed by Western blot. As shown in Figure 4.7, antichor1 antiserum detects a high molecular weight signal in all cell lines analysed. A much fainter signal was detected in the non-human cell lines (lanes 1 & 2). This implies that these cells express much less chorein than the others do, or that there is less cross-reaction of the non-human chorein homologues with the anti-chor1 antiserum.

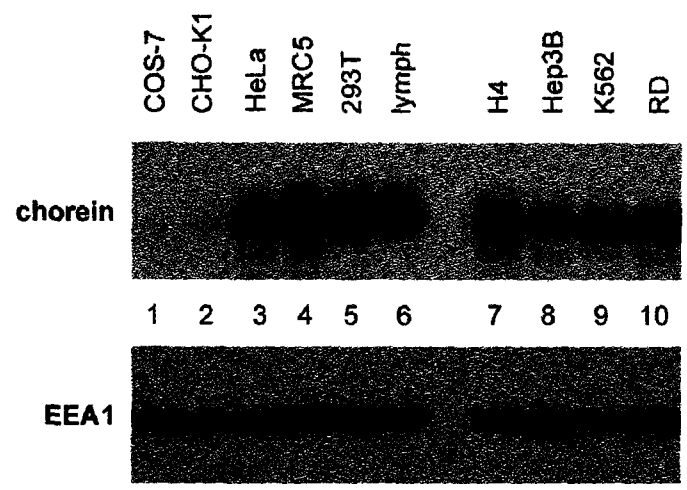

Figure 4.7 - Expression of chorein in different cell types. 20-μg protein samples from different cell lines were separated by SDS-PAGE and analysed by western blot. Cells were derived from African green monkey (lane 1), Chinese hamster (lane 2), or human (lanes 3-10) tissue. Immunodetection of early endosome antigen 1 (EEA1) shows equal loading of samples.

4.6 Expression of mutant chorein

4.6.1 Expression of mutant chorein in ChAc cell lines

Figure 4.8a shows a Western blot of lymphoblastoid protein lysates prepared from individuals from two ChAc pedigrees. As described in section 3.1.1, the affected siblings in the CHAC6 pedigree are homozygous for the missense mutation 4354T>C in exon 37 of *VPS13A*, which results in substitution of a proline for a serine residue at amino-acid position 1452 in chorein. Their unaffected brother is homozygous for the wild type. The affected son in family CHAC11 has inherited the 237del mutation in exon 4 from his mother and the 9429_9432del mutation in exon 72 from his father. In contrast to the unaffected individuals in both pedigrees, CHAC6 and CHAC11 patients (lanes 2, 4 & 7) show a markedly reduced level of chorein expression compared with the control. The complete absence of a corresponding band in the CHAC2 patient (P, lane 1) implies that the weak staining seen in the other patients is indeed chorein and not an unspecific signal. The 237delT mutation in family CHAC11 is predicted to lead to degradation of most of the mutant transcript by nonsense-mediated decay. Any protein that is produced from this allele will be severely truncated (predicted size 10 kDa). The faint signal seen for the proband must therefore derive from truncated protein generated by the 9429_9432del mutation (357 kDa); and/or chorein isoform 1B (345 kDa), which is encoded by exons 1-69 only and is theoretically unaffected by the exon 72 mutation.

As MLS can be difficult to distinguish clinically from ChAc (Danek *et al.* 2004), lymphoblasts from an MLS patient with the *XK* splice-site mutation 508+1G>A (FD in (Ho *et al.* 1994)) were also analysed to determine whether chorein detection could

discriminate between the two disorders. As shown in Figure 4.8a (M1, lane 8), the level of chorein expression in this patient was similar to that of the control.

Chorein expression in ChAc patient and control primary skin fibroblasts is shown in Figure 4.8b. Wave II patient 24 (II-24) is a compound heterozygote for the nonsense mutation S2140X in exon 48 and the frameshift mutation 9190del in exon 70. Expression of chorein in this patient is detectable (lane 1), but markedly reduced when compared with fibroblasts from a healthy control (lane 4). II-11 is heterozygous for the frameshift mutation 1125_1128del in exon 13; this was the only mutation detected upon screening of this patient's *VPS13A* gene (Table 3.2). II-2 is a compound heterozygote for two splice-site mutations: 2288+2T>C in intron 22 and 8472-1G>C in intron 61. Expression of chorein in these latter two patients was undetectable (lanes 2 & 3).

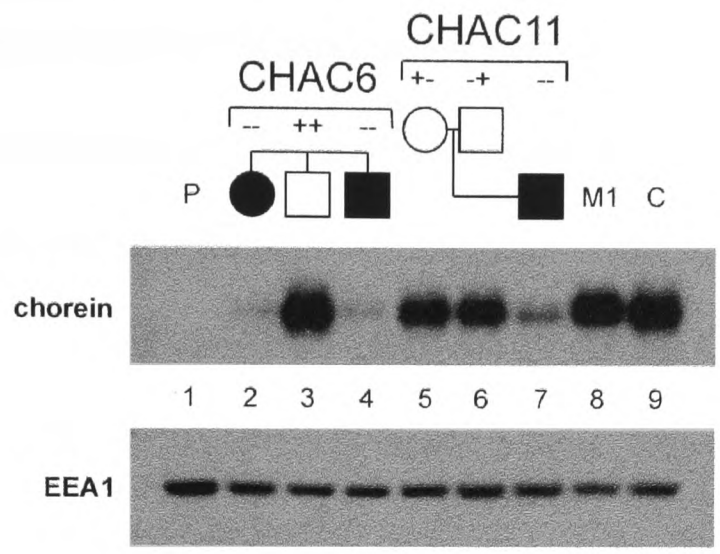

Figure 4.8 - Analysis of chorein expression in ChAc cell lines. **a**, Analysis of lymphoblastoid cell lines. 20-μg protein samples from lymphoblastoid cell lines were separated by SDS-PAGE and analysed by western blot. Cells were derived from family CHAC2 proband (P, lane 1), affected (lanes 2, 4 & 7) and unaffected (lanes 3, 5 & 6) members of CHAC6 and CHAC11 families, an individual with McLeod syndrome (M1, lane 8) and a healthy control (C, lane 9). The *VPS13A* genotype is indicated above CHAC6 and CHAC11 family members (+, wild type; -, mutant allele). Immunodetection of early endosome antigen 1 (EEA1) shows equal loading of samples. **b**, Analysis of fibroblasts. 20-μg protein samples from primary skin fibroblasts derived from ChAc patients (lanes 1-3) and a control (C, lane 4) were separated by SDS-PAGE and analysed by western blot. Immunodetection of early endosome antigen 1 (EEA1) shows equal loading of samples. The panel on the right shows a longer exposure of the anti-chor1 immunoblot.

4.6.2 Expression of chorein in erythrocyte membranes

Erythrocyte membrane fractions were prepared from frozen whole blood from seven unrelated ChAc patients and two healthy individuals (C1 & 2). Blood from an MLS patient (M2), who harbours a hemizygous deletion of *XK* exon 1 (Patient 13 in (Danek *et al.* 2001)), was also used. Blood had been stored at -20°C for different lengths of time, ranging from 8 weeks 4 days (C2) to 159 weeks 5 days (II-23). M2 blood had been stored at -192 °C for 654 weeks 3 days. Western blot analyses of these preparations are shown in Figure 4.9.

The ChAc patients were known to harbour at least one heterozygous mutation likely to disrupt *VPS13A* (Tables 3.2 & 3.3). As shown in Figure 4.9, chorein expression was not detected in erythrocyte membrane preparations from patients III-29, III-33, III-26 and II-23 (lanes 2, 3, 5 & 7). Expression of chorein in patient III-8 was detectable (lane 6), but markedly reduced when compared with controls C3 and C4. Overexposure of the immunoblot revealed a very faint signal corresponding to chorein for patients II-16 & III-7 (data not shown). For patients II-16, III-29 and III-33 the reduction or absence of signal cannot be explained by degradation of the chorein protein during storage, as they were stored for less than, or the same amount of time as, C1. Although their blood was stored for longer, this is also an unlikely explanation for reduced signal in the remaining patients, as evidenced by the integrity of the cross-reacting signal at ~220 kDa. A signal comparable in strength with the controls was observed in the MLS patient (lane 8), even though this blood had been stored for over 12 years.

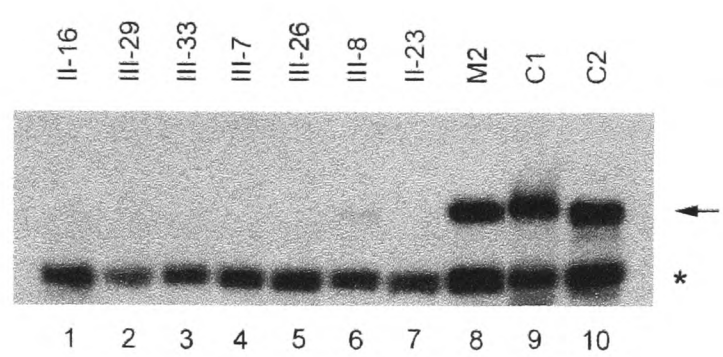

Figure 4.9 - Analysis of chorein expression in red blood cells. Red blood cell membranes were prepared from ChAc patients (lanes 1-7), an individual with McLeod syndrome (M2, lane 8) and healthy controls (C1 & 2, lanes 9 & 10). Membrane preparations were separated by SDS-PAGE and analysed by western blot. The band corresponding to chorein is arrowed - the lower band (~220 kDa, asterisked) probably results from cross-reaction of anti-chor1 with spectrin, the most abundant protein associated with the erythrocyte membrane (Marchesi *et al.*, 1976). Total protein staining of the blot prior to immunodetection demonstrated equal loading of samples (data not shown).

4.7 Summary

This chapter describes the analysis of *VPS13A* gene expression, at both the mRNA and protein levels. mRNA expression was analysed by Northern blot and RT-PCR, and was shown to be ubiquitous. For analysis of protein expression, an N-terminal region of chorein (chor1) was expressed in bacteria and purified. This was used to raise rabbit polyclonal antisera (anti-chor1). Western blot analyses using anti-chor1 suggested that chorein expression was also ubiquitous. However, chorein expression was absent or markedly reduced in lymphoblastoid cell lines, primary fibroblasts and erythrocyte membranes prepared from ChAc patients. In contrast, lymphoblastoid cell lysates and erythrocyte membrane preparations from MLS patients showed chorein levels similar to those of healthy controls.

Chapter 5: Detection of potential chorein-interacting proteins

5.1 Yeast two-hybrid screen of chorein

The yeast two-hybrid (Y2H) system is an *in vivo* technique whereby interactions between two proteins are identified through reconstitution of an active transcription factor (TF) (reviewed in (Toby and Golemis 2001)). Yeast are transformed with two fusion proteins: a TF DNA-binding domain fused to a protein of interest, A (the 'bait'), and a TF activation domain fused to a second protein, B (the 'prey'). If proteins A and B interact, the two domains of the transcription factor are brought together and transcription of reporter genes containing the relevant TF-binding site is activated. This technique can be used to reveal interactions between two known proteins, or to screen proteins encoded by a cDNA library for those that interact with a protein of interest. I used a GAL4 Y2H system from Invitrogen to search for proteins that interact directly with chorein.

5.1.1 Construction of yeast two-hybrid baits

I assembled six Y2H bait constructs containing cDNA fragments encoding chorein amino acids 1-600, 1961-2558, 2550-3174, 495-1096, 993-1597 or 1487-2090, fused to the DNA-binding domain of GAL4 (GAL4DB), according to the scheme illustrated in Figure 5.1a & b. The resultant constructs (pDEST32chacY1-6, respectively) were transformed into yeast and cultures were made of the transformants. Western blot analysis of these cultures revealed that each was expressing a GAL4DB-fusion protein of the appropriate size, although expression levels were variable (Figure 5.1c).

5.1.2 Investigation of potential homotypic interactions

I investigated the possibility that chorein fragments could form interactions with themselves. I constructed six Y2H prey constructs (pDEST22chacY1-6) encoding the same chorein regions as used for the baits, but this time fused to GAL4AD (see Figure 5.2a). Each bait and prey construct pair was transformed into yeast strain MaV203, which contains *HIS3*, *URA3*, and *lacZ* reporter genes. When activated, *HIS3* allows growth on media lacking histidine (-His), *lacZ* results in a blue colour when assayed with X-Gal, and *URA3* permits growth on media lacking uracil (-Ura) but inhibits growth on media containing 5-fluoro-orotic acid (+5FOA). Double transformants were assayed for *lacZ* activity and for growth on the relevant selection media. As shown in Figure 5.2b, no *lacZ* activity was seen, and colonies grew on +5FOA but not on -His or -Ura: this pattern of growth matched that of the negative interaction control.

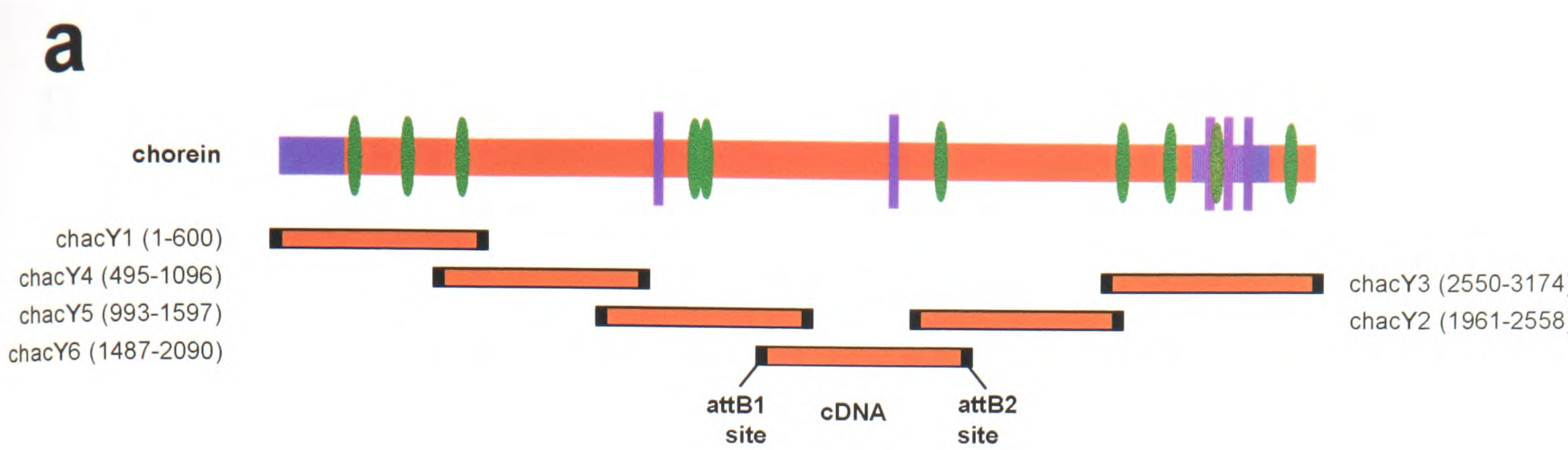

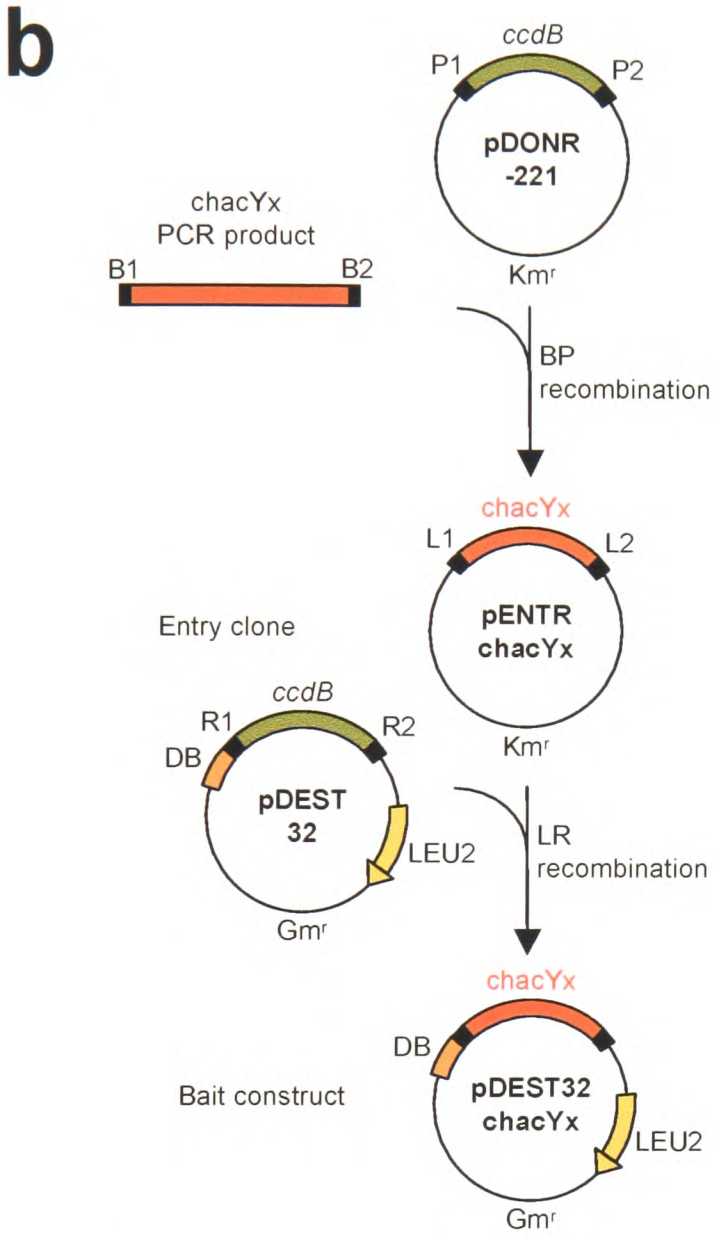

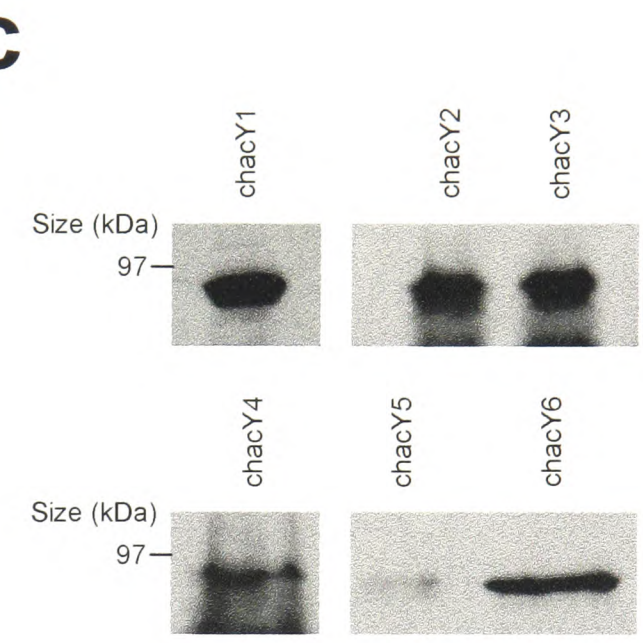

Figure 5.1 - Construction and expression of baits for yeast two-hybrid analysis. a, Schematic representation of chorein primary structure. Regions of high conservation between chorein homologues are indicated in blue; vertical bars indicate putative transmembrane domains; ellipses indicate putative tetratricopeptide repeats (discussed in section 1.8). Horizontal bars below chorein indicate the PCR products amplified from *VPS13A* cDNA for bait construction: the amino acids encoded by each bait are indicated in parentheses. **b**, Strategy for construction of pDEST32chacY1-6. The regions of interest were amplified using PCR primers with 5' attB recombination site sequences (see Appendix 1). Recombination reactions with the PCR products and pDONR vectors generated entry clones pENTRchacY1-6. The gene regions in the entry clones were transferred into the destination vector pDEST32, generating bait vectors pDEST32chacY1-6. Regions B1&2, P1&2, L1&2 and R1&2 are recombination sites. **c**, Western blot analysis of bait fusion proteins. 30 µl of crude cell lysate from yeast transformed with pDEST32chacY1-6 (see section 2.13.1) were subjected to electrophoresis on a 10% polyacrylamide gel. Immunodetection was performed with anti-GAL4 DB antibody.
Key: *ccdB*, inhibitor of DNA gyrase; DB, GAL4 DNA-binding domain; Km^r, kanamycin resistance gene; Gm^r, gentamicin resistance gene; LEU2, gene enabling growth on leucine-deficient media.

Fig 5.1

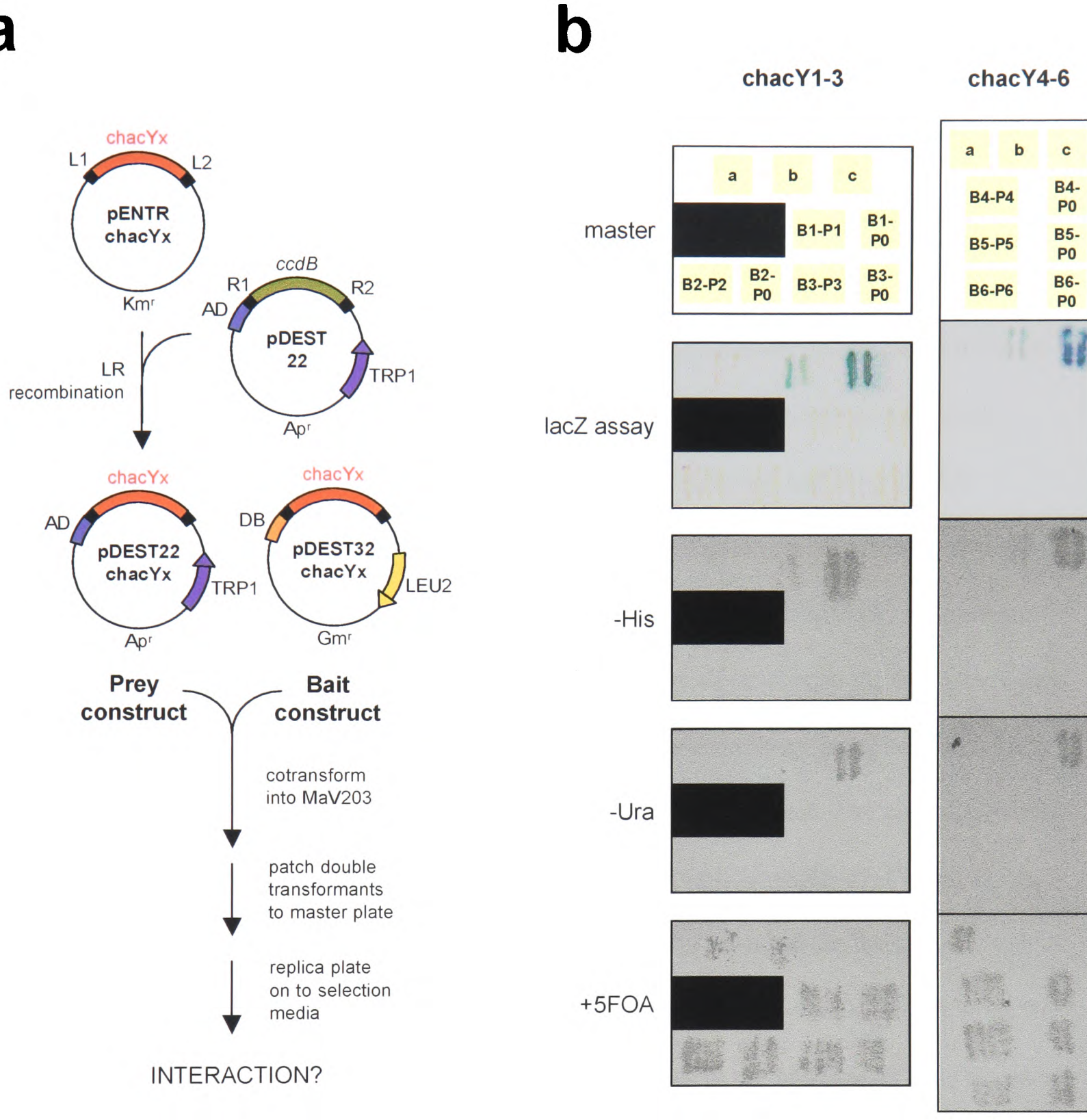

Figure 5.2 - Construction of prey vectors and investigation of homotypic interactions in chorein. a, Strategy for construction of pDEST22chacY1-6. The gene regions in the entry clones pENTRchacY1-6 were transferred into the destination vector pDEST22, generating prey vectors pDEST22chacY1-6. Bait-prey vector pairs were cotransformed into yeast strain MaV203 and double transformants were analysed for induction of reporter gene expression. **b**, Analysis of homotypic interactions. Double transformants were patched on to SC-Leu-Trp media according to the scheme in the top row (master) and incubated for 16 h at 30°C. The patches were then replica plated on to selection media and incubated at 30°C. *lacZ* activity was assayed 24 h after replica plating (second row); growth on -His, -Ura, or +5FOA media was recorded 48 h after replica plating (third, fourth & fifth rows).
Key: *ccdB*, inhibitor of DNA gyrase; AD, GAL4 transactivation domain; DB, GAL4 DNA-binding domain; Km^r, kanamycin resistance gene; Gm^r, gentamicin resistance gene; Ap^r, ampicillin resistance gene; a, negative interaction control; b, 'weak interaction'control; c, 'moderate interaction' control; B1-P1, bait construct pDEST32chacY1 cotransformed with prey construct pDEST22chacY1; B1-P0, pDEST32chacY1 cotransformed with empty prey vector pEXP-AD502.

5.1.3 Yeast two-hybrid library screen

Y2H bait constructs pDEST32chacY1-6 were used to screen an adult human brain cDNA library cloned into the prey vector pEXP-AD502. In each case, over a million clones were screened for chorein-interacting proteins (Table 5.1). Clones that grew on media lacking leucine, tryptophan and histidine (primary positive clones) were patched on to secondary selection media, testing in parallel for activation of all three reporter genes. Clones whose growth patterns implied the presence of a chorein-interacting protein (secondary positive clones) were cultured, and prey cDNA constructs were isolated. These were retested by cotransformation with the relevant bait construct or an empty pDEST32 plasmid into a new MaV203 host. Clones that gave positive results in the new host (tertiary positive clones) were deemed worthy of further investigation. As shown in Table 5.1, only seven tertiary positive clones were identified, all from the screen using pDEST32chacY2 as the bait. The prey constructs isolated from these clones were named pEXP-c1 through to pEXP-c7. (When DNA was isolated from positive clone 4, restriction analysis revealed the presence of two populations of prey constructs - these were called pEXP-c4 and pEXP-c4a.) None of these constructs promoted activation of reporter genes in the absence of chacY2, as shown in Figure 5.3. When cotransformed with pDEST32chacY2, pEXP-c1, -c3, -c5 & -c7 showed weak *lacZ* activation; pEXP-c2, -c4, & -c6 showed very weak activation of *lacZ*. pEXP-c4a did not show detectable *lacZ* activation. Consistent with these results, pEXP-c1, -c3, and -c5 transformants grew well on -His media but poorly on +5FOA media. pEXP-c7 also grew poorly on +5FOA. pEXP-c2, -c4 & c6 transformants grew on -His media; inhibition of growth on +FOA was slight but detectable. pEXP-c4a did not grow on -His media and grew well on +FOA media. Growth on -Ura media, which requires a moderately strong interaction between bait

and prey, was not observed for any test transformant. From these results, it was concluded that pEXP-c1, -c3, -c5 & -c7 constructs encoded probable weak chacY2-interactors, while pEXP-c2, -c4 & -c6 constructs encoded proteins that probably interact very weakly with chacY2. pEXP-c4a was concluded to encode a protein that does not interact with chacY2, and was therefore excluded from further analysis.

Table 5.1 - Number of clones processed in chorein yeast two-hybrid screens

Bait construct	No. clones screened	No. primary positives	No. secondary positives	No. tertiary positives
pDEST32chacY1	4.8×10^6	203[a]	5	0
pDEST32chacY2	4.4×10^6	62	10	7
pDEST32chacY3	4.7×10^6	102	10	0
pDEST32chacY4	3.5×10^6	51	8	0
pDEST32chacY5	1.2×10^6	35	6	0
pDEST32chacY6	4.2×10^6	30	5	0

[a]: The relatively large number of primary positives in this first screen probably doesn't reflect the true total, but rather the increased ability to discard obvious false positives in subsequent experiments.

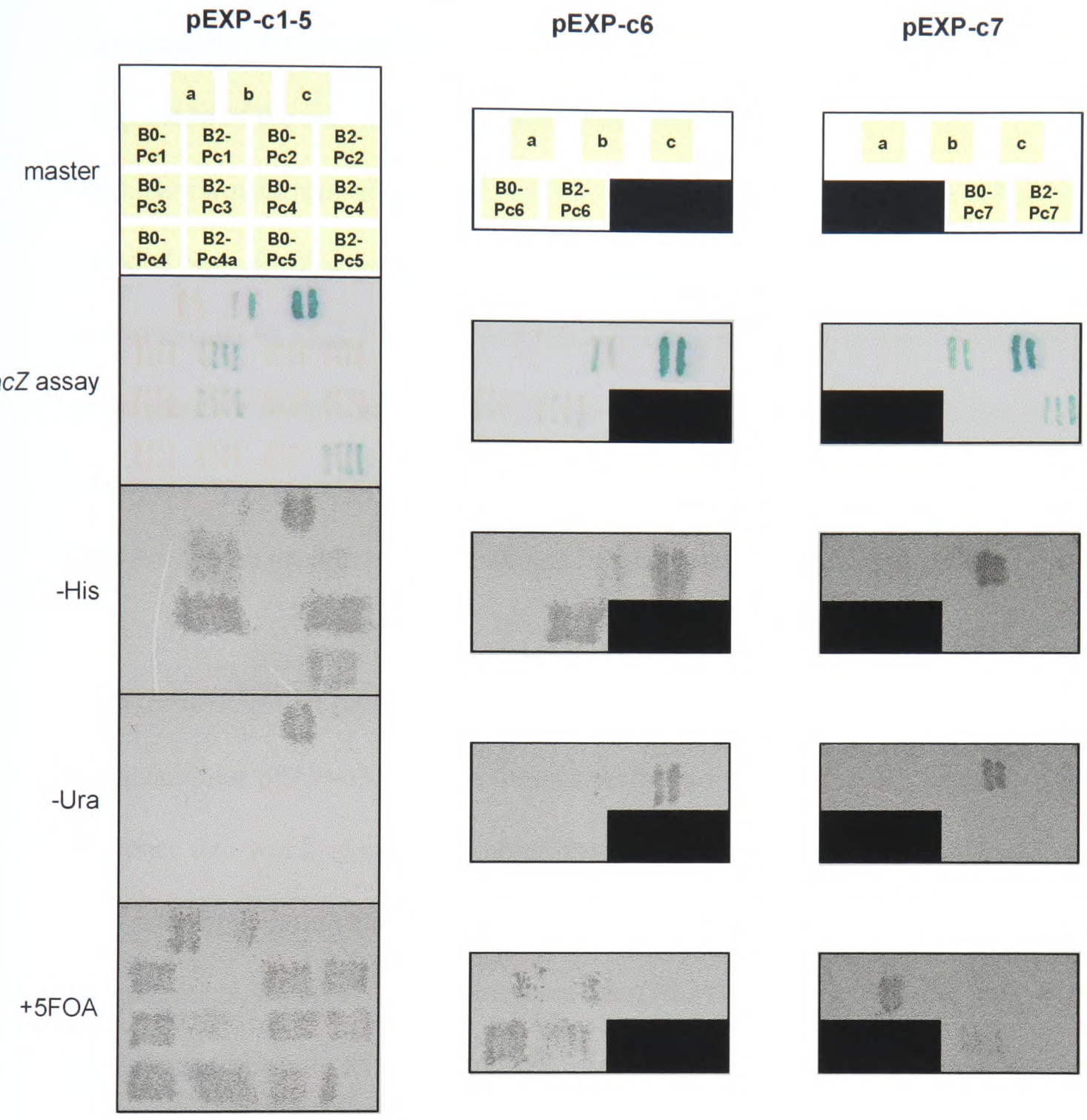

Figure 5.3 - Retransformation assays of secondary positives from chacY2 yeast two-hybrid screen.
Yeast strain MaV203 was cotransformed with bait construct pDEST32chacY2 and putative prey constructs (pEXP-c1 to pEXP-c7). Cotransformation pairs with empty bait construct pDBLeu were used as controls. Double transformants were patched on to SC-Leu-Trp media according to the scheme in the top row (master) and incubated for 16 h at 30°C. The patches were then replica plated on to selection media and incubated at 30°C. *lacZ* activity was assayed 24 h after replica plating (second row); growth on -His, -Ura, or +5FOA media was recorded 48 h after replica plating (third, fourth & fifth rows). Note that pDEST32chacY2/pEXP-c7 cotransformant grew poorly on -H media (third column, third row), but this result was consistent with the poor growth of interaction control B on this plate.
Key: a, negative interaction control; b, 'weak interaction' control; c, 'moderate interaction' control; B0-Pc1, empty bait vector pDBLeu cotransformed with prey construct pEXP-c1; B2-Pc1, bait construct pDEST32chacY1 cotransformed with pEXP-c1.

5.1.4 Characterisation of tertiary positives

The seven Y2H prey constructs that appeared to encode chacY2-interacting proteins were sequenced using pDEST22-specific primers. They were identified by BLAST comparison of the nucleotide sequence in the GenBank database (http://www.ncbi.nlm.nih.gov/BLAST/). I determined that pEXP-c1, -c5 & -c7 encoded part of mitogen-activated protein kinase kinase kinase 7 interacting-protein 2, also known as TAK1-binding protein 2 (TAB2). pEXP-c3, -c4 & -c6 encoded part of the putative protein phosphatase 2C eta (PP2Cη). pEXP-c1 encoded part of the p65 subunit of nuclear transcription factor kappa B (NF-κB). Sequencing revealed that the cDNA for each protein had been cloned in-frame with the GAL4 sequence.

5.1.5 Further Y2H investigation of chacY2 - PP2Cη interaction

Sequencing of pEXP-c3, -c4 & -c6 revealed that all three constructs contained sequence that was largely identical to the predicted ORF of cDNA FLJ39362,[2] apart from a 97-bp deletion and a 64-bp insertion. FLJ39362 bases 723-819 were deleted in the constructs; the insertion occurred between FLJ39362 bases 939 and 940, and corresponded exactly to bases 836-899 of cDNA FLJ32332. The amino-acid sequences predicted for FLJ32332 and FLJ39362 correspond exactly to PP2Cη splicing isoforms 1 and 2, respectively. Two other splicing variants are annotated for this protein - it seems likely that the inserts of pEXP-c3, -c4 & -c6 encode a fifth splicing variant of PP2Cη. In addition, pEXP-c3 contained 350 bases and pEXP-c4 & -c6 contained 320 bases upstream of the predicted initiating codon. This meant that the GAL4AD-fusion protein being expressed included either 117 aa (pEXP-c3) or 107 aa (pEXP-c4 & -c6) that were not predicted to be present in the wild-type protein. The

[2] GenBank accession numbers are reported in Appendix 2.

initial assay results (Fig. 5.3) appeared to show that pEXP-c3 led to stronger activation of *lacZ* transcription than pEXP-c4 & -c6 did. This prompted us to investigate whether the extra N-terminal amino acids predicted to be absent in the wild-type protein were contributing to the observed interaction with chacY2. I assembled a prey construct encoding GAL4AD fused to the first 117 aa only of the clone 3 protein (Figure 5.4a). This construct (pEXP-FLJ5'), along with intact pEXP-c3 & -c4, was cotransformed with pDEST32chacY2, pDEST32chacY1 or pPC97-dDP. Double transformants were assayed for *HIS3* and *lacZ* activity. As shown in Figure 5.4b, only intact pEXP-c3 & -c4 showed activation of reporter genes in combination with chacY2 bait. They did not activate transcription when cotransformed with the spurious bait constructs pDEST32chacY2 and pPC7-dDP. This time, pEXP-c3 and pEXP-c4 transformants showed roughly equivalent levels of *lacZ* activation and growth on -His media.

a

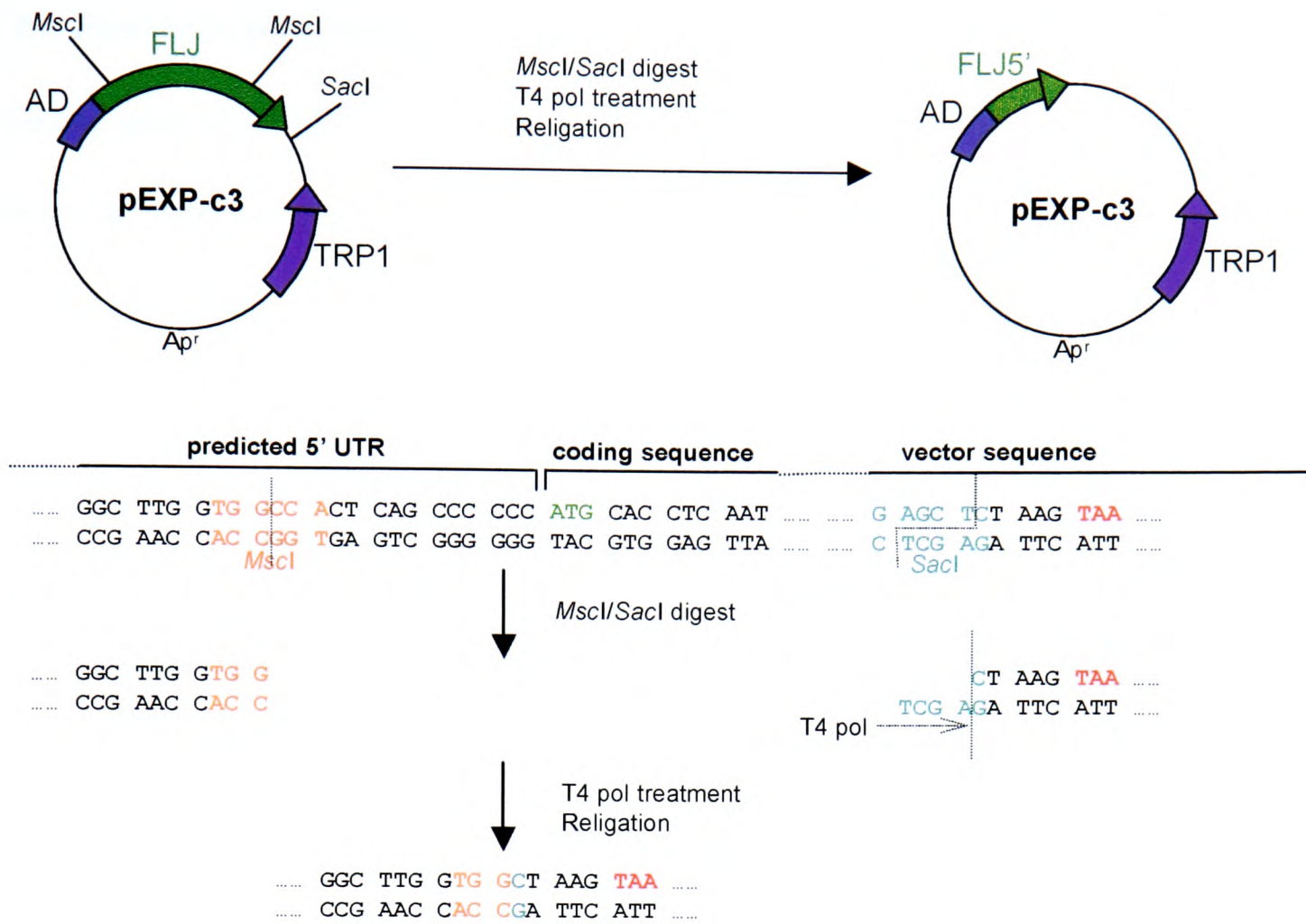

b

Figure 5.4 - Investigation of the interaction between chacY2 and PP2Cη. a, Strategy for construction of pEXP-FLJ5'. Prey construct pEXP-c3 was digested with *Msc*I and *Sac*I to remove the coding sequence of putative protein PP2Cη (the predicted initiation codon is highlighted in green). T4 DNA polymerase (T4 pol) was used to remove the 3' overhang generated by *Sac*I digestion. The fragment was then religated to generate pEXP-FLJ5'. This construct contains only sequence 5' to the putative start site, in frame with a TAA stop codon (indicated in red). **b**, Analysis of interactions between PP2Cη and chacY constructs. Yeast strain MaV203 was cotransformed with prey comprising different regions of PP2Cη cDNA (pEXP-c3, pEXP-FLJ5' or pEXP-c4), and either 'correct' bait pDEST32chacY2 or spurious baits (pDEST32chacY1 or pPC97-dDP). Transformant pairs with empty prey vector were used as controls. Double transformants were patched on to SC-Leu-Trp media according to the scheme in the left-hand panel (master) and incubated for 16 h at 30°C. The patches were then replica plated on to selection media and incubated at 30°C. *lacZ* activity was assayed 24 h after replica plating (middle panel); growth on -His media was recorded 48 h after replica plating (right-hand panel).
Key: Ap^r, Ampicillin resistance gene; AD, GAL4 transactivation domain; a, negative interaction control; b, 'weak interaction' control; c, 'moderate interaction' control; B1-Pc3, bait construct pDEST32chacY1 cotransformed with prey construct pEXP-c3; Bdp-Pf5', bait construct pPC97-dDP cotransformed with prey construct pEXP-FLJ5'; B1-P0, pDEST32chacY1 cotransformed with empty prey vector pEXP-AD502.

Fig 5.4

5.1.6 Further Y2H investigation of chacY2 - NF-κB interaction

Sequence analysis of pEXP-c2 revealed that it contained bases 170-1767 of NF-κB cDNA, encoding amino acids 91-551 of the 551-aa p65 subunit. pEXP-c2 had not shown any activation of reporter genes when transformed with an empty bait vector (Figure 5.3). However, as NF-κB is a transcription factor itself (and the Y2H assay is based on reconstitution of an active TF), we were suspicious that its interaction here was not specific to chacY2. To investigate this possibility, I cotransformed pEXP-c2 with the specific bait construct pDEST32-chacY2 or with the spurious bait constructs pDEST32-chacY1 or pPC97-dDP. As shown in Figure 5.5, only yeast cotransformed with pEXP-c2 and the specific bait displayed significant *lacZ* activity and growth on -His media.

5.2 Investigation of chorein interaction with TAB2

Sequence analysis of prey constructs containing TAB2 sequence revealed that pEXP-c1 and pEXP-c5 contained nucleotides 1125-4359 of TAB2 cDNA, encoding amino acids 318-693; while pEXP-c7 contained a slightly smaller fragment, nucleotides 1182-4355 (amino acids 337-693). This represents the 357 aa at the C-terminus of TAB2. Although two splicing variants have been reported for this cDNA, all clones were derived from splice variant 2 only. I performed co-immunoprecipitation and colocalisation studies in order to further characterise the interaction between TAB2 and chorein.

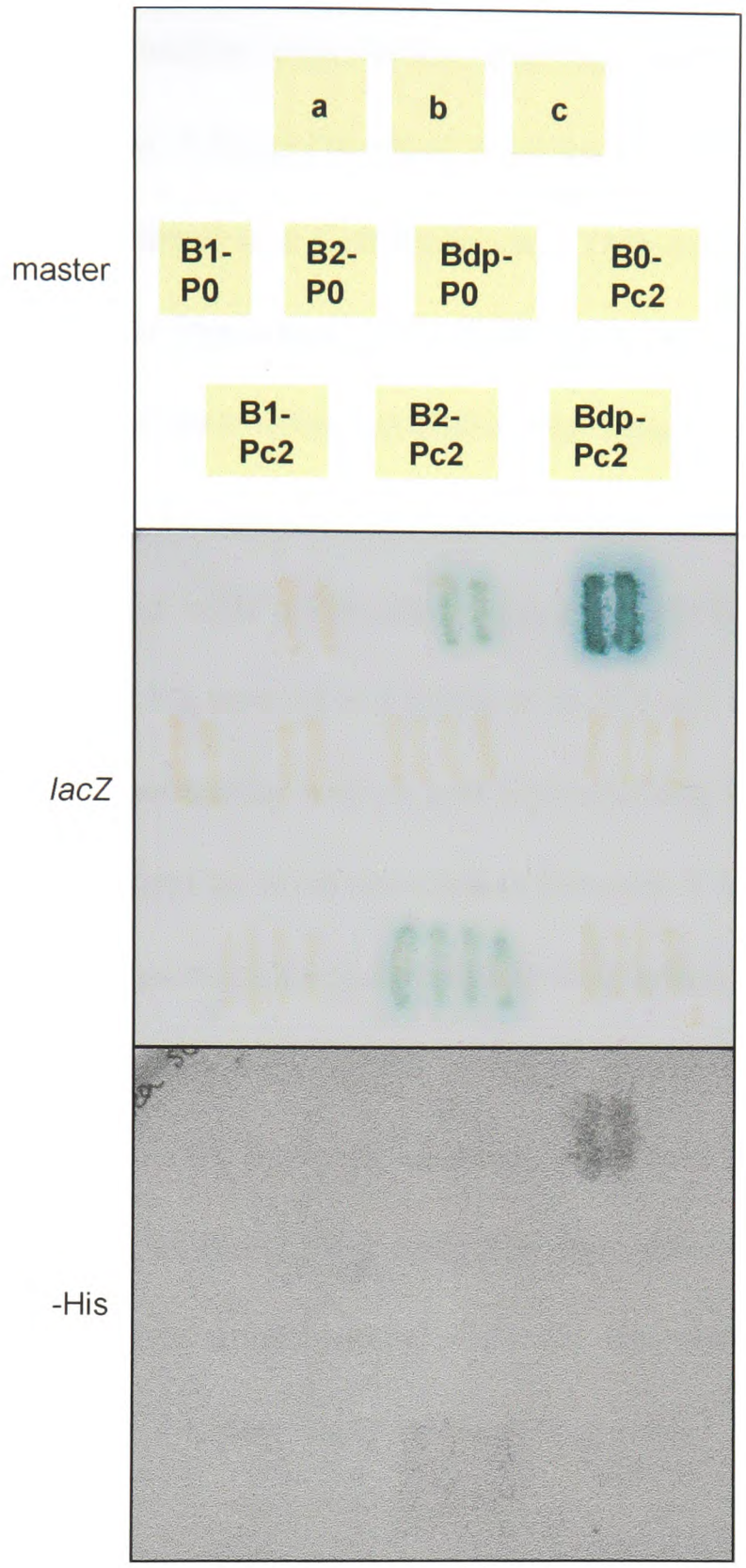

Figure 5.5 - Investigation of the interaction between chacY2 and NF-κB. Yeast strain MaV203 was cotransformed with NF- κB construct pEXP-c2 and either 'correct' bait pDEST32chacY2 or spurious baits (pDEST32chacY1 or pPC97-dDP). Transformant pairs with either empty bait or empty prey vector were used as controls. Double transformants were patched on to SC-Leu-Trp media according to the scheme in the top panel (master) and incubated for 16 h at 30°C. The patches were then replica plated on to selection media and incubated at 30°C. *lacZ* activity was assayed 24 h after replica plating (middle panel); growth on -His media was recorded 48 h after replica plating (bottom panel).
Key: a, negative interaction control; b, 'weak interaction' control; c, 'moderate interaction' control; B1-P0, bait construct pDEST32chacY1 cotransformed with empty prey vector pEXP-AD502; Bdp-P0, bait construct pPC97-dDP cotransformed with pEXP-AD502; B0-Pc2, empty prey vector pDBLeu cotransformed with prey construct pEXP-c2.

5.2.1 Co-immunoprecipitation of chorein and TAB2

I assembled the mammalian expression construct pcD4-chac2 according to the strategy set out in Figure 5.6a. pcD4-chac2 contains the cDNA encoding amino acids 1959-2558 of chorein fused to a C-terminal *myc* epitope, under control of a strong human cytomegalovirus immediate-early (CMV) promoter. pCMVT-TAB2, a kind gift from Kunihiro Matsumoto (Nagoya University, Japan), encodes full-length TAB2 fused to an N-terminal T7 epitope, also under control of the CMV promoter. 293T cells were cotransfected with pcD4-chac2 and pCMVT-TAB2. Cell extracts were immunoprecipitated with a monoclonal antibody to T7, and coprecipitated chac2-myc was detected by immunoblotting with an anti-myc antibody (Figure 5.6b, panels i-iii). These results were suggestive of an association between TAB2 and chac2. However, when the experiment was reversed and immunoprecipitation was performed with anti-myc antibody, coprecipitated T7-TAB2 could be detected even in the absence of chac2-myc (panel iv, lane 3), implying an unspecific interaction directly between T7-TAB2 and the anti-myc antibody. Repeating this experiment gave the same results. In an attempt to gain more unambiguous data for this interaction, I repeated the coimmunoprecipitation, this time using full-length chorein.

a

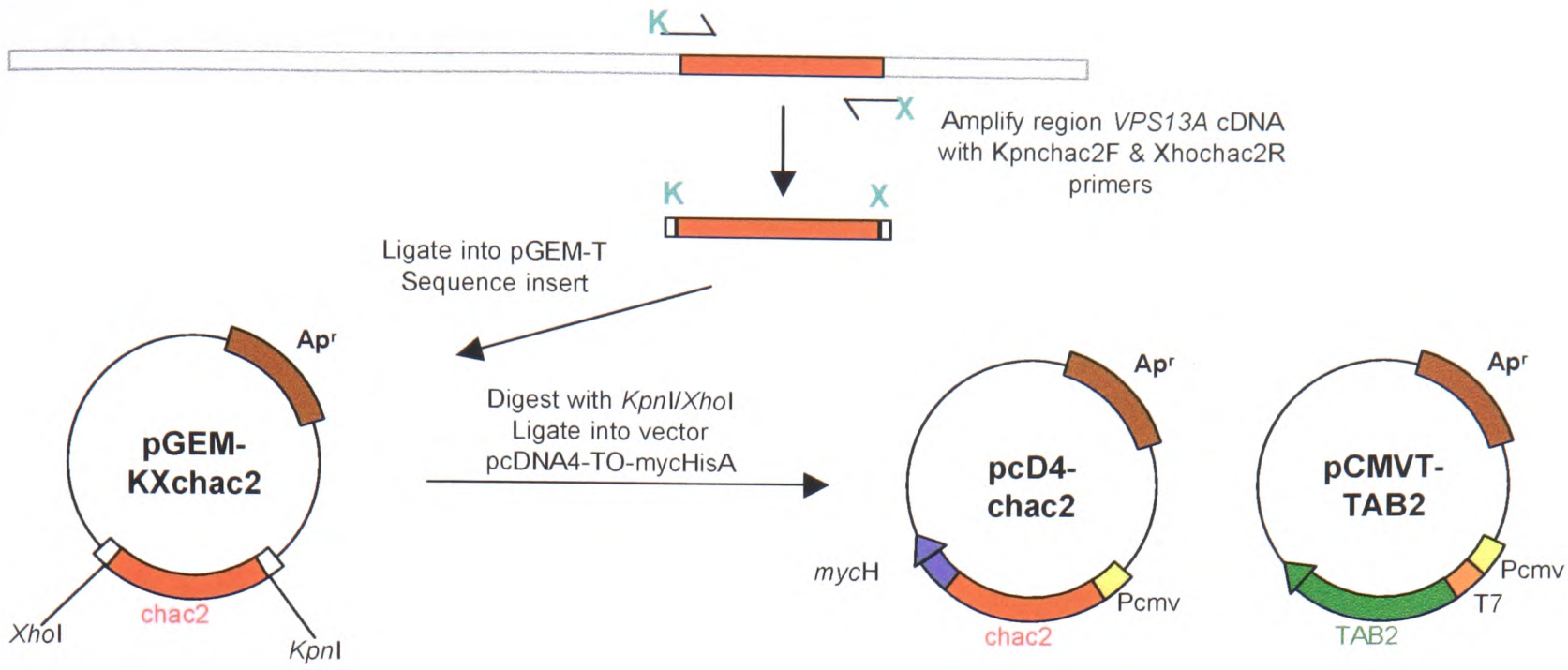

b

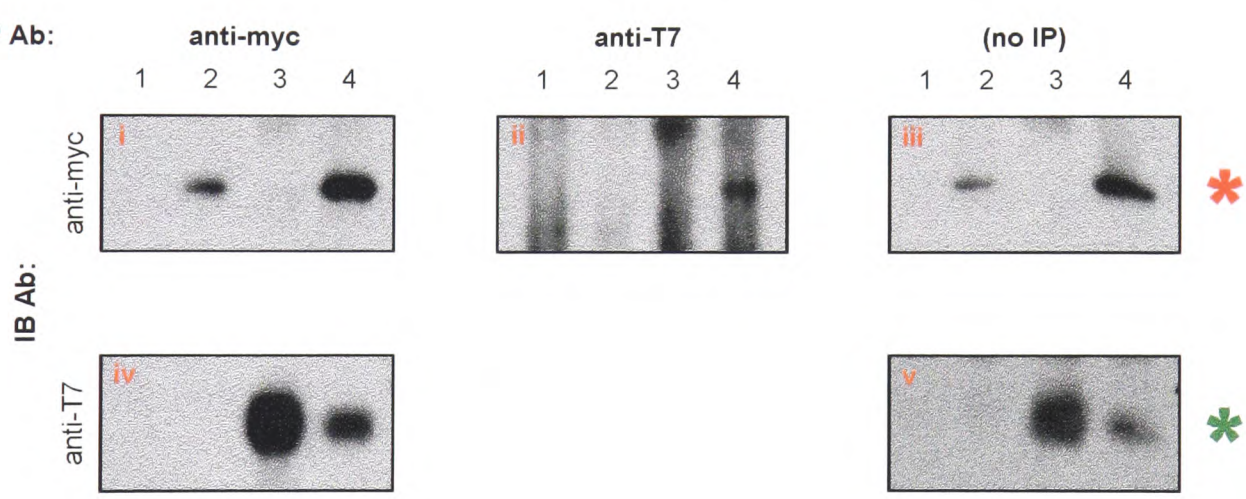

Figure 5.6 - Co-immunoprecipitation of T7-TAB2 and chac2-myc. a, Strategy for construction of pcD4-chac2. The region encoding amino-acids 1959-2558 of chorein was amplified from *VPS13A* cDNA using a forward primer containing a 5' *Kpn*I and a reverse primer containing a 5' *Xho*I site (Kpnchac2F & Xhochac2R: see Appendix 1). Purified PCR products were ligated into the TA cloning vector, pGEM-T. Inserts of the resultant constructs were fully sequenced before being liberated by *Kpn*I/*Xho*I digestion and ligated into the mammalian expression vector, pcDNA4mycHA. Ligation junction sequences were sequenced and correct constructs were used in cotransfection studies with pCMVT-TAB2 (schematic shown on the right). **b**, Coimmunoprecipitation of TAB2 and chac2**.** HEK293T cells were transfected with constructs according to the following schedule: 1 - no constructs; 2 - pcD4-chac2; 3 - pCMVT-TAB2; 4 - pcD4-chac2 & pCMVT-TAB2. Cells were lysed 48h post-transfection and the lysates immunoprecipitated (IP) with anti-myc or anti-T7 antibody. Cell lysate (no IP) and IP proteins were detected by immunoblotting (IB) with anti-myc or anti-T7. Bands corresponding to chac2-myc or T7-TAB2 are asterisked.
Construct pCMVT-TAB2 was kindly provided by K Matsumoto, Nagoya University, Japan.

pcDFchac8 is a mammalian expression vector that encodes full-length chorein fused to a C-terminal FLAG epitope, under control of the CMV promoter (see Figure 5.7a). I cotransfected 293T cells with pcDFchac8 and pCMVT-TAB2. Cell extracts were immunoprecipitated with either an anti-T7 antibody or an anti-FLAG antibody. Coprecipitated chorein-FLAG and T7-TAB2 were detected by immunoblotting with anti-T7 antibody and anti-FLAG antibody, respectively (Figure 5.7b). Chorein-FLAG was found to coprecipitate using anti-T7 antibody only in the presence of T7-TAB2 (panel ii, lane 4). In addition, T7-TAB2 was found to coprecipitate using anti-FLAG antibody only in the presence of chorein-FLAG (panel iv, lane 4).

5.2.2 Immunolocalisation of chorein-FLAG and T7-TAB2

In order to determine the biological significance of the chorein-TAB2 interaction, I investigated the subcellular localisation of exogenous chorein and TAB2. 293T and MRC-5 SV2 cells were cotransfected with chorein-FLAG and T7-TAB2. Immunofluorescence staining revealed that the transfected proteins did not appear to colocalise, as shown in Figure 5.8a. Cells transfected only with T7-TAB2 were also investigated. Immunolocalisation of endogenous chorein using anti-chor1 antiserum gave a high background signal. However, a minority of MRC-5 SV2 cells showed vesicular staining similar to that seen for transfected chorein (Figure 5.8b, panel v): this did not appear to colocalise with transfected T7-TAB2 (panel vi). Unfortunately, in the absence of an anti-TAB2 antibody, it was not possible to determine the subcellular localisation of endogenous TAB2.

a

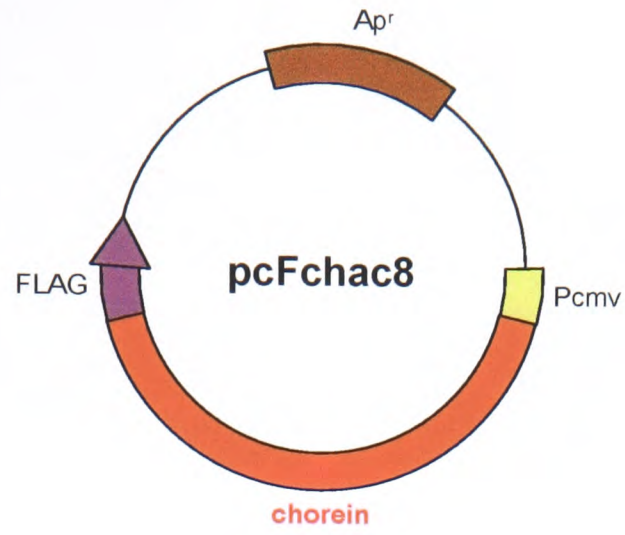

b

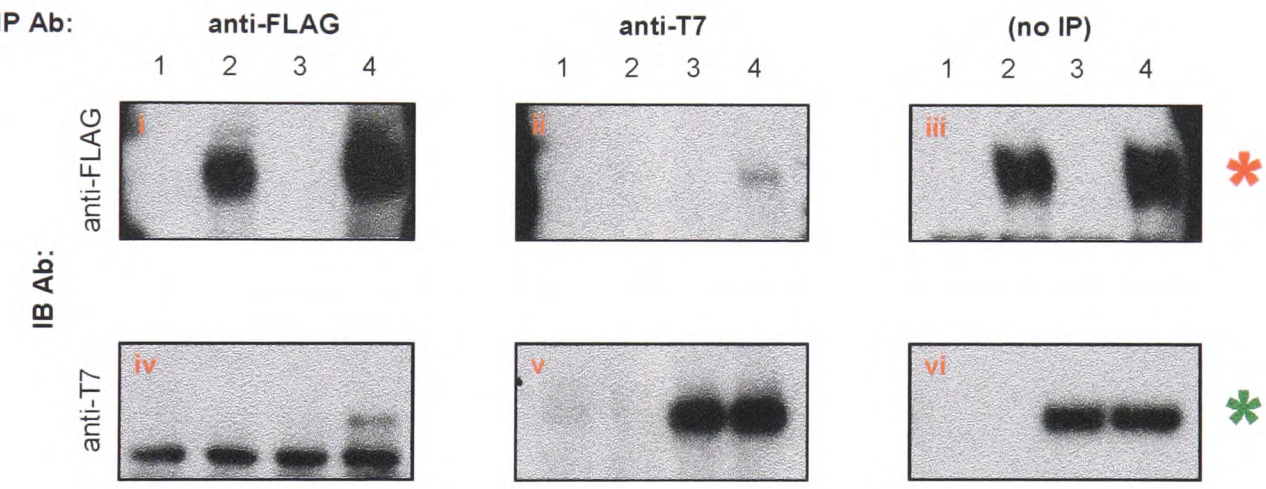

Figure 5.7 - Co-immunoprecipitation of T7-TAB2 and chorein-FLAG. a, Schematic of the mammalian expression vector pcFchac8, encoding full-length chorein fused to a C-terminal FLAG epitope, under control of a CMV promoter. For schematic of pCMVT-TAB2, see Figure 5.6a. **B,** Coimmunoprecipitation of TAB2 and chorein. HEK293T cells were transfected with constructs according to the following schedule: 1 - no constructs; 2 - pcFchac8; 3 - pCMVT-TAB2; 4 - pcFchac8 & pCMVT-TAB2.
Cells were lysed 48 h post-transfection and the lysates were immunoprecipitated (IP) with anti-FLAG or anti-T7 antibody. Cell lysate (no IP) and IP proteins were detected by immunoblotting (IB) with anti-FLAG or anti-T7. Bands corresponding to chorein-FLAG or T7-TAB2 are asterisked.
Construct pcFchac8 was kindly provided by A Velayos.

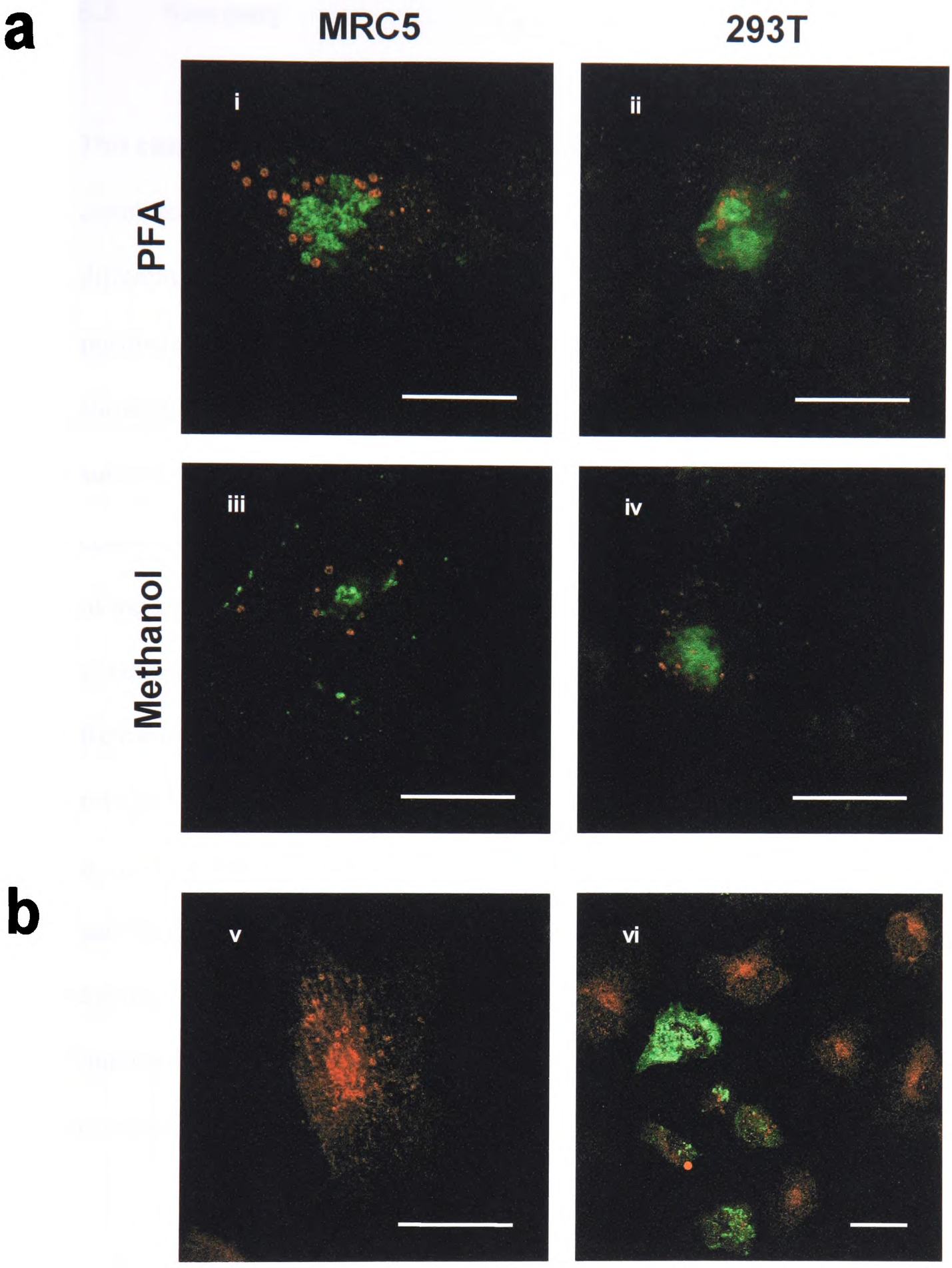

Figure 5.8 - Subcellular localisation of TAB2 and chorein. a, Localisation of T7-TAB2 and chorein-FLAG. MRC5.V2 (i & iii) and HEK293T (ii & iv) cells were grown on a coverslip and cotransfected with pcFchac8 and pCMVT-TAB2. Forty hours post-transfection, cells were fixed by incubation in 4% paraformaldehyde (PFA, panels i & ii) or methanol (iii & iv). **b, Localisation of T7-TAB2 and endogenous chorein**. MRC5.V2 cells were mock transfected (v) or transfected with pCMVT-TAB2 (vi). Forty hours post-transfection, cells were methanol-fixed.

Rabbit anti-FLAG (**a**) or rabbit anti-chor1 (**b**) and mouse anti-T7 (**a** & **b**) antibodies were used, followed by secondary staining with Alexa Fluor 594-conjugated goat anti-rabbit (red) and Alexa Fluor 488-conjugated goat anti-mouse (green). Cells were viewed by confocal fluorescent microscopy. Scale bar, 20 μm.

5.3 Summary

This chapter describes the search for proteins that may interact with chorein. This was attempted via a yeast two-hybrid screen of a human brain cDNA library, using six different regions of chorein (chacY1 - chacY6) as bait. After elimination of false positives, only seven independent prey constructs (pEXP-c1 - pEXP-c7) remained, all showing a putative interaction with chacY2. pEXP-c2 encoded a region of the p65 subunit of NF-κB: although this is itself a transcription factor, retransformation of this construct with spurious baits implied that this positive was unlikely to be an artefact of the assay. pEXP-c3, -c4 & -c6 encoded part of a putative protein phosphatase and contained some sequence predicted to be upstream of the initiating codon. Retransformation assays with a construct containing only this upstream sequence revealed that this region was not responsible for the chacY2 interaction. pEXP-c1, -c5 & -c7 encoded a C-terminal region of TAB2, a protein that interacts with mitogen-activated protein kinase kinase kinase 7. Coimmunoprecipitation studies in mammalian cells supported an interaction between TAB2 and chorein. However, immunofluorescent microscopy of cells expressing epitope-tagged chorein and TAB2 revealed that these exogenous proteins did not appear to colocalise.

Chapter 6: Discussion

6.1 Mutational analysis of *VPS13A*

6.1.1 VPS13A *is the gene mutated in chorea-acanthocytosis*

This laboratory previously located the *VPS13A* locus to a 6-cM region on chromosome 9q21-q22, in a genomewide scan of 11 families with ChAc (Rubio *et al.* 1997). After identification of a novel gene, *VPS13A*,[3] in the ChAc critical region, we initially searched for *VPS13A* mutations in these 11 families (Wave I, (Rampoldi *et al.* 2001)). We found 16 different mutations, identifying at least one mutation in each family. Every mutation co-segregated with the disease haplotype, as confirmed by sequencing or restriction analysis of family members. Of these mutations, 12 lead to a PTC, and are therefore likely to severely disrupt gene function: this demonstrates that *VPS13A* is the gene that, when mutated, causes ChAc.

We followed up this initial analysis with two additional mutation screens of 43 (Wave II, (Dobson-Stone *et al.* 2002)) and 29 (Wave III) unrelated ChAc probands. In total, we have identified 88 different mutations likely to cause chorea-acanthocytosis in 72 pedigrees. Seventy-six of these disease mutations were only identified in a single family each, indicating a strong allelic heterogeneity with no single mutation causing the majority of ChAc cases in the population. For 11 probands in this study with typical symptoms, no disease mutations in *VPS13A* were detected. As mentioned previously (section 1.5.2), a pedigree with autosomal dominant inheritance of a

[3] Originally reported as *CHAC* (Rampoldi *et al.*, 2001)

ChAc-like phenotype was found to be associated with the Huntington's disease-like-2 expansion in the *junctophilin-3* gene (Walker *et al.* 2003). We therefore screened for this expansion in all ChAc probands in this study without identified *VPS13A* mutations: however, all allele sizes observed were within the wild-type range (data not shown).

As there is little evidence for additional locus heterogeneity of ChAc, it could be that the 'missing' mutations are located within the 5' or 3' UTRs, or within intronic sequences not screened in this study; deletions and rearrangements preventing amplification of one allele will also not be detected with our screening method. For the 12 probands with only one heterozygous mutation detected, this is almost certain to be the case. Since seven deletions of entire exons have already been identified ((Ueno *et al.* 2001) and work described in this thesis) and the *VPS13A* gene is spread over such a large genomic region (about 240 kb), it is conceivable that many ChAc patients could harbour heterozygous deletions. Such deletions will only be detected by comprehensive Southern blot analysis of the entire gene or quantitative PCR.

6.1.2 Mode of inheritance of ChAc

Although the majority of reported ChAc pedigrees are consistent with autosomal recessive inheritance, a few studies have reported autosomal dominant (AD) inheritance of ChAc (Levine *et al.* 1968; Marson *et al.* 2003; Saiki *et al.* 2003). In this study, two ChAc pedigrees with apparent AD inheritance were analysed (II-5 & II-8). In family II-8, we found that the father, who displayed some mild dyskinesia, was homozygous for the splicing mutation (9474G>A) he passed on to his affected daughter (Figure 3.2b). Perhaps this mutation permits some correct splicing of

transcript and it is only in combination with an additional mutation (observed in proband II-8) that the full-blown ChAc phenotype is seen. In family II-5, we found that the proband and his affected mother and sister were all homozygous for the same nonsense mutation (Figure 3.2a). The mother and father are first cousins - the mutation results, coupled with haplotype analysis showing homozygosity of the *CHAC* critical region in the mother (data not shown) imply that the maternal grandparents were also related. Therefore, both families in fact display pseudodominant inheritance. Saiki *et al.* (2003) found that the proband and her affected sibling in an AD ChAc pedigree were heterozygous for a splicing mutation in *VPS13A* exon 57, which was absent in the unaffected mother. They were not able to screen the presumptively affected father. It is therefore conceivable that, as in II-8, the father was homozygous for this mutation, an additional undetected mutation being inherited from the heterozygous mother. By extension, pseudodominant inheritance is a possible explanation for other cases of apparent AD transmission: this highlights the need for careful genetic analysis of all such pedigrees.

6.1.3 VPS13A *mutation distribution*

Figure 6.1 shows that there does not seem to be any 'clustering' of mutations identified in *VPS13A* so far. However, conclusions can be drawn about the relative importance of its various splice forms. As mentioned previously (section 1.7.3), the two main splice forms as identified by expressed sequence tag analysis are isoform 1A, the result of splicing exons 1-68 and 70-73; and isoform 1B, from exons 1-69 only. Ten mutations in this study (Tables 3.1-3.3) are predicted to affect only transcript 1A. Four probands are in fact homozygous for transcript 1A-specific mutations: probands II-42, III-6 & III-24 (deletion of exons 70-73) and proband III-18 (a 2-bp deletion in exon 72). Given that these patients display symptoms typical for ChAc, we can deduce that isoform 1B, and other splice forms lacking exons 70-73, cannot compensate for absence of full-length chorein in this disorder.

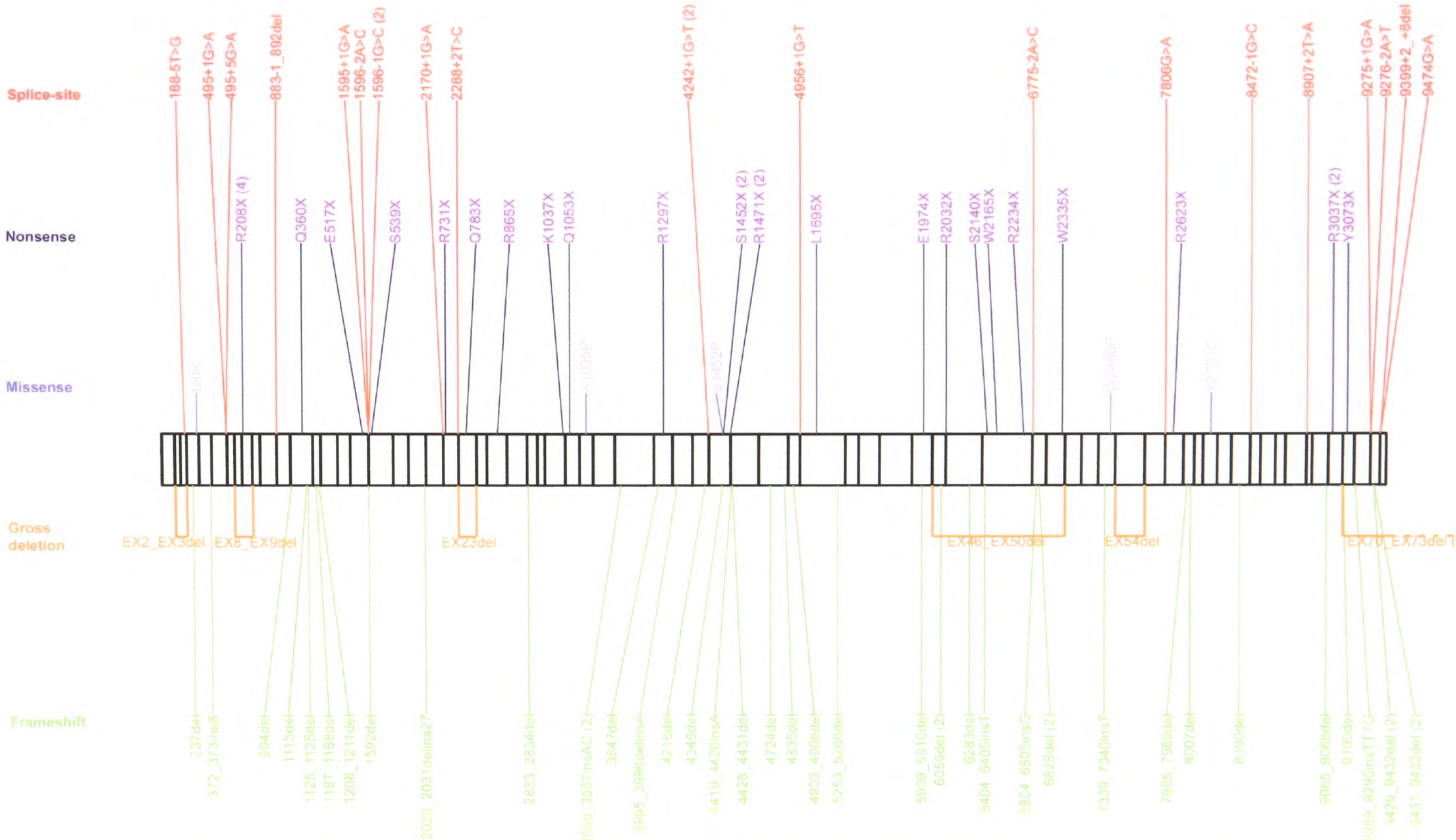

Figure 6.1 - Spectrum of *VPS13A* mutations identified in this study. The coding sequence of *VPS13A* transcript 1A is illustrated in the middle, with exon junctions indicated by vertical lines. The number of probands in which identical mutations were identified is shown in parentheses.

Fig 6.1

6.1.4 Recurrent VPS13A *mutations*

Twelve mutations reported here were found in multiple probands within this study, as shown in Table 6.1. Probands II-12 and II-39 are heterozygous and II-27 is homozygous for the mutation 622C>T (R208X), which was also found in Wave I family CHAC3. Family CHAC3 and proband II-12 both originate from Italy and so it is conceivable that their mutation was inherited from a common ancestor. However, II-27 originates from Japan and II-39 has inherited the mutation from a Danish mother. As it is unlikely that these individuals are related to the other pedigrees, it seems logical to conclude that the 622C>T mutation has arisen at least three times independently. Supporting this hypothesis is the fact that the cytosine involved is part of a CG dinucleotide and as such is especially vulnerable to methylation and spontaneous deamination to thymine (Cooper and Youssoufian 1988). The same explanation is appropriate for the probable recurrence of the 9109C>T (R3037X) mutation in the Mexican family CHAC7 and the German proband II-1, and the 4411C>T (R1471X) mutation in Japanese II-26 and Italian III-3. This mechanism may also explain the overrepresentation of R>X substitutions in this study (9/22 nonsense mutations). Proband II-34 and CHAC11 both originate from the UK and therefore inheritance of the 9429_9432del allele from a common ancestor cannot be ruled out. The deletion is of the tetranucleotide AGAG within the tandem repeat AGAGAG, however, and so it is plausible that this mutation has arisen twice through replication slippage. The existence of a smaller deletion within the same region in II-29 & III-18 (9431_9432del, deletion of the dinucleotide AG) supports the latter hypothesis. The duplication of the dinucleotide AC in the mutation shared by the North American CHAC4 family and Mexican III-31 (3557_3558insAC) may have arisen by the same mechanism.

The shared geographical origin of most of the remaining probands with identical mutations suggests that these have been inherited from common ancestors. We could not perform haplotype analysis on certain probands in this study, so it was not possible to determine unambiguously whether they are related. However, haplotype analysis of the French Canadian families of II-42, III-6 and III-24, each harbouring a homozygous deletion (EX70_73del), revealed that the affected individuals were homozygous for a common haplotype spanning ~4 cM around *VPS13A* (haplotype A in Figure 6.2). French Canadian proband III-11 and her affected sister, both homozygous for the 4242+1G>T mutation, are homozygous for a different haplotype, as expected (haplotype B in Figure 6.2). However, two affected brothers in a different branch of the family are heterozygous for haplotypes A & B. This implies that these two brothers, who show classic symptoms of ChAc despite having only one copy of the 'family' mutation 4242+1G>T, may be heterozygous in addition for the EX70_73del mutation. Efforts are now being made to develop a junction PCR to amplify across the exon 70-73 deletion and unequivocally determine whether this is indeed the case.

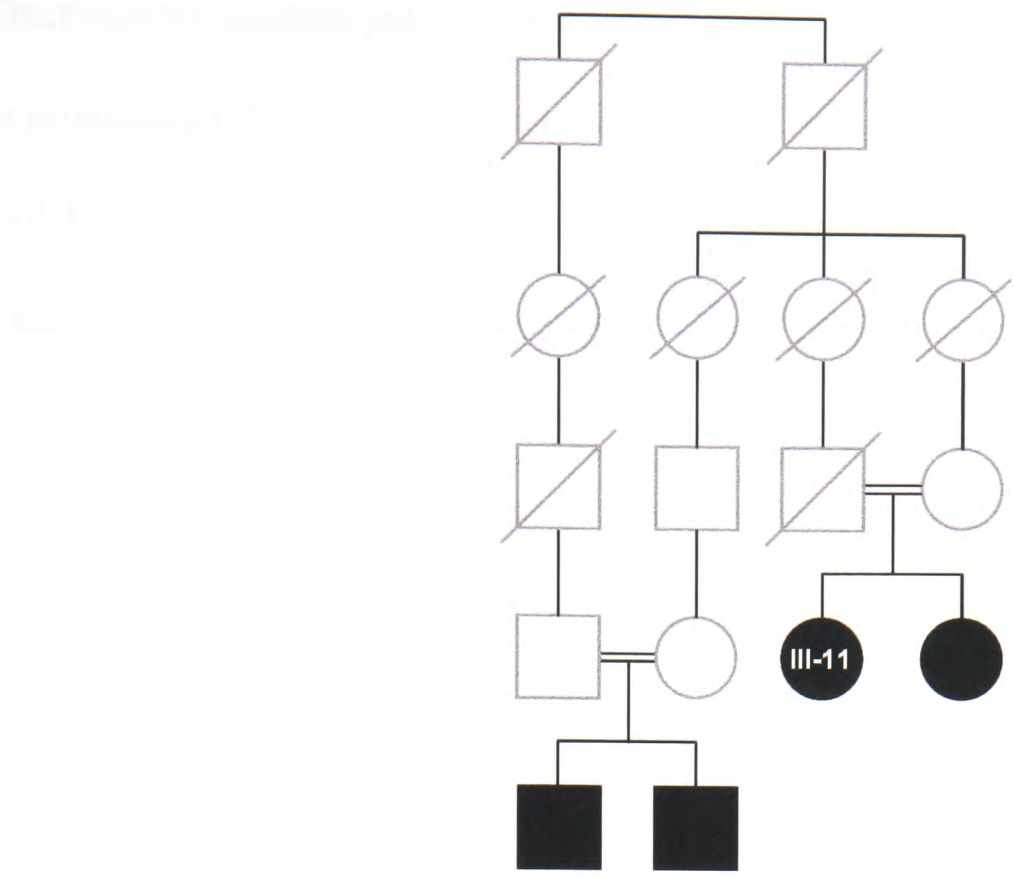

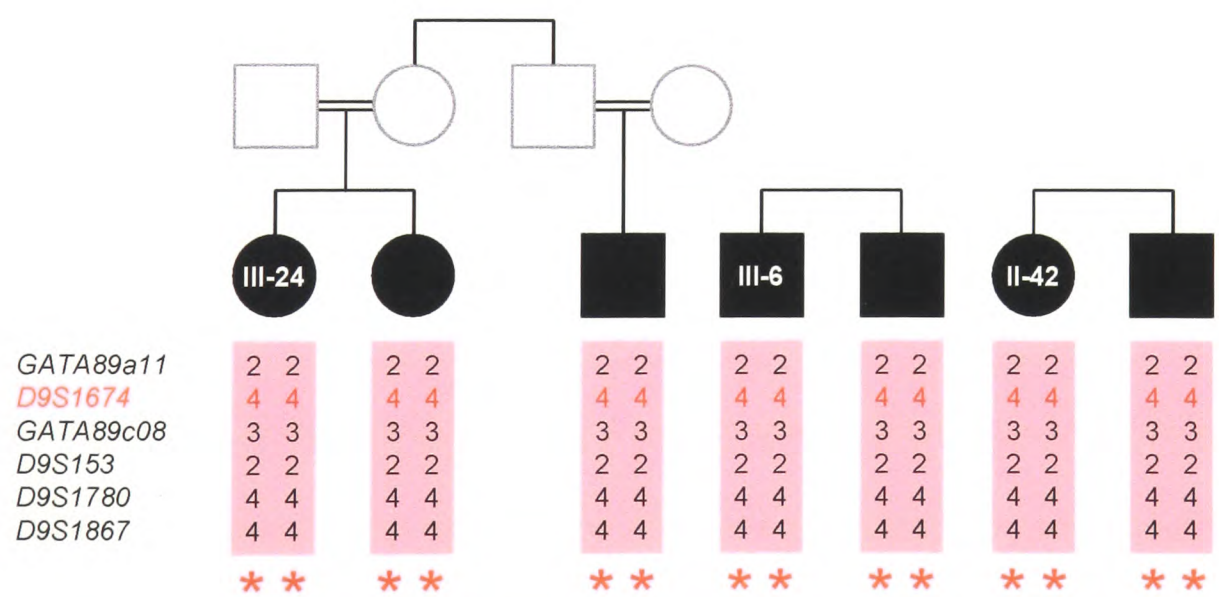

Figure 6.2 - Haplotype analysis of French Canadian ChAc families. Haplotypes of affected individuals from four apparently unrelated families segregating ChAc are shown (probands labelled in white): the *D9S1674* marker, which is internal to *VPS13A*, is indicated in red. Haplotype A is in pink, haplotype B is light yellow. Red asterisks denote where a homozygous deletion of exons 70-73 has been found by PCR analysis. Yellow asterisks denote where the splice-site mutation 4242+1G>T has been identified.
Key: *, heterozygous for mutation; **, homozygous for mutation.

The French Canadian population is of great interest to geneticists: it was founded by approximately 8500 settlers in the 17th century and has since increased in relative isolation to about six million people in Quebec province (Scriver 2001). Many Mendelian diseases occur at unusually high frequency in its subpopulations: for example, oculopharyngeal muscular dystrophy (OPMD, OMIM 164300) is found worldwide but is at greatest concentration in Southeastern Quebec. Analysis of haplotypes in 42 French Canadian OPMD families pointed to a single OPMD-associated haplotype in the patients, indicating a founder effect for this disorder (Brais *et al.* 1995). The discovery of four French Canadian families sharing a ChAc-associated haplotype indicates that ChAc may also show a founder effect in this population. Routine testing for the EX70_73del mutation may therefore be an option for rapid diagnosis of ChAc in French Canadian patients with relevant symptoms. Testing for the 4242+1G>T mutation, which was observed in a French proband (II-40), may also be worthwhile.

Interestingly, the EX70_73del mutation seems also to span the terminal two exons of *GNA14*, which encodes Gα subunit 14 (Figure 3.4). The α-subunits of G-proteins form heterotrimeric complexes with β- and γ-subunits; these complexes are involved in signal transduction from cell surface receptors to a variety of intracellular effectors. *GNA14* is positioned just upstream of the gene encoding Gα subunit q, *GNAQ*: the two genes have probably arisen through tandem duplication (Wilkie *et al.* 1992). Although *GNAQ* is expressed in a wide range of tissues, *GNA14* mRNA is virtually undetectable in adult tissue and appears to be restricted to foetal lung, kidney and liver, at levels far lower than *GNAQ* (Rubio *et al.* 1999). Preliminary investigations appear to show that the individuals who harbour the deletion of the 3' termini of

VPS13A and *GNA14* have no obvious phenotypic differences from those who have mutations affecting *VPS13A* only. This would imply that either Gα14 function does not depend on the presence of its carboxy-terminal region, or that its absence is fully compensated for by, e.g., other Gα subunit proteins. Indeed, many biochemical activities ascribed to Gα14 have also been observed in other Gα proteins (e.g., (Nakamura *et al.* 1995; Maeda *et al.* 1996; Xu *et al.* 1998; Day *et al.* 2003)). However, detailed clinical analysis of individuals harbouring the *GNA14* deletion may reveal subtle differences in phenotype that could give clues to Gα14's physiological role.

Table 6.1 - *VPS13A* mutations identified in two or more ChAc probands

DNA change[a]	Probands with mutation	Proband ancestry[b]
622C>T	CHAC3 (ht)	Italian
	II-12 (ht)	Italian
	II-27 (hm)	Japanese
	II-39 (ht)	Danish
1596-1G>C	II-35 (ht)	Lithuanian
	III-29 (ht)	East German
3557_3558insAC	CHAC4 (hm)	North American
	III-31 (hm)	Mexican
4242+1G>T	II-40 (hm)	*France*
	III-11 (hm)	French Canadian
4355C>G	II-35 (ht)	Lithuanian
	III-29 (ht)	East German
4411C>T	II-26 (ht)	Japanese
	III-3 (hm)	Italian
6059del	II-37 (hm)	Israeli-Jewish
	III-2 (hm)	Israeli-Jewish
6828del	II-41 (ht)	Italian
	III-9 (ht)	Italian
9109C>T	CHAC7 (ht)	Mexican
	II-1 (ht)	German
EX70_EX73del	II-42 (hm)	French Canadian
	III-6 (hm)	French Canadian
	III-24 (hm)	French Canadian
9429_9432del	CHAC11 (ht)	English
	II-34 (ht)	English
9431_9432del	II-29 (ht)	British
	III-18 (hm)	Irish

[a]: Nucleotides and amino acids are numbered according to the cDNA sequence of *VPS13A* isoform 1A, reported by Rampoldi *et al.* (2001) as *CHAC* isoform A (GenBank accession no. NM_033305), with the adenosine of the initiation codon assigned position 1. [b]: Where we have no data on proband ancestry, the country in which the proband was examined is given in italics.
Key: ht, heterozygous; hm, homozygous

6.1.5 *Predicted effects of* VPS13A *mutations on function*

Fifty-eight of the 88 *VPS13A* mutations identified in this study (66%) are nonsense or insertion/deletion mutations that lead to PTCs and therefore predict absence or marked reduction of mutated *VPS13A* transcript via nonsense-mediated decay (Hentze and Kulozik 1999). This is in accordance with the recessive inheritance of chorea-acanthocytosis, where lack of chorein is the primary cause of the disease.

Nineteen out of the 88 *VPS13A* disease mutations described here (22%) are changes affecting splicing. A survey of point mutants that result in human genetic disease revealed that, on average, 10-15% were at splice junctions (Krawczak *et al.* 1992). A likely explanation for the relatively high percentage of splice-site mutations in ChAc is the large number of splice sites contained within *VPS13A*: its 143 splice sites presumably present quite a large target for mutation. In the absence of RNA from affected patients, it is difficult to predict exactly what effect these mutations have at the transcript level. However, as every splice-site mutation described here alters the respective exon/intron junction such that it does not score on the SpliceView program, it is likely that normal splicing will be markedly reduced in each case.

Only five of the *VPS13A* mutations that are predicted to cause disease in this study (5/88, 6%) are missense mutations (shown in Figure 6.3). They are non-conservative substitutions and were not found in at least 100 control chromosomes (384 control chromosomes were tested for Wave II mutations), which suggests that they do not represent benign polymorphisms. The substitution I90K occurs within the 190-aa amino-terminal region that is highly conserved among VPS13 homologues. The position is occupied by a hydrophobic amino acid in the chromosome 15 paralogue of

VPS13A (VPS13C), as well as in VPS13A homologues in *Drosophila melanogaster*, *Caenorhabditis elegans*, *Schizosaccharomyces pombe* and *Saccharomyces cerevisiae*. The introduction of a positively charged residue here is likely to disrupt chorein structure and/or function.

The site of substitution A1095P is moderately well conserved, being occupied by a hydrophobic amino acid in all homologues described above. The introduction of the cyclic structure of proline here is likely to profoundly influence protein architecture, as it is often found in the bends of folded protein chains (Stryer 1995).

Although the identity of the amino acid is not so well conserved at the S1452P site, the introduction of a proline between the well-conserved hydrophobic amino acid at 1451 and leucine at 1453 is also likely to have steric consequences - as discussed below (section 6.2.2), this mutation leads to markedly reduced chorein levels. Intriguingly, the equivalent leucine residue is mutated to arginine in the VPS13B protein of a patient with Cohen syndrome, and is the sole missense mutation observed so far (L2193R, in (Kolehmainen *et al.* 2003)). Perhaps the precise architecture of this region is crucial to maintain protein integrity in VPS13 homologues.

The tryptophan site of the W2460R mutation is occupied by an aromatic or large aliphatic amino acid in all VPS13A orthologues studied: its replacement for a positively charged amino acid is therefore likely to have a deleterious effect.

Substitution Y2721C is in a locally well-conserved region – the introduction of the reactive sulphydryl group in cysteine may significantly influence the chemistry of this area. The fact that just five out of 12 amino-acid variants reported here (Tables 3.1, 3.2 & 3.4) are believed to be pathogenic is perhaps an indication that much of chorein is tolerant to substitution.

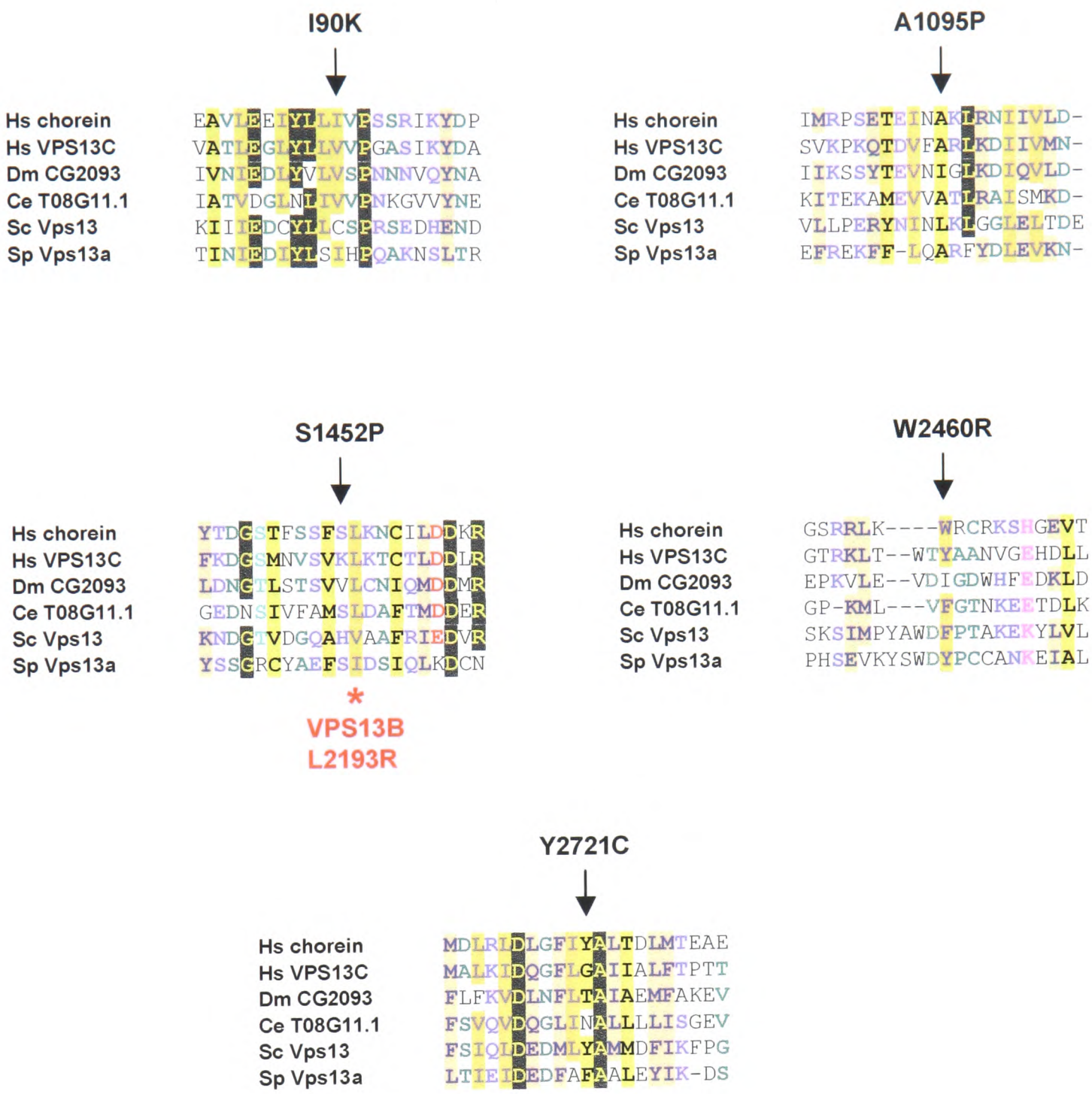

Figure 6.3 - Alignment of *VPS13A* missense mutations. Alignment of the amino-acid sequence surrounding the five missense mutations identified in this study. Sequences from chorein and homologues were aligned and coloured using the T-Coffee (Notredame *et al.*, 2000) and CHROMA (Goodstadt *et al.*, 2001) programs, respectively. The missense mutation site is arrowed. The equivalent position of the missense mutation L2193R reported in *VPS13B* is asterisked.
Key: Hs, *Homo sapiens;* Dm, *Drosophila melanogaster;* Ce, *Caenorhabditis elegans;* Sc, *Saccharomyces cerevisiae;* Sp, *Schizosaccharomyces pombe.*

6.2 Analysis of *VPS13A* expression

6.2.1 Distribution of VPS13A *mRNA and protein*

Northern and RT-PCR analysis revealed that *VPS13A* mRNA is ubiquitously expressed (Figure 4.1). This is consistent with the fact that the 5'UTR of *VPS13A* contains a CpG island, a feature characteristic of 'housekeeping' genes, and with the ubiquitous expression of its three human gene homologues (Velayos-Baeza *et al.* 2004). Development of a polyclonal antiserum against chorein revealed that chorein is expressed in cell lines derived from a wide variety of human tissues, as well as primary skin fibroblasts and erythrocytes (Figures 4.7 - 4.9), which lends further support to the ubiquitous expression of this gene. Although the *VPS13A* mRNA signal is weak (Figure 4.1), and experiments with the yeast homologue Vps13p indicate that its cell copy number is very low (Brickner and Fuller 1997), we found that endogenous chorein is expressed at a level sufficient to be detected by immunoblot assays of cell lysates.

6.2.2 Expression of mutant chorein in ChAc cell lines

We have demonstrated that five classes of *VPS13A* mutations (nonsense, frameshift, splice-site, missense, exon deletion) can lead to absence or marked reduction of chorein expression in ChAc patients (Figures 4.5, 4.7- 4.9). The affected siblings in family CHAC6 show very little expression of chorein (Figure 4.8a), implying that the missense mutation S1452P must adversely affect stability at the transcript or protein level. The fact that this missense mutation simply alters protein dosage is consistent with the theory that absence of chorein, rather than a functional defect of chorein, causes ChAc in the majority of patients. The affected son in CHAC11 is heterozygous

for an exon 72 mutation that should only affect the longer isoform of chorein, isoform 1A: isoform 1B expression (and that of other isoforms that don't include exon 72) should in theory be unaffected. The fact that there is very little expression of chorein in this patient (Figure 4.8a) implies that isoform 1B is expressed at much lower levels than isoform 1A. As mentioned previously (section 6.1.3), we have demonstrated that isoform 1B and others cannot compensate for absence of chorein isoform 1A in chorea-acanthocytosis. It is therefore possible that exons 70-73 encode one or more protein domains that are essential for some functions of chorein. The relatively poor expression of isoforms lacking these exons, as demonstrated here, may provide an alternative reason for their inability to substitute for full-length chorein in this disorder.

6.2.3 Chorein detection for diagnosis of ChAc

We have shown that chorein can be detected in association with the erythrocyte membrane (Figure 4.9). It is still possible to detect chorein from blood that has been frozen for several months, with little apparent degradation of chorein in the samples. This has obvious implications for diagnosis of ChAc. At present, if the *VPS13A* gene has not been screened, ChAc can only be diagnosed by excluding other clinically similar disorders. Unlike in McLeod syndrome and abetalipoproteinemia (see sections 1.2 and 1.3), no simple biochemical test is at present possible. In contrast to Huntington's disease (Kremer *et al.* 1994), no single mutation is responsible for the majority of cases of ChAc. Nor do the mutations cluster to a particular area of *VPS13A*: so far, ChAc disease mutations have been identified in 51/73 exons, implying that all regions of the gene must be screened for efficient mutation detection. As *VPS13A* is a large gene with many exons, screening is costly, labour-intensive and

time-consuming. Western blotting of patient erythrocyte membranes could perhaps give an early indication of the disorder before a precise diagnosis is given by a *VPS13A* gene screen.

Although chorein was absent or markedly reduced in all patient erythrocytes analysed so far, one cannot exclude ChAc as a diagnosis if chorein is present in a sample. It is possible that some patients harbour missense mutations that do not affect chorein dosage but produce functionally defective chorein nevertheless. Also, some mutations may allow almost normal expression levels of mutant chorein lacking only a few exons, which might not be resolved from wild-type chorein due to its large size. However, as missense changes comprise less than 6% of *VPS13A* mutations described so far (this study and (Ueno *et al.* 2001), and the majority of transcripts containing premature stop codons are believed to be rapidly degraded (Hentze and Kulozik 1999), we anticipate that this would not be a significant problem. In any case, if chorein is absent in a patient sample, the most likely diagnosis will be chorea-acanthocytosis.

6.3 Identification of potential chorein-interacting proteins

With only data from *VPS13A* homologues to draw on, it is clear that determination of chorein function is in its infancy. We used the yeast two-hybrid approach to search for proteins that may interact with chorein, in an attempt to infer the function of chorein from the function of its binding partners, and/or to dissect the pathological pathways that lead from chorein absence to development of ChAc. Although six ~600-aa regions of chorein were used as baits, and nearly 2.3 x 10^7 yeast transformants were screened, only seven independent clones, representing three distinct proteins, were identified. All were weak or very weak interactors with a single bait, chacY2 (Figure 5.3).

6.3.1 Limitations of the assay

It is likely that some physiological interactors with chorein have been missed in this screen. This could have been due to the bait selection. Due to its size, a Y2H screen using full-length chorein was unlikely to be successful, so baits comprising portions of the protein were designed. Logical bait design should take account of known domains of the protein, and of localisation signals that could interfere with nuclear localisation of the bait. However, due to limited structural information for chorein, this was not possible; and so functional domains of the protein may have been destroyed or mislocalised by bait selection. The recent discovery of the human chorein homologues on chromosomes 1, 8 and 15 has permitted further computer analysis of domains in chorein and some new conserved regions, such as 'domain of unknown function' 1162 and the R domains (as shown in Figure 6.4) have been identified. These regions could prove fruitful in future assays of chorein interactions.

Interactions may also have been missed due to bait sequestration by interaction with endogenous yeast orthologues of its physiological partners, or bait misfolding induced by expression as a fusion with GAL4 DB. In addition, post-translational modifications of the bait may be required for some interactions (Toby and Golemis 2001). Even if bait proteins were fully available, correctly folded and modified, some chorein-interactors may not have been represented in this cDNA library, due to low copy number in the brain. Screening of additional brain cDNA libraries, and libraries made from other tissues, may address this issue.

6.3.2 Potential chorein-binding partners

The potential chorein-interactors identified in this Y2H screen were TAB2, the putative protein PP2Cη and the p65 subunit of NF-κB (Figures 5.3-5.5). As three independent clones encoding TAB2 were identified, and TAB2 has already been characterised in other studies (e.g., Takaesu *et al.* 2000), we investigated the TAB2-chorein interaction further by co-immunoprecipitation studies in mammalian cells (Figures 5.6 & 5.7). The fact that some TAB2-T7 appears to be coprecipitated when chorein-FLAG is immunoprecipitated (and vice versa) implies that chorein and TAB2 may interact *in vivo*. The relatively low levels of *lacZ* activity induced by the chacY2-TAB2 interaction in the yeast two-hybrid studies and the fact that only a small amount of partner protein is coprecipitated in transfected cells implies that any *in vivo* interaction between chorein and TAB2 is likely to be transient and/or weak.

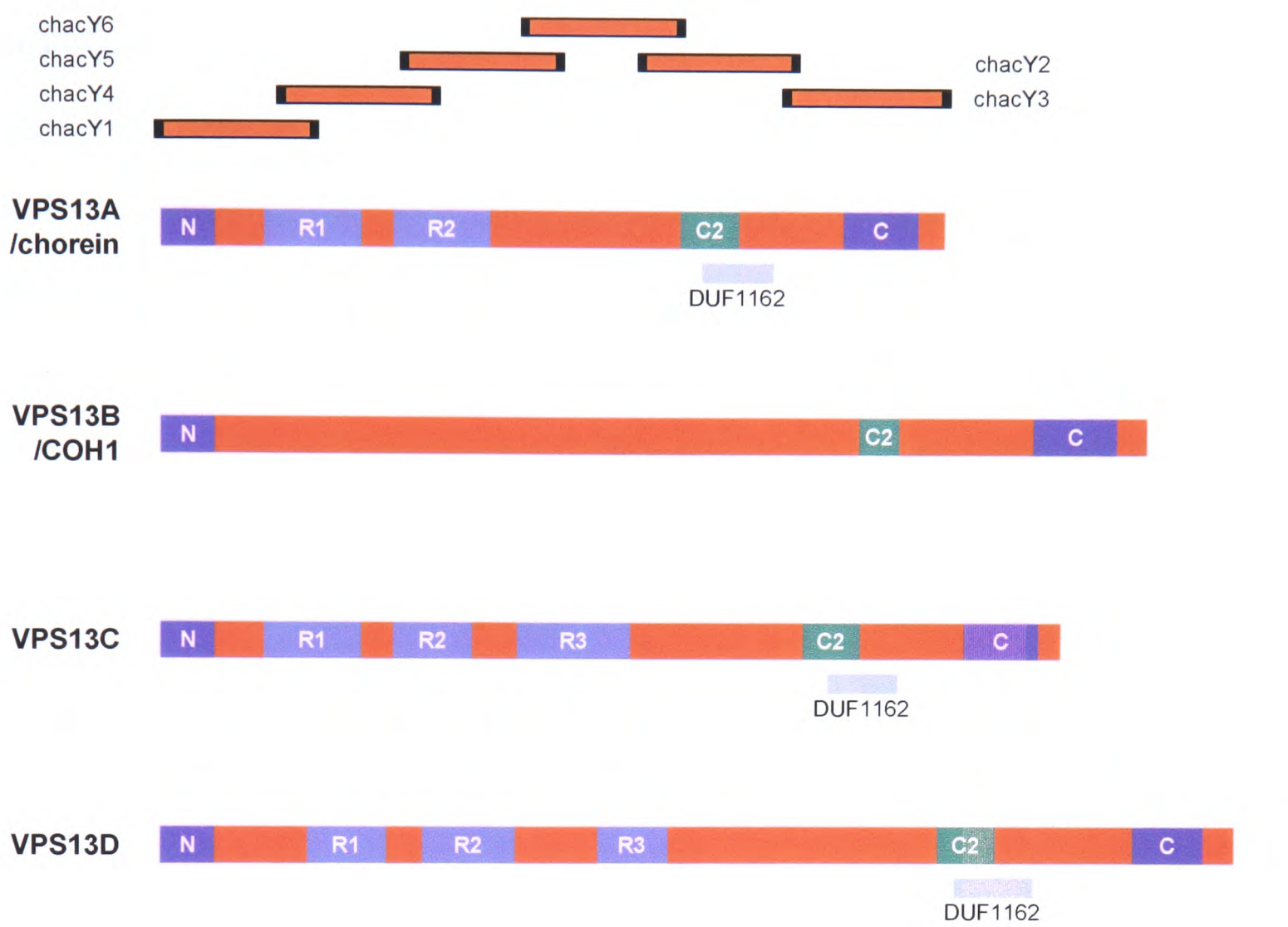

Figure 6.4 - Features of human VPS13 proteins. Schematic of VPS13A-D, splice form 1A. The amino (N) and carboxy (C) regions of high conservation are indicated in dark blue. The recent identification of this gene family and subsequent computer analysis of homologue alignments (Velayos-Baeza *et al.*, 2004) has enabled elucidation of additional conserved regions: repeat regions 1-3 (R1-3) and carboxy-terminal region 2 (C2). Domain of unknown function 1162 (DUF1162) is a further region of homology shared between VPS13A, C and D. The chorein regions used for yeast two-hybrid analysis are indicated above the chorein plot. (*After Velayos-Baeza* et al., *2004*)

We have not yet been able to determine the nature of the vesicular structures observed in immunofluorescent staining of chorein. Preliminary investigations of transiently transfected cells revealed that these structures did not colocalise with markers for the endoplasmic reticulum, Golgi, TGN, endosomes or other subcellular compartments (data not shown). Localisation studies in stably transfected cell lines are currently underway. Although transfected TAB2 and chorein did not colocalise (Figure 5.8), there is a possibility that the high expression levels of the recombinant proteins could result in mislocalisation and the true subcellular localisation of TAB2 is elsewhere. It would be interesting to repeat the immunofluorescent studies using an antibody for detection of endogenous TAB2, e.g., in neuronal cell lines, to resolve this issue. Subcellular fractionation studies indicate that IL-1 stimulation alters the distribution of TAB2 (Jiang *et al.* 2002); this implies that future chorein-TAB2 immunolocalisation studies could also benefit from different cytokine treatment conditions.

6.3.3 Possible relationships between chorein-interacting proteins

Intriguingly, experiments on TAB2, the type 2C protein phosphatases and NF-κB have illuminated potential relationships between these proteins. Some of the evidence linking them to each other and the same or similar complex signalling pathways is outlined below.

TAB1 & TAB2 were originally identified in a yeast two-hybrid screen as binding partners for transforming growth factor β (TGFβ)-activated kinase 1 (TAK1), a protein involved in the mitogen-activated protein (MAP) kinase cascade (Shibuya *et al.* 1996). TAK1 is a MAP kinase kinase kinase (MAPKKK) that is involved in

signalling mediated by interleukin-1 (IL-1), TGFβ and stress-related signals (Yamaguchi *et al.* 1995; Shirakabe *et al.* 1997). Jiang *et al.* (2002) proposed the following model of IL-1 signalling. Components from the stimulated IL receptor complex dissociate and interact with a complex of TAK1, TAB1 & TAB2 on the membrane. This leads to phosphorylation of TAK1 & TAB2 and translocation of the complex to the cytosol, where TAK1 is activated. TAK1 is implicated in the activation of IκB kinase (IKK) (Wang *et al.* 2001), which leads to NF-κB activation, as discussed below.

The PP2C proteins are the defining members of the PPM family of serine/threonine phosphatases. One of their roles is to reverse protein kinase cascades that become activated because of stress signals, including environmental stimuli and proinflammatory cytokines (Tamura *et al.* 2002). As mentioned above, TAK1 is one of the kinases involved in the stress response. PP2Cβ-1 and PP2Cε have both been shown to dephosphorylate and inactivate TAK1 (Hanada *et al.* 2001; Li *et al.* 2003). No experimental evidence yet exists for the human putative protein PP2Cη, but the orthologue in mouse has recently been characterised. Mouse PP2Cη shows strongest expression in testis, but modest expression was also observed in lung, kidney and brain (Komaki *et al.* 2003). Intriguingly, aa 64-368 of TAB1 are annotated in the SWISSPROT database as containing a PP2C-like domain and TAB1 aa 164-232 share 56% similarity with aa 53-120 of PP2Cη isoform 2; however, no phosphatase activity has been reported for TAB1.

NF-κB in its inactive form is present in the cytosol as a three-subunit complex, which usually comprises the transcription factor dimer of p50 & p65 and the inhibitory subunit IκB. Activation is effected by IKK: it causes the phosphorylation and subsequent degradation of IκB, leaving the p65-p50 dimer free to translocate to the nucleus and activate transcription of a wide range of genes. The activation of NF-κB in brain tissue by a diverse range of signals, including tumour necrosis factor alpha, nerve growth factor, glutamate and intracellular hydrogen peroxide has been documented (Mattson and Camandola 2001). Studies suggest that NF-κB plays important roles in cellular responses to injury of the nervous system in both acute and chronic neurodegenerative conditions. The consequences of NF-κB activation are complex: generally, in neurons it induces the expression of antiapoptotic gene products and other neuroprotective proteins, while NF-κB activation in microglia leads to expression of genes whose products promote neuronal degeneration (Mattson and Camandola 2001). Interestingly, mice lacking the p50 subunit of NF-κB undergo increased striatal neuron degeneration and have increased motor dysfunction when exposed to the mitochondrial toxin 3-nitropropionic acid, in an animal model of Huntington's disease (Yu *et al.* 2000).

6.4 Potential functions for chorein

Although it has been established that mutations in *VPS13A* are the primary cause of chorea-acanthocytosis, it is not yet known how chorein functions or how its abolition brings about the neurological and erythrocyte changes that make up the ChAc phenotype. Clinical data is currently being gathered for an exhaustive comparison of genotype and phenotype. However, as most of the *VPS13A* mutations identified so far result in a null allele, and substantial intrafamilial phenotypic variation has been observed (e.g., in Aasly *et al.* 1999), significant genotype-phenotype correlation is not likely. It may not be possible, therefore, to identify what clinical consequences are seen when different parts of the protein are ablated. As chorein also has no identifiable domains that can give clues to its normal function(s), information has to be derived from studies on its homologues.

6.4.1 Chorein: a protein sorter?

As discussed previously (section 1.8.1), the chorein homologue that has been most studied is Vps13p in *Saccharomyces cerevisiae* (Redding *et al.* 1996; Brickner and Fuller 1997). Vps13p is involved in the intracellular trafficking of Kex2p and other proteins: if we extrapolate from this finding, we can speculate that chorein may play a similar role in humans. Proteins that could be sorted by chorein include furin-like proteases, mammalian homologues of Kex2p. Furin has been shown to cycle between the TGN, endosomes and the plasma membrane (Nakayama 1997) and is therefore a good candidate for protein trafficking. Cytoskeletal components may also be mislocalised. In McLeod syndrome, the destabilisation of the Kell-XK complex and

the consequent disruption of contacts with the underlying membrane skeleton might lead to the structural changes thought to be related to acanthocyte formation (Terada *et al.* 1999). It is known that mice lacking the erythrocyte membrane protein 4.1R exhibit neurobehavioural deficits and abnormal erythrocyte morphology (Walensky *et al.* 1998). Perhaps mislocalisation of a similar protein or proteins in the absence of functional chorein could cause the haematological and neurological abnormalities seen in ChAc.

Additional potential targets for chorein protein sorting have been provided by the Y2H screen performed in this study. Again, it is feasible that chorein may be involved in the trafficking of one or more of these proteins: e.g., in shuttling of NF-κB between nucleus and cytosol, or movement of TAB2 between membrane and cytosol. The weakness of the interaction between chorein and TAB2 *in vitro* (and of chacY2 and its prey constructs in the Y2H screen) may be a reflection of the necessarily transient nature of an interaction between a sorting protein and its cargo. As NF-κB, TAB2 and PP2Cs all have links with the pathways involved in the cellular response to metabolic and environmental stress, mislocalisation of any of these proteins could possibly lead to a perturbation in the stress response. Under conditions of metabolic-excitotoxic stress, neurons with inadequate or inappropriate stress responses may be more liable to apoptose, thus leading to the marked neurodegeneration seen in the latter stages of chorea-acanthocytosis.

6.4.2 Possible redundancy in function of VPS13 proteins

A pertinent question is why the symptoms of ChAc appear to be limited to neuronal, muscular and erythroid cells, given the apparently ubiquitous expression of chorein. As mentioned previously (section 1.8.2), we have recently identified a novel human gene family comprising *VPS13A* and three other genes on chromosomes 1, 8 and 15. The proteins encoded by these genes show significant similarity with yeast Vps13p, notably at the amino- and carboxy-terminal regions (Velayos-Baeza *et al.* 2004). It is possible that these family members share some functions in the cell and that other VPS13 proteins can compensate for lack of chorein in most tissues. Only certain cells where chorein plays a non-redundant role would therefore be vulnerable in ChAc patients.

6.4.3 Future analysis of chorein function

Analysis of the few missense mutations that have been identified in this study might give important clues as to which amino acids are critical for chorein function. For example, the Y2H bait chacY2 is the site of the missense mutation W2460R: although time constraints prohibited further analysis, it would be interesting to see what effect the substitution of this residue has on the interactions between chacY2 and its putative binding partners. However, as we have shown, at least one of the missense changes appears simply to have an effect on protein dosage (Figure 4.8a), implying that a functional study of this mutant protein may not be biologically relevant. Western blotting of patient cells with missense mutations could be used to exclude such 'dosage effect' substitutions from further analysis, enabling efforts to be concentrated

on substitutions that may have functional implications. Functional analysis of these mutants is now needed in order to elucidate the exact role that chorein plays, both in the pathogenesis of ChAc and within the context of normal brain processes.

References

Aasly J, Skandsen T, Ro M (1999) Neuroacanthocytosis--the variability of presenting symptoms in two siblings. *Acta Neurol Scand* 100:322-325

Abiko Y (1967) Investigations on pantothenic acid and its related compounds. IX. Biochemical studies.4. Separation and substrate specificity of pantothenate kinase and phosphopantothenoylcysteine synthetase. *J Biochem (Tokyo)* 61:290-299

Aden DP, Fogel A, Plotkin S, Damjanov I, Knowles BB (1979) Controlled synthesis of HBsAg in a differentiated human liver carcinoma-derived cell line. *Nature* 282:615-616

Afshar K, Gonczy P, DiNardo S, Wasserman SA (2001) fumble encodes a pantothenate kinase homolog required for proper mitosis and meiosis in Drosophila melanogaster. *Genetics* 157:1267-1276

Al-Shali K, Wang J, Rosen F, Hegele RA (2003) Ileal adenocarcinoma in a mild phenotype of abetalipoproteinemia. *Clin Genet* 63:135-138

Allen FH, Jr., Krabbe SM, Corcoran PA (1961) A new phenotype (McLeod) in the Kell blood-group system. *Vox Sang* 6:555-560

Alonso ME, Teixeira F, Jimenez G, Escobar A (1989) Chorea-acanthocytosis: report of a family and neuropathological study of two cases. *Can J Neurol Sci* 16:426-431

Arnstein P, Taylor DO, Nelson-Rees WA, Huebner RJ, Lennette EH (1974) Propagation of human tumors in antithymocyte serum-treated mice. *J Natl Cancer Inst* 52:71-84

Asano K, Osawa Y, Yanagisawa N, Takahashi Y, Oshima M (1985) Erythrocyte membrane abnormalities in patients with amyotrophic chorea with acanthocythosis. Part 2. Abnormal degradation of membrane proteins. *J Neurol Sci* 68:161-173

Atzel A, Wetterau JR (1994) Identification of two classes of lipid molecule binding sites on the microsomal triglyceride transfer protein. *Biochemistry* 33:15382-15388

Ballas SK, Bator SM, Aubuchon JP, Marsh WL, Sharp DE, Toy EM (1990) Abnormal membrane physical properties of red cells in McLeod syndrome. *Transfusion* 30:722-727

Banta LM, Robinson JS, Klionsky DJ, Emr SD (1988) Organelle assembly in yeast: characterization of yeast mutants defective in vacuolar biogenesis and protein sorting. *J Cell Biol* 107:1369-1383

Bassen FA, Kornzweig AL (1950) Malformation of the erythrocyte in a case of atypical retinitis pigmentosa. *Blood* 5:381-387

Berriot-Varoqueaux N, Aggerbeck LP, Samson-Bouma M, Wetterau JR (2000) The role of the microsomal triglygeride transfer protein in abetalipoproteinemia. *Annu Rev Nutr* 20:663-697

Bertelson CJ, Pogo AO, Chaudhuri A, *et al.* (1988) Localization of the McLeod locus (XK) within Xp21 by deletion analysis. *Am J Hum Genet* 42:703-711

Bharucha EP, Bharucha NE (1989) Choreo-acanthocytosis. *J Neurol Sci* 89:135-139

Bieri JG, Hoeg JM, Schaefer EJ, Zech LA, Brewer HB, Jr. (1984) Vitamin A and vitamin E replacement in abetalipoproteinemia. *Ann Intern Med* 100:238-239

Bird TD, Cederbaum S, Valey RW, Stahl WL (1978) Familial degeneration of the basal ganglia with acanthocytosis: a clinical, neuropathological, and neurochemical study. *Ann Neurol* 3:253-258

Blatch GL, Lassle M (1999) The tetratricopeptide repeat: a structural motif mediating protein-protein interactions. *Bioessays* 21:932-939

Bohlega S, Al-Jishi A, Dobson-Stone C, *et al.* (2003) Chorea-acanthocytosis: clinical and genetic findings in three families from the Arabian peninsula. *Mov Disord* 18:403-407

Bohlega S, Riley W, Powe J, Baynton R, Roberts G (1998) Neuroacanthocytosis and aprebetalipoproteinemia. *Neurology* 50:1912-1914

Bosman GJ, Bartholomeus IG, De Grip WJ, Horstink MW (1994) Erythrocyte anion transporter and antibrain immunoreactivity in chorea-acanthocytosis. A contribution to etiology, genetics, and diagnosis. *Brain Res Bull* 33:523-528

Bostantjopoulou S, Katsarou Z, Kazis A, Vadikolia C (2000) Neuroacanthocytosis presenting as parkinsonism. *Mov Disord* 15:1271-1273

Brais B, Xie YG, Sanson M, *et al.* (1995) The oculopharyngeal muscular dystrophy locus maps to the region of the cardiac alpha and beta myosin heavy chain genes on chromosome 14q11.2-q13. *Hum Mol Genet* 4:429-434

Brecher G, Bessis M (1972) Present status of spiculed red cells and their relationship to the discocyte-echinocyte transformation: a critical review. *Blood* 40:333-344

Brickner JH, Fuller RS (1997) SOI1 encodes a novel, conserved protein that promotes TGN-endosomal cycling of Kex2p and other membrane proteins by modulating the function of two TGN localization signals. *J Cell Biol* 139:23-36

Brooks DJ, Ibanez V, Playford ED, *et al.* (1991) Presynaptic and postsynaptic striatal dopaminergic function in neuroacanthocytosis: a positron emission tomographic study. *Ann Neurol* 30:166-171

Bruce LJ, Kay MM, Lawrence C, Tanner MJ (1993) Band 3 HT, a human red-cell variant associated with acanthocytosis and increased anion transport, carries the mutation Pro-868-->Leu in the membrane domain of band 3. *Biochem J* 293 (Pt 2):317-320

Burbaud P, Rougier A, Ferrer X, *et al.* (2002) Improvement of severe trunk spasms by bilateral high-frequency stimulation of the motor thalamus in a patient with chorea-acanthocytosis. *Mov Disord* 17:204-207

Caballero FM, Buchanan GR (1980) Abetalipoproteinemia presenting as severe vitamin K deficiency. *Pediatrics* 65:161-163

Cabantchik ZI, Rothstein A (1974) Membrane proteins related to anion permeability of human red blood cells. I. Localization of disulfonic stilbene binding sites in proteins involved in permeation. *J Membr Biol* 15:207-226

Carter ND, Morgan JE, Monaco AP, Schwartz MS, Jeffery S (1990) Dystrophin expression and genotypic analysis of two cases of benign X linked myopathy (McLeod's syndrome). *J Med Genet* 27:345-347

Chang BH, Liao W, Li L, Nakamuta M, Mack D, Chan L (1999) Liver-specific inactivation of the abetalipoproteinemia gene completely abrogates very low density lipoprotein/low density lipoprotein production in a viable conditional knockout mouse. *J Biol Chem* 274:6051-6055

Ching KH, Westaway SK, Gitschier J, Higgins JJ, Hayflick SJ (2002) HARP syndrome is allelic with pantothenate kinase-associated neurodegeneration. *Neurology* 58:1673-1674

Chitale AA, Sterling RK, Post AB, Silver BJ, Mulligan DC, Schulak JA (1998) Resolution of spur cell anemia with liver transplantation: a case report and review of the literature. *Transplantation* 65:993-995

Clark MR, Aminoff MJ, Chiu DT, Kuypers FA, Friend DS (1989) Red cell deformability and lipid composition in two forms of acanthocytosis: enrichment of acanthocytic populations by density gradient centrifugation. *J Lab Clin Med* 113:469-481

Cogan U, Schachter D (1981) Asymmetry of lipid dynamics in human erythrocyte membranes studied with impermeant fluorophores. *Biochemistry* 20:6396-6403

Collins JC, Scheinberg IH, Giblin DR, Sternlieb I (1989) Hepatic peroxisomal abnormalities in abetalipoproteinemia. *Gastroenterology* 97:766-770

Cooper DN, Youssoufian H (1988) The CpG dinucleotide and human genetic disease. *Hum Genet* 78:151-155

Cooper RA (1977) Abnormalities of cell-membrane fluidity in the pathogenesis of disease. *N Engl J Med* 297:371-377

Cooper RA, Gulbrandsen CL (1971) The relationship between serum lipoproteins and red cell membranes in abetalipoproteinemia: deficiency of lecithin:cholesterol acyltransferase. *J Lab Clin Med* 78:323-335

Cooper RA, Sawyer WH, Leslie MH, Hill JS, Gill FM, Wiley JS (1980) Normal fluidity of red cell membranes in hereditary spherocytosis. *Br J Haematol* 46:299-301

Critchley EM, Clark DB, Wikler A (1968) Acanthocytosis and neurological disorder without betalipoproteinemia. *Arch Neurol* 18:134-140

Dacie J (1985) *The haemolytic anaemias*. Vol 1. Churchill Livingstone, Edinburgh

Danek A (2002) [Progress in molecular chorea diagnosis. McLeod syndrome and chorea acanthocytosis]. *Nervenarzt* 73:564-569

Danek A, Jung HH, Melone MAB, Rampoldi L, Broccoli V, Walker RH (2004) Neuroacanthocytosis: new developments in a neglected group of dementing disorders. *J Neurol Sci (submitted)*

Danek A, Rubio JP, Rampoldi L, *et al.* (2001) McLeod neuroacanthocytosis: genotype and phenotype. *Ann Neurol* 50:755-764

Danek A, Uttner I, Vogl T, Tatsch K, Witt TN (1994) Cerebral involvement in McLeod syndrome. *Neurology* 44:117-120

Day PW, Carman CV, Sterne-Marr R, Benovic JL, Wedegaertner PB (2003) Differential interaction of GRK2 with members of the G alpha q family. *Biochemistry* 42:9176-9184

Day RS, 3rd, Ziolkowski CH (1979) Human brain tumour cell strains with deficient host-cell reactivation of N-methyl-N'-nitro-N-nitrosoguanidine-damaged adenovirus 5. *Nature* 279:797-799

de Yebenes JG, Brin MF, Mena MA, *et al.* (1988) Neurochemical findings in neuroacanthocytosis. *Mov Disord* 3:300-312

Delecluse F, Deleval J, Gerard JM, Michotte A, Zegers de Beyl D (1991) Frontal impairment and hypoperfusion in neuroacanthocytosis. *Arch Neurol* 48:232-234

Delpre G, Kadish U, Glantz I, Avidor I (1978) Endoscopic assessment in abetalipoproteinemia (Bassen-Kornzweig-syndrome). *Endoscopy* 10:59-62

den Dunnen JT, Antonarakis SE (2000) Mutation nomenclature extensions and suggestions to describe complex mutations: a discussion. *Hum Mutat* 15:7-12

Dische MR, Porro RS (1970) The cardiac lesions in Bassen-Kornzweig syndrome. Report of a case, with autopsy findings. *Am J Med* 49:568-571

Dobson-Stone C, Danek A, Rampoldi L, *et al.* (2002) Mutational spectrum of the CHAC gene in patients with chorea-acanthocytosis. *Eur J Hum Genet* 10:773-781

Dodge JT, Mitchell C, Hanahan DJ (1963) The preparation and chemical characteristics of hemoglobin-free ghosts of human erythrocytes. *Arch Biochem Biophys* 100:119-130

Doll DC, List AF, Dayhoff DA, Loy TS, Ringenberg QS, Yarbro JW (1989) Acanthocytosis associated with myelodysplasia. *J Clin Oncol* 7:1569-1572

Dotti MT, Battisti C, Malandrini A, *et al.* (2000) McLeod syndrome and neuroacanthocytosis with a novel mutation in the XK gene. *Mov Disord* 15:1282-1284

Dubinsky RM, Hallett M, Levey R, Di Chiro G (1989) Regional brain glucose metabolism in neuroacanthocytosis. *Neurology* 39:1253-1255

Dubowitz V (1985) *Muscle biopsy. A practical approach*. Baillière Tindall, London

Ehrenreich H, Nau TR, Dembowski C, *et al.* (2000) Endothelin b receptor deficiency is associated with an increased rate of neuronal apoptosis in the dentate gyrus. *Neuroscience* 95:993-1001

Estes JW, Morley TJ, Levine IM, Emerson CP (1967) A new hereditary acanthocytosis syndrome. *Am J Med* 42:868-881

Faillace RT, Kingston WJ, Nanda NC, Griggs RC (1982) Cardiomyopathy associated with the syndrome of amyotrophic chorea and acanthocytosis. *Ann Intern Med* 96:616-617

Feinberg TE, Cianci CD, Morrow JS, *et al.* (1991) Diagnostic tests for choreoacanthocytosis. *Neurology* 41:1000-1006

Fitch CD, Dinning JS (1963) Vitamin E deficiency in the monkey. V. Estimated requirements and the influence of fat deficiency and antioxidants on the syndrome. *J Nutr* 79:69-78

Flamm M, Schachter D (1982) Acanthocytosis and cholesterol enrichment decrease lipid fluidity of only the outer human erythrocyte membrane leaflet. *Nature* 298:290-292

Francke U, Ochs HD, de Martinville B, *et al.* (1985) Minor Xp21 chromosome deletion in a male associated with expression of Duchenne muscular dystrophy, chronic granulomatous disease, retinitis pigmentosa, and McLeod syndrome. *Am J Hum Genet* 37:250-267

Frangioni JV, Neel BG (1993) Solubilization and purification of enzymatically active glutathione S-transferase (pGEX) fusion proteins. *Anal Biochem* 210:179-187

Frezal J, Rey J, Polonovski J, Levy G, Lamy M (1961) [Congenital absence of beta-lipoproteins: study of fat absorption after exsanguinotransfusion measuring the half-life of injected beta-lipoproteins]. *Rev Fr Etud Clin Biol* 6:677-683

Fuchs E, Weber K (1994) Intermediate filaments: structure, dynamics, function, and disease. *Annu Rev Biochem* 63:345-382

Fujimoto Y, Isozaki E, Yokochi F, Yamakawa K, Takahashi H, Hirai S (1997) [A case of chorea-acanthocytosis successfully treated with posteroventral pallidotomy]. *Rinsho Shinkeigaku* 37:891-894

Galey WR, Evan AP, Van Nice PS, Dail WG, Wimer BM, Cooper RA (1978) Morphology and physiology of the McLeod erythrocyte. I. Scanning electron microscopy and electrolyte and water transport properties. *Vox Sang* 34:152-161

Gascard P, Mohandas N (2000) New insights into functions of erythroid proteins in nonerythroid cells. *Curr Opin Hematol* 7:123-129

Gervais FG, Singaraja R, Xanthoudakis S, *et al.* (2002) Recruitment and activation of caspase-8 by the Huntingtin-interacting protein Hip-1 and a novel partner Hippi. *Nat Cell Biol* 4:95-105

Gluzman Y (1981) SV40-transformed simian cells support the replication of early SV40 mutants. *Cell* 23:175-182

Goebl M, Yanagida M (1991) The TPR snap helix: a novel protein repeat motif from mitosis to transcription. *Trends Biochem Sci* 16:173-177

Goodstadt L, Ponting CP (2001) CHROMA: consensus-based colouring of multiple alignments for publication. *Bioinformatics* 17:845-846

Gordon DA, Jamil H (2000) Progress towards understanding the role of microsomal triglyceride transfer protein in apolipoprotein-B lipoprotein assembly. *Biochim Biophys Acta* 1486:72-83

Gradstein L, Danek A, Grafman J, Fitzgibbon EJ (2003) Eye movements in chorea-acanthocytosis. *Invest Ophthalmol Vis Sci* 44:1934

Graham FL, Smiley J, Russell WC, Nairn R (1977) Characteristics of a human cell line transformed by DNA from human adenovirus type 5. *J Gen Virol* 36:59-74

Gross KB, Skrivanek JA, Carlson KC, Kaufman DM (1985) Familial amyotrophic chorea with acanthocytosis. New clinical and laboratory investigations. *Arch Neurol* 42:753-756

Hackam AS, Yassa AS, Singaraja R, *et al.* (2000) Huntingtin interacting protein 1 induces apoptosis via a novel caspase-dependent death effector domain. *J Biol Chem* 275:41299-41308

Hanada M, Ninomiya-Tsuji J, Komaki K, *et al.* (2001) Regulation of the TAK1 signaling pathway by protein phosphatase 2C. *J Biol Chem* 276:5753-5759

Hardie RJ, Pullon HW, Harding AE, *et al.* (1991) Neuroacanthocytosis. A clinical, haematological and pathological study of 19 cases. *Brain* 114 (Pt 1A):13-49

Hayflick SJ (2003) Unraveling the Hallervorden-Spatz syndrome: pantothenate kinase-associated neurodegeneration is the name. *Curr Opin Pediatr* 15:572-577

Hayflick SJ, Westaway SK, Levinson B, *et al.* (2003) Genetic, clinical, and radiographic delineation of Hallervorden-Spatz syndrome. *N Engl J Med* 348:33-40

Hegele RA, Miskie BA (2002) Acanthocytosis in a patient with homozygous familial hypobetalipoproteinemia due to a novel APOB splice site mutation. *Clin Genet* 61:101-103

Hentze MW, Kulozik AE (1999) A perfect message: RNA surveillance and nonsense-mediated decay. *Cell* 96:307-310

Herbert PN, Assman G, Gotto AMJ, Fredrickson DS (1983) Familial lipoprotein deficiency: abetalipoproteinemia; hypobetalipoproteinemia and Tangier's disease. In: Stanbury JB, Wyngaarden JB, Fredrickson DS, Goldstein JL, Brown MS (eds) *The metabolic bases of inherited disease*. McGraw-Hill, New York, pp 605-607

Higuchi I, Yamano T, Kuriyama M, *et al.* (1993) Histochemical and ultrastructural pathology of skeletal muscle in a patient with abetalipoproteinemia. *Acta Neuropathol (Berl)* 86:529-531

Hirano T, Kinoshita N, Morikawa K, Yanagida M (1990) Snap helix with knob and hole: essential repeats in S. pombe nuclear protein nuc2+. *Cell* 60:319-328

Hirayama M, Hamano T, Shiratori M, *et al.* (1997) Chorea-acanthocytosis with polyclonal antibodies to ganglioside GM1. *J Neurol Sci* 151:23-24

Ho M, Chelly J, Carter N, Danek A, Crocker P, Monaco AP (1994) Isolation of the gene for McLeod syndrome that encodes a novel membrane transport protein. *Cell* 77:869-880

Ho MF, Monaco AP, Blonden LA, *et al.* (1992) Fine mapping of the McLeod locus (XK) to a 150-380-kb region in Xp21. *Am J Hum Genet* 50:317-330

Holmes SE, O'Hearn E, Rosenblatt A, *et al.* (2001) A repeat expansion in the gene encoding junctophilin-3 is associated with Huntington disease-like 2. *Nat Genet* 29:377-378

Hosokawa S, Ichiya Y, Kuwabara Y, *et al.* (1987) Positron emission tomography in cases of chorea with different underlying diseases. *J Neurol Neurosurg Psychiatry* 50:1284-1287

Houlden H, Lincoln S, Farrer M, Cleland PG, Hardy J, Orrell RW (2003) Compound heterozygous PANK2 mutations confirm HARP and Hallervorden-Spatz syndromes are allelic. *Neurology* 61:1423-1426

Huschtscha LI, Holliday R (1983) Limited and unlimited growth of SV40-transformed cells from human diploid MRC-5 fibroblasts. *J Cell Sci* 63:77-99

Ishikawa S, Tachibana N, Tabata KI, *et al.* (2000) Muscle CT scan findings in McLeod syndrome and chorea-acanthocytosis. *Muscle Nerve* 23:1113-1116

Jiang Z, Ninomiya-Tsuji J, Qian Y, Matsumoto K, Li X (2002) Interleukin-1 (IL-1) receptor-associated kinase-dependent IL-1-induced signaling complexes phosphorylate TAK1 and TAB2 at the plasma membrane and activate TAK1 in the cytosol. *Mol Cell Biol* 22:7158-7167

Johnson SE, Dahl A, Sjaastad O (1998) Progressive pseudobulbar paresis, early choreiform movements, and later rigidity: appearance in two sets of dizygotic twins in the same family. *Mov Disord* 13:556-562

Jung HH, Brandner S (2002) Malignant McLeod myopathy. *Muscle Nerve* 26:424-427

Jung HH, Hergersberg M, Kneifel S, *et al.* (2001a) McLeod syndrome: a novel mutation, predominant psychiatric manifestations, and distinct striatal imaging findings. *Ann Neurol* 49:384-392

Jung HH, Hergersberg M, Vogt M, *et al.* (2003) McLeod phenotype associated with a XK missense mutation without hematologic, neuromuscular, or cerebral involvement. *Transfusion* 43:928-938

Jung HH, Russo D, Redman C, Brandner S (2001b) Kell and XK immunohistochemistry in McLeod myopathy. *Muscle Nerve* 24:1346-1351

Kao FT, Puck TT (1968) Genetics of somatic mammalian cells, VII. Induction and isolation of nutritional mutants in Chinese hamster cells. *Proc Natl Acad Sci U S A* 60:1275-1281

Kartsounis LD, Hardie RJ (1996) The pattern of cognitive impairments in neuroacanthocytosis. A frontosubcortical dementia. *Arch Neurol* 53:77-80

Kataoka Y, Koizumi S, Kohzuma M, *et al.* (1995) NMDA receptor involvement in endothelin neurotoxicity in rat striatal slices. *Eur J Pharmacol* 273:285-289

Kay MM (1981) Isolation of the phagocytosis-inducing IgG-binding antigen on senescent somatic cells. *Nature* 289:491-494

Kay MM, Bosman G, Johnson RC, Poulin J, Lawrence C, Goodman J (1994) Molecular basis of human band-3 mutation associated with increased anion transport. *Exp Clin Immunogenet* 11:209-221

Kay MM, Goodman J, Goodman S, Lawrence C (1990a) Membrane protein band 3 alteration associated with neurologic disease and tissue-reactive antibodies. *Exp Clin Immunogenet* 7:181-199

Kay MM, Goodman J, Lawrence C, Bosman G (1990b) Membrane channel protein abnormalities and autoantibodies in neurological disease. *Brain Res Bull* 24:105-111

Khamlichi S, Bailly P, Blanchard D, Goossens D, Cartron JP, Bertrand O (1995) Purification and partial characterization of the erythrocyte Kx protein deficient in McLeod patients. *Eur J Biochem* 228:931-934

Kito S, Itoga E, Hiroshige Y, Matsumoto N, Miwa S (1980) A pedigree of amyotrophic chorea with acanthocytosis. *Arch Neurol* 37:514-517

Kivitie-Kallio S, Norio R (2001) Cohen syndrome: essential features, natural history, and heterogeneity. *Am J Med Genet* 102:125-135

Kliman HJ, Steck TL (1980) Association of glyceraldehyde-3-phosphate dehydrogenase with the human red cell membrane. A kinetic analysis. *J Biol Chem* 255:6314-6321

Knowles BB, Howe CC, Aden DP (1980) Human hepatocellular carcinoma cell lines secrete the major plasma proteins and hepatitis B surface antigen. *Science* 209:497-499

Kolehmainen J, Black GC, Saarinen A, *et al.* (2003) Cohen syndrome is caused by mutations in a novel gene, COH1, encoding a transmembrane protein with a presumed role in vesicle-mediated sorting and intracellular protein transport. *Am J Hum Genet* 72:1359-1369

Komaki K, Katsura K, Ohnishi M, *et al.* (2003) Molecular cloning of PP2Ceta, a novel member of the protein phosphatase 2C family. *Biochim Biophys Acta* 1630:130-137

Krawczak M, Reiss J, Cooper DN (1992) The mutational spectrum of single base-pair substitutions in mRNA splice junctions of human genes: causes and consequences. *Hum Genet* 90:41-54

Kremer B, Goldberg P, Andrew SE, *et al.* (1994) A worldwide study of the Huntington's disease mutation. The sensitivity and specificity of measuring CAG repeats. *N Engl J Med* 330:1401-1406

Kuroiwa Y, Ohnishi A, Sato Y, Kanazawa I (1984) Chorea acanthocytosis: clinical pathological and biochemical aspects. *Int J Neurol* 18:64-74

Kuypers FA, van Linde-Sibenius Trip M, Roelofsen B, Op den Kamp JA, Tanner MJ, Anstee DJ (1985) The phospholipid organisation in the membranes of McLeod and Leach phenotype erythrocytes. *FEBS Lett* 184:20-24

Lamb JR, Tugendreich S, Hieter P (1995) Tetratrico peptide repeat interactions: to TPR or not to TPR? *Trends Biochem Sci* 20:257-259

Lee S, Lin M, Mele A, *et al.* (1999) Proteolytic processing of big endothelin-3 by the kell blood group protein. *Blood* 94:1440-1450

Lee S, Russo D, Redman C (2000) Functional and structural aspects of the Kell blood group system. *Transfus Med Rev* 14:93-103

Lee S, Zambas ED, Marsh WL, Redman CM (1991) Molecular cloning and primary structure of Kell blood group protein. *Proc Natl Acad Sci U S A* 88:6353-6357

Lepke S, Fasold H, Pring M, Passow H (1976) A study of the relationship between inhibition of anion exchange and binding to the red blood cell membrane of 4,4'-diisothiocyano stilbene-2,2'-disulfonic acid (DIDS) and its dihydro derivative (H2DIDS). *J Membr Biol* 29:147-177

Levine IM, Estes JW, Looney JM (1968) Hereditary neurological disease with acanthocytosis. A new syndrome. *Arch Neurol* 19:403-409

Li MG, Katsura K, Nomiyama H, *et al.* (2003) Regulation of the interleukin-1-induced signaling pathways by a novel member of the protein phosphatase 2C family (PP2Cepsilon). *J Biol Chem* 278:12013-12021

Limos LC, Ohnishi A, Sakai T, Fujii N, Goto I, Kuroiwa Y (1982) "Myopathic" changes in chorea-acanthocytosis. Clinical and histopathological studies. *J Neurol Sci* 55:49-58

Linton MF, Farese RV, Jr., Young SG (1993) Familial hypobetalipoproteinemia. *J Lipid Res* 34:521-541

Loomis WF (1982) *The development of Dictyostelium discoideum.* Academic Press, San Diego

Lozzio BB, Lozzio CB, Bamberger EG, Feliu AS (1981) A multipotential leukemia cell line (K-562) of human origin. *Proc Soc Exp Biol Med* 166:546-550

Machlin LJ, Filipski R, Nelson J, Horn LR, Brin M (1977) Effects of a prolonged vitamin E deficiency in the rat. *J Nutr* 107:1200-1208

Maeda S, Wu S, Juppner H, *et al.* (1996) Cell-specific signal transduction of parathyroid hormone (PTH)-related protein through stably expressed recombinant PTH/PTHrP receptors in vascular smooth muscle cells. *Endocrinology* 137:3154-3162

Malandrini A, Fabrizi GM, Palmeri S, *et al.* (1993) Choreo-acanthocytosis like phenotype without acanthocytes: clinicopathological case report. A

contribution to the knowledge of the functional pathology of the caudate nucleus. *Acta Neuropathol (Berl)* 86:651-658

Malandrini A, Fabrizi GM, Truschi F, *et al.* (1994) Atypical McLeod syndrome manifested as X-linked chorea-acanthocytosis, neuromyopathy and dilated cardiomyopathy: report of a family. *J Neurol Sci* 124:89-94

Mann CJ, Anderson TA, Read J, *et al.* (1999) The structure of vitellogenin provides a molecular model for the assembly and secretion of atherogenic lipoproteins. *J Mol Biol* 285:391-408

Marchesi VT, Furthmayr H, Tomita M (1976) The red cell membrane. *Annu Rev Biochem* 45:667-698

Marsh WL, Marsh NJ, Moore A, Symmans WA, Johnson CL, Redman CM (1981) Elevated serum creatine phosphokinase in subjects with McLeod syndrome. *Vox Sang* 40:403-411

Marsh WL, Oyen R, Nichols ME, Allen FH, Jr. (1975a) Chronic granulomatous disease and the Kell blood groups. *Br J Haematol* 29:247-262

Marsh WL, Taswell HF, Oyen R, Nichols ME, Vergara MS, Pineda AA (1975b) Kx antigen of the Kell system and its relationship to chronic granulomatous disease. Evidence that the Kx gene is X-linked. *Transfusion* 15:527

Marson AM, Bucciantini E, Gentile E, Geda C (2003) Neuroacanthocytosis: clinical, radiological, and neurophysiological findings in an Italian family. *Neurol Sci* 24:188-189

Mattson MP, Camandola S (2001) NF-kappaB in neuronal plasticity and neurodegenerative disorders. *J Clin Invest* 107:247-254

McAllister RM, Melnyk J, Finkelstein JZ, Adams EC, Jr., Gardner MB (1969) Cultivation in vitro of cells derived from a human rhabdomyosarcoma. *Cancer* 24:520-526

Medalia A, Merriam A, Sandberg M (1989) Neuropsychological deficits in choreoacanthocytosis. *Arch Neurol* 46:573-575

Melone MA, Di Fede G, Peluso G, *et al.* (2002) Abnormal accumulation of tTGase products in muscle and erythrocytes of chorea-acanthocytosis patients. *J Neuropathol Exp Neurol* 61:841-848

Mohandas N, Chasis JA (1993) Red blood cell deformability, membrane material properties and shape: regulation by transmembrane, skeletal and cytosolic proteins and lipids. *Semin Hematol* 30:171-192

Mohandas N, Gascard P (1999) What do mouse gene knockouts tell us about the structure and function of the red cell membrane? *Baillieres Best Pract Res Clin Haematol* 12:605-620

Nakamura F, Kato M, Kameyama K, *et al.* (1995) Characterization of Gq family G proteins GL1 alpha (G14 alpha), GL2 alpha (G11 alpha), and Gq alpha expressed in the baculovirus-insect cell system. *J Biol Chem* 270:6246-6253

Nakayama K (1997) Furin: a mammalian subtilisin/Kex2p-like endoprotease involved in processing of a wide variety of precursor proteins. *Biochem J* 327 (Pt 3):625-635

Neuman RJ, Yuan B, Gerhard DS, *et al.* (2002) Replication of linkage of familial hypobetalipoproteinemia to chromosome 3p in six kindreds. *J Lipid Res* 43:407-415

Nishi M, Hashimoto K, Kuriyama K, *et al.* (2002) Motor discoordination in mutant mice lacking junctophilin type 3. *Biochem Biophys Res Commun* 292:318-324

Nishi M, Mizushima A, Nakagawara K, Takeshima H (2000) Characterization of human junctophilin subtype genes. *Biochem Biophys Res Commun* 273:920-927

Notredame C, Higgins DG, Heringa J (2000) T-Coffee: A novel method for fast and accurate multiple sequence alignment. *J Mol Biol* 302:205-217

Ohnishi A, Sato Y, Nagara H, *et al.* (1981) Neurogenic muscular atrophy and low density of large myelinated fibres of sural nerve in chorea-acanthocytosis. *J Neurol Neurosurg Psychiatry* 44:645-648

Olivieri O, De Franceschi L, Bordin L, *et al.* (1997) Increased membrane protein phosphorylation and anion transport activity in chorea-acanthocytosis. *Haematologica* 82:648-653

Olofsson SO, Asp L, Boren J (1999) The assembly and secretion of apolipoprotein B-containing lipoproteins. *Curr Opin Lipidol* 10:341-346

Ong B, Devathasan G, Chong PN (1989) Choreoacanthocytosis in a Chinese patient--a case report. *Singapore Med J* 30:506-508

Oshima M, Osawa Y, Asano K, Saito T (1985) Erythrocyte membrane abnormalities in patients with amyotrophic chorea with acanthocytosis. Part 1. Spin labeling studies and lipid analyses. *J Neurol Sci* 68:147-160

Peppard RF, Lu CS, Chu NS, Teal P, Martin WR, Calne DB (1990) Parkinsonism with neuroacanthocytosis. *Can J Neurol Sci* 17:298-301

Puck TT, Cieciura SJ, Robinson A (1958) Genetics of somatic mammalian cells. III. Long-term cultivation of euploid cells from human and animal subjects. *J Exp Med* 108:945-956

Raabe M, Flynn LM, Zlot CH, *et al.* (1998) Knockout of the abetalipoproteinemia gene in mice: reduced lipoprotein secretion in heterozygotes and embryonic lethality in homozygotes. *Proc Natl Acad Sci U S A* 95:8686-8691

Raabe M, Veniant MM, Sullivan MA, *et al.* (1999) Analysis of the role of microsomal triglyceride transfer protein in the liver of tissue-specific knockout mice. *J Clin Invest* 103:1287-1298

Rampoldi L, Danek A, Monaco AP (2002) Clinical features and molecular bases of neuroacanthocytosis. *J Mol Med* 80:475-491

Rampoldi L, Dobson-Stone C, Rubio JP, *et al.* (2001) A conserved sorting-associated protein is mutant in chorea-acanthocytosis. *Nat Genet* 28:119-120

Raymond CK, Howald-Stevenson I, Vater CA, Stevens TH (1992) Morphological classification of the yeast vacuolar protein sorting mutants: evidence for a prevacuolar compartment in class E vps mutants. *Mol Biol Cell* 3:1389-1402

Redding K, Brickner JH, Marschall LG, Nichols JW, Fuller RS (1996) Allele-specific suppression of a defective trans-Golgi network (TGN) localization signal in Kex2p identifies three genes involved in localization of TGN transmembrane proteins. *Mol Cell Biol* 16:6208-6217

Redman CM, Marsh WL, Scarborough A, Johnson CL, Rabin BI, Overbeeke M (1988) Biochemical studies on McLeod phenotype red cells and isolation of Kx antigen. *Br J Haematol* 68:131-136

Rinne JO, Daniel SE, Scaravilli F, Harding AE, Marsden CD (1994a) Nigral degeneration in neuroacanthocytosis. *Neurology* 44:1629-1632

Rinne JO, Daniel SE, Scaravilli F, Pires M, Harding AE, Marsden CD (1994b) The neuropathological features of neuroacanthocytosis. *Mov Disord* 9:297-304

Roth AM, Hepler RS, Mukoyama M, Cancilla PA, Foos RY (1971) Pigmentary retinal dystrophy in Hallervorden-Spatz disease: clinicopathological report of a case. *Surv Ophthalmol* 16:24-35

Rothman JE, Lenard J (1977) Membrane asymmetry. *Science* 195:743-753

Rubio JP, Danek A, Stone C, *et al.* (1997) Chorea-acanthocytosis: genetic linkage to chromosome 9q21. *Am J Hum Genet* 61:899-908

Rubio JP, Levy ER, Dobson-Stone C, Monaco AP (1999) Genomic organization of the human galpha14 and Galphaq genes and mutation analysis in chorea-acanthocytosis (CHAC). *Genomics* 57:84-93

Russo D, Redman C, Lee S (1998) Association of XK and Kell blood group proteins. *J Biol Chem* 273:13950-13956

Russo D, Wu X, Redman CM, Lee S (2000) Expression of Kell blood group protein in nonerythroid tissues. *Blood* 96:340-346

Russo DC, Lee S, Reid ME, Redman CM (2002) Point mutations causing the McLeod phenotype. *Transfusion* 42:287-293

Saiki S, Sakai K, Kitagawa Y, Saiki M, Kataoka S, Hirose G (2003) Mutation in the CHAC gene in a family of autosomal dominant chorea-acanthocytosis. *Neurology* 61:1614-1616

Sakai T, Antoku Y, Iwashita H, Goto I, Nagamatsu K, Shii H (1991) Chorea-acanthocytosis: abnormal composition of covalently bound fatty acids of erythrocyte membrane proteins. *Ann Neurol* 29:664-669

Sakai T, Iwashita H, Kakugawa M (1985) Neuroacanthocytosis syndrome and choreoacanthocytosis (Levine-Critchley syndrome). *Neurology* 35:1679

Sakai T, Mawatari S, Iwashita H, Goto I, Kuroiwa Y (1981) Choreoacanthocytosis. Clues to clinical diagnosis. *Arch Neurol* 38:335-338

Salhany JM, Shaklai N (1979) Functional properties of human hemoglobin bound to the erythrocyte membrane. *Biochemistry* 18:893-899

Sambrook J, Fritsch EF, Maniatis T (1989) *Molecular Cloning: A Laboratory Manual (2nd edn)*. Cold Spring Harbor Laboratory Press, New York

Scherer WF, Hoogasian AF (1954) Preservation at subzero temperatures of mouse fibroblasts (strain L) and human epithelial cells (strain HeLa). *Proc Soc Exp Biol Med* 87:480-487

Schonfeld G (2003) Familial hypobetalipoproteinemia: a review. *J Lipid Res* 44:878-883

Schonfeld G, Patterson BW, Yablonskiy DA, *et al.* (2003) Fatty liver in familial hypobetalipoproteinemia: triglyceride assembly into VLDL particles is affected by the extent of hepatic steatosis. *J Lipid Res* 44:470-478

Schwartz JF, Rowland LP, Eder HA, *et al.* (1961) Bassen-Kornweig syndrome. Neuromuscular disorder resembling Friedreich's ataxia associated with

retinitis pigmentosa, acanthocytosis, steatorrhea, and an abnormality of lipid metabolism. *Trans Am Neurol Assoc* 86:49-53

Scriver CR (2001) Human genetics: lessons from Quebec populations. *Annu Rev Genomics Hum Genet* 2:69-101

Serra S, Xerra A, Arena A (1986) Amyotrophic choreo-acanthocytosis: a new observation in southern Europe. *Acta Neurol Scand* 73:481-486

Serra S, Xerra A, Scribano E, Meduri M, Di Perri R (1987) Computerized tomography in amyotrophic choreo-acanthocytosis. *Neuroradiology* 29:480-482

Sharp D, Blinderman L, Combs KA, *et al.* (1993) Cloning and gene defects in microsomal triglyceride transfer protein associated with abetalipoproteinaemia. *Nature* 365:65-69

Sheetz MP, Singer SJ (1974) Biological membranes as bilayer couples. A molecular mechanism of drug-erythrocyte interactions. *Proc Natl Acad Sci U S A* 71:4457-4461

Shibasaki H, Sakai T, Nishimura H, Sato Y, Goto I, Kuroiwa Y (1982) Involuntary movements in chorea-acanthocytosis: a comparison with Huntington's chorea. *Ann Neurol* 12:311-314

Shibuya H, Yamaguchi K, Shirakabe K, *et al.* (1996) TAB1: an activator of the TAK1 MAPKKK in TGF-beta signal transduction. *Science* 272:1179-1182

Shirakabe K, Yamaguchi K, Shibuya H, *et al.* (1997) TAK1 mediates the ceramide signaling to stress-activated protein kinase/c-Jun N-terminal kinase. *J Biol Chem* 272:8141-8144

Sikorski RS, Boguski MS, Goebl M, Hieter P (1990) A repeating amino acid motif in CDC23 defines a family of proteins and a new relationship among genes required for mitosis and RNA synthesis. *Cell* 60:307-317

Simon ER, Ways P (1964) Incubation Hemolysis and Red Cell Metabolism in Acanthocytosis. *J Clin Invest* 43:1311-1321

Simon MI, Strathmann MP, Gautam N (1991) Diversity of G proteins in signal transduction. *Science* 252:802-808

Singleton BK, Green CA, Renaud S, Fuhr P, Poole J, Daniels GL (2003) McLeod syndrome resulting from a novel XK mutation. *Br J Haematol* 122:682-685

Sobue G, Mukai E, Fujii K, Mitsuma T, Takahashi A (1986) Peripheral nerve involvement in familial chorea-acanthocytosis. *J Neurol Sci* 76:347-356

Sorrentino G, De Renzo A, Miniello S, Nori O, Bonavita V (1999) Late appearance of acanthocytes during the course of chorea-acanthocytosis. *J Neurol Sci* 163:175-178

Sotaniemi KA (1983) Chorea-acanthocytosis. Neurological disease with acanthocytosis. *Acta Neurol Scand* 68:53-56

Spitz MC, Jankovic J, Killian JM (1985) Familial tic disorder, parkinsonism, motor neuron disease, and acanthocytosis: a new syndrome. *Neurology* 35:366-370

Stanfield GM, Horvitz HR (2000) The ced-8 gene controls the timing of programmed cell deaths in C. elegans. *Mol Cell* 5:423-433

Stege JT, Laub MT, Loomis WF (1999) tip genes act in parallel pathways of early Dictyostelium development. *Dev Genet* 25:64-77

Stevenson VL, Hardie RJ (2001) Acanthocytosis and neurological disorders. *J Neurol* 248:87-94

Storch A, Kornhass M, Schwarz J (2004) Acanthocytosis in movement disorders: How much is normal? *(Manuscript in preparation)*

Strapazon E, Steck TL (1977) Interaction of the aldolase and the membrane of human erythrocytes. *Biochemistry* 16:2966-2971

Stryer L (1995) Protein Structure and Function. In: *Biochemistry*. W. H. Freeman and Company, New York

Swash M, Schwartz MS, Carter ND, Heath R, Leak M, Rogers KL (1983) Benign X-linked myopathy with acanthocytes (McLeod syndrome). Its relationship to X-linked muscular dystrophy. *Brain* 106 (Pt 3):717-733

Symmans WA, Shepherd CS, Marsh WL, Oyen R, Shohet SB, Linehan BJ (1979) Hereditary acanthocytosis associated with the McLeod phenotype of the Kell blood group system. *Br J Haematol* 42:575-583

Takaesu G, Kishida S, Hiyama A, *et al.* (2000) TAB2, a novel adaptor protein, mediates activation of TAK1 MAPKKK by linking TAK1 to TRAF6 in the IL-1 signal transduction pathway. *Mol Cell* 5:649-658

Takashima H, Sakai T, Iwashita H, *et al.* (1994) A family of McLeod syndrome, masquerading as chorea-acanthocytosis. *J Neurol Sci* 124:56-60

Takeshima H, Komazaki S, Nishi M, Iino M, Kangawa K (2000) Junctophilins: a novel family of junctional membrane complex proteins. *Mol Cell* 6:11-22

Takeshita J, Arai Y, Hirose N, Tsukamoto H, Shirahase J (2002) Abetalipoproteinemia-like lipid profile and acanthocytosis in a young woman with anorexia nervosa. *Am J Med Sci* 324:281-284

Tamura S, Hanada M, Ohnishi M, Katsura K, Sasaki M, Kobayashi T (2002) Regulation of stress-activated protein kinase signaling pathways by protein phosphatases. *Eur J Biochem* 269:1060-1066

Tanaka M, Hirai S, Kondo S, *et al.* (1998) Cerebral hypoperfusion and hypometabolism with altered striatal signal intensity in chorea-acanthocytosis: a combined PET and MRI study. *Mov Disord* 13:100-107

Tarugi P, Lonardo A (1997) Heterozygous familial hypobetalipoproteinemia associated with fatty liver. *Am J Gastroenterol* 92:1400-1402

Terada N, Fujii Y, Ueda H, *et al.* (1999) Ultrastructural changes of erythrocyte membrane skeletons in chorea-acanthocytosis and McLeod syndrome revealed by the quick-freezing and deep-etching method. *Acta Haematol* 101:25-31

Thomas JG, Baneyx F (1997) Divergent effects of chaperone overexpression and ethanol supplementation on inclusion body formation in recombinant Escherichia coli. *Protein Expr Purif* 11:289-296

Toby GG, Golemis EA (2001) Using the yeast interaction trap and other two-hybrid-based approaches to study protein-protein interactions. *Methods* 24:201-217

Towfighi J (1981) Effects of chronic vitamin E deficiency on the nervous system of the rat. *Acta Neuropathol (Berl)* 54:261-267

Ueno E, Oguchi K, Yanagisawa N (1982) Morphological abnormalities of erythrocyte membrane in the hereditary neurological disease with chorea, areflexia and acanthocytosis. *J Neurol Sci* 56:89-97

Ueno S, Maruki Y, Nakamura M, *et al.* (2001) The gene encoding a newly discovered protein, chorein, is mutated in chorea-acanthocytosis. *Nat Genet* 28:121-122

Velayos-Baeza A, Vettori A, Copley RR, Dobson-Stone C, Monaco AP (2004) Analysis of the human *VPS13* gene family. *Genomics (submitted)*

Villegas A, Moscat J, Vazquez A, *et al.* (1987) A new family with hereditary choreo-acanthocytosis. *Acta Haematol* 77:215-219

Vita G, Serra S, Dattola R, *et al.* (1989) Peripheral neuropathy in amyotrophic chorea-acanthocytosis. *Ann Neurol* 26:583-587

Vonsattel JP, Myers RH, Stevens TJ, Ferrante RJ, Bird ED, Richardson EP, Jr. (1985) Neuropathological classification of Huntington's disease. *J Neuropathol Exp Neurol* 44:559-577

Wahli W (1988) Evolution and expression of vitellogenin genes. *Trends Genet* 4:227-232

Walensky LD, Shi ZT, Blackshaw S, *et al.* (1998) Neurobehavioral deficits in mice lacking the erythrocyte membrane cytoskeletal protein 4.1. *Curr Biol* 8:1269-1272

Walker RH, Morgello S, Davidoff-Feldman B, *et al.* (2002) Autosomal dominant chorea-acanthocytosis with polyglutamine-containing neuronal inclusions. *Neurology* 58:1031-1037

Walker RH, Rasmussen A, Rudnicki D, *et al.* (2003) Huntington's disease-like 2 can present as chorea-acanthocytosis. *Neurology* 61:1002-1004

Wang C, Deng L, Hong M, Akkaraju GR, Inoue J, Chen ZJ (2001) TAK1 is a ubiquitin-dependent kinase of MKK and IKK. *Nature* 412:346-351

Wang J, Hegele RA (2000) Microsomal triglyceride transfer protein (MTP) gene mutations in Canadian subjects with abetalipoproteinemia. *Hum Mutat* 15:294-295

Ward PC (1979) Investigation of poikilocytic normochromic normocytic anemia. 2. Spiculated forms. *Postgrad Med* 65:229-231, 234-225

Wetterau JR, Aggerbeck LP, Bouma ME, *et al.* (1992) Absence of microsomal triglyceride transfer protein in individuals with abetalipoproteinemia. *Science* 258:999-1001

Wichman A, Buchthal F, Pezeshkpour GH, Gregg RE (1985) Peripheral neuropathy in abetalipoproteinemia. *Neurology* 35:1279-1289

Wihl G, Volkmann J, Allert N, Lehrke R, Sturm V, Freund HJ (2001) Deep brain stimulation of the internal pallidum did not improve chorea in a patient with neuro-acanthocytosis. *Mov Disord* 16:572-575

Wilkie TM, Gilbert DJ, Olsen AS, *et al.* (1992) Evolution of the mammalian G protein alpha subunit multigene family. *Nat Genet* 1:85-91

Wimer BM, Marsh WL, Taswell HF, Galey WR (1977) Haematological changes associated with the McLeod phenotype of the Kell blood group system. *Br J Haematol* 36:219-224

Witt TN, Danek A, Reiter M, Heim MU, Dirschinger J, Olsen EG (1992) McLeod syndrome: a distinct form of neuroacanthocytosis. Report of two cases and literature review with emphasis on neuromuscular manifestations. *J Neurol* 239:302-306

Xu X, Croy JT, Zeng W, *et al.* (1998) Promiscuous coupling of receptors to Gq class alpha subunits and effector proteins in pancreatic and submandibular gland cells. *J Biol Chem* 273:27275-27279

Yamaguchi K, Shirakabe K, Shibuya H, *et al.* (1995) Identification of a member of the MAPKKK family as a potential mediator of TGF-beta signal transduction. *Science* 270:2008-2011

Yamamoto T, Hirose G, Shimazaki K, Takado S, Kosoegawa H, Saeki M (1982) Movement disorders of familial neuroacanthocytosis syndrome. *Arch Neurol* 39:298-301

Young SG, Bertics SJ, Curtiss LK, Witztum JL (1987) Characterization of an abnormal species of apolipoprotein B, apolipoprotein B-37, associated with familial hypobetalipoproteinemia. *J Clin Invest* 79:1831-1841

Young SG, Northey ST, McCarthy BJ (1988) Low plasma cholesterol levels caused by a short deletion in the apolipoprotein B gene. *Science* 241:591-593

Yu Z, Zhou D, Cheng G, Mattson MP (2000) Neuroprotective role for the p50 subunit of NF-kappaB in an experimental model of Huntington's disease. *J Mol Neurosci* 15:31-44

Yuan B, Neuman R, Duan SH, *et al.* (2000) Linkage of a gene for familial hypobetalipoproteinemia to chromosome 3p21.1-22. *Am J Hum Genet* 66:1699-1704

Zhang B, Chang A, Kjeldsen TB, Arvan P (2001) Intracellular retention of newly synthesized insulin in yeast is caused by endoproteolytic processing in the Golgi complex. *J Cell Biol* 153:1187-1198

Zhou B, Westaway SK, Levinson B, Johnson MA, Gitschier J, Hayflick SJ (2001) A novel pantothenate kinase gene (PANK2) is defective in Hallervorden-Spatz syndrome. *Nat Genet* 28:345-349

Appendix 1: PCR primers used in this study

A1.1 Primers for amplification of *VPS13A* exons

Exon	Forward primer[a]	Reverse primer[a]	Amplicon size (bp)	AT (°C)[b], [Mg] (mM)
1	ACCGCCTCCGTCTCTCGCTGG	GAAGCCCCGAGAACGCAG	362	62, 2*
2	CTGATTATGACAGGAATGAAG	TAAGGTGACAAACTGAATCAGG	212	58, 2.5
3	GTTGATGATAAGGAAATGTGTAAG	GCTCAGAAACATGAAAAATATCAC	275	54, 3
4	AGAAAATAGACTAACCATAAATGC	CAAAGTTGCCAAAAATGTAGAG	339	58, 2.5
5	CCAATTAATGATTATTTGTAAGG	GAAATAATCTCAGCATCTCCAG	295	54, 2.5
6	ATTTCAGCAAGGCAACGTAAGC	CTTTTGGGATTTAACAGATTGG	312	58, 2.5
7	GGGAGCCGCTGCACATTGACAG	GACACCTATTTCTGATGCTGGC	249	58, 2.5
8	TGAAAGGGACATTGGTCTAGGG	TTAAGTGAGCCATATCACAGAG	288	58, 2.5
9	TTTAACTCTGTGATATGGCTCAC	GTATAGTTACACACATCTTCACC	342	58, 2.5
10	TGGCATGAATATAAATAAAAGC	TGCAGCGTGATCTTACTATTTCG	469	58, 2.5
11	CCACACATGGTTCATCTGACTG	TTGCTTTTATCAAACAATAATTCAC	343	54, 3
12	CCCTAAAAAGTCAGTAATGTAAC	CTCAATAAGCTAAAGCAGCTAC	360	58, 2.5
13	TGTTGTTAGAGTAGAAGCAATG	GGAATGAAAGGTAGGGAGTATC	342	58, 2.5
14	GAATGTTCTGTTGTTTGCTTCC	ACTAAAAAGCAAATTGAACCAC	315	58, 2.5
15	GCTCAAGAGGATAAGTTCTCAG	GACACCCAGTGATTAACTATGC	274	58, 2.5
16	TTTATTAAAGGCAGATACATTGTG	TATATTCTAAGGTATAAGGCAAG	207	58, 3
17	GGGGTCAATGTGATGATTCTTG	ACTAAGATTGTGACCTAATGTC	360	58, 2.5
18	ATTGTATGTCTTCTTTGATGGG	CTATACTATTCACTGTCCTCTG	434	58, 2.5
19	AATTTAGTTTGCTTTGAGTTTGTG	CTAGGTATGAACTTTCTGAGTG	367	54, 2.5
20	TTGGAAGTATTTTGCTGAGGTC	AACAAAGAAACACCCCAAATGC	333	58, 2.5
21	TACTTGTGAATTTATCCTCTCC	ATCACTTCAACAAAATCAATCAAC	292	58, 2.5
22	AATGGAATGTGTGACTATGAAG	AGGAAGAGTCAGTTAAGTATGG	291	58, 2.5
23	TAAGACGGAAATTGGAATAGAG	TGTGGACTTTCTTAATTCATGC	327	58, 2.5
24	GCGGTGAATAAACATTTTTGTGC	CTTCCTCTGTGTGGTCCTTTGAG	230	62, 2.5
25	AGAGAGCCTTAGTGTTTTAGTG	GAGTGACCAAGAATCACACAGC	402	58, 2.5
26	GTGTATTGTATGTCTGTGTGGG	TCTAGCAGGTAGTCAAACAATG	374	58, 2.5
27	CATTTATTTTCAGTTACCTTTCC	TACAAAGAGATTATGTTACAGTG	254	54, 2.5
28	TGATTGTATATGTATGTCTTCC	GCTGATTTTTCCTCTGATTGC	414	58, 2.5
29	TCTAACTGGAATTGTAAGATCC	CCTGGCATATAATGAATCCTTC	444	54, 2.5
30	AGTAGGGAATATCATACCTTGC		519	58, 2.5
31		CCTATGACCACTCTTAAAGGAC		
32	CAGTTACAGTAGAATTGTTGCC	CTAGTCTTCATCCATATTTGAC	398	58, 2.5
33	AATAATGCTTGGTTGTATCAAG	TCTCACTGTAAACAGACTACTC	522	58, 2.5
34	GATATTTTCCCTTTATACCCAAC	TCAAATGATGCCTTATGTCCCC	360	58, 2.5
35	GTGGTAGAGGATTGAAACAGTC	GAGATGTCTGAATGGAATTAGC	473	58, 2.5
36	GCCAGAAGTTACTGAGTTTTAC	TTCTCAGAGGGACAGATACTAC	412	58, 2.5
37	GCCTTTCATTAGAGCCCTTCGG	TACGAGCTGACTGAATTGAAGC	445	58, 2.5
38	TTCCCAAGAGACATGACTTCAG	AAGGCTAATCAAGGTTAAGTCC	424	58, 2.5
39	GGTTGTAGTTGATTCCTTTGGG	TTACAGAGCAAGGTTGGAAAGC	477	58, 3
40	AGATATTAGGTTCTAGATGTCC	CACACCTATTTTGTTTGCATAAC	384	54, 2.5
41	TGACGTAGTATGTTTGAAAGTG	TACACAAGATTCCATAATATTCC	508	58, 2.5
42	TACTGAATGGCATGTAGACTGG	TGATGAGACAACCTGAACCTTG	488	58, 2.5

Exon	Forward primer[a]	Reverse primer[a]	Amplicon size (bp)	AT (°C)[b], [Mg] (mM)
43	CCTTTCTAATGTTGGTATTGGG	ATGACAAGGAGAACAGTAAAGG	360	58, 2.5
44	ACTTGTCTGATTGATCTGTCTG	CCTTGCTAAGATTCTACAAAAGAG	474	58, 2.5
45	TGCTGGCTTCTTAAAATATCCC	ACTGTTACGGTTTATATTCTTTC	433	58, 2.5
46	GCCTGATAGTTCCTTTGTTAAG	CACTGAAACCTAAATACGTTAG	337	58, 2.5
47	ACTACAATATTATGAAAGGAGG	CTGCATTACCTATTCTTTACTAG	523	54, 2
48	GACTTGTTCTGATAGGTATTTC	TTAACAAGTTATTTCTACCAAG	631	54, 4
49	GAAACTTGGATAGAAATAACTTG	ATCATTTCCTTCTTCAGCCACTG	528	58, 2.5
50	CTGAAAATGGACTATCAAGTGAG	GGGGAGAGTTAAAACATTACATGG	382	58, 2.5
51	CTAGAGCAGTGTTAAAACAGG	ATCTTAGATCTCTGTTTCCTTC	417	58, 3
52	TGAATTGTTTTCTCAGTCATCC	TCAGAGACTCCTAACAAACTC	321	58, 2.5
53	CAGAACGATCACAGATCTCAG	AAAGGCTGCTGGGAACACC	283	58, 2.5
54	CCACTAACCCCATGAAGTAGG	AGCACTACCACAGTATCAATG	491	58, 2.5
55	GCTCACTTGTAATTGAGGCTG	TATACAAGGTATGTATGACAGG	410	58, 2.5
56	TGTGAATTTTATGGACATGGG	GCTAGCACAACATTGAAACTG	411	58, 2.5
57	GTGCTTGGTCACCGCTAGAC	GTGTATAGTACTTGCTGGTCC	350	58, 2.5
58	GTAGTAGATTTTGCCAATATCAG	TGCTTAAATCTTTGACTTGTCC	319	54, 2
59	TTGCTGTTATTAACAGTGTTCC	AAGGTATGTACCACAAGAGAG	412	58, 2.5
60	CCTTCTGAGGCAATCATAAGC	GCTATAGGTGGCTCCACATG	435	58, 2.5
61	TAGTGATTTTAACATAATCCAG	GCCTATGATCTGCAACGTAC	393	58, 2.5
62	ACTAGAAGGAAAGGTTTGGAG	ATTCTGAGGAAAATACCCATGC	338	58, 2.5
63	TGGCATTAAAGGTGTTGGCCTG	CCTCTTACCATTGTTTGCTGC	373	58, 2.5
64	AGTGAATATAACTCACTCACTC		498	54, 2.5
65		ACCCACTGCTCTTAAAATATCC		
66	TACTTAGGAGATCTGTTAATTC		473	56, 2
67		ATGCCTGAAGCCAAAGAGCAG		
68	GACTTAAACTTCTCTATAGTTCTG	TTAAGCAAAATAGATAAAAGCCC	416	54, 2
69	TAATTACAGTCTGAGTCATAGC	TATGGGCATTATGGTATAAGTC	317	54, 2.5
70	GTTTGCCCCATTGAGAAATGG	GAAGACCCAAGAATCAGTGTG	309	58, 2.5
71	TTTGCACTTGCGATTCATTCG	AAGCCTGGGTAAGATAGCAGG	366	58, 2.5
72	AGGGACACTTTAGGCATACAG	AGTCTGGGGTAAATATTATCTGG	349	58, 2.5
73	ATTGGCTGTCAGTATTACACC	AGCATCCAGAATACAGGGTAC	294	54, 2.5

[a]: When exons were amplified as a single amplicon, the forward primer is indicated on the row of the exon most 5', the reverse primer on the row of the exon most 3'. [b]: A 'touchdown' program was used to amplify exons for DHPLC analysis (see section 2.2.2)
Key: AT, annealing temperature; [Mg], $MgCl_2$ concentration; * addition of deaza dGTP (see section 2.2.2)

A1.2 Primers for amplification of *VPS13A* cDNA

Region amplified (nt)[a]	Primer name (direction)	Primer sequence	Amplicon size (bp)	AT (°C), [Mg] (mM)
2193-2755	KIAArt13 (F)	AAACTCAGTGTATCTACCCAGC	563	60, 2
	KIAArt11 (R)	TCTCAATTTCTGCACCCAATCC		
516-1543	KIAArt22 (F)	GCTGTCATTTGGTATTTCCCTTC	1028	58, 2.5
	KIAArt15 (R)	TTACAATATCTACCAGCTCAGG		
8871-9580	222006fp6 (F)	AGAAGGCATCACTCGTGGAGG	710	60, 2
	BCD3239fp1 (R)	GTAGTCTAGGAGCTGTAATCAC		

[a]: Nucleotides are numbered according to the cDNA sequence of *CHAC* isoform A reported by Rampoldi *et al.* (2001) (Genbank accession no. NM_033305), with the adenosine of the initiation codon assigned position 1.
Key: F, forward; R, reverse; AT, annealing temperature; [Mg], $MgCl_2$ concentration

A1.3 Primers for amplification of Chromosome 9 microsatellite markers

Marker	Primer sequence	Label[a]	Amplicon size range (bp)	AT (°C), [Mg] (mM)
GATA89a11	F: GCTTCTGAAAGCTTCTAGTTTACC	TET	186-210	55, 2
	R: AATAGTAATGCCATTTGTGATAGG			
D9S1674	F: GGCCTACCCTGTAGACTGAC	FAM	216-232	53, 1.5
	R: TTAGAAGTGAGCCAAACTCAAA			
GATA89c08	F: AGCCCAAGCTTTTAACCACT	FAM	342-366	58, 2
	R: GCTGCTTAGCTAAACATGGC			
D9S153	F: TTATGGCAGCCCAAATGGACTA	FAM	143-155	58, 1.5
	R: GCAGAATGTTGCCCAAAACTCA			
D9S1780	F: ACATTGTGTCTTATTCTGCATGA	TET	241-259	55, 1.5
	R: CGCTTTGTAAAGATAGCCTCA			
D9S1867	F: GTGAACTGCATCAGCCG	HEX	172-210	55, 2
	R: ATCAGCCAGGGTTTCAACA			

[a]: Fluorescent label was attached to forward primer only
Key: F, forward primer; R, reverse primer; AT, annealing temperature; [Mg], $MgCl_2$ concentration;

A1.4 Primers for preparation of plasmid constructs

Construct name	Primer name	Primer sequence[a]	Amplicon size (bp)	Notes[b]
pGEX-RT1	XhoRT1F	CCG**CTCGAG**CTCTCTCTGGGCATCTGGAAAGG	918	*Xho*I site
	XhoRT1R	CCG**CTCGAG**ATGGTGGTGAAGAGGCACATCAGG		*Xho*I site
pGEX-RT2	CHACRT1 (F)	CCG**CTCGAG**CTGGAATGGCTGCTACTGGTG	955	*Xho*I site
	XhoRT2R	CCG**CTCGAG**AAGACCGCATCAGTCACACAACC		*Xho*I site
pGEX-RT1	XhoRT3F	CCG**CTCGAG**TTAGTAGATCAATCACAAGTCAGCC	916	*Xho*I site
	XhoRT3R	CCG**CTCGAG**CATCCCTCAACCTGTACGGTCTG		*Xho*I site
pENTR-chacY1	attB1-chac1f	GGGG**ACAAGTTTGTACAAAAAAGCAGGCT**TCATGGT TTTCGAGTCGGTGGTC	1864	*att*B1 site
	attB2-chac1r	GGGG**ACCACTTTGTACAAGAAAGCTGGGT**CCTAACT ATTCACTGTCCTTGCATC		*att*B2 site
pENTR-chacY2	attB1-chac2f	GGGG**ACAAGTTTGTACAAAAAAGCAGGCT**CACGTCT GTACACTGTAAGACAC	1855	*att*B1 site
	attB2-chac2r	GGGG**ACCACTTTGTACAAGAAAGCTGGGT**CCTATGT TTCCCAAACCACATCAGAAC		*att*B2 site
pENTR-chacY3	attB1-chac3f	GGGG**ACAAGTTTGTACAAAAAAGCAGGCT**GTTCTGA TGTGGTTTGGGAAACA	1939	*att*B1 site
	attB2-chac3r	GGGG**ACCACTTTGTACAAGAAAGCTGGGT**CTCAGAG GCTCGGAGAAGGTTCTC		*att*B2 site
pENTR-chacY4	attB1-chac4f	GGGG**ACAAGTTTGTACAAAAAAGCAGGCT**TCAAAAG TATGTCTATTGTTCTAAGAG	1870	*att*B1 site
	attB2-chac4r	GGGG**ACCACTTTGTACAAGAAAGCTGGGT**CCTACTT TGCGTTTATTTCAGTTTCTG		*att*B2 site
pENTR-chacY5	attB1-chac5f	GGGG**ACAAGTTTGTACAAAAAAGCAGGCT**CCTCTTT GGATATTCATTTACAC	1879	*att*B1 site
	attB2-chac5r	GGGG**ACCACTTTGTACAAGAAAGCTGGGT**CCTAAGT CATTGTACTATTTTCAAGG		*att*B2 site
pENTR-chacY6	attB1-chac6f	GGGG**ACAAGTTTGTACAAAAAAGCAGGCT**TTATAAA GTACAGGAAAGTCAGAG	1876	*att*B1 site
	attB2-chac6r	GGGG**ACCACTTTGTACAAGAAAGCTGGGT**CCTAAGA TGTTAAATTATCTTTTTCTGG		*att*B2 site
pcD4chac2	Kpn-chac2F	C**GGTACC**ATGGGACGACGTCTGTACACTG	1814	*Kpn*I site
	Xho-chac2R	C**CTCGAG**TGTTTCCCAAACCACATCAGAAC		*Xho*I site

[a]: Restriction enzyme sites or recombination sites introduced by the primers are shown in bold. [b]: PCRs were all performed with annealing temperature of 60°C and magnesium acetate concentration of 1 mM, using r*Tth* enzyme (section 2.2.3)
Key: F, forward; R, reverse; AT, annealing temperature; [Mg], $MgCl_2$ concentration

A1.5 Primers to introduce restriction sites for *VPS13A* RFLP analysis

Primer name	Primer sequence	Amplicon size (bp)	AT (°C), [Mg] (mM)	Enzyme site created	Base change analysed
AKex18RDf	GTCTTCATTGGATGATGCAATGCCAC	188	58, 2.5	*Mwo*I	1695C>G
AKex18RDr	CATCATTAACACAAACTCAAAGCAAAC				
AKex31RDf	AAATTTCACAAAAAGCAAATTAAAAG	148	50, 2.5	*Bst*XI	3283G>C
AKex31RDr	GAATCTAAAACAATTATATTCCATAGC				
AKex38RDf	AAAAAGACATGATGGATATAAAGTGC	166	58, 2.5	*Bsg*I	4469G>A
AKex38RDr	TGCACACTGGTTTCTACAGCAG				
AKex54RDf	TGCCTATAGATTTGGGGGAAAAGTC	135	58, 2.5	*Hin*cII	7457T>C
AKex54RDr	GCTCTGCTAACTCTGCTTTCTCAC				

Key: AT, annealing temperature; [Mg], $MgCl_2$ concentration

A1.6 Primers for amplification of *GNA14* exons

Exon	Primer name	Primer sequence	Amplicon size (bp)	AT (°C), [Mg] (mM)
1	hG145'UTRfp2	CCGTCTTTTCTTTCCACACCCCTGTG	185	58, 2.5
	hG14int1rp2	CCTCCGGGAGGGCTCGGTAG		
2	hG14int1fp2	TCCCTTCCAAATCCAACCCATCAG	415	58, 2.5
	hG14int2rp2	TTCTTCTGGCTCTGACAAAGCACTGA		
3	hG14int2fp2	TCTCCAAATCCACAGACCAGGGCAAG	356	58, 2.5
	hG14int3rp2	CTGTGCACCGCATTTCAGCAGCGTTC		
4	hG14int3fp2	CTGTGTGGGGCTCACTGTGAGTG	353	58, 2.5
	hG14int4rp2	GAGAGGGTCACTCTGTCCTAAGAG		
5	hG14int4fp2	TTACTGAGGACTCCAAGAGCACTG	353	54, 2.5
	hG14int5rp2	GTAGCAAGACTGTTTGACCTAATG		
6	hG14int5fp2	GACTGCGGCGGGGCAAGGGAAG	325	58, 2.5
	hG14int6rp2	TAGACTGATGCCCGGGAGGT		
7	hG14int6fp2	GGAGGACATGGTGTTAAGTCTGTG	342	58, 2.5
	hG143'UTRrp2	TGGGGCTGGCTCTGGTGATGTCAG		

Key: AT, annealing temperature; [Mg], $MgCl_2$ concentration

A1.7 Primers for amplification and sequencing of *XK* exons

Exon	Primer name (direction)[a]	Primer sequence	Amplicon size (bp)	AT (°C), [Mg] (mM)
1	**XKbfp1 (F)**	**TGACGCGCGGAGATGAAATTC**	432	61, 1.5
	XKrp1 (R)	**ATGATTCGTCGCGTTCCTGACT**		
	XKseq1 (R)	AGATCAGGCTACAGGACCGAGGCT		(Sequencing)
2	**XKbfp2 (F)**	**AGGACTGCATACTGAGAACTGGTC**	625	61, 1.5
	XKrp2 (R)	**CCCTGCCTAGAATGCAGAGTCATA**		
	XKseq2.1 (F)	GTTCAGAGTAGCCAAGTCAAGGCT		(Sequencing)
	XKseq2.2 (R)	GAGCATAGTAACTAGAACACAGATTC		(Sequencing)
3	**XKbfp3 (F)**	**AACTGGAAGTCAGGCTGTGCACAT**	1217	65, 1.5
	XKrp3 (R)	**GGCCAGTAATGCCTAGAAGAACAC**		
	XKseq3.1 (F)	TATCCCTGTTGTCCATTGTGTATG		(Sequencing)
	XK3.1bis (F)	TGACAGAGTGTCTGCTGCAGTAG		(Sequencing)
	XKseq3.2 (R)	ACCAGGACTACAACTCGAGTGGC		(Sequencing)
	XKseq3.3 (R)	ATCTCTGGATGACTGTAGATCTTC		(Sequencing)
	XKseq3.4 (F)	GAACATAGAGAAGGCCCTCAGTAG		(Sequencing)

[a]: Primers used for PCR amplification are shown in bold.
Key: AT, annealing temperature; [Mg], $MgCl_2$ concentration

Appendix 2: GenBank accession numbers for sequences used in this study

This appendix lists the accession numbers for cDNA and protein sequences deposited at the GenBank database at the National Centre for Biotechnology Information (http://www.ncbi.nlm.nih.gov/).

A2.1 Accession numbers for cDNA sequences

H sapiens FLJ39362	AK096681
H sapiens FLJ32332	NM_144641
H sapiens NF-κB p65 subunit	M62399
H sapiens TAB2 splice variant 2	NM_145342
H sapiens VPS13A (*CHAC*) splice variant 1A	NM_033305
H sapiens VPS13A (*CHAC*) splice variant 1B	NM_015186

A2.2 Accession numbers for protein sequences

A thaliana AT1g48090.1	NP_175242
A thaliana VPS13-like protein	CAC08248
A thaliana O23559	CAB80985
A thaliana O23557	CAB80983
C elegans T08G11.1	T24692
D discoideum TipC	AAC31916
D melanogaster CG2093	AAF59228
H sapiens chorein variant 1A	NP_150648
H sapiens chorein variant 1B	NP_056001
H sapiens NF-κB p65 subunit	AAA36408
H sapiens PP2Cη	Q96MI6
H sapiens TAB1	Q15750
H sapiens TAB2 variant 2	NP_663317
H sapiens VPS13B variant 1A	CAE75584
H sapiens VPS13C variant 1A	CAE75582
H sapiens VPS13D variant 1A	CAE75586
S cerevisiae Vps13p/Soi1p	NP_013060
S pombe T39553	T39553
S pombe VPS13 orthologue	NP_596800

Appendix 3: Publications arising from this study

Dobson-Stone C, Velayos-Baeza A, Filippone LA, Westbury S, Storch A, Erdmann T, Wroe SJ, Leenders KL, Lang AE, Dotti MT, Federico A, Mohiddin SA, Fananapazir L, Daniels G, Danek A, Monaco AP.
Chorein detection for the diagnosis of chorea-acanthocytosis
Ann Neurol (in press)

Velayos-Baeza A, Vettori A, Copley RR, **Dobson-Stone C**, Monaco AP.
Analysis of the human *VPS13* gene family
Genomics (in press)

Bohlega S, Al-Jishi A, **Dobson-Stone C**, Rampoldi L, Saha P, Murad H, Kareem A, Roberts G, Monaco AP.
Chorea-acanthocytosis: Clinical and genetic findings in three families from the Arabian peninsula
Mov Dis. (2003) 18:403-407.

Dobson-Stone C, Danek A, Rampoldi L, *et al.*
Mutational spectrum of the CHAC gene in patients with chorea-acanthocytosis.
Eur J Hum Genet. (2002) 10:773-781.

Danek A, Rubio JP, Rampoldi L, Ho M, **Dobson-Stone C**, Tison F, Symmans WA, Oechsner M, Kalckreuth W, Watt JM, Corbett AJ, Hamdalla HH, Marshall AG, Sutton I, Dotti MT, Malandrini A, Walker RH, Daniels G, Monaco AP.
McLeod neuroacanthocytosis: genotype and phenotype.
Ann Neurol. (2001) 50:755-764.

Rampoldi L, **Dobson-Stone C**, Rubio JP, Danek A, Chalmers RM, Wood NW, Verellen C, Ferrer X, Malandrini A, Fabrizi GM, Brown R, Vance J, Pericak-Vance M, Rudolf G, Carre S, Alonso E, Manfredi M, Nemeth AH, Monaco AP.
A conserved sorting-associated protein is mutant in chorea-acanthocytosis.
Nat Genet. (2001) 28:119-120.